PARAMETRIC AND NON-PARAMETRIC APPROACHES TO QUANTITATING PHARMACODYNAMIC RESPONSE

Emily Renee Olson

A dissertation submitted to the faculty of the University of North Carolina at Chapel Hill in partial fulfillment of the requirements for the degree of Doctor of Philosophy in the School of Pharmacy

Chapel Hill
2008

Approved by:

Advisor: Gary M. Pollack, Ph.D.

Reader: Robert E. Dupuis, Pharm.D., BCPS

Reader: J. Heyward Hull, Pharm.D., M.S

Reader: Adam M. Persky, Ph.D.

Reader: Joseph Polli, Ph.D.

ABSTRACT

EMILY RENEE OLSON: Parametric and Non-Parametric Approaches to Quantitating Pharmacodynamic Response
(Under the direction of Gary M. Pollack, Ph.D.)

The goal of this project was to evaluate factors that impact pharmacokinetic-pharmacodynamic (PK-PD) relationships, and to develop novel approaches for analysis of those relationships utilizing opioids as a model pharmacologic class. The role of protein binding in *in vitro*-to-preclinical and preclinical-to-clinical estimates of opioid potency was investigated; the optimal metric for characterizing *in vivo* potency was unbound brain EC_{50}. The role of P-glycoprotein (P-gp) efflux at the blood brain barrier (BBB) in attenuating central nervous system (CNS) concentrations and pharmacologic response was evaluated in mice receiving loperamide, methadone, alfentanil or fentanyl. An integrated PK-PD model fit to the time course of antinociception and serum/brain concentrations revealed the influence of P-gp on brain:plasma ratio and brain:plasma equilibration half-life. The influence of behavioral responses in the hotplate latency antinociception assay was investigated for loperamide, methadone and sufentanil. PK-PD modeling suggested that processed responses, jumping and hind-paw licking, reflected centrally-mediated processes, whereas reflexive responses, lifting or shaking of the hind paw, were mediated predominately in the periphery, with a slight additive central contribution. The influence of truncating the dynamic range of pharmacologic effect on recovery of PD parameters was investigated with fentanyl and morphine. Incorporating E_{max} as a parameter, as opposed to a fixed value, in

PK-PD modeling improved model predictions when compared to assigning a fixed value at an artificial ceiling. The utility of area bounded by a hysteresis loop (ABH) as a non-parametric descriptor of dissociation between pharmacodynamics and pharmacokinetics was assessed with five opioids administered to P-gp-competent and P-gp-deficient mice. A Matlab routine was developed to calculate ABH, and this novel quantitative approach was evaluated relative to image analysis of the hysteresis loop. ABH correlated with area under the curve (AUC) and the model-derived parameters EC_{50} and k_{e0}. Taken together, these approaches provide a framework for understanding the multiplicity of factors that influence drug concentrations and pharmacologic effect, and provide insight into how information derived from parametric and non-parametric analyses can be used to characterize PK-PD relationships and predict the behavior of PK-PD systems.

ACKNOWLEDGEMENTS

I would like to thank my advisor, Dr. Gary Pollack, for his dedication of time, insight, and support. By taking a chance on an unknown student from Kalamazoo College, Dr. Pollack shaped the course of my life and for that, I am grateful.

I extend many thanks to my committee members, Drs. Bob Dupuis, Adam Persky, Heyward Hull, and Joe Polli, for their guidance and insight.

I am grateful for the incredible opportunities, invaluable advice and solid scientific foundation provided by Elizabeth Schanhals, and Drs. D. Blaine Moore, Laura Furge, and Natilie Hosea.

I thank the former, current and future members of the Pollack and Brouwer labs. In particular, I thank Dr. J. Cory Kalvass for his attention to detail, willingness to collaborate and scientific insight. Thanks to Dr. Rong Zhao and Jeannie Padowski for their friendship, support and patience. I thank Dr. Maciej Zamek-Gliszczynski for his friendship, academic and career insight, and for always providing a great story.

Finally, I would like to thank my parents, Steve and Kathryn Bandstra and Tom and Linda Olson, for their dedication, encouragement and unwavering love. I am grateful for the strength, devotion and sense of humor possessed by my mother. I thank my father for always putting things in perspective and reminding me that there is always time to take a breath and enjoy the ride. I thank my brothers, Devin and Jared, for their love, humor and stories. I thank Dr. John Dumas for his love, inspiration, and friendship.

TABLE OF CONTENTS

LIST OF TABLES viii

LIST OF FIGURES ix

LIST OF ABBREVIATIONS AND SYMBOLS xiv

CHAPTER

1. PROJECT OVERVIEW 1

2. OPIOID TOLERANCE DEVELOPMENT: A PHARMACOKINETIC-PHARMACODYNAMIC PERSPECTIVE 21

PART I: USE OF CLASSICAL APPROACHES TO IMPROVE THE LINK BETWEEN PHARMACOKINETICS AND PHARMACODYNAMICS 69

3. PHARMACOKINETICS AND PHARMACODYNAMICS OF SEVEN OPIOIDS IN PGP-COMPETENT MICE ASSESSMENT OF UNBOUND BRAIN EC50S AND CORRELATION OF IN VITRO, PRECLINICAL, AND CLINICAL DATA 70

4. INFLUENCE OF BLOOD-BRAIN BARRIER P-GLYCOPROTEIN ON BRAIN PENETRATION AND ANTINOCICEPTIVE EFFECTS OF MODEL OPIOIDS 105

5. PHARAMCOKINETICS AND PHARMACODYNAMICS OF ALFENTANIL IN P-GLYCOPROTEIN-COMPETENT AND P-GLYCOPROTEIN-DEFICIENT MICE: P-GLYCOPROTEIN EFFLUX ALTERS ALFENTANIL BRAIN DISPOSITION AND ANTINOCICEPTION. 130

PART II: NOVEL APPROACHES TO CHARACTERIZING PHARMACOKINETICS AND PHARMACODYNAMICS 151

6. USE OF A PHARMACOKINETIC-PHARMACODYNAMIC (PK-PD) MODEL INCORPORATING SERUM AND BRAIN CONCENTRATIONS TO EXAMINE CENTRAL AND PERIPHERAL CONTRIBUTIONS TO ANTINOCICEPTION 154

7. INFLUENCE OF TRUNCATING THE DYNAMIC RANGE OF PHARMACOLOGIC EFFECT MEASUREMENTS ON PHARMACODYNAMIC PARAMETER ESTIMATES 183

8. THE INFLUENCE OF PHARMACOKINETIC AND PHARMACODYNAMIC PARAMETERS ON HYSTERESIS LOOP AREA 207

9. RELATIONSHIP BETWEEN AREA BOUNDED BY THE ANTINOCICEPTION-SERUM CONCENTRATION HYSTERESIS AND PHARMACOKINETIC-PHARMACODYNAMIC PARAMETER ESTIMATES FOR A SERIES OF OPIOIDS..... 231

10. CONCLUSIONS..... 268

APPENDIX: MATLAB CODE..... 281

LIST OF TABLES

Table 2.1. Categorization of the common opioids based on structural similarities. 47

Table 2.2. Pharmacokinetic/pharmacodynamic parameter estimates and corresponding coefficients of variation obtained from simultaneous modeling of morphine disposition, NO production, and antinociceptive effects. 48

Table 3.1. Additional parameters used for correlation of i*n vitro*, preclinical, and clinical data..... 91

Table 3.2. Parameter estimates from PK-PD modeling. 92

Table 4.1. Parameter estimates from PK-PD modeling. 119

Table 4.2. Parameter estimates for loperamide in FVB mice 120

Table 5.1. PK-PD parameters for alfentanil in *mdr1a*(-/-) and *mdr1a*(+/+) mice..... 143

Table 6.1. Pharmacokinetic parameter estimates [mean (% CV)] derived using non-linear regression analysis..... 171

Table 6.2. Pharmacodynamic parameter estimates [mean (% CV)] by fitting Model 1 to the standard effect data using non-linear regression analysis. 172

Table 6.3. Pharmacodynamic parameter estimates [mean (% CV)] derived by fitting Model 2 to the modified effect data using non-linear regression analysis. 173

Table 7.1. Final parameter estimates from traditional PK-PD modeling..... 195

Table 7.2. Final parameter estimates from traditional PK-PD modeling..... 196

Table 8.1. Influence of model parameters on ABH. 221

Table 9.1. Parameter estimates from PK-PD modeling. 247

LIST OF FIGURES

Figure 1.1. PK-PD model depicting a direct relationship between plasma drug concentration and pharmacologic response. 14

Figure 1.2. Depiction of clockwise (A) and counterclockwise (B) hysteresis loops. Arrows represent the progression of time. 15

Figure 1.3. Time-dependent PK-PD models include (A) production of an active metabolite, (B) indirect pharmacologic response, and (C) drug distribution between plasma and effect compartment which mediates pharmacologic response. 16

Figure 2.1. Downstream mediators of antinociception following opioid agonist binding to the MOR. 49

Figure 2.2. Scheme depicting the PK-PD model of tolerance following multiple morphine i.v. bolus doses 50

Figure 2.3. Relationship between antinociceptive response and morphine concentrations in blood during continuous infusion at the time of peak response (*circles*) or at 12 hr into the infusion (*triangles*) 51

Figure 2.4. Time course of antinociceptive response during morphine infusion in rats. 52

Figure 2.5. Recovery of antinociceptive response to a 2-mg/kg bolus dose of morphine following termination of a 12-hr morphine infusion (2 mg/kg/hr) 53

Figure 2.6. PK-PD model for L-arginine-associated stimulation of nitric oxide production in rats.. 54

Figure 2.7. Concentration-time profiles for brain NO during (A) saline or administration of L-arginine [(B) 250 mg/kg/hr, (C) 500 mg/kg/hr, or (D) 1000 mg/kg/hr].. 55

Figure 2.8. Scheme depicting the PK-PD model of morphine disposition, NO production and antinociceptive effect.. 56

Figure 2.9. Blood morphine concentrations, brain morphine concentrations, and antinociceptive effect during and following an 8-hr morphine infusion.. 58

Figure 3.1. Pharmacokinetic/pharmacodynamic model for opioid disposition and antinociception in mice.. 93

Figure 3.2. Time course of antinociception (◇), serum (●) and brain (▲) concentrations. 95

Figure 3.3. Relationship between plasma concentration and antinociception for μ-opioid agonists. 96

Figure 3.4. Relationship between brain concentration and antinociception for μ-opioid agonists.. 97

Figure 3.5. Time course of opioid $K_{p,brain}$ in CF-1 *mdr1a*(+/+)..... 98

Figure 3.6. Correlation analysis for various in vivo measures relative to in vitro potency. 99

Figure 3.7. Correlation between mouse serum and human plasma EC_{50}s. 100

Figure 3.8. Correlation of equipotent clinical dose with in vitro K_i values, mouse ED_{50} values, and mouse EC_{50} values. 101

Figure 3.9. The correlation between human plasma-biophase equilibration half-life ($t_{1/2,Ke0}$) and mouse brain equilibration half-life ($t_{1/2eq,brain}$)..... 102

Figure 4.1. Pharmacokinetic-pharmacodynamic model for opioid disposition and antinociception in mice. 121

Figure 4.2. Time course of serum (●) and brain (□) concentrations following s.c. administration of opioids 122

Figure 4.3. Time course of antinociception following s.c. administration of opioids. 123

Figure 4.4. Relationship between antinociception and opioid serum concentration. 124

Figure 4.5. Relationship between antinociception and opioid brain concentration..... 125

Figure 4.6. Time course of opioid $K_{p,brain}$ in *mdr1a*(-/-) and *mdr1a*(+/+) mice. 126

Figure 4.7. Pharmacokinetics/pharmacodynamics of loperamide in FVB mice..... 127

Figure 5.1. Pharmacokinetic-pharmacodynamic model for alfentanil disposition and antinociception in mice. 144

Figure 5.2. Time course of serum (●) and brain (▲) concentrations following a 0.067- or 0.2-mg/kg s.c. dose of alfentanil in *mdr1a*(–/–) or *mdr1a*(+/+) mice..... 145

Figure 5.3. Time course of antinociception following a 0.067- or 0.2-mg/kg s.c. dose of alfentanil in *mdr1a*(–/–) or *mdr1a*(+/+) mice. 146

Figure 5.4. Relationship between antinociception and serum concentration of alfentanil following a 0.067-mg/kg s.c. dose [*mdr1a*(–/–)] or 0.2-mg/kg s.c. dose [*mdr1a*(+/+)]. 147

Figure 5.5. Relationship between antinociception and brain concentration of alfentanil following a 0.067-mg/kg s.c. dose [*mdr1a*(–/–)]or 0.2-mg/kg s.c. dose [*mdr1a*(+/+)]. 148

Figure 5.6. Time course of alfentanil $K_{p,brain}$ in mice following a 0.067-mg/kg s.c. dose [*mdr1a*(–/–)] or 0.2-mg/kg s.c. dose [*mdr1a*(+/+)]. 149

Figure 6.1. Pharmacokinetic-pharmacodynamic models characterizing opioid disposition and antinociception..... 174

Figure 6.2. Time course of observed and predicted opioid serum and brain concentrations following subcutaneous administration of loperamide, methadone and sufentanil. 175

Figure 6.3. Time course of observed and predicted opioid standard and modified antinociceptive effect following administration of loperamide, methadone, and sufentanil. 176

Figure 6.4. Relationship between standard antinociceptive effect and concentration for loperamide, methadone, and sufentanil..... 177

Figure 6.5. Relationship between modified antinociceptive effect and serum or brain concentrations for loperamide, methadone and sufentanil. 178

Figure 6.6. Contribution of serum (solid gray line) and brain (dashed black line) to overall observed (symbols; n = 4 to 36) and predicted (solid black line) modified antinociceptive effect for loperamide (○), methadone (◇) and sufentanil (△). 179

Figure 6.7. Pharmacodynamic parameter estimates for modified antinociceptive effect were used to simulate serum and brain mediated contributions to modified effect for loperamide, methadone and sufentanil 180

Figure 7.1. Scheme of the pharmacokinetic-pharmacodynamic model for opioid disposition and antinociception in mice..... 197

Figure 7.2. Influence of E_{max} fixed at 100% on the time course of antinociception..... 198

Figure 7.3. Influence of a variable E_{max} on the predicted time course of antinociception..... 199

Figure 7.4. Influence of E_{max} truncation on estimates of k_{e0}, EC_{50} and γ for fentanyl and morphine. 200

Figure 7.5. Effect versus concentration relationships expressed as actual response or relative to the maximum allowable response. 201

Figure 7.6. Effect versus concentration relationships expressed as actual response or relative to the maximum allowable response 202

Figure 7.7. Effect versus concentration relationships expressed as actual response or relative to the maximum allowable response. 203

Figure 7.8. Relationship between the apparent EC_{50} and the maximum allowable response for truncated effect data 204

Figure 8.1. Scheme of the model used to generate concentration and effect profiles. 222

Figure 8.2. Method of calculating ABH utilized by Matlab. 223

Figure 8.3. Representative pharmacokinetic and pharmacodynamic model output. 224

Figure 8.4. Relationship between ABH calculated using ImageJ and Matlab 225

Figure 8.5. The influence of PK-PD parameter values on measures of ABH. 226

Figure 8.6. Influence of PK parameter values on the effect versus blood concentration hysteresis 227

Figure 8.7. The influence of PD parameter values on the effect versus blood concentration hysteresis. 228

Figure 9.1. Scheme of the pharmacokinetic-pharmacodynamic model for opioid disposition and antinociception in mice 248

Figure 9.2. Time course of antinociception, serum, and effect compartment concentrations following subcutaneous opiod administration 254

Figure 9.3. Relationship between opioid antinociception and serum or effect compartment concentrations. 260

Figure 9.4. Relationship between ABH calculated using observed data versus predicted fit of the model for a series of opioids. 261

Figure 9.5. Relationship between ABH and AUC for a series of opioids. 262

Figure 9.6. Relationship between ABH and $1/k_{e0}$ for a series of opioids in P-gp competent and deficient mice. 263

Figure 9.7. Correlation between ABH normalized by EC_{50} or $EC_{50,u}$ and $1/k_{e0}$ for data obtained experimentally or adapted from literature. 264

Figure 9.8. Relationship between $1/k_{e0}$ and the normalized time between maximum serum and effect compartment concentrations. 265

LIST OF ABBREVIATIONS AND SYMBOLS

γ	Hill factor
$\gamma_{,B}$	Hill factor for brain
$\gamma_{,S}$	Hill factor for serum
ABC	ATP-binding cassette
ABH	area bounded by the hysteresis
AC	adenylyl cyclase
AIC	Akikes information criteria
AUC	area under the curve
BBB	blood brain barrier
C_A	arterial concentration
C_B	brain (or blood concentration) concentration
C_E	effect compartment concentration
Cl	systemic clearance
Cl_{ef}	efflux clearance
C_{in}	afferent concentration
Cl_{up}	uptake clearance
C_{out}	efferent concentration
CNS	central nervous system
CREB	cAMP-responsive element binding protein
C_S	serum concentration
CSF	cerebrospinal fluid
C_V	venous concentration

CYP	cytochrome P450
DOR	δ-opioid receptor
EC_{50}	concentration at 50% of the maximum effect
$EC_{50,B}$	brain concentration at 50% of the maximum modified effect
$EC_{50,S}$	serum concentration at 50% of the maximum modified effect
ED_{50}	dose that produces 50% of the maximum effect
E_M	modified antinociceptive effect
E_{max}	maximum effect
E_s	standard antinociceptive effect
GABA	γ-amino-butyric acid
GPCR	G-protein coupled receptor
GRK	G-protein receptor kinase
GTPγS	guanosine 5'-*O*-(3-thio)triphosphate
HPLC-MS/MS	high-performance liquid chromatography-tandem mass spectrometry.
hPXR	human pregnane X receptor
k_a	first-order rate of absorption
k_{e0}	rate of effect offset
KOR	κ-opioid receptor
$K_{p,brain}$	brain-to-serum ratio
L-Arg	L-arginine (L-Arg)
L-Cit	L-citrulline (L-Cit)
M3G	morphine-3-glucuronide
M6G	morphine-6-glucuronide

MOR	μ-opioid receptor
MPR	maximal possible response
NMDA	*N*-methyl-D-aspartate
nNOS	neuronal nitric oxide synthase
NRA	*N*-methyl-D-aspartate receptor antagonist
OR	opioid receptors
PD	pharmacodynamic
PK	pharmacokinetic
P-gp	P-glycoprotein
PK	pharmacokinetic
PKA	protein kinase A
PSD-95	post-synaptic density complex
sGC	soluble guanylyl cyclase
SNP	single nucleotide polymorphism
T	time
UGT	uridine-5'-diphosphate-glucuronosyltranserase
V	volume of distribution
V_B	brain volume of distribution
V_S	serum volume of distribution
X_0	dose
X_A	mass of drug at the absorption site
X_B	mass of drug in brain
X_S	mass of drug in serum

CHAPTER 1

PROJECT OVERVIEW

Pharmacokinetic-pharmacodynamic (PK-PD) modeling is increasingly being recognized as a critical component of the drug development process. Advances in computational power and bioanalytical specificity, sensitivity and reproducibility over the last twenty years have led to the inclusion of PK-PD analysis as a routine part of drug development programs. While tremendous progress has been made in describing drug disposition and effect since Gerhard Levy (1966) commented that "the multiplicity of factors which are expected to be involved in the response of intact animals to drugs seems to have discouraged investigations of the kinetics of gross pharmacologic effect," the underlying problem remains, and a satisfactory definition of what pharmacologic response is and how it shall be interpreted is missing. This deficiency can, in part, be attributed to the "multiplicity of factors" that mediate pharmacologic effect, including the ability of receptor populations in physiologically distinct locales to produce the same pharmacologic response, multiple responses mediated by one drug molecule, and intra- and inter-individual assay variability and insensitivity.

This project overview has been constructed to 1) review concepts associated with characterizing pharmacokinetics and pharmacodynamic response, 2) introduce the challenges associated with characterizing central nervous system (CNS) PK-PD, 3) explain why the opioids are an ideal drug class for examining CNS penetration and response as fundamental

processes, and 4) lay out the parametric and non-parametric techniques used in this dissertation project to quantify pharmacodynamic response.

PRINCIPLES OF PHARMACOKINETIC-PHARMACODYNAMIC MODELING

Characterizing the relationship between drug administration, the time course of drug concentrations, and the pharmacologic effect produced by these concentrations is a critical component of any drug development program. Integrating what the body does to a drug, pharmacokinetics, with what the drug does to the body, pharmacodynamics, forms a therapeutically-relevant relationship that can be used to predict responses following changes to the system (i.e. dose route, frequency or concentration). The following sections will serve as an introduction to modeling time-independent and time-dependent relationships between drug kinetics and response. In addition, methods that address dissociations between effect and concentration will be addressed.

Time-independent relationship between effect and concentration

When pharmacologic effect is receptor-mediated, the magnitude of biologic response is assumed to be proportional to the fraction of the receptor population occupied at a particular drug concentration. If concentrations in the receptor biophase (C_E) are in immediate equilibrium with concentrations in blood (C_B), and the effect (E) is instantaneously reversible and time-invariant, the relationship between E and C_B can be described using a parametric model such as the sigmoidal E_{max} (or Hill) equation (Figure 1.1). More detailed descriptions of commonly used PD models can be found in a number of articles (Holford and Sheiner 1982; Meibohm and Derendorf 1997; Bellissant, Sebille et al., 1998). The neuromuscular blocker turbocurarine holds true to these assumptions, and a sigmoidal relationship between the degree of paralysis and blood concentrations can be

demonstrated (Gibaldi and Levy 1972). The scenario where pharmacologic response is directly related to plasma concentrations is atypical, however, with few drugs conforming to the strict assumptions associated with this model.

Time-dependent relationships between effect and concentration

A far more common occurrence is the presence of a time-dependent dissociation between drug disposition and pharmacologic effect. The development of acute tolerance, such as occurs in response to nasally-administered cocaine, is a classic example of time-dependent changes in the concentration-effect relationship (Jones 1990). In this example, blood cocaine concentrations initially increase and produce a commensurate increase in euphoria. Receptor desensitization ensues and, despite continued increases in concentration, euphoria rapidly diminishes. The relationship between the euphoric effect and blood concentration reveals what is known as a hysteresis loop that progresses temporally in a clockwise direction (Figure 1.2A).

While tolerance is manifested as a clockwise hysteresis, the more common situation is the presence of a counterclockwise hysteresis loop. Dissociation between effect and blood concentrations producing counterclockwise hysteresis behavior can result from a number of physiologic processes: indirect responses following drug-receptor binding, production of a pharmacologically active metabolite, or drug distribution to a structurally distinct compartment containing the receptor biophase (Figure 1.3). Drug concentrations at the receptor biophase often are unknown, and the PK-PD model therefore must characterize the relationship between drug response and serum concentrations. For example, an intravenous bolus dose of morphine initially will produce high blood concentrations, but the onset of effect will lag behind the maximum concentration (C_{max}) because of the temporal delay in

morphine distribution to the brain (the presumed locale of response). Similarly, just as slow accumulation in brain can result in delayed onset of effect, prolonged residence of drug in the brain can result in an offset of effect slower than would be predicted based on the rate of decline in blood concentrations. Assuming that the receptor biophase is in equilibrium with brain concentrations, a time-independent sigmoidal relationship will be observed between pharmacologic response and brain concentrations, while the temporal dissociation between response and blood concentrations will produce a hysteresis loop that temporally progresses counterclockwise (Figure 1.2B).

Techniques used to address pharmacokinetic-pharmacodynamic hysteresis loops

In the presence of hysteresis behavior, recovery of PD parameter estimates from the relationship between effect and central compartment (blood) concentrations is not feasible. For example, in the presence of significant hysteresis, two distinct concentrations will correspond to 50% of maximal effect, neither of which will be representative of the true EC_{50}. This effect-concentration disconnect is most commonly addressed with the application of the indirect-link PK-PD model, which uses the temporal relationships for effect and blood concentrations to predict the time course of drug concentrations in a hypothetical effect compartment (Holford and Sheiner 1982). Estimates of fundamental pharmacodynamic parameters (EC_{50} and γ) then can be recovered from effect versus effect compartment concentration relationship. This analytical process is referred to as "collapsing the hysteresis loop". An alternative approach taken by Gastonguay and Schwartz (1994) characterized pharmacodynamics in the presence of processes that result in competing hysteresis behavior: distributional delays of drug presentation to the receptor biophase and onset of acute pharmacodynamic tolerance. This approach was based on computationally minimizing the

contribution of distribution to the net hysteresis behavior. While these approaches address distribution-based hysteresis loops, other methods have been explored to rectify hysteresis behavior resulting from other physiologic processes.

Hysteresis loops can be attributed to differences in venous, arterial and effect compartment concentrations. For example, a drug that equilibrates rapidly between arterial and venous blood, but exhibits slow distribution from arterial blood to the effect site, will be associated with a counterclockwise hysteresis between pharmacologic response and venous concentrations. Verotta et al. (1989) developed a semiparametric model that incorporates distribution between arterial and venous blood, together with distribution between arterial blood and the effect compartment, to address the hysteresis resulting from the dissociation between effect and sampled venous blood concentrations. By incorporating the rate constants recovered from this analysis, the hysteresis collapses and the ensuing relationship between pharmacologic response and effect compartment concentrations can be used to recover estimates of fundamental pharmacodynamic parameters.

CENTRAL NERVOUS SYSTEM PHARMACOKINETICS AND PHARMACODYNAMICS

Describing the link between pharmacologic effect and drug concentrations is particularly challenging for drugs with central nervous system (CNS) activity. Systemic concentrations of a drug are influenced primarily by lumped absorption, distribution, metabolism and elimination (ADME) processes, whereas CNS concentrations, and consequently pharmacologic effect, are determined by protein binding, blood-brain barrier (BBB) permeability, active transport, local metabolism, and cerebrospinal fluid (CSF) turnover. Access to the brain and CSF is highly regulated by the BBB and blood-cerebrospinal fluid barrier (BCSFB), respectively. While the BCSFB is poorly characterized

compared to the BBB, it serves a largely protective role by regulating the entry of potential neurotoxins and metabolizing and/or effluxing xenobiotics from the CSF, via many of the same active transporters and metabolizing enzymes found in the BBB (de Lange 2004; Graff and Pollack 2004). Due to the small surface area of the BCSFB (~0.02% of the BBB surface area), the BBB is considered the primary interface between systemic concentrations and the CNS (Kusuhara and Sugiyama 2001). The following sections provide an introduction to mechanisms of brain uptake, experimental approaches to assessing brain disposition and the use of opioids as model CNS active drugs.

Central Nervous System Disposition

The BBB is an anatomical, biochemical, and functional barrier situated between the CNS and systemic circulation that serves to supply the brain with essential nutrients and to regulate entry and efflux of endogenous and exogenous substances. The primary physical attributes that restrict brain penetration are the highly-developed tight junctions that link brain capillary endothelial cells, adjacent brain parenchymal cells (glial cells and astrocytes), an absence of microvascular fenestrations, and minimal pinocytotic activity (Engelhardt 2003; Ohtsuki and Terasaki 2007). While chemical structure and physicochemical properties (molecular weight, polar surface area, lipophilicity, and hydrogen bonding) dictate passive diffusion across the BBB, with small, lipophilic compounds being more permeable, the presence of active uptake and efflux transporters enables the passage of many substrates into and out of the brain (Feng 2002; Mahar Doan, Humphreys et al. 2002). CNS homeostasis is, in part, maintained by specific transporters for essential nutrients and physiologic substrates: glucose, neuropeptides, monocarboxylic acids, amino acids, hormones, and electrolytes (Graff and Pollack 2004; Hawkins, O'Kane et al. 2006).

The presence of efflux transporters at the BBB limits the brain exposure of many pharmacologic agents and should be considered in the evaluation of new compounds. The predominant transmembrane efflux transporters expressed at the BBB belong to the ABC (ATP-binding cassette) superfamily and include P-glycoprotein (P-gp; *ABCB1*), breast cancer resistance protein (BCRP; *ABCG2*), and multidrug resistance proteins (MRP; *ABCC* family), in addition to the organic cation transporters (OCTs; *SLC2*s) and organic anion transporting polypeptides (OATPs; *SLCO*s) that also are present (Golden and Pollack 2003; Hagenbuch and Meier 2004). A comprehensive overview of BBB (and BCSFB) uptake and efflux transporters is provided by Graff and Pollack (2004). Ultimately, pharmacologic response of a CNS active agent is, in part, dictated by the relative balance achieved between passive and active uptake and efflux at the BBB.

Initially identified in tumor cells with a multi-drug resistance phenotype, P-gp is a 170-kDa, ATP-dependent membrane bound transport protein encoded by the multidrug resistance gene ABCB1 (formerly *MDR1*) in humans and *mdr1a* and *mdr1b* in rodents (Sharma, Inoue et al. 1992). P-gp serves to attenuate intestinal absorption, secrete drugs into bile and urine, and protect sanctuary tissues such as the CNS and reproductive organs from toxic drug exposure (Matheny, Lamb et al. 2001). The latter role, impeding the entry of potential toxins into a sanctuary site, is achieved by P-gp expression on the luminal surface of brain endothelial cells (Cordon-Cardo, O'Brien et al. 1989). The role of active and passive transport at the BBB has received considerable attention, and a number of methods have been developed to identify substrates of P-gp efflux at the BBB.

While the collection of blood and urine is relatively straightforward and can be repeated over time, characterizing CNS drug disposition is more challenging and often

requires invasive, labor-intensive, and costly approaches. For this reason, *in vitro* systems such as cultured brain microvessel endothelial cells (BMECs) and transfected Madin-Darby canine kidney (MDCK) cells have been used as surrogate models to characterize BBB permeability and transporter-mediated efflux (Biegel, Spencer et al. 1995; Johnson and Anderson 1999; Letrent, Polli et al. 1999; Mahar Doan, Humphreys et al. 2002). These systems can be used in coordination with chemical inhibitors or transfected cells to identify the role of P-gp and other BBB transporter proteins on brain penetration. While these methods have proven useful, they differ from the intact BBB and exhibit increased paracellular permeability, leaky tight junctions and decreased transendothelial electrical resistance (TEER) compared to *in vivo* estimates (Wolburg, Neuhaus et al. 1994). Recent techniques have attempted to improve *in vitro* methodology by co-culturing BMECs with astrocytes and with the use of specific cellular markers to verify BMEC composition. Nevertheless, *in vivo* studies provide more reliable and relevant results (Yamagata, Tagami et al. 1997; Yousif, Marie-Claire et al. 2007).

Two strains of mice deficient in P-gp are commonly used to characterize the impact of P-gp efflux: the CF-1 strain, which possess a naturally occurring mutation in the *mdr1a(*-/-) gene and the FVB strain, which serves as the platform for creating knockout mice deficient in both *mdr1* isoforms expressed in brain, *mdr1a* and *mdr1b* (Schinkel, Wagenaar et al. 1996; Lankas, Cartwright et al. 1997; Schinkel, Mayer et al. 1997; Umbenhauer, Lankas et al. 1997). The collection of whole tissues from intact animals (Chen and Pollack 1998) or the use of *in situ* brain perfusion in P-gp-competent and P-gp-deficient mice (Dagenais, Rousselle et al. 2000) are frequently-used methods of determining net distribution across the BBB and initial brain uptake of compounds, respectively. Other techniques, including brain

microdialysis and CSF sampling, have been utilized but are highly invasive and, in the case of microdialysis, limited to preclinical species. An alternative, non-invasive technique that can be used in both humans and preclinical species is positron emission tomography (PET) (Hsiao, Sasongko et al. 2006; Hsiao, Bui et al. 2007). However, the lack of metabolite specificity, the need for specialized facilities, and cost have limited the widespread adoption of this approach.

Opioids: A model pharmacologic class with central nervous system activity

The diversity in chemical structure, BBB penetration, physicochemical properties, potency and duration of effect, make opioids an ideal group of compounds for probing a multiplicity of phenomena that determine CNS pharmacokinetics and pharmacodynamics. This class of drugs is well understood in preclinical and clinical settings, and extensive attention has been paid to elucidating the post-receptor binding signal transduction pathways that mediate analgesia and the undesirable effects of respiratory depression, decreased gastrointestinal motility, and tolerance development (Bailey and Connor 2005; Lotsch 2005). Moreover, pharmacologic effect is easily assessed over time by characterizing alterations in rate, frequency or time of response following exposure to a noxious stimulus (Le Bars, Gozariu et al. 2001). Moreover, the different categories of noxious stimuli that can be used to assess antinociception has led to adoption of numerous assays. While most opioids produce analgesia via opioid receptors in central locales, others (i.e., loperamide) do not cross the BBB readily and are devoid of centrally-mediated effects at therapeutic doses (Niemegeers, McGuire et al. 1979). The use of knockout mice has been instrumental in assessing the role of P-gp in attenuating brain uptake and antinociception of loperamide,

methadone, DPDPE ([D-penicillamine(2,5)] enkephalin) (Chen and Pollack 1998; Thompson, Koszdin et al. 2000; Dagenais, Graff et al. 2004).

Characterizing pharmacologic response of opioids

Assessing pharmacologic effect can be particularly challenging because drugs can produce multiple responses, drug-receptor interactions in distinct compartments can mediate the same overt effect, and homeostatic mechanisms and counter-adaptations can influence observed response. In addition, physiologic differences between preclinical species and humans often necessitate the use of different assay methodologies. An obvious difference is the absence of verbal communication in animals that requires the investigator to interpret vocal and behavioral responses to a noxious stimulus (the hot plate latency assay, the paw pressure test, the tail flick assay, and electrical vocalization stimulation). In contrast, opioid-induced antinociception can be assessed in humans using verbal responses to a stimulus by referencing numerical- or image-based pain scales, through use of transcutaneous electrical stimuli, with pupillometry, or by the extent of respiratory depression (Le Bars, Gozariu et al. 2001; Lotsch 2005). While assay overlap between species exists in the form of electroencephalogram (EEG) power spectrum analysis, the most commonly-used animal assays monitor behavioral responses following exposure to a painful stimulus.

A number of disadvantages, primarily related to the influence of ancillary physiologic processes, accompany the use of behavioral assays. For example, thermal assays and pressure tests are nondiscriminatory in the activation of nociceptors and either thermoreceptors or low-threshold mechanoreceptors, respectively (Le Bars, Gozariu et al. 2001). Some drugs elicit motor incoordination that may delay response time following exposure to the noxious stimulus, leading to a potential underestimate of the EC_{50} for

antinociception. In these instances, parallel motor incoordination assays may be necessary (Parsons 2001). One also must consider the influence of learning on performance in behavioral assays when a subject is repeatedly exposed to a noxious stimulus (Milne, Gamble et al. 1989). Moreover, one common criticism of preclinical antinociceptive assays is the lack of clinically relevant, persistent pain states. While this is an assay limitation, ethical considerations dictate the minimization of exposure to noxious stimuli, accomplished with stimulus removal upon observation of the desired response. Overall, characterizing antinociception, particularly in preclinical settings, is challenging, and the experimenter must carefully consider and, to the extent possible, control for all processes that influence responsivity.

PROJECT OVERVIEW

Time-dependent dissociations between pharmacologic effect and drug concentration are a particularly challenging aspect of pharmacokinetic-pharmacodynamic data analysis and modeling. While mathematical and experimental approaches have been developed to address such dissociations, they often are inadequate or require hypothetical constructs that limit their utility. The goal of this dissertation project was to develop model-dependent and model-independent methods of characterizing and quantitating the relationship between drug response and systemic drug exposure. Consequently, this dissertation is divided into two sections. Part I communicates the results of an experimentally-based approach to describe opioid pharmacokinetic-pharmacodynamic relationships and to improve predictions between *in vitro*, preclinical, and clinical predictions of potency. Part II is based on the development of novel model-dependent and –independent approaches to characterizing the relationship between between response and concentration.

Opioids frequently are used to treat acute, severe, and chronic pain. Repeat exposure results in the rapid development of tolerance to the analgesic effects but tolerance to the side effects develops less rapidly, often limiting dose increases. A number of kinetic and dynamic alterations have been proposed as contributing to the onset of analgesic tolerance, and multiple PK-PD models have been developed to characterize the time-dependent decrease in response. A comprehensive review of these mechanisms and the corresponding mathematical models used to describe opioid tolerance is provided in Chapter 2.

The use of cell culture models of the BBB is a popular strategy in drug discovery to screen compounds for CNS penetration. These *in vitro* models differ from whole organism studies of brain disposition in that they represent just one of multiple routes of central penetration, they lack the complex cytoarchitecture that comprises the BBB, and they exhibit greater cell permeability. Preclinical *in vivo* studies are useful for predicting CNS disposition and response in humans, but differences in transporter and metabolism expression, blood flow and intrinsic potency can influence these observations. In order to determine the best preclinical measure of CNS intrinsic potency, the relationship between either *in vitro*-to-preclinical or preclinical-to-clinical potency and receptor binding affinity was evaluated using a series of seven opioids (Chapter 3). The role of P-gp efflux in attenuating brain uptake and antinociception was assessed using a compound set consisting of four opioids (Chapters 4 and 5). Loperamide, a known P-gp substrate, was used as a probe to identify potential differences in drug disposition and response between the two P-gp-deficient mouse strains, CF-1 [*mdr1a*(-/-)] and FVB [*mdr1a*(-/-) and *mdr1b*(-/-)] (Chapter 4).

Preclinical models of antinociception often fail to predict opioid efficacy in humans. While humans are able to communicate degree of discomfort verbally, preclinical models of

nociception often rely on interpretation of behavioral responses to assess antinociception. The role of behavioral endpoint criteria in determining quantitative measures of antinociception with the hotplate latency assay was investigated and used in a novel approach to isolate central and peripheral nervous system contributions to overall observed antinociception (Chapter 6). Another common problem associated with the hotplate latency assay is the imposition of an artificial effect ceiling resulting from a 60 sec cut-off exposure time. Chapter 7 presents an alternative approach to modeling data where the value of E_{max} is truncated.

Counterclockwise hysteresis loops represent time-dependent dissociations between pharmacologic effect and drug concentration. Methods to collapse the hysteresis loop and recover relevant PD parameters such as EC_{50} and γ are well-established, but possess well-understood deficiencies. A key hypothesis underlying Part II of this dissertation project was that the size of the hysteresis loop may provide an additional, non-parametric parameter to describe the extent of temporal dissociation between concentration and effect. A quantitative method to assess area bounded by the hysteresis loop was developed and used to characterize the influence of fundamental pharmacokinetic-pharmacodynamic parameters on hysteresis area (Chapter 8). This approach was validated by quantifying the area of the opioid effect-concentration hysteresis loops and relating the area bounded by the hysteresis to model-derived parameters (Chapter 9). Finally, the results of this research effort are discussed in the context of the existing literature, and suggestions for a research agenda that will extend the present results are provided (Chapter 10).

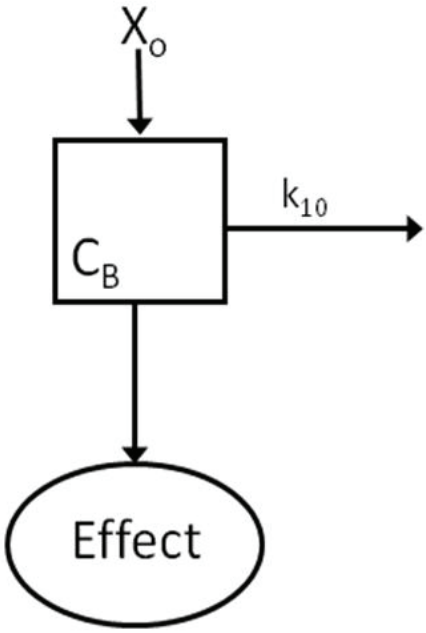

Figure 1.1. PK-PD model depicting a direct relationship between plasma drug concentration and pharmacologic response.

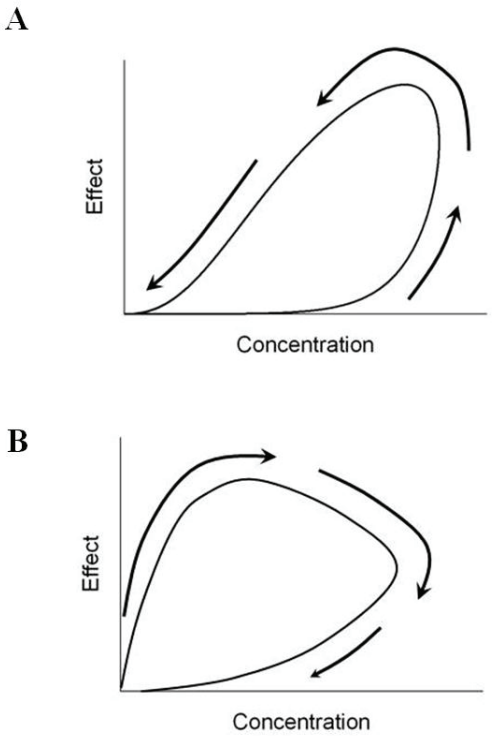

Figure 1.2. Depiction of clockwise (A) and counterclockwise (B) hysteresis loops. Arrows represent the progression of time.

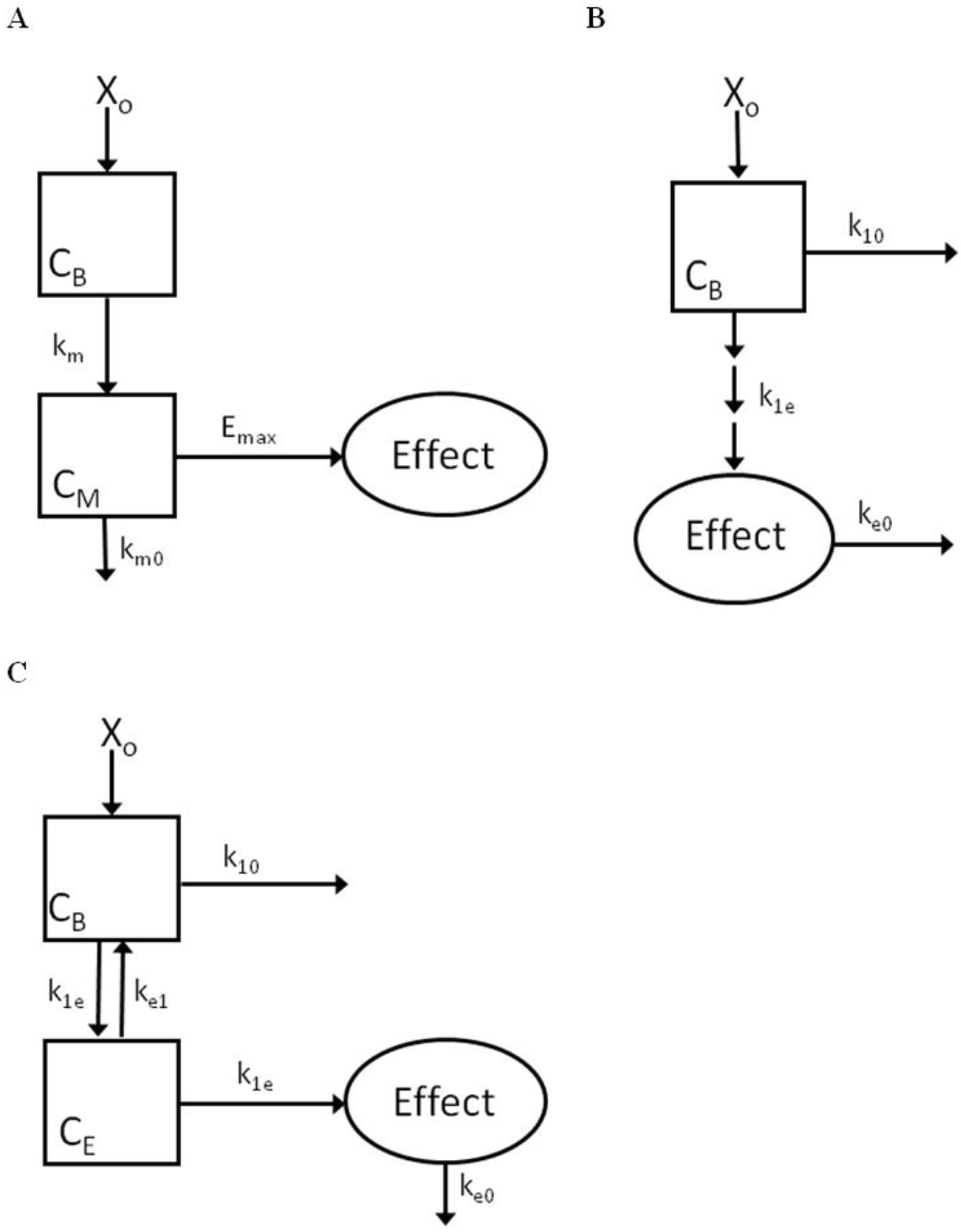

Figure 1.3. Time-dependent PK-PD models include (A) production of an active metabolite, (B) indirect pharmacologic response, and (C) drug distribution between plasma and effect compartment which mediates pharmacologic response.

REFERENCES

Bailey, C. P. and M. Connor (2005). "Opioids: cellular mechanisms of tolerance and physical dependence." Curr Opin Pharmacol **5**(1): 60-8.

Bellissant, E., V. Sebille, et al. (1998). "Methodological issues in pharmacokinetic-pharmacodynamic modelling." Clin Pharmacokinet **35**(2): 151-66.

Biegel, D., D. D. Spencer, et al. (1995). "Isolation and culture of human brain microvessel endothelial cells for the study of blood-brain barrier properties in vitro." Brain Res **692**(1-2): 183-9.

Chen, C. and G. M. Pollack (1998). "Altered disposition and antinociception of [D-penicillamine(2,5)] enkephalin in mdr1a-gene-deficient mice." J Pharmacol Exp Ther **287**(2): 545-52.

Cordon-Cardo, C., J. P. O'Brien, et al. (1989). "Multidrug-resistance gene (P-glycoprotein) is expressed by endothelial cells at blood-brain barrier sites." Proc Natl Acad Sci U S A **86**(2): 695-8.

Dagenais, C., C. L. Graff, et al. (2004). "Variable modulation of opioid brain uptake by P-glycoprotein in mice." Biochem Pharmacol **67**(2): 269-76.

Dagenais, C., C. Rousselle, et al. (2000). "Development of an in situ mouse brain perfusion model and its application to mdr1a P-glycoprotein-deficient mice." J Cereb Blood Flow Metab **20**(2): 381-6.

de Lange, E. C. (2004). "Potential role of ABC transporters as a detoxification system at the blood-CSF barrier." Adv Drug Deliv Rev **56**(12): 1793-809.

Engelhardt, B. (2003). "Development of the blood-brain barrier." Cell Tissue Res **314**(1): 119-29.

Feng, M. R. (2002). "Assessment of blood-brain barrier penetration: in silico, in vitro and in vivo." Curr Drug Metab **3**(6): 647-57.

Gastonguay, M. R. and S. L. Schwartz (1994). "The use of multiple doses and pharmacodynamic system analysis to distinguish between dispositional delays and time-variant pharmacodynamics." Pharm Res **11**(12): 1825-8.

Gibaldi, M. and G. Levy (1972). "Dose-dependent decline of pharmacologic effects of drugs with linear pharmacokinetic characteristics." J Pharm Sci **61**(4): 567-9.

Golden, P. L. and G. M. Pollack (2003). "Blood-brain barrier efflux transport." J Pharm Sci **92**(9): 1739-53.

Graff, C. L. and G. M. Pollack (2004). "Drug transport at the blood-brain barrier and the choroid plexus." Curr Drug Metab **5**(1): 95-108.

Hagenbuch, B. and P. J. Meier (2004). "Organic anion transporting polypeptides of the OATP/ SLC21 family: phylogenetic classification as OATP/ SLCO superfamily, new nomenclature and molecular/functional properties." Pflugers Arch **447**(5): 653-65.

Hawkins, R. A., R. L. O'Kane, et al. (2006). "Structure of the blood-brain barrier and its role in the transport of amino acids." J Nutr **136**(1 Suppl): 218S-26S.

Holford, N. H. and L. B. Sheiner (1982). "Kinetics of pharmacologic response." Pharmacol Ther **16**(2): 143-66.

Hsiao, P., T. Bui, et al. (2007). "In Vitro to In Vivo Prediction of P-glycoprotein Based Drug Interactions at the Human and Rodent Blood-Brain Barrier." Drug Metab Dispos.

Hsiao, P., L. Sasongko, et al. (2006). "Verapamil P-glycoprotein transport across the rat blood-brain barrier: cyclosporine, a concentration inhibition analysis, and comparison with human data." J Pharmacol Exp Ther **317**(2): 704-10.

Johnson, M. D. and B. D. Anderson (1999). "In vitro models of the blood-brain barrier to polar permeants: comparison of transmonolayer flux measurements and cell uptake kinetics using cultured cerebral capillary endothelial cells." J Pharm Sci **88**(6): 620-5.

Jones, R. T. (1990). Euphoria vs. cocaine plasma concentrations after nasal administration (20% solution). NIDA Research Monograph 99 (Research Findings on Smoking of Abused Substances). C. N. Chiang and R. L. Hawks**:** 30-41.

Kusuhara, H. and Y. Sugiyama (2001). "Efflux transport systems for drugs at the blood-brain barrier and blood-cerebrospinal fluid barrier (Part 1)." Drug Discov Today **6**(3): 150-156.

Lankas, G. R., M. E. Cartwright, et al. (1997). "P-glycoprotein deficiency in a subpopulation of CF-1 mice enhances avermectin-induced neurotoxicity." Toxicol Appl Pharmacol **143**(2): 357-65.

Le Bars, D., M. Gozariu, et al. (2001). "Animal Models of Nociception." Pharmacol Rev **53**(4): 597-652.

Letrent, S. P., J. W. Polli, et al. (1999). "P-glycoprotein-mediated transport of morphine in brain capillary endothelial cells." Biochem Pharmacol **58**(6): 951-7.

Levy, G. (1966). "Kinetics of pharmacologic effects." Clin Pharmacol Ther **7**(3): 362-72.

Lotsch, J. (2005). "Pharmacokinetic-pharmacodynamic modeling of opioids." J Pain Symptom Manage **29**(5 Suppl): S90-103.

Mahar Doan, K. M., J. E. Humphreys, et al. (2002). "Passive permeability and P-glycoprotein-mediated efflux differentiate central nervous system (CNS) and non-CNS marketed drugs." J Pharmacol Exp Ther **303**(3): 1029-37.

Matheny, C. J., M. W. Lamb, et al. (2001). "Pharmacokinetic and pharmacodynamic implications of P-glycoprotein modulation." Pharmacotherapy **21**(7): 778-96.

Meibohm, B. and H. Derendorf (1997). "Basic concepts of pharmacokinetic/pharmacodynamic (PK/PD) modelling." Int J Clin Pharmacol Ther **35**(10): 401-13.

Milne, R. J., G. D. Gamble, et al. (1989). "Behavioural tolerance to morphine analgesia is supraspinally mediated: a quantitative analysis of dose-response relationships." Brain Res **491**(2): 316-27.

Niemegeers, C. J., J. L. McGuire, et al. (1979). "Dissociation between opiate-like and antidiarrheal activities of antidiarrheal drugs." J Pharmacol Exp Ther **210**(3): 327-33.

Ohtsuki, S. and T. Terasaki (2007). "Contribution of carrier-mediated transport systems to the blood-brain barrier as a supporting and protecting interface for the brain; importance for CNS drug discovery and development." Pharm Res **24**(9): 1745-58.

Parsons, C. G. (2001). "NMDA receptors as targets for drug action in neuropathic pain." Eur J Pharmacol **429**(1-3): 71-8.

Schinkel, A. H., U. Mayer, et al. (1997). "Normal viability and altered pharmacokinetics in mice lacking mdr1-type (drug-transporting) P-glycoproteins." Proc Natl Acad Sci U S A **94**(8): 4028-33.

Schinkel, A. H., E. Wagenaar, et al. (1996). "P-glycoprotein in the blood-brain barrier of mice influences the brain penetration and pharmacological activity of many drugs." J Clin Invest **97**(11): 2517-24.

Sharma, R. C., S. Inoue, et al. (1992). "Peptide transport by the multidrug resistance pump." J Biol Chem **267**(9): 5731-4.

Thompson, S. J., K. Koszdin, et al. (2000). "Opiate-induced analgesia is increased and prolonged in mice lacking P-glycoprotein." Anesthesiology **92**(5): 1392-9.

Umbenhauer, D. R., G. R. Lankas, et al. (1997). "Identification of a P-glycoprotein-deficient subpopulation in the CF-1 mouse strain using a restriction fragment length polymorphism." Toxicol Appl Pharmacol **146**(1): 88-94.

Upton, R. N. and D. J. Doolette (2002). "A quantitative alternative to the hysteresis plot for measurement of drug transit time." J Pharmacol Toxicol Methods **47**(1): 45-51.

Verotta, D., S. L. Beal, et al. (1989). "Semiparametric approach to pharmacokinetic-pharmacodynamic data." Am J Physiol **256**(4 Pt 2): R1005-10.

Wolburg, H., J. Neuhaus, et al. (1994). "Modulation of tight junction structure in blood-brain barrier endothelial cells. Effects of tissue culture, second messengers and cocultured astrocytes." J Cell Sci **107 (Pt 5)**: 1347-57.

Yamagata, K., M. Tagami, et al. (1997). "Astrocyte-conditioned medium induces blood-brain barrier properties in endothelial cells." Clin Exp Pharmacol Physiol **24**(9-10): 710-3.

Yousif, S., C. Marie-Claire, et al. (2007). "Expression of drug transporters at the blood-brain barrier using an optimized isolated rat brain microvessel strategy." Brain Res **1134**(1): 1-11.

CHAPTER 2

OPIOID TOLERANCE DEVELOPMENT: A PHARMACOKINETIC-PHARMACODYNAMIC PERSPECTIVE

This chapter is an invited review that has been submitted for publication to *The AAPS Journal* and is presented in the style of that journal.

ABSTRACT

The opioids are commonly used to treat acute, severe, and chronic pain. Long-term opioid administration eventually reaches a dose ceiling that is attributable to the rapid onset of analgesic tolerance coupled with the slow development of tolerance to the untoward side effects of respiratory depression, nausea and decreased gastrointestinal motility. The need for effective-long term analgesia remains. In order to develop new therapeutics and novel strategies for current use of current analgesics, the processes that mediate tolerance must be understood. This review highlights potential pharmacokinetic (changes in metabolite production, metabolizing enzyme expression, and transporter function) and pharmacodynamic (receptor type, location and functionality; alterations in signaling pathways and cross-tolerance) aspects of opioid tolerance development, and presents several pharmacodynamic modeling strategies that have been used to characterize time-dependent attenuation of opioid analgesia.

INTRODUCTION

Opioid analgesics are commonly used to treat acute, severe, and chronic pain associated with surgical interventions or disease states such as cancer. Opioids produce a diverse spectrum of centrally- and peripherally-mediated responses, including respiratory depression, nausea, sedation, euphoria or dysphoria, decreased gastrointestinal motility, and itching (1). Long-term use of opioids can be problematic due to the rapid development of profound tolerance to the analgesic effects coupled with slow development of tolerance to many of the untoward effects of these agents. It is the inability to tolerate these undesirable side effects that eventually limits dose escalations and analgesic efficacy.

The World Health Organization (WHO) has recommended adoption of a three-step "analgesic ladder" to meet the therapeutic challenges presented by opioid tolerance. In this approach, analgesic therapy is initiated with a non-opioid analgesic co-administered, if necessary, with an adjuvant. As the underlying condition progresses and pain becomes more intractable, a weak opioid is substituted for the non-opioid. Eventually, a strong opioid is introduced as a final step (2). While these recommendations are designed to improve quality of life for chronic pain sufferers, the underlying problem of opioid tolerance persists, and the clear and compelling need for effective long-term analgesics, or for effective strategies for applying existing analgesics to control chronic pain, remains. This goal may be achieved through the specific design and development of new agents that are not subject to tolerance development, or through the use of adjunct treatments that can minimize or reverse tolerance. In either case, a comprehensive understanding of the mechanisms underlying tolerance, as well as the kinetics of tolerance development and regeneration of responsivity, is required.

The purpose of this paper is to review the pharmacokinetic and pharmacodynamic mechanisms involved in the development of opioid tolerance. Pharmacokinetic

considerations such as the production of metabolites, alterations in metabolic enzyme activity, and modulation of drug transporter expression or function are addressed. Pharmacodynamic processes such as receptor binding type and location, alterations in signal transduction, and cross-tolerance also are considered. Finally, approaches to comprehensive pharmacokinetic and pharmacodynamic (PK-PD) modeling of opioid antinociception and tolerance development are discussed.

ETIOLOGY OF TOLERANCE

Tolerance is defined as a decrease in pharmacologic response following repeated or prolonged drug administration. Tolerance can be separated into two main classifications: innate or acquired. Innate tolerance is a predisposition to exhibit drug sensitivity or insensitivity due to pharmacogenetic makeup. In most situations, innate tolerance is determined upon administration of the initial dose. In contrast, acquired tolerance is a consequence of repeated drug exposure, and can be subdivided into three general types based on the prevailing mechanism: pharmacokinetic, pharmacodynamic, or learned. Pharmacokinetic tolerance occurs when drug disposition or metabolism is altered as a function of time, often a consequence of the drug being an inducer or inhibitor of a specific metabolic enzyme or transporter system, resulting in a time-dependent decrease in presentation of the active moiety to the receptor biophase. Pharmacodynamic tolerance occurs when the intrinsic responsivity of the receptor system diminishes over time.

Acute tolerance is mediated predominantly by pharmacodynamic mechanisms, manifested as a decreased response following a single administration of the agent or during repeat-dosing but over a short time frame. This phenomenon is exemplified by nasally-administered cocaine. Initially, the relationship between cocaine-associated euphoria and

blood cocaine concentrations is proportionate. However, at later points in time, the euphoric response decreases despite continued, or even increased, circulating concentration (3). In contrast to acute tolerance, chronic tolerance can be mediated through either pharmacokinetic or pharmacodynamic mechanisms, with an end result of a long-term decrease in drug response in the face of constant systemic exposure. In cases in which chronic tolerance develops, cross-tolerance within the pharmacologic class also may occur. Replacing the initial drug with a comparable agent will result in a lower pharmacologic response compared to that experienced by a drug-naive individual. Cross-tolerance is the principle underlying methadone substitution in the treatment of heroin addicts. Although methadone produces opioid effects in heroin-addicted subjects, euphoria and side effects are minimized by the tolerance produced by long-term heroin exposure. The significance of pharmacokinetic and pharmacodynamic mechanisms in relation to tolerance development will be examined in depth in subsequent sections of this review.

The final class of acquired tolerance is attributed to learning, either behavioral or conditioned. Behavioral tolerance occurs when an individual learns to function despite repeat exposure to a drug. Chronic alcohol abusers, for example, may not exhibit an outward appearance of motor impairment as a consequence of intoxication because of learned motor function adaptations and awareness of their impairment. Conditioned tolerance follows "Pavlovian" principles in which situational cues are associated with drug administration. Removal of these environmental cues will result in an enhancement in pharmacologic effect. For example, when morphine-tolerant rats are placed in a novel environment and challenged with morphine, antinociceptive tolerance is reduced (4). Analysis of behavioral tolerance has been reviewed in detail elsewhere (5).

MORPHINE AND RELATED AGONISTS

The medicinal value of opium has been acknowledged for centuries. Despite possessing an extensive side-effect profile, morphine, isolated from opium more than 200 years ago, remains the gold standard for treating pain. Structurally similar, semisynthetic morphine-like derivatives as well as structurally distinct opioids have been synthesized in a search for compounds that improve analgesia and minimize side effects. The common, clinically-used opioid analgesics are semisynthetic morphine derivatives, as well as synthetic phenylpiperidine, anilidopiperidine, and diphenylpropylamine derivatives (Table 2.1). Due to the structural similarities between these drugs and morphine, they primarily bind to the same receptor subtypes (μ-opioid receptors), produce analgesia, and exhibit similar side effect profiles. However, divergence in congener pharmacokinetic-pharmacodynamic parameter values allows the clinician to select a drug based on specific patient needs (1). For example, an ideal drug for a short surgical procedure would have rapid onset and offset of effect, such as the piperidine derivative alfentanil. Overall, opioid selection depends on a number of factors, including the nature of pain, predisposition to opioid responsivity, and previous opioid exposure.

PHARMACOKINETIC MEDIATORS OF OPIOID TOLERANCE

Receptor occupancy theory holds that pharmacologic response will be proportional to the fraction of the target receptor population that is occupied at a particular drug concentration (6). As the drug concentration in the vicinity of the receptor increases, the likelihood of drug binding to the receptor and producing an effect also increases. Gibaldi and Levy (7) applied this principle in describing the sigmoidal relationship between tubocurarine-mediated paralysis and dose or blood concentration. For this simplest of pharmacodynamic

systems, drug concentrations in the receptor biophase must be in immediate equilibrium with concentrations in blood, and response must be instantaneous, reversible and time-independent. However, the relationship between the magnitude or time course of drug response and the kinetics of drug disposition generally is more complex, evidenced by time-dependent dissociations between pharmacologic response and systemic pharmacokinetics. A variety of factors, including slow equilibration of drug between the target receptor and blood or slowly-elaborated pharmacologic responses post-receptor binding, can cause such kinetic-dynamic dissociation. However, a particularly complicated underlying factor is the development of tolerance.

Metabolic and Distributional Mediators of Tolerance

One source of the extensive variability in drug concentrations, and consequently, response, within a population can be attributed to differences in drug absorption, distribution and metabolism. The opioids undergo significant Phase I and II biotransformation, and polymorphisms in the cytochrome P450s (CYPs) and uridine-5'-diphosphate-glucuronosyltranserases (UGTs) will influence individual opioid disposition and response. For example, depending on the allelic combinations of the highly polymorphic CYP2D6, patients are characterized as one of four phenotypes: poor, intermediate, extensive and ultrarapid metabolizers (8). Subjects who exhibit the poor-metabolizer phenotype will not convert codeine to morphine efficiently, and therefore will exhibit a reduced effect compared to patients who can form morphine (9). In addition to the important role these enzymes play in mediating opioid concentrations and responses, it has been suggested that biotransformation processes contribute to morphine tolerance secondary to induced enzymatic expression (10, 11). However, there is a lack of evidence to support this

observation, as long-term administration of methadone or morphine does not alter the parent drug to metabolite concentration ratios, indicating that autoinduction is unlikely (12, 13). Ultimately, metabolite formation could influence tolerance development through pharmacodynamic mechanisms, but there is a lack of evidence supporting time-dependent changes in the formation clearance of opioid metabolites.

In addition to metabolism, drug transport can play a significant role in mediating drug exposure at the target site, and therefore the time course and magnitude of pharmacologic response. Many of the common opioids are substrates of the efflux transporter P-glycoprotein (P-gp), an ATP-dependant, 170-kDa transmembrane protein encoded by the *MDR1* (human) and *mdr1a*/*mdr1b* (rodent) genes (14). P-gp is expressed in a number of tissues in which it plays a protective role as a barrier transporter, limiting absorption from the intestines or penetration into organs such as testes or brain, as well as an excretory transport system in the kidney and liver (15). P-gp also functions to modulate the secretion of centrally synthesized opioid peptides and neurotransmitters from the brain to the systemic circulation (16).

Studies with P-gp-deficient mice have revealed that P-gp-mediated efflux attenuates the brain-to-serum ratio ($K_{p,brain}$) and antinociceptive effect of fentanyl, methadone and loperamide by ~2-, 7-, and 45-fold, respectively (17). Considering the extent to which P-gp mediates transport of some opioids, upregulation of this barrier transporter could further limit CNS penetration and antinociceptive effects of some opioids. Indeed, exposing transgenic mice expressing human pregnane X receptor (hPXR) to rifampin, an acute P-gp inhibitor and long-term P-gp inducer, upregulated expression of P-gp in brain capillary endothelium and attenuated the antinociceptive effect of the P-gp substrate methadone by 70% (18). Based on

the results of this study, if an opioid is both a substrate and inducer of P-gp, chronic treatment could result in higher blood brain barrier (BBB) P-gp expression, with a consequent decrease in CNS penetration and antinociception (i.e., pharmacokinetic tolerance). Although autoinduction of BBB P-gp remains a possible mechanism underlying opioid tolerance, increases in P-gp expression following chronic treatment with morphine and oxycodone appear to be modest (2- and 1.3-fold, respectively; (19, 20). This minor increase in expression (≤ 2-fold) coupled with a negligible alteration in function (a 1.4-fold reduction in paclitaxel brain distribution) suggests that opioid-mediated P-gp upregulation, at least in experimental animals, does not influence opioid antinociceptive tolerance to an extent that can be distinguished from population PK-PD variability (19).

Metabolite Contributions to Opioid Response and Tolerance

Tolerance also may result from the production of metabolites that accumulate in the systemic circulation over time, penetrate the site of action, and interfere with pharmacologic response whether by competing with the parent compound for receptor binding (e.g., antagonists or partial agonists) or by down-regulating the responsivity of the receptor system or downstream events. The contribution of derived metabolites to morphine pharmacodynamics has received significant attention. In humans, morphine is metabolized in the liver by UGT2B7 to form morphine-3-glucuronide (M3G) and morphine-6-glucuronide (M6G). Although morphine is metabolized preferentially to M3G (~5:1 M3G to M6G formation ratio), this metabolite does not contribute to antinociceptive response. In contrast, M6G is considered to be an unusual Phase II metabolite in that it is biologically active, and in fact appears to be somewhat more potent (2- to 4-fold) than morphine (21).

Some studies have suggested that, rather than contributing to antinociception, M3G attenuates the response to morphine. In this scenario, time-dependent M3G accumulation could be responsible for the appearance of morphine tolerance. For example, Smith and Smith (22) observed an inverse relationship between morphine-associated antinociception and M3G concentrations. However, careful examination of the influence of M3G pretreatment on morphine antinociception in rats revealed that acute M3G exposure, at concentrations similar to those produced by pharmacologically-relevant doses of morphine, does not attenuate antinociception to a significant extent (23, 24). In contrast, M3G concentrations that are far in excess of those produced by pharmacologic doses of the parent drug can evoke neuroexcitatory behavioral responses that oppose the analgesic effects mediated by morphine binding to opioid receptors. Such neuroexcitation would account for the observed M3G-associated decrease in morphine-related antinociception (25). These excitatory responses are independent of the opioid receptor system, as evidenced by the absence of naloxone reversibility, and may be mediated through interactions at the *N*-methyl-D-aspartate (NMDA) and the γ-amino-butryic acid ($GABA_A$) receptors (25, 26). Overall, it appears that M3G may influence antinociception and tolerance, although through a mechanism other than μ-opioid receptor (MOR)-mediated interactions, and it is unlikely that accumulation of this metabolite formed from morphine contributes substantially to the development of functional morphine tolerance.

PHARMACODYNAMIC MEDIATORS OF OPIOID TOLERANCE

While inherent inter-individual pharmacokinetic variability can influence analgesia within a population, time-dependent changes in systemic disposition appear to play a minimal role in the development of opioid tolerance. In contrast, a number of

pharmacodynamic processes have been characterized as potential mediators of opioid tolerance. These adaptations include, but are not exclusively limited to, genetic predisposition, receptor subtypes, cross-tolerance, receptor affinity, alterations in secondary mediators such as the nitric oxide synthase pathway and transcription alterations, and receptor binding in the central versus the peripheral nervous system.

Mu Opioid Receptor-Mediated Changes

The biologic effects that are characteristic of opioids are a consequence of agonist binding to opioid receptors with subsequent alterations in signal transduction and ion conductance that reduce neuronal pain transmission. The three major mammalian types of opioid receptors (OR) are designated μ, δ, and κ (27-29). Pharmacologic studies with opioid receptor ligands and receptor knockout mice identified the μ-opioid receptor (MOR) as the primary mediator of both the therapeutic and side effects associated with opioids such as morphine (30-32). The role of the δ- and κ-opioid receptors in mediating analgesia and tolerance will be discussed more thoroughly in subsequent sections of this review.

The MOR is a seven-transmembrane protein belonging to the G-protein coupled receptor (GPCR) superfamily. Binding of an agonist to the MOR results in the replacement of the α-subunit GDP with GTP and the subsequent dissociation of the α- and βγ-subunits from the Gαβγ heterotrimer (33, 34). These mechanisms result in acute inhibition of neuronal transmission due to alterations in the conductance of ion channels (Na^+, K^+, Ca^{2+}), the stimulation of protein kinase A (PKA), and the transient inhibition of the adenylyl cyclase (AC) pathway (35). Chronic opioid use enhances the cAMP pathway via the superactivation of AC, alterations in ion channel conductance, an increase in neurotransmitter release, and altered gene expression through changes in cAMP-responsive

element binding protein (CREB) phosphorylation and expression (36, 37). Overall, antinociception is mediated through a complex sequence of downstream effectors, which can differ following acute versus chronic opioid exposure.

In addition to alterations in signaling, opioid tolerance is associated with decreases in opioid receptor sensitivity and expression in the plasma membrane. Following receptor binding of some, but not all (e.g., morphine), opioids, the MOR is phosphorylated by G-protein receptor kinase (GRKs), with opioid efficacy related to the extent of phosphorylation (38, 39). Receptor phosphorylation is the first step in the desensitization and internalization of the MOR, and precedes association of β-arrestin to the receptor complex, which uncouples the receptor from G proteins. This uncoupling event desensitizes the receptor and attenuates the second messenger signal cascade, reducing agonist efficacy (40). The role of β-arrestin in receptor desensitization was characterized in β-arrestin KO mice that exhibited enhanced and prolonged analgesia with a lack of antinociceptive tolerance (41, 42). β-arrestin also can modulate tolerance by recruiting adaptor proteins that link the receptor complex to clathrin, resulting in endocytosis in clathrin-coated pits. Following internalization, the receptor is retained and recycled to the plasma membrane as a resensitized receptor or, upon recognition of an interaction with the GPCR-associated sorting protein (GASP), the receptor will be sent to the lysosome for degradation (33, 43). Agonist binding therefore results in diverse cellular adaptations that mediate antinociception and onset of tolerance.

The mechanisms underlying morphine tolerance appear to be different from those of other opioid agonists. Despite significant and prolonged efforts directed towards understanding morphine tolerance, the specific pathway has remained obscure. In contrast to most opioids, morphine-receptor binding does not initiate GRK-mediated MOR

phosphorylation that results in receptor internalization (40). This observation is further supported by the absence of increased membrane internalization protein expression (e.g. β-arrestin and GRK) that accompanies most opioids (44). Even in the absence of receptor internalization, the interaction between the morphine-bound receptor and β-arrestin persists, evidenced by a reduction in tolerance in β-arrestin KO mice, suggesting that morphine induces tolerance by sustaining signaling pathways and cellular adaptations such as AC superactivation (41, 45). An alternative explanation for the reduction in morphine tolerance observed in β-arrestin KO mice is that, although it is not an internalizing opioid, morphine binds to MORs that exist as heterodimers, with the second OR subtype interacting with β-arrestin and the subsequent internalization of the morphine-heterodimer complex (46, 47). However, the validity of this hypothesis appears unlikely, as the results were not reproducible in later experiments and depended on the co-administration of morphine with an internalizing opioid for dimer endocytosis, and chronic morphine exposure does not change MOR expression (46, 48, 49).

Another contributor to morphine tolerance is the slow recovery of resensitized MORs because morphine desensitized receptors do not participate in the traditional pathway of internalization, recycling and reinsertion into the plasma membrane (50). Ultimately, the specific molecular mechanisms governing morphine tolerance have not been fully elucidated, and the possibility that mechanisms of morphine tolerance vary depending on the specific brain and spinal cord region requires further investigation (51).

MOR Receptor Polymorphisms

Analgesic variability within a population can, in part, be attributed to opioid pharmacogenetics. The human MOR has over 100 identified single nucleotide

polymorphisms (SNPs), some of which are thought to influence opioid responsiveness, abuse potential, and tolerance (52, 53). Of these SNPs, the most well-characterized is the A118G nucleotide substitution, which changes the amino-acid sequence at position 40 from asparginine to aspartic acid, eliminating an extracellular N-linked glycosylation site (54, 55). Clinically, this variant reduces the analgesic effects of alfentanil and M6G (56, 57). These alterations are not likely a consequence of altered binding affinity, as *in vitro* studies demonstrated that the N40D substitution did not affect binding of the exogenous opioids morphine, fentanyl, or methadone, nor that of the endogenous opioids Met- and Leu-enkephalin, endomorphin-1 and-2 and D-Ala^2, *N*-methyl-Phe^4, Glycol^5]enkephalin (DAMGO) (54). Although this study demonstrated a 3-fold increase in binding affinity of the endogenous opioid peptide β-endorphine, subsequent studies did not detect any difference in β-endorphine binding, or receptor endocytosis, desensitization or resensitization in the N40D substitution (54, 58, 59). Additional work on human MOR polymorphisms characterized amino acid substitutions of N15D, R265H, and S268P. The latter substitution, located in the intracellular domain, exhibited a significant loss of receptor signaling (58). The human MOR intracellular loop polymorphisms reduced the extent of MOR-calcium calmodulin CaM interactions (R265H and S268P) and the R260H and R265H variants exhibited a reduction in basal MOR signaling (60).

Despite these detailed studies, the relationship between MOR polymorphisms and binding affinity, signaling pathways and ion channel conductance is not entirely clear. These alterations may, in part, mediate differential development of opioid tolerance within a population. For example, individuals expressing the N40D variant exhibit decreased analgesia, and may require larger opioid doses to achieve equipotent pain relief. It is

conceivable that this dose differential could influence the development of tolerance in these subjects compared to normal MOR expressers. Research focused on MOR polymorphisms is continuing, and should shed light on the specific physiologic implications of these variants, including opioid responsivity and tolerance development.

Multiple Opioid Receptors

While less is known about the specific roles of the two remaining ORs, δ and κ, these proteins are expressed throughout the body and mediate antinociception, although to a lesser extent than the MOR (61-64). The κ-opioid receptor (KOR) exhibits tolerance following prolonged opioid exposure, a consequence of GRK-mediated phosphorylation of the KOR that initiates receptor internalization (65, 66). While dephosphorylation is the typical mechanism of recovering receptor sensitivity, the KOR appears to require regeneration and reassembly of the receptor complex for restoration of antinociception (67). The net effect of these processes is a reduction in KOR expression that results in a decreased pharmacologic response following long-term opioid exposure. Similar to the KOR, the δ-opioid receptor (DOR) manifests tolerance to specific DOR-agonists via receptor phosphorylation and internalization (68, 69). Despite receiving less attention than the MOR, opioid binding to the DOR and KOR also can result in antinociception and tolerance.

Cross-tolerance

Long-term exposure to one drug often results in the development of tolerance to the effects of other structurally similar drugs in the same pharmacologic class. This phenomenon is termed cross-tolerance. Although opioids frequently exhibit cross-tolerance, it is rarely complete, as evidenced by the utility of opioid rotation from morphine to hydromorphone or oxycodone, particularly in treatment of cancer pain (70, 71). However, complete cross

tolerance can develop, as evidenced by the lack of analgesia elicited by high-dose morphine in patients receiving methadone maintenance therapy (72). The more common scenario of incomplete cross tolerance has been attributed to multiple pharmacologic mechanisms. This preservation of effect may be a function of the inverse relationship between intrinsic opioid efficacy and tolerance, as well as that in situations of tolerance, replacing a low efficacy opioid such as morphine with fentanyl, a high-efficacy opioid with a high receptor reserve, will enhance analgesia (73, 74). Furthermore, multiplicity in MOR subtypes may play an important role in determining the magnitude of cross-tolerance. For example, when one opioid is substituted for another, the secondary opioid may bind to a different receptor subtype than the initial compound, thereby limiting the apparent extent of cross-tolerance (75). Alternatively, incomplete cross tolerance may be attributed to the ability of the opioid receptors to homo- and heterodimerize. For example, substituting an initial opioid with an agonist that binds to a different dimer combination can result in the recovery of analgesia because of incomplete tolerance to the new opioid-receptor combination. (47, 76). Further investigation of the interplay between opioid receptors likely will reveal novel mechanisms that mediate antinociception and contribute to opioid tolerance. Clinically, opioid cross-tolerance presents a challenge when a patient switches to a new opioid regimen. Despite this possibility, the lack of complete tolerance generally results in a reduction in pain and fewer side effects compared to the initial, tolerant regimen.

NMDA Receptor Contributions to Opioid Tolerance

In addition to the direct actions of opioids, neurotransmitters such as dopamine, serotonin and glutamine have been implicated as mediators of opioid tolerance and antinociception (77-79). Of particular interest is the NMDA-sensitive glutamate receptor.

The intertwined relationship between the MOR and NMDA receptor systems is in part attributed to co-localization in central tissues (80, 81). Mg^{2+} is bound to the receptor channel of the NMDA receptor under normal physiologic conditions, and serves to block the entrance of ions such as Ca^{2+} (Fig. 2.1). Small changes in synaptic cleft concentrations of glutamate and inorganic ions can temporarily displace Mg^{2+} and allow an influx of Ca^{2+}, which will bind to and activate the neuronal nitric oxide synthase (nNOS), CaM and PSD-95 complex, which converts L-arginine (L-arg) to L-citrulline (L-Cit) and nitric oxide (82, 83). Finally, NO mediates the conversion of GTP to cGMP, a mediator of tolerance, via soluble guanylyl cyclase (sGC). Chronic opioid exposure enhances NMDA receptor function by increasing intracellular Ca^{2+}, NO and cGMP levels, which contribute to the development of opioid tolerance. The use of NMDA receptor antagonists or inhibitors of NOS production from L-arginine to enhance antinociception and delay the onset of tolerance has proven effective (82). Of these approaches, the use of NMDA receptor antagonists has shown preclinical and clinical potential in minimizing opioid tolerance. The potential role of NOS in determining the time course and magnitude of opioid tolerance is considered in detail in the final section of this review.

Initially viewed as a "miracle" drug class, the clinical use of NMDA receptor antagonists has yet to be fully realized. NMDA receptor antagonists are particularly promising drug targets due to a number of modulatory sites with different structural subunit combinations, most commonly the NR1 subunit combined with NR2A-D or NR3A-B subunits (84, 85). These modulatory sites result in four general classes of NMDA receptor antagonists: the uncompetitive receptor channel blockers (MK-801, ketamine, PCP, memantine), the competitive glutamate antagonists (LY235959, D-CPPene), the glycine site

antagonists [(+)(R)-HA-966], and the polyamine site antagonists (86). Preclinical and clinical models have been used to demonstrate that NMDA receptor antagonists can attenuate tolerance development and enhance antinociception, the latter effect allowing decreases in dose which may delay tolerance onset (87).

The majority of studies characterized the NMDA receptor antagonists as enhancing or having no effect on analgesia, whereas a minority demonstrated attenuation of acute morphine analgesia (88-93). One challenge in this area is the absence of consistent results identifying which opioids exhibit NMDA receptor antagonist-enhanced antinociception. For example, Redwine and Trujillo (94) found that morphine analgesia was enhanced only when co-administered with LY235959 (3 mg/kg); fentanyl analgesia was enhanced in the presence of LY235959 (3 mg/kg), dextromethorphan (30 mg/kg) and (+)(R)-HA-966 (30 mg/kg); and no difference was observed for morphine or fentanyl when co-administered with MK-801 (0.1 and 0.3 mg/kg), memantine (3 and 10 mg/kg), or ifendopril (1 and 3 mg/kg). Additional work clearly is needed to identify the specific interactions between each opioid and NMDA receptor antagonist. For example, NMDA receptor antagonist pharmacokinetics are poorly characterized. However, it is clear that they are capable of penetrating central tissues, evidenced by the appearance of centrally-mediated side effects such as hallucinations, memory impairment, blood pressure elevation, catatonia and anesthesia (95). NMDA receptor antagonists of greater selectivity and lower affinity were developed in response to these undesirable central effects, and promising alternatives may include the use of low affinity channel blockers (e.g., memantine), NR2B subunit selective drugs (ifendopril), or the partial glycine site antagonists (96). Based on these varied observations, further characterization of the underlying pharmacologic mechanisms and

pharmacokinetic/pharmacodynamic relationships between the opioids and NRAs remains to be elucidated.

The Role of Peripheral Opioid and NMDA Receptors in Mediating Antinociception

While NMDA receptor antagonists may represent a feasible approach to delay the onset and attenuate the extent of tolerance, these compounds manifest intolerable central side effects that limit use. One alternative strategy that may prove effective in treating pain is targeting non-centrally located NMDA receptors and/or ORs to achieve antinociception while minimizing centrally-mediated side effects and, potentially, the development of tolerance. The feasibility of this approach is, in part, supported by the broad peripheral distribution of these receptors. For example, MORs are present in a number of peripheral tissues, including the small and large intestines, kidney, lung, spleen, testis, ovaries and uterus (97). While these sites are important in mediating a number of physiologic processes, molecular and functional studies suggest that MORs and NMDA receptors localized on unmyelinated, cutaneous sensory axons contribute to antinociception (98). Moreover, the density of ORs and NMDA receptors on peripheral sensory axons increases in conditions of inflammation, suggesting a role in mediating pain perception (99, 100). Overall, the physiologic distribution of the ORs and NMDA receptors suggests a role in mediating peripheral antinociception.

The functionality of peripheral ORs was demonstrated when a systemically inactive, subcutaneous dose of morphine into the rat tail exhibited naloxone-reversible antinociception (101, 102). Additional studies identified the ability of locally-administered morphine and loperamide to mediate antinociception in a radiant heat tail-flick assay and in an inflammatory model, respectively (103). Furthermore, repeated immersion of the tail in

opioid-containing DMSO solutions resulted in local antinociception and tolerance development, the latter being reversible following topical or systemic administration of the NMDA receptor antagonist MK-801 (104-106). These results suggest that peripherally-restricted opioids contribute to antinociception and tolerance, which may be minimized by co-administration with non-centrally penetrating NMDA receptor antagonists.

PHARMACOKINETIC-PHARMACODYNAMIC MODELS OF OPIOID TOLERANCE

"Black-Box" Approach

Although it is clear that complex cellular, mechanistic and homeostatic alterations contribute to tolerance development, PK-PD models, including those that incorporate tolerance as a time-dependent loss of intrinsic activity, often utilize a black-box approach that accounts for changes in the response-concentration relationship over time rather than incorporating specific biologic mechanisms that serve to drive the development of tolerance. Such empirical models tend to exhibit a broad applicability, are useful in characterizing and summarizing the temporal aspects of loss of drug response, and can be used to describe numerous tolerance scenarios (107). One such model developed by Porchet et al. (108) characterized acute tolerance to the cardioaccelerating effects of nicotine by integrating a hypothetical noncompetitive antagonist formed by a first-order process, with nicotine concentrations serving as the driving force for formation. Furthermore, optimal recovery from acute nicotine tolerance corresponded with longer intervals between nicotine exposure (108).

The generic approach to modeling tolerance development, which included consideration of the relationship between the development of opioid tolerance and administration strategy, was utilized by Ouellet and Pollack (109) for two morphine

treatment regimens: multiple increasing i.v. bolus doses over a 12-hr period (24 mg/kg total exposure in 7 doses) or one i.v. bolus dose per day (beginning with 1.85 mg/kg on day 1, and increasing to 6 mg/kg maximum) for 13 days. The hypothesis underlying this experimental design was that tolerance development would be attenuated in the once-daily administration group if the kinetics of tolerance offset were rapid (i.e., if significant return to basal responsivity occurred within 24 hr after morphine exposure). Morphine disposition did not differ significantly between the 12-hr and 13-day treatment groups, indicating that changes in systemic morphine disposition could not account for tolerance development. Concentration-normalized peak analgesic effects remained relatively constant over 12 hr, while the 13-day treatment group exhibited a decrease in normalized peak effect from day 1 to 8. In addition, the extent of analgesic tolerance development was similar whether morphine was administered as a multiple i.v. bolus or constant infusion. Taken together, these observations suggested that morphine tolerance development was dependent on systemic drug concentrations (i.e., the extent of exposure), but was independent of the kinetics of morphine administration (i.e., the rate of morphine exposure or the presence of relatively brief "drug holidays" in the administration regimen).

The apparent independence of the rate or extent of tolerance development and the kinetics of drug administration was an unexpected observation, as conventional wisdom suggested that continuous presentation of opioids such as morphine would result in the production of profound tolerance. An explanation for this observation was formulated through comprehensive PK-PD modeling of morphine concentration-time and antinociceptive effect-time data obtained from rats during and following continuous morphine infusion (109). In this experiment, morphine was infused for 12 hr at several

different rates to achieve one of five preselected steady-state concentrations. Blood morphine concentrations and antinociceptive response (tail flick) were determined at timed intervals during infusion. Separate groups of rats were studied for 18 days after termination of a 12-hr morphine infusion, with pharmacologic response compared to that produced 15 min after a single intravenous bolus dose (presumably representing a "no-tolerance" state. The data were fit with a tolerance model similar to that displayed schematically in Figure 2.2. This model assumed accumulation of a hypothetical "inhibitor" that was formed from morphine by a first-order process; several different "inhibitor" scenarios (reverse agonist, competitive antagonist, non-competitive antagonist, or partial agonist) were evaluated, with the net effect (E) produced under each scenario shown in Equations 2.1-4, respectively:

$$E = \frac{E_{\max} \bullet C_e^{\gamma}}{EC_{50}^{\gamma} + C_e^{\gamma}} - \frac{I_{\max} \bullet C_i^{\gamma}}{IC_{50}^{\gamma} + C_i^{\gamma}} \qquad \text{(Equation 2.1)}$$

$$E = \frac{E_{\max} \bullet C_e^{\gamma}}{C_e^{\gamma} + \left(EC_{50}^{\gamma} / IC_{50}^{\gamma}\right) \bullet C_i^{\gamma} + EC_{50}^{\gamma}} \qquad \text{(Equation 2.2)}$$

$$E = \frac{E_{\max} \bullet IC_{50}^{\gamma} \bullet C_e^{\gamma}}{EC_{50}^{\gamma} \bullet IC_{50}^{\gamma} + C_e^{\gamma} \bullet IC_{50}^{\gamma} + C_i^{\gamma} \bullet EC_{50}^{\gamma} + C_e^{\gamma} \bullet C} \qquad \text{(Equation 2.3)}$$

$$E = \frac{E_{\max} \bullet IC_{50}^{\gamma} \bullet C_e^{\gamma} + I_{\max} \bullet C_i^{\gamma} \bullet EC_{50}^{\gamma}}{EC_{50}^{\gamma} \bullet IC_{50}^{\gamma} + C_e^{\gamma} \bullet IC_{50}^{\gamma} + C_i^{\gamma} \bullet EC_{50}^{\gamma}} \qquad \text{(Equation 2.4)}$$

The results of this study indicated that morphine tolerance development was dependent on both morphine concentration and the duration of morphine exposure. As morphine concentrations increased, the net change in antinociceptive response (peak effect

minus effect at 12 hr) increased; regardless of the steady-state concentration produced, antinociceptive responses at 12 hr were similar, resulting in a truncated effect versus concentration relationship at 12 hr (Figure 2.3). The PK-PD model was capable of describing the time course of loss (Figure 2.4) and return (Figure 2.5) of pharmacologic effect. When the loss-of-response data were fit alone, it was not possible to distinguish between the four alternative "inhibitor" scenarios. However, the return-of-response data suggested that the kinetics of morphine tolerance behaved as if driven by a partial agonist with a very low intrinsic activity (<10% of the maximum response to morphine) and a high affinity (IC_{50} ~ 14 ng/ml). In addition, the combined data set allowed estimation of the rate constant associated with tolerance offset (~0.12 day^{-1}), which corresponded to a half-life of 5.7 days.

This modeling effort revealed the explanation, if not the underlying mechanism, for the apparent independence between the kinetics of tolerance development and the kinetics of morphine administration, a situation starkly different from that for nicotine. In fully-tolerant animals, a "drug holiday" of nearly six days would be required in order to regenerate 50% of the intrinsic responsivity to morphine lost during the development of tolerance. In contrast, the half-life associated with return of responsivity to nicotine (35 min) is consistent with nearly complete recovery and resensitization when doses are separated by 3 or more hours (108, 109).

As these examples demonstrate, "black-box" modeling of tolerance can provide useful information regarding system dynamics, are capable of describing the loss or return of pharmacologic effect over time, and can predict responsiveness under differing administration scenarios. By their very nature these models have a limited ability to reflect

the specific mechanisms underlying tolerance development in a given system. However, when used appropriately, such modeling efforts can direct further mechanistic experimentation. Subsequent elaboration of mechanistic detail then can be used to inform the PK-PD model of tolerance, which in turn provides additional understanding of system dynamics and an increased capacity to predict system response under differing conditions. An example of this iterative approach to modeling opioid tolerance is provided in the next section of this review.

Mechanistic Approach

When the specific physiologic alterations that lead to time-dependent loss of pharmacologic effect are known, they can be incorporated into mechanistic PK-PD models. As discussed earlier in this review, chronic opioid exposure enhances NMDA receptor function thereby permitting greater Ca^{2+} influx; Ca^{2+} will attach to and activate the NOS complex that mediates the conversion of L-Arg to NO. One method of limiting NO production is to coadminister an opioid with an NMDA antagonist or a NOS inhibitor (85, 87, 110). Furthermore, coadministering exogenous L-Arg with an opioid increased NO levels and attenuated antinociception (84, 111, 112). These observations suggested an important, and perhaps causative, role of NO in the induction of opioid tolerance.

The significance of NO in mediating the time dependent loss of morphine-associated antinociception was elaborated in a series of experiments by Heinzen and coworkers. Following long-term morphine administration, the extent of antinociceptive tolerance that developed in mice deficient in neuronal nitric oxide synthase (nNOS) was significantly less than that in wild-type mice (30% versus 80% loss of effect, respectively) (113). In rats, infusion of the NO precursor L-arg increased the concentration of NO in brain tissue and

decreased the intrinsic antinociceptive activity of morphine (114-116). An integrated PK-PD model was developed (Figure 2.6) that was capable of describing the time course of changes in brain NO in response to L-arg infusion (Figure 2.7). This model required inclusion of circadian control of NO production to accurately describe the observed data. Furthermore, morphine administration increased the brain concentration of NO, and the temporal pattern of apparent nNOS stimulation by morphine was consistent with the time course of loss of morphine-associated antinociception due to tolerance development (116). Subsequent experiments at the receptor level confirmed that NO alters mu-opioid receptor function (117). Taken together, these observations demonstrate that elevated brain content of NO is both necessary and sufficient to induce functional antinociceptive tolerance to morphine in rats and mice.

The relationship between morphine concentrations in blood and brain tissue (measured by microdialysis sampling), NO production in brain (measured with an indwelling amperometric probe), and the development of antinociceptive tolerance (measured by electrical stimulation vocalization) was characterized with a comprehensive PK-PD model (116). In this model (Figure 2.8), a two-compartment PK model was fit to morphine blood and brain concentrations during and after an 8 hour i.v. morphine infusion in rats. A multi-component PD submodel was required to incorporate morphine-associated changes in the production of neuronal NO, morphine associated agonism of the mu-opioid receptor (expressed as an increase in the threshold for electrical stimulation vocalization), and NO-associated decreases in the threshold for electrical stimulation vocalization. This relatively complex PK-PD model was similar in structure to preceding "black-box" approaches, but utilized an experimentally-determined variable (brain concentration of NO), rather than a

hypothetical construct, as the driving force for tolerance development. The model was able to provide a good description of the time course of morphine-associated antinociception during and following infusion in relation to changes in the blood and brain tissue concentrations of morphine (Figure 2.9). Despite the complexity of the model, the data obtained were capable of supporting parameter estimates with a reasonable degree of precision (Table 2.2).

Two aspects of the comparison between the "black box" and "mechanistic" modeling approaches for morphine tolerance are noteworthy. First, although both models are capable of describing the time course of changes in pharmacologic response, there are fundamental differences in the interpretation of those models. With the "black box" approach, the hypothetical "inhibitor" of response appeared to be a partial agonist of low intrinsic activity and high affinity; in the "mechanistic" approach, NO (presumably the analog of the hypothetical "inhibitor" clearly functioned as a reverse agonist. This difference underscores the difficulty in extrapolating specific mechanisms from compartmental modeling when mechanistic information is absent. Secondly, although the "black box" approach did not provide mechanistic detail, it influenced further experimentation that was target towards obtaining the missing mechanistic information. Thus, such modeling efforts can be extraordinarily useful in the design and interpretation of studies aimed as elucidating fundamental mechanisms of kinetic or dynamic behavior. As additional steps in the NO pathway for opioid tolerance development are elaborated, or as alternative pathways for opioid tolerance are elucidated, for the development of opioid tolerance, more detailed mechanistic models can be developed, assuming that the relevant steps in those pathways can be studied in vivo.

CONCLUSIONS

Opioid tolerance is a complex phenomenon mediated by diverse behavioral and cellular adaptations. Many of the specific alterations in intracellular signaling, trafficking and neurotransmitter activity have been thoroughly characterized using in vitro approaches and knockout mice. Despite these advances, there is in general a lack of integrative system approaches characterizing how these cellular adaptations interact within the whole organism. Such an approach will be critical in developing comprehensive understanding of opioid tolerance. As mechanistic information continues to be generated, increasingly sophisticated PK-PD models, with increasing biologic relevance, can be developed. The availability of such models, in turn, will support diverse activities ranging from drug discovery to adjunct therapy in order to minimize or reverse opioid tolerance. The ability to control the tolerance process is a requisite step in devising appropriate pharmacologic strategies for the treatment of chronic pain.

Table 2.1. Categorization of the common opioids based on structural similarities.

Semisynthetic derivatives	Synthetic derivatives
Morphine-related agonists	*Phenylpiperidines*
Hydromorphone	Meperidine
Hydrocodone	Loperamide
Oxycodone	*Diphenylpropylamines*
Oxymorphone	Methadone
Codeine	Propoxyphene
Morphine-related partial agonists and antagonists	*Piperidines*
	Fentanyl
Buprenorphine	Alfentanil
Naloxone	Sufentanil
Naltrexone	Remifentanil

Table 2.2. Pharmacokinetic/pharmacodynamic parameter estimates and corresponding coefficients of variation obtained from simultaneous modeling of morphine disposition, NO production, and antinociceptive effects. See Figure 2.6 for model structure. From Heinzen and Pollack (116).

Parameter	Estimate	CV %
V_{BL} (L/kg)	2.5	25.9
V_{BR} (L/kg)	26	22.6
k_{10} (hr^{-1})	2.17	26.3
k_{12} (hr^{-1})	2.15	45.2
k_{21} (hr^{-1})	1.77	10.8
$Emax_{,S}$ (% stim)	0.19	36.8
$EC50_{,S}$ (ng/mL)	15.2	36.7
$\gamma_{,S}$	3.1	115
k_{ON}	258	126
k_{OFF}	25.8	127
$Emax_{,E}$ (% MPE)	100	21.9
$EC50_{,E}$ (ng/mL)	26.8	29.8
$\gamma_{,E}$	1.04	14.8
$Imax_{,E}$ (% MPE)	2726	133
$IC50_{,E}$ (% SAL)	264	157
$\gamma_{,I}$	5.2	52.4
$keo_{,\text{low dose morphine}}$ (hr^{-1})	1.56	19.3
$keo_{,\text{intermediate dose morphine}}$ (hr^{-1})	1.01	15.8
$keo_{,\text{high dose morphine}}$ (hr^{-1})	0.61	21.4

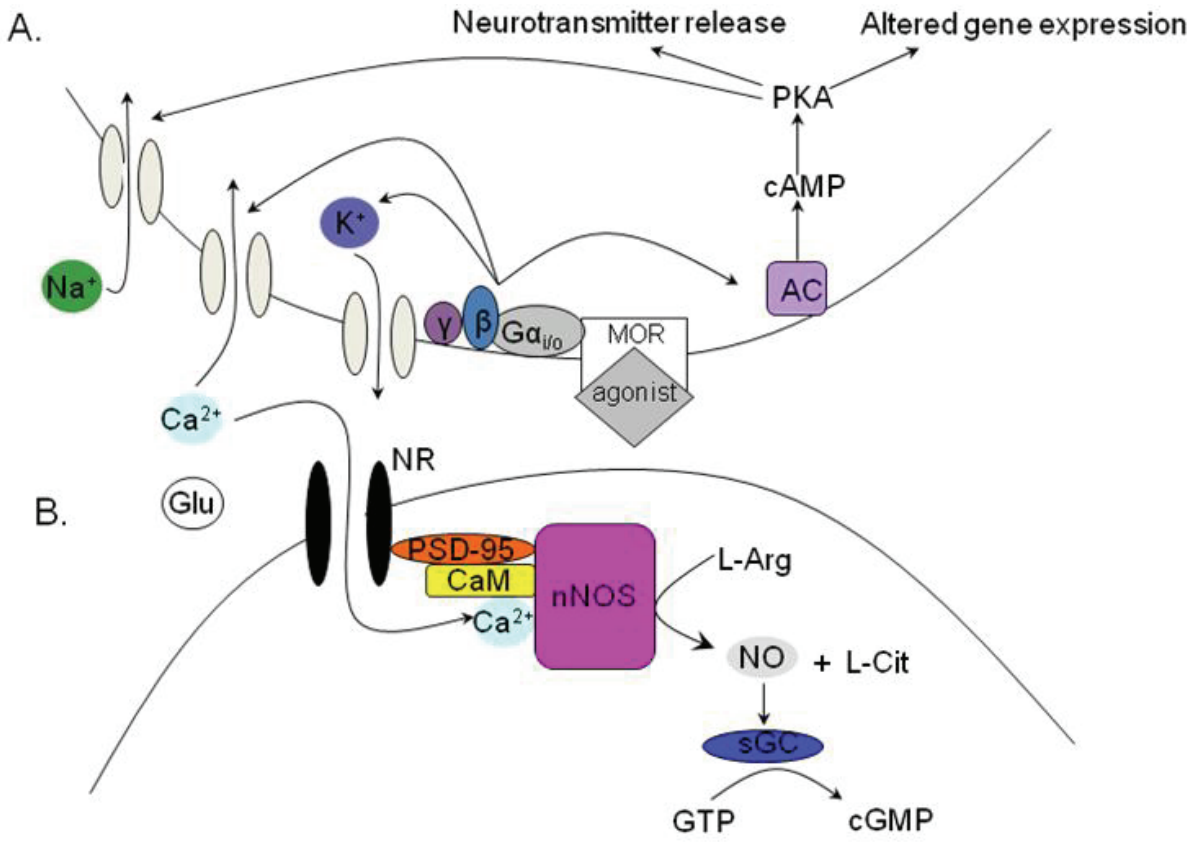

Figure 2.1. Downstream mediators of antinociception following opioid agonist binding to the MOR. A. Binding of the agonist changes in ion channel conductance and alters the cAMP pathway. Bold arrows indicate up- or down-regulation of pathways following chronic opioid exposure. B. Activation of the NMDA receptor/NO pathway. Chronic opioid exposure alters synaptic cleft ion conductance and glutamate expression, leading to the the displacement of the Mg^{2+} block of the NMDA receptor, an influx of Ca^{2+} and conversion of L-Arg to NO, a mediator of tolerance. Administering an NMDA receptor antagonist attenuates and delays the onset of tolerance by blocking Ca^{2+} influx and associated alterations.

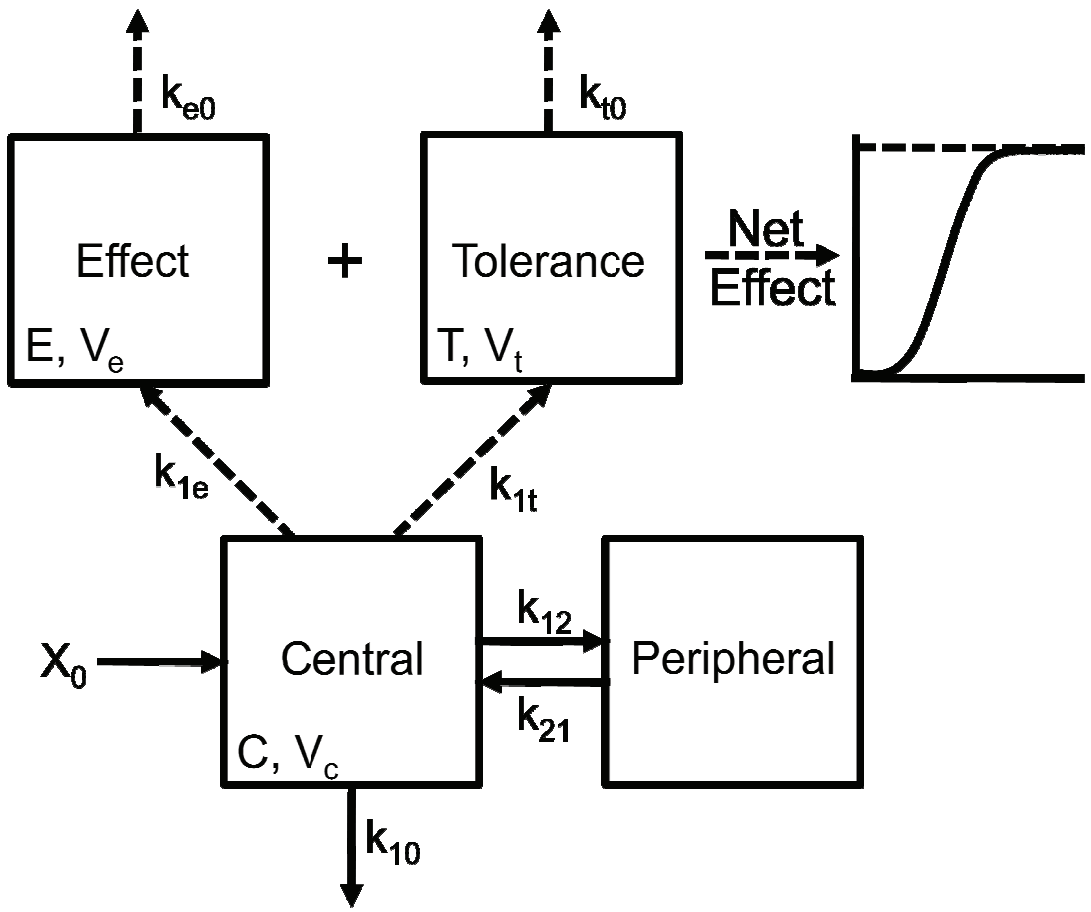

Figure 2.2. Scheme depicting the PK-PD model of tolerance following multiple morphine i.v. bolus doses. The time course of morphine concentrations following multiple i.v. bolus doses was described by a two-compartment model with a central volume of distribution V_c, distribution between the central and peripheral compartment according to the rate constants k_{12} and k_{21}, and elimination from the central compartment by the first-order rate constant k_{10}. The time course of antinociception was described using an approach derived by Porchet (108) where the first-order rate constants of effect onset, k_{1e} and k_{1t}, link the central compartment to the effect (E) and tolerance (T) compartments of volumes V_e and V_t and, effect offset is governed by the first-order rate constants k_{e0} and k_{t0}. Adapted from Ouellet and Pollack (118).

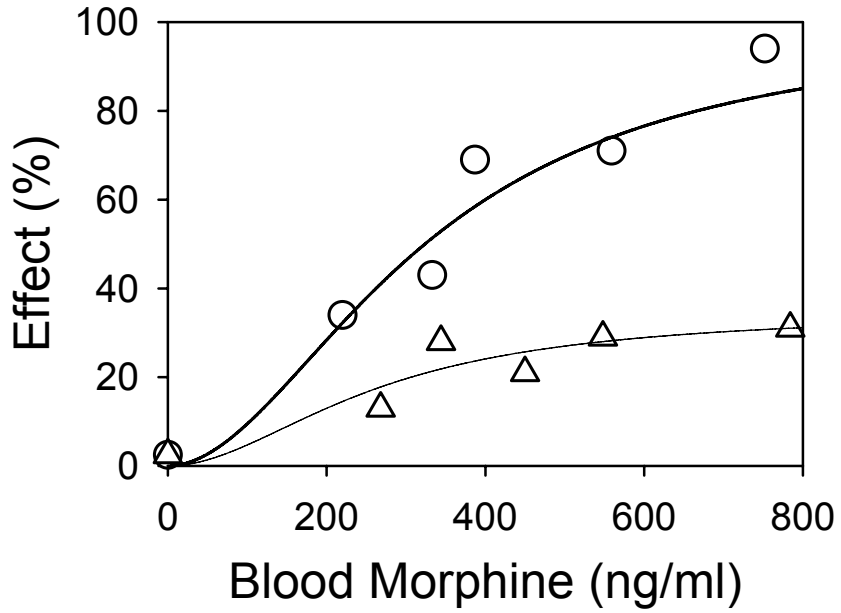

Figure 2.3. Relationship between antinociceptive response and morphine concentrations in blood during continuous infusion at the time of peak response (*circles*) or at 12 hr into the infusion (*triangles*). Data are presented as mean for clarity; lines indicate the fit of the Hill equation to the data with the following parameter values: peak effect vs. concentration data (E_{max} = 100%, EC_{50} = 324 ng/ml, γ = 1.92); effect at 12 hr vs. concentration (E_{max} = 34.8%, EC_{50} = 262 ng/ml, γ = 1.92). Data were obtained from Ouellet and Pollack (119).

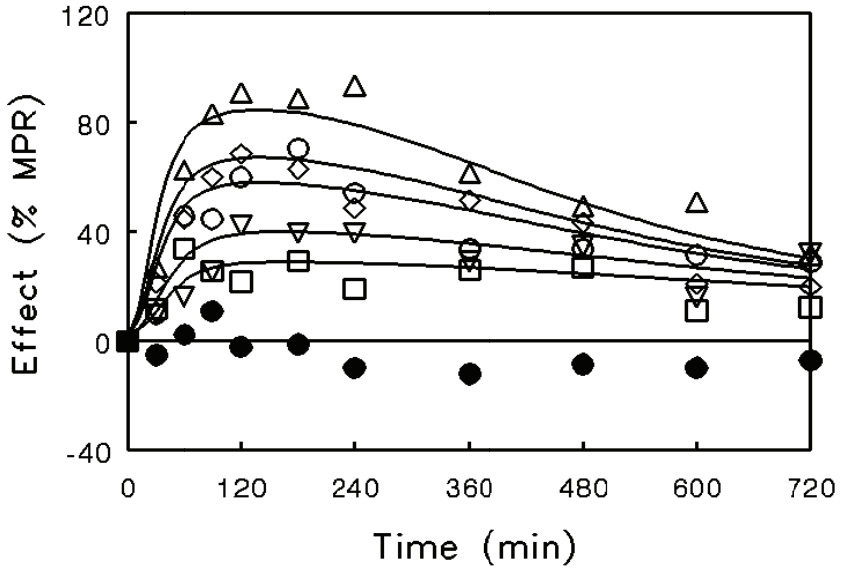

Figure 2.4. Time course of antinociceptive response during morphine infusion in rats. Infusion rates were selected to produce steady-state concentrations of 200-299 ng/ml (*squares*), 300-399 ng/ml (*inverted triangles*), 400-499 ng/ml (*diamonds*), 500-599 ng/ml (*circles*), or > 600 ng/ml (*triangles*). Closed circles indicate animals that did not receive morphine. Data are represented as mean for clarity; lines indicate the fit of an integrated PK-PD model (Figure 2.2) with the assumption that tolerance is driven by accumulation of a hypothetical partial agonist (Equation 2.4). Adapted from Ouellet and Pollack (119).

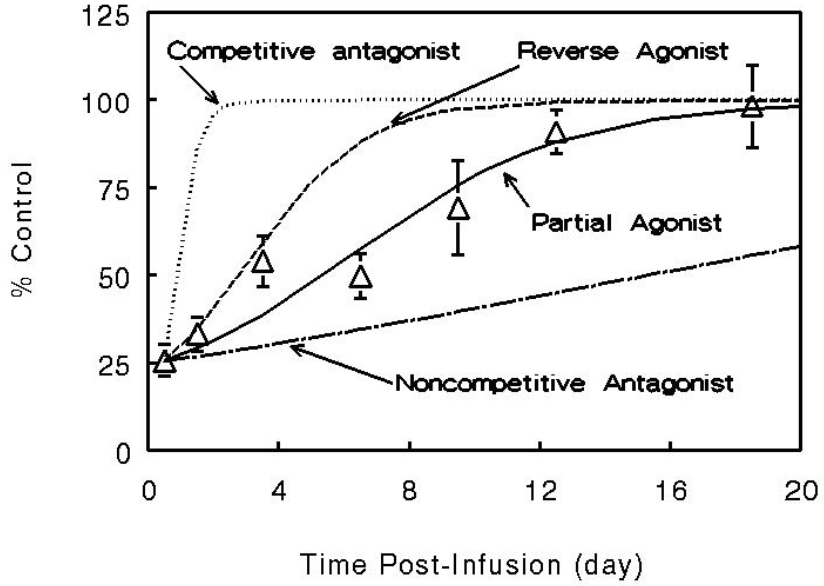

Figure 2.5. Recovery of antinociceptive response to a 2-mg/kg bolus dose of morphine following termination of a 12-hr morphine infusion (2 mg/kg/hr). Data are presented as mean ± SE; lines indicate model simulations based on an assumption that tolerance is driven by accumulation of a hypothetical reverse agonist (dashed line),competitive antagonist (dotted line), non-competitive antagonist (dot-dashed line), or partial agonist (solid line). Adapted from Ouellet and Pollack (119).

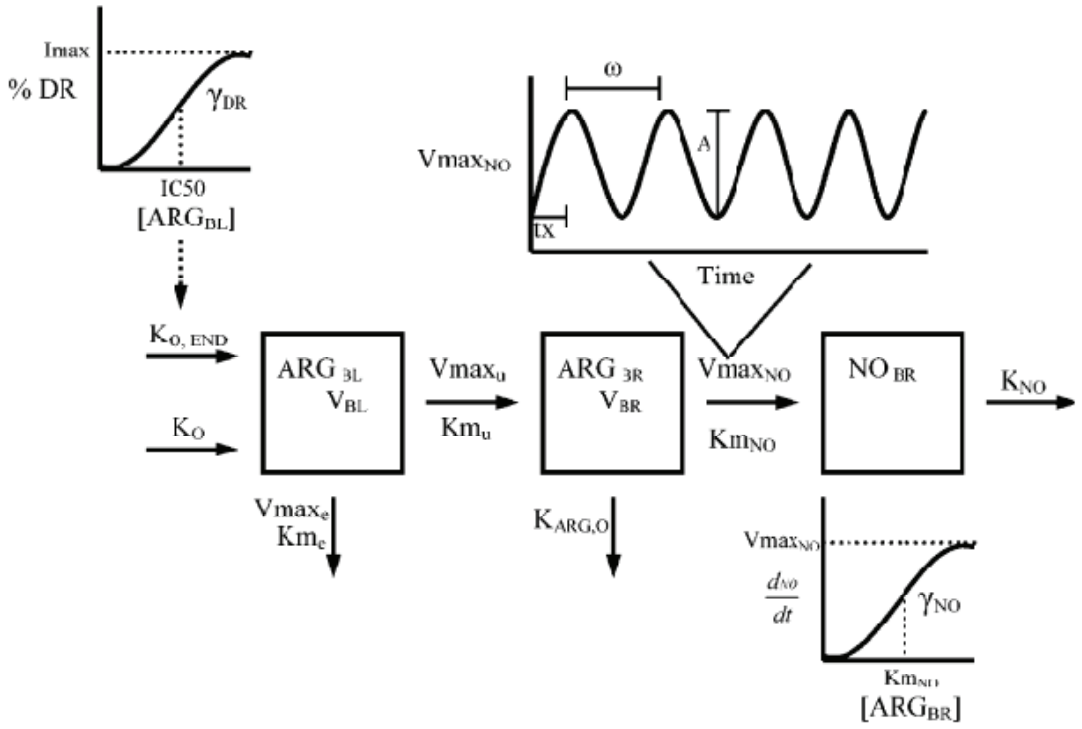

Figure 2.6. PK-PD model for L-arginine-associated stimulation of nitric oxide production in rats. From Heinzen and Pollack (115).

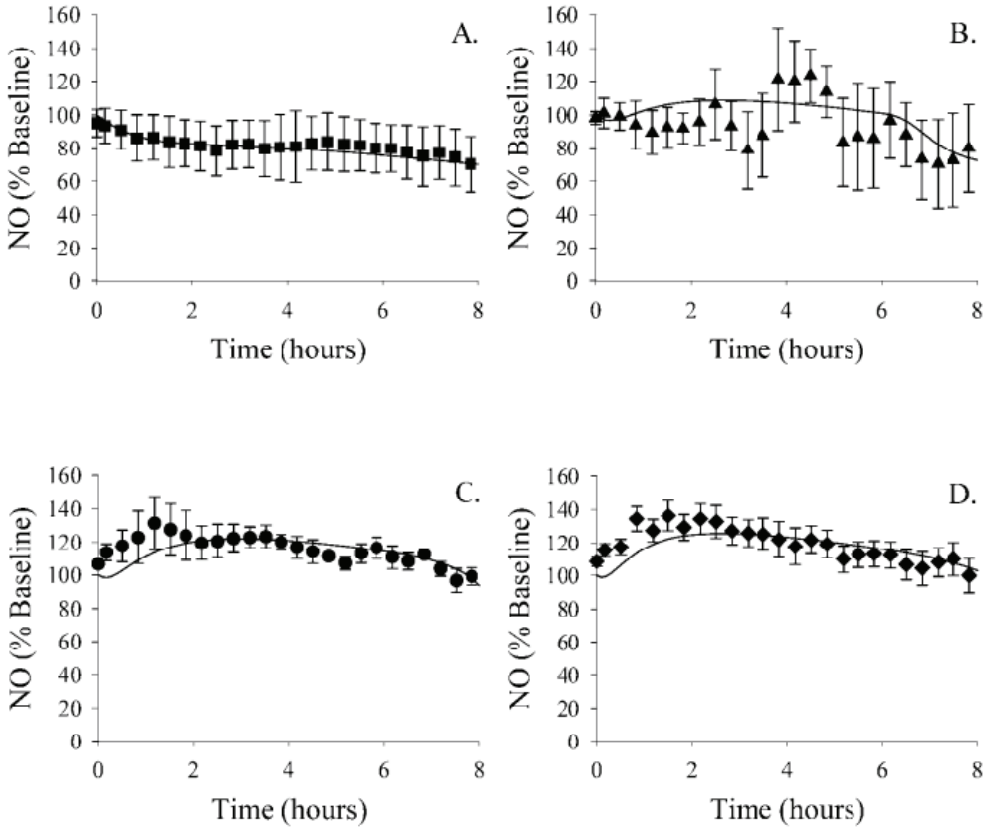

Figure 2.7. Concentration-time profiles for brain NO during (A) saline or administration of L-arginine [(B) 250 mg/kg/hr, (C) 500 mg/kg/hr, or (D) 1000 mg/kg/hr]. Data are mean±SE. Lines indicate the fit of the PK-PD model (Figure 2.6) to the data. From Heinzen and Pollack (115).

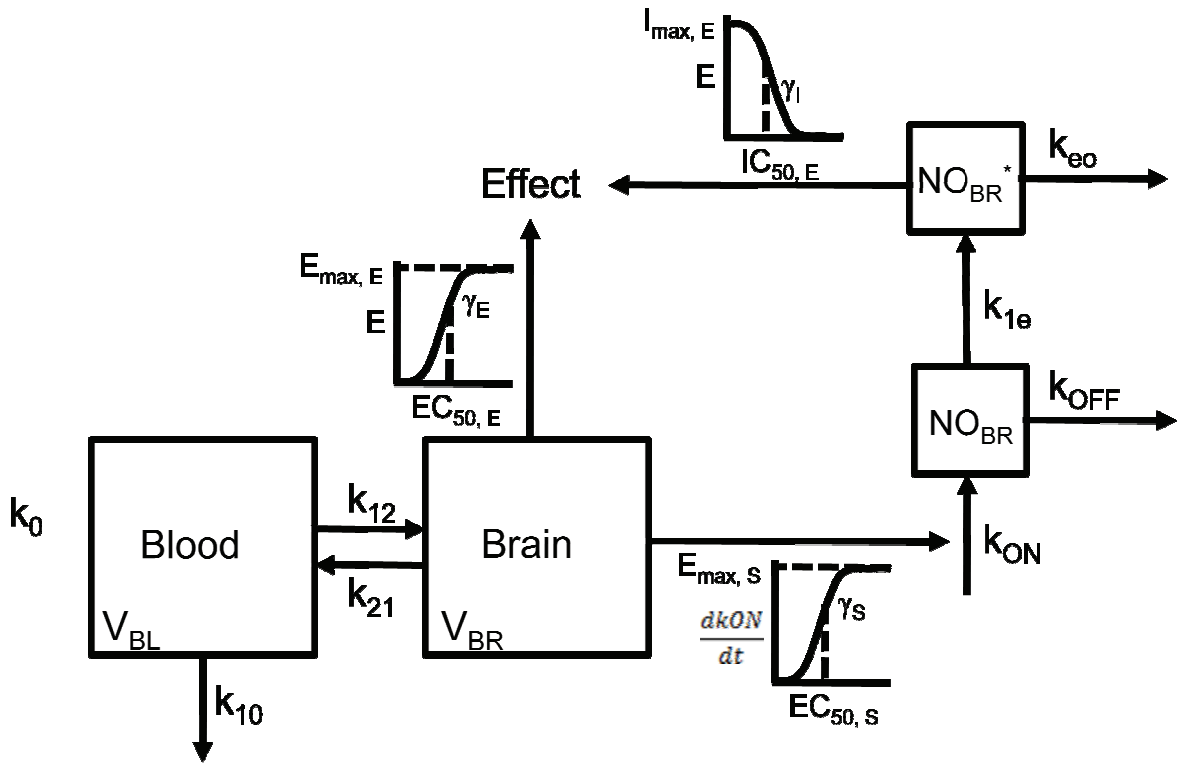

Figure 2.8. Scheme depicting the PK-PD model of morphine disposition, NO production and antinociceptive effect. The disposition qof morphine administered as a zero-order infusion (k_0) into the blood of volume V_{BL} was described by the first-order rate constants of transfer between the blood and brain, k_{12} and k_{21}, and by the first-order rate constant of elimination k_{10} from the blood. Antinociception was mediated by morphine in the brain of volume V_{BR} by acting as an agonist at the MOR and by indirectly stimulating the production of NO, which indirectly inhibited antinociception. The actions of morphine on NO production and antinociception was described using sigmoidal Emax models, where $E_{max,\ E\ or\ S}$ is maximum effect or stimulation; $EC_{50,E\ or\ S}$ is the concentration that elicits 50% effect or stimulation; $\gamma_{\ E\ or\ S}$ is the shape factor dictating the relationship between concentration and effect or stimulation of NO production (k_{ON}); k_{OFF} is the first-order rate constant of NO degradation; NO_{BR}* is the concentration of NO in the hypothetical compartment that indirectly inhibits effect; $I_{max,E}$ is the maximum inhibitory effect of NO; $IC_{50,E}$ is the

concentration of NO that inhibits 50% of the effect; and $\gamma_{,I}$ is the shape factor of the inhibitory effect of NO on antinociception. Adapted from Heinzen and Pollack (109,119).

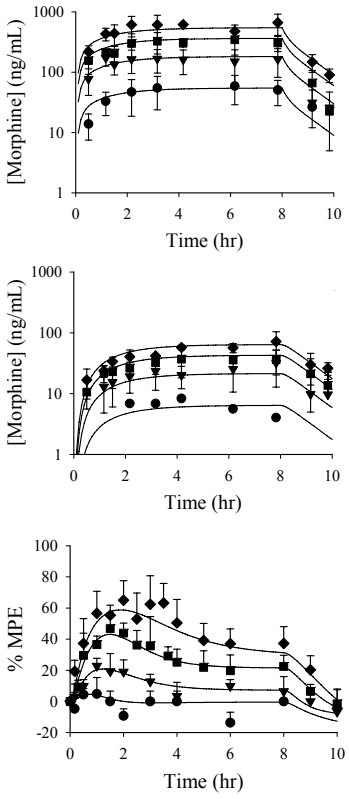

Figure 2.9. Blood morphine concentrations (top), brain morphine concentrations (middle), and antinociceptive effect (bottom) during and following an 8-hr morphine infusion at 0.3- (*circles*), 1- (*triangles*), 2- (*squares*), or 3- (*diamonds*) mg/kg/hr. Lines indicate the fit of the PK/PD model to data. Adapted from Heinzen and Pollack (116).

REFERENCES

1. Inturrisi, C. E., Clinical pharmacology of opioids for pain. Clin J Pain 2002, 18, (4 Suppl), S3-13.

2. World Health Organization, Cancer Pain Relief, Second Edition. In World Health Organization: Geneva, Switzerland, 1996; pp 1-69.

3. Jones, R. T., Euphoria vs. cocaine plasma concentrations after nasal administration (20% solution). In *NIDA Research Monograph 99 (Research Findings on Smoking of Abused Substances)*, Chiang, C. N.; Hawks, R. L., Eds. 1990; pp 30-41.

4. Siegel, S., Morphine analgesic tolerance: its situation specificity supports a Pavlovian conditioning model. *Science* **1976,** 193, (4250), 323-5.

5. van Ree, J. M.; Gerrits, M. A.; Vanderschuren, L. J., Opioids, reward and addiction: An encounter of biology, psychology, and medicine. *Pharmacol Rev* **1999,** 51, (2), 341-96.

6. Ross, E. M.; Kenakin, T. P., Pharmacodynamics: Mechanisms of Drug Action and the Relationship Between Drug Concentration and Effect. In *Goodman and Gilman's the Pharmacological Basis of Therapeutics*, 10th ed.; Hardman, J. G.; Limbird, L. E., Eds. McGraw Hill: 2001; pp 31-43.

7. Gibaldi, M.; Levy, G., Dose-dependent decline of pharmacologic effects of drugs with linear pharmacokinetic characteristics. *J Pharm Sci* **1972,** 61, (4), 567-9.

8. Bernard, S.; Neville, K. A.; Nguyen, A. T.; Flockhart, D. A., Interethnic differences in genetic polymorphisms of CYP2D6 in the U.S. population: clinical implications. *Oncologist* **2006,** 11, (2), 126-35.

9. Desmeules, J.; Gascon, M. P.; Dayer, P.; Magistris, M., Impact of environmental and genetic factors on codeine analgesia. *Eur J Clin Pharmacol* **1991,** 41, (1), 23-6.

10. Berkowitz, B. A., The relationship of pharmacokinetics to pharmacological activity: morphine, methadone and naloxone. *Clin Pharmacokinet* **1976,** 1, (3), 219-30.

11. Sawe, J., High-dose morphine and methadone in cancer patients. Clinical pharmacokinetic considerations of oral treatment. *Clin Pharmacokinet* **1986,** 11, (2), 87-106.

12. Fredheim, O. M.; Borchgrevink, P. C.; Klepstad, P.; Kaasa, S.; Dale, O., Long term methadone for chronic pain: a pilot study of pharmacokinetic aspects. *Eur J Pain* **2007,** 11, (6), 599-604.

13. Sawe, J.; Svensson, J. O.; Rane, A., Morphine metabolism in cancer patients on increasing oral doses--no evidence for autoinduction or dose-dependence. *Br J Clin Pharmacol* **1983,** 16, (1), 85-93.

14. Dagenais, C.; Graff, C. L.; Pollack, G. M., Variable modulation of opioid brain uptake by P-glycoprotein in mice. *Biochem Pharmacol* **2004,** 67, (2), 269-76.

15. Matheny, C. J.; Lamb, M. W.; Brouwer, K. R.; Pollack, G. M., Pharmacokinetic and pharmacodynamic implications of P-glycoprotein modulation. *Pharmacotherapy* **2001,** 21, (7), 778-96.

16. King, M.; Su, W.; Chang, A.; Zuckerman, A.; Pasternak, G. W., Transport of opioids from the brain to the periphery by P-glycoprotein: peripheral actions of central drugs. *Nat Neurosci* **2001,** 4, (3), 268-74.

17. Kalvass, J. C.; Olson, E. O.; Pollack, G. M., Influence of Blood-Brain Barrier P-glycoprotein on Brain Penetration and Antinociceptive Effects of Model Opioids. *Drug Metabolism and Disposition* **Submitted**.

18. Bauer, B.; Yang, X.; Hartz, A. M.; Olson, E. R.; Zhao, R.; Kalvass, J. C.; Pollack, G. M.; Miller, D. S., In vivo activation of human pregnane X receptor tightens the blood-brain barrier to methadone through P-glycoprotein up-regulation. *Mol Pharmacol* **2006,** 70, (4), 1212-9.

19. Hassan, H. E.; Myers, A. L.; Lee, I. J.; Coop, A.; Eddington, N. D., Oxycodone induces overexpression of P-glycoprotein (ABCB1) and affects paclitaxel's tissue distribution in Sprague Dawley rats. *J Pharm Sci* **2007,** 96, (9), 2494-506.

20. Aquilante, C. L.; Letrent, S. P.; Pollack, G. M.; Brouwer, K. L., Increased brain P-glycoprotein in morphine tolerant rats. *Life Sci* **2000,** 66, (4), PL47-51.

21. Wittwer, E.; Kern, S. E., Role of morphine's metabolites in analgesia: concepts and controversies. *Aaps J* **2006,** 8, (2), E348-52.

22. Smith, G. D.; Smith, M. T., Morphine-3-glucuronide: evidence to support its putative role in the development of tolerance to the antinociceptive effects of morphine in the rat. *Pain* **1995,** 62, (1), 51-60.

23. Gardmark, M.; Karlsson, M. O.; Jonsson, F.; Hammarlund-Udenaes, M., Morphine-3-glucuronide has a minor effect on morphine antinociception. Pharmacodynamic modeling. *J Pharm Sci* **1998,** 87, (7), 813-20.

24. Ouellet, D. M.; Pollack, G. M., Effect of prior morphine-3-glucuronide exposure on morphine disposition and antinociception. *Biochem Pharmacol* **1997,** 53, (10), 1451-7.

25. Smith, M. T., Neuroexcitatory effects of morphine and hydromorphone: evidence implicating the 3-glucuronide metabolites. *Clin Exp Pharmacol Physiol* **2000,** 27, (7), 524-8.

26. Bartlett, S. E.; Cramond, T.; Smith, M. T., The excitatory effects of morphine-3-glucuronide are attenuated by LY274614, a competitive NMDA receptor antagonist,

and by midazolam, an agonist at the benzodiazepine site on the GABAA receptor complex. *Life Sci* **1994,** 54, (10), 687-94.

27. Evans, C. J.; Keith, D. E., Jr.; Morrison, H.; Magendzo, K.; Edwards, R. H., Cloning of a delta opioid receptor by functional expression. *Science* **1992,** 258, (5090), 1952-5.

28. Chen, Y.; Mestek, A.; Liu, J.; Hurley, J. A.; Yu, L., Molecular cloning and functional expression of a mu-opioid receptor from rat brain. *Mol Pharmacol* **1993,** 44, (1), 8-12.

29. Li, S.; Zhu, J.; Chen, C.; Chen, Y. W.; Deriel, J. K.; Ashby, B.; Liu-Chen, L. Y., Molecular cloning and expression of a rat kappa opioid receptor. *Biochem J* **1993,** 295 (Pt 3), 629-33.

30. Kieffer, B. L., Opioids: first lessons from knockout mice. *Trends Pharmacol Sci* **1999,** 20, (1), 19-26.

31. Matthes, H. W.; Maldonado, R.; Simonin, F.; Valverde, O.; Slowe, S.; Kitchen, I.; Befort, K.; Dierich, A.; Le Meur, M.; Dolle, P.; Tzavara, E.; Hanoune, J.; Roques, B. P.; Kieffer, B. L., Loss of morphine-induced analgesia, reward effect and withdrawal symptoms in mice lacking the mu-opioid-receptor gene. *Nature* **1996,** 383, (6603), 819-23.

32. Sora, I.; Takahashi, N.; Funada, M.; Ujike, H.; Revay, R. S.; Donovan, D. M.; Miner, L. L.; Uhl, G. R., Opiate receptor knockout mice define mu receptor roles in endogenous nociceptive responses and morphine-induced analgesia. *Proc Natl Acad Sci U S A* **1997,** 94, (4), 1544-9.

33. Williams, J. T.; Christie, M. J.; Manzoni, O., Cellular and synaptic adaptations mediating opioid dependence. *Physiol Rev* **2001,** 81, (1), 299-343.

34. Tso, P. H.; Wong, Y. H., Molecular basis of opioid dependence: role of signal regulation by G-proteins. *Clin Exp Pharmacol Physiol* **2003,** 30, (5-6), 307-16.

35. Smart, D.; Hirst, R. A.; Hirota, K.; Grandy, D. K.; Lambert, D. G., The effects of recombinant rat mu-opioid receptor activation in CHO cells on phospholipase C, [Ca2+]i and adenylyl cyclase. *Br J Pharmacol* **1997,** 120, (6), 1165-71.

36. Nestler, E. J.; Aghajanian, G. K., Molecular and cellular basis of addiction. *Science* **1997,** 278, (5335), 58-63.

37. Taylor, D. A.; Fleming, W. W., Unifying perspectives of the mechanisms underlying the development of tolerance and physical dependence to opioids. *J Pharmacol Exp Ther* **2001,** 297, (1), 11-8.

38. Zhang, L.; Yu, Y.; Mackin, S.; Weight, F. F.; Uhl, G. R.; Wang, J. B., Differential mu opiate receptor phosphorylation and desensitization induced by agonists and phorbol esters. *J Biol Chem* **1996,** 271, (19), 11449-54.

39. Yu, Y.; Zhang, L.; Yin, X.; Sun, H.; Uhl, G. R.; Wang, J. B., Mu opioid receptor phosphorylation, desensitization, and ligand efficacy. *J Biol Chem* **1997,** 272, (46), 28869-74.

40. Zhang, J.; Ferguson, S. S.; Barak, L. S.; Bodduluri, S. R.; Laporte, S. A.; Law, P. Y.; Caron, M. G., Role for G protein-coupled receptor kinase in agonist-specific regulation of mu-opioid receptor responsiveness. *Proc Natl Acad Sci U S A* **1998,** 95, (12), 7157-62.

41. Bohn, L. M.; Gainetdinov, R. R.; Lin, F. T.; Lefkowitz, R. J.; Caron, M. G., Mu-opioid receptor desensitization by beta-arrestin-2 determines morphine tolerance but not dependence. *Nature* **2000,** 408, (6813), 720-3.

42. Bohn, L. M.; Lefkowitz, R. J.; Gainetdinov, R. R.; Peppel, K.; Caron, M. G.; Lin, F. T., Enhanced morphine analgesia in mice lacking beta-arrestin 2. *Science* **1999,** 286, (5449), 2495-8.

43. Thompson, D.; Pusch, M.; Whistler, J. L., Changes in G Protein-coupled Receptor Sorting Protein Affinity Regulate Postendocytic Targeting of G Protein-coupled Receptors. *J Biol Chem* **2007,** 282, (40), 29178-85.

44. Narita, M.; Suzuki, M.; Narita, M.; Niikura, K.; Nakamura, A.; Miyatake, M.; Yajima, Y.; Suzuki, T., mu-Opioid receptor internalization-dependent and -independent mechanisms of the development of tolerance to mu-opioid receptor agonists: Comparison between etorphine and morphine. *Neuroscience* **2006,** 138, (2), 609-19.

45. Dang, V. C.; Williams, J. T., Morphine-Induced mu-opioid receptor desensitization. *Mol Pharmacol* **2005,** 68, (4), 1127-32.

46. He, L.; Fong, J.; von Zastrow, M.; Whistler, J. L., Regulation of opioid receptor trafficking and morphine tolerance by receptor oligomerization. *Cell* **2002,** 108, (2), 271-82.

47. Jordan, B. A.; Devi, L. A., G-protein-coupled receptor heterodimerization modulates receptor function. *Nature* **1999,** 399, (6737), 697-700.

48. Bailey, C. P.; Couch, D.; Johnson, E.; Griffiths, K.; Kelly, E.; Henderson, G., Mu-opioid receptor desensitization in mature rat neurons: lack of interaction between DAMGO and morphine. *J Neurosci* **2003,** 23, (33), 10515-20.

49. Stafford, K.; Gomes, A. B.; Shen, J.; Yoburn, B. C., mu-Opioid receptor downregulation contributes to opioid tolerance in vivo. *Pharmacol Biochem Behav* **2001,** 69, (1-2), 233-7.

50. Finn, A. K.; Whistler, J. L., Endocytosis of the mu opioid receptor reduces tolerance and a cellular hallmark of opiate withdrawal. *Neuron* **2001,** 32, (5), 829-39.

51. Sim-Selley, L. J.; Scoggins, K. L.; Cassidy, M. P.; Smith, L. A.; Dewey, W. L.; Smith, F. L.; Selley, D. E., Region-dependent attenuation of mu opioid receptor-mediated G-protein activation in mouse CNS as a function of morphine tolerance. *Br J Pharmacol* **2007,** 151, (8), 1324-33.

52. LaForge, K. S.; Yuferov, V.; Kreek, M. J., Opioid receptor and peptide gene polymorphisms: potential implications for addictions. *Eur J Pharmacol* **2000,** 410, (2-3), 249-268.

53. Kreek, M. J.; Bart, G.; Lilly, C.; LaForge, K. S.; Nielsen, D. A., Pharmacogenetics and human molecular genetics of opiate and cocaine addictions and their treatments. *Pharmacol Rev* **2005,** 57, (1), 1-26.

54. Bond, C.; LaForge, K. S.; Tian, M.; Melia, D.; Zhang, S.; Borg, L.; Gong, J.; Schluger, J.; Strong, J. A.; Leal, S. M.; Tischfield, J. A.; Kreek, M. J.; Yu, L., Single-nucleotide polymorphism in the human mu opioid receptor gene alters beta-endorphin binding and activity: possible implications for opiate addiction. *Proc Natl Acad Sci U S A* **1998,** 95, (16), 9608-13.

55. Surratt, C. K.; Johnson, P. S.; Moriwaki, A.; Seidleck, B. K.; Blaschak, C. J.; Wang, J. B.; Uhl, G. R., -mu opiate receptor. Charged transmembrane domain amino acids are critical for agonist recognition and intrinsic activity. *J Biol Chem* **1994,** 269, (32), 20548-53.

56. Romberg, R. R.; Olofsen, E.; Bijl, H.; Taschner, P. E.; Teppema, L. J.; Sarton, E. Y.; van Kleef, J. W.; Dahan, A., Polymorphism of mu-opioid receptor gene (OPRM1:c.118A>G) does not protect against opioid-induced respiratory depression despite reduced analgesic response. *Anesthesiology* **2005,** 102, (3), 522-30.

57. Oertel, B. G.; Schmidt, R.; Schneider, A.; Geisslinger, G.; Lotsch, J., The mu-opioid receptor gene polymorphism 118A>G depletes alfentanil-induced analgesia and protects against respiratory depression in homozygous carriers. *Pharmacogenet Genomics* **2006,** 16, (9), 625-36.

58. Befort, K.; Filliol, D.; Decaillot, F. M.; Gaveriaux-Ruff, C.; Hoehe, M. R.; Kieffer, B. L., A single nucleotide polymorphic mutation in the human mu-opioid receptor severely impairs receptor signaling. *J Biol Chem* **2001,** 276, (5), 3130-7.

59. Beyer, A.; Koch, T.; Schroder, H.; Schulz, S.; Hollt, V., Effect of the A118G polymorphism on binding affinity, potency and agonist-mediated endocytosis, desensitization, and resensitization of the human mu-opioid receptor. *J Neurochem* **2004,** 89, (3), 553-60.

60. Wang, D.; Quillan, J. M.; Winans, K.; Lucas, J. L.; Sadee, W., Single nucleotide polymorphisms in the human mu opioid receptor gene alter basal G protein coupling and calmodulin binding. *J Biol Chem* **2001,** 276, (37), 34624-30.

61. Millan, M. J., Kappa-opioid receptor-mediated antinociception in the rat. I. Comparative actions of mu- and kappa-opioids against noxious thermal, pressure and electrical stimuli. *J Pharmacol Exp Ther* **1989,** 251, (1), 334-41.

62. Millan, M. J.; Czlonkowski, A.; Lipkowski, A.; Herz, A., Kappa-opioid receptor-mediated antinociception in the rat. II. Supraspinal in addition to spinal sites of action. *J Pharmacol Exp Ther* **1989,** 251, (1), 342-50.

63. Heyman, J. S.; Mulvaney, S. A.; Mosberg, H. I.; Porreca, F., Opioid delta-receptor involvement in supraspinal and spinal antinociception in mice. *Brain Res* **1987,** 420, (1), 100-8.

64. Wittert, G.; Hope, P.; Pyle, D., Tissue distribution of opioid receptor gene expression in the rat. *Biochem Biophys Res Commun* **1996,** 218, (3), 877-81.

65. Leighton, G. E.; Rodriguez, R. E.; Hill, R. G.; Hughes, J., kappa-Opioid agonists produce antinociception after i.v. and i.c.v. but not intrathecal administration in the rat. *Br J Pharmacol* **1988,** 93, (3), 553-60.

66. Narita, M.; Khotib, J.; Suzuki, M.; Ozaki, S.; Yajima, Y.; Suzuki, T., Heterologous mu-opioid receptor adaptation by repeated stimulation of kappa-opioid receptor: up-regulation of G-protein activation and antinociception. *J Neurochem* **2003,** 85, (5), 1171-9.

67. McLaughlin, J. P.; Myers, L. C.; Zarek, P. E.; Caron, M. G.; Lefkowitz, R. J.; Czyzyk, T. A.; Pintar, J. E.; Chavkin, C., Prolonged kappa opioid receptor phosphorylation mediated by G-protein receptor kinase underlies sustained analgesic tolerance. *J Biol Chem* **2004,** 279, (3), 1810-8.

68. Okura, T.; Varga, E. V.; Hosohata, Y.; Navratilova, E.; Cowell, S. M.; Rice, K.; Nagase, H.; Hruby, V. J.; Roeske, W. R.; Yamamura, H. I., Agonist-specific down-regulation of the human delta-opioid receptor. *Eur J Pharmacol* **2003,** 459, (1), 9-16.

69. Lecoq, I.; Marie, N.; Jauzac, P.; Allouche, S., Different regulation of human delta-opioid receptors by SNC-80 [(+)-4-[(alphaR)-alpha-((2S,5R)-4-allyl-2,5-dimethyl-1-piperazinyl)-3-meth oxybenzyl]-N,N-diethylbenzamide] and endogenous enkephalins. *J Pharmacol Exp Ther* **2004,** 310, (2), 666-77.

70. de Stoutz, N. D.; Bruera, E.; Suarez-Almazor, M., Opioid rotation for toxicity reduction in terminal cancer patients. *J Pain Symptom Manage* **1995,** 10, (5), 378-84.

71. Riley, J.; Ross, J. R.; Rutter, D.; Wells, A. U.; Goller, K.; du Bois, R.; Welsh, K., No pain relief from morphine? Individual variation in sensitivity to morphine and the

need to switch to an alternative opioid in cancer patients. *Support Care Cancer* **2006,** 14, (1), 56-64.

72. Athanasos, P.; Smith, C. S.; White, J. M.; Somogyi, A. A.; Bochner, F.; Ling, W., Methadone maintenance patients are cross-tolerant to the antinociceptive effects of very high plasma morphine concentrations. *Pain* **2006,** 120, (3), 267-75.

73. Duttaroy, A.; Yoburn, B. C., The effect of intrinsic efficacy on opioid tolerance. *Anesthesiology* **1995,** 82, (5), 1226-36.

74. Walker, E. A.; Richardson, T. M.; Young, A. M., Tolerance and cross-tolerance to morphine-like stimulus effects of mu opioids in rats. *Psychopharmacology (Berl)* **1997,** 133, (1), 17-28.

75. Pasternak, G. W., Multiple opiate receptors: deja vu all over again. *Neuropharmacology* **2004,** 47 Suppl 1, 312-23.

76. Gupta, A.; Decaillot, F. M.; Devi, L. A., Targeting opioid receptor heterodimers: strategies for screening and drug development. *Aaps J* **2006,** 8, (1), E153-9.

77. Zarrindast, M. R.; Alaei-Nia, K.; Shafizadeh, M., On the mechanism of tolerance to morphine-induced Straub tail reaction in mice. *Pharmacol Biochem Behav* **2001,** 69, (3-4), 419-24.

78. Luccarini, P.; Perrier, L.; Degoulange, C.; Gaydier, A. M.; Dallel, R., Synergistic antinociceptive effect of amitriptyline and morphine in the rat orofacial formalin test. *Anesthesiology* **2004,** 100, (3), 690-6.

79. Sawynok, J.; Esser, M. J.; Reid, A. R., Antidepressants as analgesics: an overview of central and peripheral mechanisms of action. *J Psychiatry Neurosci* **2001,** 26, (1), 21-9.

80. Gracy, K. N.; Svingos, A. L.; Pickel, V. M., Dual ultrastructural localization of mu-opioid receptors and NMDA-type glutamate receptors in the shell of the rat nucleus accumbens. *J Neurosci* **1997,** 17, (12), 4839-48.

81. Commons, K. G.; van Bockstaele, E. J.; Pfaff, D. W., Frequent colocalization of mu opioid and NMDA-type glutamate receptors at postsynaptic sites in periaqueductal gray neurons. *J Comp Neurol* **1999,** 408, (4), 549-59.

82. Zhao, M.; Joo, D. T., Subpopulation of dorsal horn neurons displays enhanced N-methyl-D-aspartate receptor function after chronic morphine exposure. *Anesthesiology* **2006,** 104, (4), 815-25.

83. Snyder, S. H., Opiate receptors and beyond: 30 years of neural signaling research. *Neuropharmacology* **2004,** 47 Suppl 1, 274-85.

84. Kolesnikov, Y. A.; Pick, C. G.; Ciszewska, G.; Pasternak, G. W., Blockade of tolerance to morphine but not to kappa opioids by a nitric oxide synthase inhibitor. *Proc Natl Acad Sci U S A* **1993,** 90, (11), 5162-6.

85. Babey, A. M.; Kolesnikov, Y.; Cheng, J.; Inturrisi, C. E.; Trifilletti, R. R.; Pasternak, G. W., Nitric oxide and opioid tolerance. *Neuropharmacology* **1994,** 33, (11), 1463-70.

86. Kemp, J. A.; McKernan, R. M., NMDA receptor pathways as drug targets. *Nat Neurosci* **2002,** 5 Suppl, 1039-42.

87. Herman, B. H.; Vocci, F.; Bridge, P., The effects of NMDA receptor antagonists and nitric oxide synthase inhibitors on opioid tolerance and withdrawal. Medication development issues for opiate addiction. *Neuropsychopharmacology* **1995,** 13, (4), 269-93.

88. Lauretti, G. R.; Lima, I. C.; Reis, M. P.; Prado, W. A.; Pereira, N. L., Oral ketamine and transdermal nitroglycerin as analgesic adjuvants to oral morphine therapy for cancer pain management. *Anesthesiology* **1999,** 90, (6), 1528-33.

89. Allen, R. M.; Dykstra, L. A., Attenuation of mu-opioid tolerance and cross-tolerance by the competitive N-methyl-D-aspartate receptor antagonist LY235959 is related to tolerance and cross-tolerance magnitude. *J Pharmacol Exp Ther* **2000,** 295, (3), 1012-21.

90. Fischer, B. D.; Carrigan, K. A.; Dykstra, L. A., Effects of N-methyl-D-aspartate receptor antagonists on acute morphine-induced and l-methadone-induced antinociception in mice. *J Pain* **2005,** 6, (7), 425-33.

91. Medvedev, I. O.; Malyshkin, A. A.; Belozertseva, I. V.; Sukhotina, I. A.; Sevostianova, N. Y.; Aliev, K.; Zvartau, E. E.; Parsons, C. G.; Danysz, W.; Bespalov, A. Y., Effects of low-affinity NMDA receptor channel blockers in two rat models of chronic pain. *Neuropharmacology* **2004,** 47, (2), 175-83.

92. Suzuki, M.; Kinoshita, T.; Kikutani, T.; Yokoyama, K.; Inagi, T.; Sugimoto, K.; Haraguchi, S.; Hisayoshi, T.; Shimada, Y., Determining the plasma concentration of ketamine that enhances epidural bupivacaine-and-morphine-induced analgesia. *Anesth Analg* **2005,** 101, (3), 777-84.

93. Sethna, N. F.; Liu, M.; Gracely, R.; Bennett, G. J.; Max, M. B., Analgesic and cognitive effects of intravenous ketamine-alfentanil combinations versus either drug alone after intradermal capsaicin in normal subjects. *Anesth Analg* **1998,** 86, (6), 1250-6.

94. Redwine, K. E.; Trujillo, K. A., Effects of NMDA receptor antagonists on acute mu-opioid analgesia in the rat. *Pharmacol Biochem Behav* **2003,** 76, (2), 361-72.

95. Willetts, J.; Balster, R. L.; Leander, J. D., The behavioral pharmacology of NMDA receptor antagonists. *Trends Pharmacol Sci* **1990,** 11, (10), 423-8.

96. Chen, H. S.; Lipton, S. A., The chemical biology of clinically tolerated NMDA receptor antagonists. *J Neurochem* **2006,** 97, (6), 1611-26.

97. Cosman, K. M.; Boyle, L. L.; Porsteinsson, A. P., Memantine in the treatment of mild-to-moderate Alzheimer's disease. *Expert Opin Pharmacother* **2007,** 8, (2), 203-14.

98. Coggeshall, R. E.; Zhou, S.; Carlton, S. M., Opioid receptors on peripheral sensory axons. *Brain Res* **1997,** 764, (1-2), 126-32.

99. Carlton, S. M.; Zhou, S.; Coggeshall, R. E., Evidence for the interaction of glutamate and NK1 receptors in the periphery. *Brain Res* **1998,** 790, (1-2), 160-9.

100. Carlton, S. M.; Hargett, G. L.; Coggeshall, R. E., Localization and activation of glutamate receptors in unmyelinated axons of rat glabrous skin. *Neurosci Lett* **1995,** 197, (1), 25-8.

101. Carlton, S. M.; Coggeshall, R. E., Inflammation-induced changes in peripheral glutamate receptor populations. *Brain Res* **1999,** 820, (1-2), 63-70.

102. Pol, O.; Puig, M. M., Expression of opioid receptors during peripheral inflammation. *Curr Top Med Chem* **2004,** 4, (1), 51-61.

103. Kolesnikov, Y. A.; Jain, S.; Wilson, R.; Pasternak, G. W., Peripheral morphine analgesia: synergy with central sites and a target of morphine tolerance. *J Pharmacol Exp Ther* **1996,** 279, (2), 502-6.

104. Reichert, J. A.; Daughters, R. S.; Rivard, R.; Simone, D. A., Peripheral and preemptive opioid antinociception in a mouse visceral pain model. *Pain* **2001,** 89, (2-3), 221-227.

105. Shannon, H. E.; Lutz, E. A., Comparison of the peripheral and central effects of the opioid agonists loperamide and morphine in the formalin test in rats. *Neuropharmacology* **2002,** 42, (2), 253-261.

106. Kolesnikov, Y.; Cristea, M.; Oksman, G.; Torosjan, A.; Wilson, R., Evaluation of the tail formalin test in mice as a new model to assess local analgesic effects. *Brain Res* **2004,** 1029, (2), 217-23.

107. Gardmark, M.; Brynne, L.; Hammarlund-Udenaes, M.; Karlsson, M. O., Interchangeability and predictive performance of empirical tolerance models. *Clin Pharmacokinet* **1999,** 36, (2), 145-67.

108. Porchet, H. C.; Benowitz, N. L.; Sheiner, L. B., Pharmacodynamic model of tolerance: application to nicotine. *J Pharmacol Exp Ther* **1988,** 244, (1), 231-6.

109. Ouellet, D. M.; Pollack, G. M., Pharmacodynamics and tolerance development during multiple intravenous bolus morphine administration in rats. *J Pharmacol Exp Ther* **1997,** 281, (2), 713-20.

110. Lutfy, K.; Hurlbut, D. E.; Weber, E., Blockade of morphine-induced analgesia and tolerance in mice by MK-801. *Brain Res* **1993,** 616, (1-2), 83-8.

111. Bhargava, H. N.; Sharma, S. S.; Bian, J. T., Evidence for a role of N-methyl-D-aspartate receptors in L-arginine-induced attenuation of morphine antinociception. *Brain Res* **1998,** 782, (1-2), 314-7.

112. Bhargava, H. N.; Bian, J. T.; Kumar, S., Mechanism of attenuation of morphine antinociception by chronic treatment with L-arginine. *J Pharmacol Exp Ther* **1997,** 281, (2), 707-12.

113. Heinzen, E. L.; Pollack, G. M., The development of morphine antinociceptive tolerance in nitric oxide synthase-deficient mice. *Biochem Pharmacol* **2004,** 67, (4), 735-41.

114. Heinzen, E. L.; Pollack, G. M., Use of an electrochemical nitric oxide sensor to detect neuronal nitric oxide production in conscious, unrestrained rats. *J Pharmacol Toxicol Methods* **2002,** 48, (3), 139-46.

115. Heinzen, E. L.; Pollack, G. M., Pharmacokinetics and pharmacodynamics of L-arginine in rats: a model of stimulated neuronal nitric oxide synthesis. *Brain Res* **2003,** 989, (1), 67-75.

116. Heinzen, E. L.; Pollack, G. M., Pharmacodynamics of morphine-induced neuronal nitric oxide production and antinociceptive tolerance development. *Brain Res* **2004,** 1023, (2), 175-84.

117. Heinzen, E. L.; Booth, R. G.; Pollack, G. M., Neuronal nitric oxide modulates morphine antinociceptive tolerance by enhancing constitutive activity of the mu-opioid receptor. *Biochem Pharmacol* **2005,** 69, (4), 679-88.

118. Holford, N. H.; Sheiner, L. B., Kinetics of pharmacologic response. *Pharmacol Ther* **1982,** 16, (2), 143-66.

119. Ouellet, D. M.; Pollack, G. M., A pharmacokinetic-pharmacodynamic model of tolerance to morphine analgesia during infusion in rats. *J Pharmacokinet Biopharm* **1995,** 23, (6), 531-49.

PART I

USE OF CLASSICAL APPROACHES TO IMPROVE THE LINK BETWEEN PHARMACOKINETIC-PHARMACODYNAMICS

CHAPTER 3

PHARMACOKINETICS AND PHARMACODYNAMICS OF SEVEN OPIOIDS IN PGP-COMPETENT MICE ASSESSMENT OF UNBOUND BRAIN EC50S AND CORRELATION OF IN VITRO, PRECLINICAL, AND CLINICAL DATA

This chapter has been published in *Journal of Pharmacology and Experimental Therapeutics* and is presented in the style of that journal.

ABSTRACT

This study was conducted to assess the utility of unbound brain EC_{50} ($EC_{50,u}$) as a measure of in vivo potency for centrally active drugs. Seven μ-opioid agonists (alfentanil, fentanyl, loperamide, methadone, meperidine, morphine, and sufentanil) were selected as model central nervous system drugs because they elicit a readily measurable central effect (antinociception) and their clinical pharmacokinetics/pharmacodynamics are wecll understood. Mice received an equipotent subcutaneous dose of one of the model opioids. The time course of antinociception and the serum and brain concentrations were determined. A pharmacokinetic/pharmacodynamic model was used to estimate relevant parameters. In vitro measures of opioid binding affinity (K_i) and functional activity [EC_{50} for agonist stimulated guanosine 5'-*O*-(3-[^{35}S]thio)triphosphate binding] and relevant clinical parameters were obtained to construct in vitro-to-preclinical and preclinical-to-clinical correlations. The strongest in vitro-to-in vivo correlation was observed between K_i and unbound brain $EC_{50,u}$ (r^2 =0.8). A strong correlation between mouse serum and human plasma EC_{50} was observed (r^2 = 0.949); the correlation was improved when corrected for protein binding (r^2 = 0.995). Clinical equipotent i.v. dose was only moderately related to K_i. However, estimates of ED_{50}

and EC_{50} (total serum, unbound serum, total brain, and unbound brain) were significant predictors of clinical equipotent i.v. dose; the best correlation was observed for brain $EC_{50,u}$ ($r^2 = 0.982$). For each opioid, brain equilibration half-life in mice was almost identical to the human plasma effect-site equilibration half-life measured clinically. These results indicate that the mouse is a good model for opioid human brain disposition and clinical pharmacology and that superior in vitro-to-preclinical and preclinical to-clinical correlations can be achieved with relevant unbound concentrations.

INTRODUCTION

In drug discovery, in vitro assays and preclinical animal studies are widely used to assess compound potency and to identify compound(s) that may have a desirable clinical response. Several options for assessing compound potency are available, including in vitro (receptor binding or functional assays) and in vivo (animal studies to determine dose-response or concentration-response relationships) protocols. In vitro binding and functional assays, by nature, are designed to estimate the intrinsic affinity or potency at the receptor of interest, whereas in vivo experiments take into account the full spectrum of pharmacokinetic and pharmacodynamic processes that ultimately determine biological response.

Ideally, in vitro potency would translate to or predict in vivo potency. Often, this is the case, and significant correlations between in vivo ED_{50} or EC_{50} and in vitro potency have been established for a variety of therapeutic targets (Leysen et al., 1983; Visser et al., 2003). However, when there is no correlation between in vivo and in vitro potency measures, the validity of the in vitro assay, the animal model, and the target may be questioned. Therefore, establishing strong in vitro-to-in vivo relationships is a necessity for drug development, because it aids in target validation and it boosts confidence in the in vitro and in vivo pharmacology models. Historically, in vitro-to-in vivo correlations have been established by comparing an in vitro measure of affinity or potency, such as K_i or EC_{50} from a receptor binding or a cell-based functional assay, with ED_{50}. Although the ED_{50} is not necessarily the best measure of intrinsic drug potency, it has been widely used because it is a straightforward, robust, and readily attainable metric. In vitro-to-in vivo correlations with ED_{50} are most likely to be successful for a compound set, within a discrete pharmacological class, that consists of members with large differences in intrinsic potency and relatively similar pharmacokinetics.

For compounds that evidence large differences in pharmacokinetics, improved in vitro-to-in vivo correlations may be obtained by using EC_{50} as opposed to ED_{50}. Commonly, EC_{50} is estimated from the effect versus plasma concentration relationship. Pharmacokinetic/pharmacodynamic (PK/PD) modeling often is used to obtain estimates of EC_{50} from in vivo data, and it is a powerful tool for enhancing mechanistic understanding of drug disposition and action.

In vitro-to-in vivo potency relationships have maximum predictability when the relationship between biological response and biophase concentration is known. Total plasma and unbound plasma concentrations are most widely used surrogates for biophase concentrations. However, systemic concentrations do not always reflect biophase concentrations, regardless of whether or not protein binding is taken into account. This is especially true for compounds that act on targets within the central nervous system (CNS). The blood-brain barrier (BBB) restricts the CNS distribution of many compounds, and in many cases, it results in temporal dissociation between biophase and systemic concentrations. Therefore, it is important to accurately determine CNS biophase concentration, or a closely related surrogate, to make better in vitro-to-in vivo correlations for centrally active compounds. When compounds have "good" BBB permeability and they are not substrates for transporters, in vitro-to-in vivo correlations can be constructed using unbound plasma or cerebrospinal fluid (CSF) concentrations as a surrogate for CNS biophase concentrations. When unbound plasma or CSF concentrations are not reflective of CNS biophase concentrations, such as when a compound has "poor" BBB permeability or it is subject to active BBB transport, other means for estimating CNS biophase concentrations may be

needed. One method for estimating CNS biophase concentrations is simply to multiply total brain concentrations by brain unbound fraction ($f_{u,brain}$).

The present study was conducted to test the hypothesis that the brain $EC_{50,u}$ is the best in vivo measure of CNS intrinsic potency. Seven μ-opioid agonists (alfentanil, fentanyl, loperamide, methadone, meperidine, morphine, and sufentanil) were selected as probe CNS drugs. These agents were selected on the bases of having pronounced differences in potency toward the μ-opioid receptor (Terenius, 1975; Leysen et al., 1983), differing physiochemical properties (i.e., lipophilicity, unbound fractions, and permeability), and differing extent of CNS distribution (i.e., P-gp or non-P-gp substrate) (Dagenais et al., 2004). PK/PD studies were conducted in mice to determine five measures of in vivo potency (ED_{50}; total and unbound EC_{50} for both serum and brain) for each opioid. Estimates of in vitro affinity and potency (K_i and EC_{50} for agonist-stimulated [^{35}S]GTPγS binding, respectively) as well as relevant clinical parameters were obtained and used to construct in vitro-to-preclinical and preclinical-to-clinical comparisons. The most useful measure of in vivo of potency was determined by correlation analysis with the in vitro and clinical potency data.

MATERIALS AND METHODS

Materials.

Alfentanil was purchased from Taylor Pharmaceuticals (Decatur, IL). Fentanyl, loperamide, methadone, morphine, and oxycodone were purchased from Sigma-Aldrich (St. Louis, MO). Meperidine was obtained from Spectrum Chemicals and Laboratory Products (Gardena, CA). Sufentanil was purchased from Abbott Laboratories (North Chicago, IL). [^{35}S]GTPγS (1250 Ci/mmol) was purchased from PerkinElmer Life and Analytical Sciences (Boston, MA). All opioid drugs used in the [^{35}S]GTPγS binding assay were obtained from the

Drug Supply Program of the National Institute on Drug Abuse (Bethesda, MD). Adenosine deaminase, GTPγS, and GDP were purchased from Sigma-Aldrich. All other reagents were obtained from common sources, and they were of reagent grade or better.

Animals.

Male CF-1 *mdr1a*(+/+) mice (30–40 g; Charles River Laboratories, Inc., Wilmington, MA) were maintained on a 12-h light/dark cycle in a temperature- and humidity-controlled room with access to water and food ad libitum. All procedures involving mice were approved by either The Institutional Animal Care and Use Committee of the University of North Carolina or The Institutional Animal Care and Use Committee at Virginia Commonwealth University, and they were conducted in accordance with Principles of Laboratory Animal Care (National Institutes of Health Publication 85-23, revised in 1985).

Agonist Stimulated [^{35}S]GTPγS Binding in Membrane Homogenates.

Mice were sacrificed by decapitation, and the thalamus was dissected on ice. Tissue was homogenized in membrane buffer (50 mM Tris-HCl, 3 mM $MgCl_2$, and 1 mM EGTA, pH 7.4) with a Polytron homogenizer (Brinkmann Instruments, Westbury, NY), centrifuged at 50,000*g* for 10 min at 4°C, resuspended in membrane buffer, and stored in aliquots of ~2 mg/ml at –80°C until use. Membranes were thawed and diluted 10-fold in assay buffer, centrifuged as described above, resuspended in assay buffer (50 mM Tris-HCl, 3 mM $MgCl_2$, 50 mM KCl, 50 mM NaCl, and 0.2 mM EGTA, pH 7.4), and preincubated for 10 min at 30°C with 4 mU/ml adenosine deaminase to remove endogenous adenosine. Protein was then determined by the Bradford method (Bradford, 1976). Each assay tube contained membranes (10 μg protein/tube), 0.1 nM [^{35}S]GTPγS, 10 μM GDP, and appropriate agonist in a 1-ml total volume. Basal binding was assessed in the absence of agonist, and nonspecific binding

was measured with 20 μM unlabeled GTPγS. Assay tubes were incubated for 2 h at 30°C. The reaction was terminated by filtration under vacuum through Whatman GF/B glass fiber filters (Whatman, Maidstone, UK), followed by three washes with ice-cold Tris buffer. Bound radioactivity was determined by liquid scintillation spectrophotometry, at 95% efficiency for ^{35}S, after overnight extraction of the filters. Agonist-stimulated [^{35}S]GTPγS binding was determined from four to six separate experiments performed in duplicate for each opioid. Net agonist-stimulated [^{35}S]GTPγS binding was defined as agonist-stimulated minus basal binding. Percentage of stimulation was defined as (net agonist-stimulated [^{35}S]GTPγS binding/basal binding) x 100%. Percentage of maximal stimulation was defined as (net stimulation by agonist/net stimulation by 10 μM [D-Ala^2,*N*-Me-Phe^4,Gly^5-ol]-enkephalin) x 100%. EC_{50} and E_{max} values were determined by nonlinear regression analyses of concentration-effect curves by iterative curve-fitting using GraphPad Prism 4 (GraphPad Software Inc., San Diego, CA).

Pharmacokinetic/Pharmacodynamic Study.

Based on the results of pilot experiments, 36 *mdr1a*(+/+) CF-1 mice in total received a single equipotent subcutaneous dose of alfentanil (0.2 mg/kg), fentanyl (0.09 mg/kg), loperamide (50 mg/kg), methadone (0.6 mg/kg), meperidine (25 mg/kg), morphine (3.6 mg/kg), or sufentanil (0.001 mg/kg). Fentanyl and loperamide were prepared in 50:50 propylene glycol/water, whereas the remaining opioids were prepared in 0.9% saline. Antinociception was assessed at selected time points, and four mice per opioid were sacrificed by decapitation for collection of brain tissue and blood samples. Trunk blood was collected in 1.5-ml microcentrifuge tubes, and it was allowed to clot for ~30 min at room

temperature. Serum was harvested after centrifugation. Brain and serum samples were stored at –20°C until analysis by HPLC-MS/MS.

Assessment of Antinociception.

Antinociception was assessed with the hot-plate latency test as described previously (Chen and Pollack, 1997). Before opioid administration, baseline hot-plate latency was determined for each animal in triplicate. Hot-plate latency was defined as the time interval between placement on the hot-plate (55°C; Columbus Instruments, Columbus, OH) and the first observation of a jump or lick of a hind limb. Only animals with an average baseline latency <25 s were used in this study. A cut-off latency of 60 s was established to avoid tissue damage. The degree of antinociception, expressed as percent maximal possible response (%MPR), was calculated as follows:

$$\%MPR = \frac{Test\ latency - Control\ latency}{60 - Control\ latency} x\ 100\% \qquad \text{(Eqn. 3.1)}$$

Evaluation of Protein Binding.

Plasma and brain unbound fractions were determined in a 96-well equilibrium dialysis apparatus (HTDialysis, Gales Ferry, CT) using a previously reported method (Kalvass and Maurer, 2002). In brief, fresh mouse plasma and brain tissue were obtained the day of the study. Spectra-Por 2 membranes obtained from Spectrum Laboratories Inc. (Rancho Dominguez, CA) were conditioned in HPLC water for 15 min, followed by 30% ethanol for 15 min, and 100 mM sodium phosphate, pH 7.4, buffer for 15 min. Brain tissue was diluted 3-fold with 100 mM sodium phosphate, pH 7.4, buffer, and it was homogenized with a sonic probe. The drug of interest was added to samples of plasma and brain tissue homogenate (3

and 1 μM, respectively), and 150-μl aliquots (n = 6) were loaded into the 96-well equilibrium dialysis apparatus and dialyzed against an equal volume of 100 mM sodium phosphate, pH 7.4, buffer for 4.5 h in a 155-rpm shaking water bath maintained at 37°C. Prior experience with the equilibrium dialysis apparatus indicated that equilibrium would be achieved by the end of the specified incubation period (data not shown). After incubation, 10 μl of matrix (plasma or brain homogenate) and 50 μl of buffer were removed from the apparatus and added directly to HPLC vials containing 100 μl of an appropriate internal standard in methanol. A 50-μl aliquot of control buffer was added to the brain homogenate and plasma samples, and a 10-μl aliquot of either control brain homogenate or control plasma was added to the buffer samples, to yield identical matrix composition for all samples before analysis. The samples were vortex-mixed and centrifuged, and the supernatant was analyzed by the HPLC-MS/MS as described below. Plasma unbound fraction was calculated from the ratio of concentrations determined in buffer versus plasma samples. Equation 3.2, which accounts for the effect of tissue dilution on unbound fraction (Kalvass and Maurer, 2002), was used to calculate the brain unbound fraction:

$$Undiluted\ f_u = \frac{\frac{1}{D}}{\left(\left(\frac{1}{f_{u,measured}}\right) - 1\right) + \frac{1}{D}} \qquad \text{(Eqn. 3.2)}$$

where D represents the -fold dilution of brain tissue, and $f_{u,measured}$ is the ratio of concentrations determined in buffer versus brain homogenate samples.

Quantitation of Serum and Brain Concentrations.

Opioid brain and serum concentrations were measured using previously described methods with slight variation (Kalvass et al., 2007a). In brief, brain samples were

homogenized in water [1:2 (v/v)] via sonic probe. An aliquot (2–25 µl) of homogenate or serum was transferred to an HPLC vial, and protein was precipitated with 4 to 125 volumes of methanol containing internal standard (5 ng/ml loperamide for alfentanil, fentanyl, meperidine, methadone, and sufentanil; 20 ng/ml methadone for loperamide; and 100 ng/ml oxycodone for morphine). The sample was vortex-mixed and centrifuged, and the supernatant was analyzed by HPLC-MS/MS. Samples were injected (2–10 µl; autosampler, CTC Analytics, Zwingen, Switzerland) onto a Gemini 110A column (2.0 x 30 mm; 5 µm) (Phenomenex, Torrance, CA) maintained at room temperature. The total run time was 3 min. Analytes were eluted with a linear gradient consisting of 10 mM ammonium acetate, pH 6.8 (A), and methanol (B) produced by two LC-10ADVP binary pumps (Shimadzu, Kyoto, Japan). An initial condition of 5% B was ramped to 95% B over 2 min, held for 0.5 min, and then returned initial condition of 5% B in a single step to re-equilibrate the column. During the run, the flow rate was increased from 750 to 1500 µl/min over the first 2 min, held at 1500 µl/min for 1 min, and then returned the initial flow rate of 750 µl/min in a single step. For the morphine samples, the initial conditions were held for 0.5 min before ramping the gradient and flow rate. The entire column effluent was diverted from the source of the PE Sciex API-4000 quadrupole mass spectrometer (Turbo V Ionspray source, 700°C; PerkinElmerSciex Instruments, Boston, MA) for the first 0.8 min and last 0.5 min of the run. Alfentanil, fentanyl, loperamide, methadone, meperidine, morphine, oxycodone, and sufentanil were measured in positive ionization mode using multiple reaction monitoring (417.3→268.3, 337.1→188.3, 477.4→266.0, 248.3→220.3, 310.3→265.2, 286.1→201.1, 316.0→298.0, and 387.2→238.4, respectively). Standard curves were prepared in brain

homogenate, serum, plasma, or buffer, and they were identical in composition to corresponding samples. Accuracy of standards and interassay variability was within ± 20%.

Pharmacokinetic/Pharmacodynamic Analysis.

A compartmental modeling approach with distribution between serum and brain tissue was used to describe opioid pharmacokinetics. The pharmacokinetic model in Fig. 3.1 was fitted simultaneously to the serum concentration- and brain concentration-time data using nonlinear least-squares regression (WinNonlin 4.1; Pharsight Corporation, Mountain View, CA). The brain volume (V_{Br}) was fixed at 13.4 ml/kg, assuming a specific gravity of 1.0 g/ml (Kalvass et al., 2007b). All other pharmacokinetic parameters were obtained from fitting the kinetic model to the data. The pharmacodynamic parameters EC_{50} and γ were determined from fitting a sigmoidal E_{max} model to the antinociception versus brain concentration (C) data.

$$\%MPR = \frac{E_{\max}\ x\ C^{\gamma}}{EC_{50} + C^{\gamma}} \qquad \text{(Eqn. 3.3)}$$

E_{max} was defined as 100%. Serum EC_{50} was calculated from the following equation:

$$Serum\ EC_{50} = \frac{Brain\ EC_{50}}{K_{p,brain,ss}} \qquad \text{(Eqn. 3.4)}$$

The ED_{50} was calculated, assuming linear pharmacokinetics, from the maximum brain concentration predicted by the PK model (brain C_{max}), the opioid dose (X_0), and the brain EC_{50}.

$$ED_{50} = \frac{Brain\ EC_{50}}{Brain\ C_{max}} x\ X_0 \qquad \text{(Eqn. 3.5)}$$

The time course of the brain-to-serum ratio ($K_{p,brain}$) for each opioid was used to estimate the brain equilibration rate constant (k_{eq}) and steady-state brain-to-serum ratio ($K_{p,brain,ss}$) for that compound according to the following equation:

$$K_{p,brain} = K_{p,brain,ss}\,(1 - e^{-k_{eq}\,x\,t}) \qquad \text{(Eqn. 3.6)}$$

The brain equilibration half-life ($t_{1/2eq,brain}$) was obtained from k_{eq} as follows:

$$t_{\frac{1}{2},eq,brain} = \frac{0.693}{k_{eq}} \qquad \text{(Eqn. 3.7)}$$

RESULTS

The dose administered to produce equivalent antinociception in mice varied by more than 4 orders of magnitude between the most and least potent opioid (0.001 versus 50 mg/kg for sufentanil and loperamide, respectively). Likewise, the calculated mouse ED_{50} varied by nearly 5 orders of magnitude (Table 3.1). The large range of effective doses was advantageous for subsequent construction of relationships between various in vitro and in vivo metrics of response.

The pharmacokinetic/pharmacodynamic model adequately described the time course of antinociception, as well as the brain tissue concentration versus time and serum concentration versus time relationships, for each of the opioids studied (Fig. 3.2, A-G). With the exception of fentanyl, the systemic pharmacokinetics of all of the opioids were most effectively modeled with a single compartment system and first-order absorption from the site of administration (Table 3.2; Fig. 3.2). The disposition of fentanyl required addition of a peripheral distributional compartment with associated parameters [apparent peripheral distributional space (V_p); distributional clearance (Cl_d)]. Estimates of relevant pharmacokinetic parameters for each of the opioids are reported in Table 3.2.

Pharmacokinetic/pharmacodynamic modeling revealed counterclockwise hysteresis in the antinociception versus serum concentration relationship for each opioid (Fig. 3.3), consistent with delayed distribution between serum concentrations and biophase concentrations. In contrast, all of the opioids exhibited a sigmoidal relationship between antinociception and brain tissue concentration, with no evidence of significant hysteresis behavior associated with temporal dissociation between CNS pharmacokinetics and pharmacodynamics (Fig. 3.4). Brain EC_{50} and γ values are reported in Table 3.2. Brain EC_{50} estimates differed by more than 2000-fold between the most (sufentanil) and the least (meperidine) potent opioid. Similarly the serum, unbound serum, and unbound brain EC_{50} estimates evidenced a wide range among the seven opioids. Depending on the particular EC_{50} value used as a metric (total brain, unbound brain, total serum, or unbound serum), the rank order of opioid potency differed considerably as a consequence of large differences in $K_{p,brain,ss}$, $f_{u,plasma}$, and $f_{u,brain}$ among the opioids.

$K_{p,brain,ss}$ values differed by more than 50-fold among the opioids (Table 3.2; Fig. 3.5). The lowest $K_{p,brain,ss}$ was observed for loperamide (0.115), and the highest was for meperidine (6.8). The $t_{1/2eq,brain}$ ranged from 1 to 74 min, with alfentanil and morphine having the shortest and longest $t_{1/2eq,brain}$, respectively (Table 3.2).

The in vitro K_i (obtained from the literature) and GTPγS EC_{50} values were strongly correlated ($r^2 > 0.9$; data not shown). In every case, the in vitro-to-in vivo correlation using K_i was stronger than the corresponding correlation using GTPγSEC_{50} (data not shown). However, the strengths of the various in vitro-to-in vivo correlations were the same relative to each other whether K_i or GTPγS EC_{50} was used. Therefore, only the in vitro-to-in vivo relationships with K_i are reported. In vitro-to-in vivo relationships (Fig. 3.6) revealed that

mouse serum EC_{50} and brain EC_{50} correlated poorly with in vitro K_i ($r^2 < 0.5$). A modest improvement was observed for the correlation between unbound serum $EC_{50,u}$ and K_i ($r^2 = 0.583$). The strongest relationship observed was between unbound brain $EC_{50,u}$ and K_i ($r^2 < 0.799$).

Preclinical-to-clinical relationships indicated that mouse serum and human plasma EC_{50} estimates were well correlated ($r^2 = 0.949$). Despite the strength of this relationship, the correlation was improved when the EC_{50} values were corrected for binding to plasma proteins ($r^2 = 0.995$) (Fig. 3.7). Correlations also were explored between human equipotent clinical i.v. dose of the opioids and various estimates of in vitro and in vivo potency (Fig. 3.8). The relationship between equipotent clinical dose and K_i was relatively poor ($r^2 = 0.677$). Equipotent clinical i.v. dose correlated more strongly with mouse ED_{50} ($r^2 = 0.932$). Equipotent clinical i.v. dose also correlated equally well with total and unbound mouse serum EC_{50} ($r^2 = 0.922$ and $r^2 = 0.937$, respectively). Somewhat surprisingly, equipotent clinical i.v. dose did not correlate as well with total brain EC_{50} ($r^2 = 0.878$) compared with the relationships with metrics obtained from plasma. However, the equipotent clinical i.v. dose correlated most strongly with unbound brain $EC_{50,u}$ values in the mouse ($r^2 = 0.982$).

The brain equilibration half-life in mouse determined in the present study ($t_{1/2eq,brain}$) was compared with the apparent plasma-biophase equilibration half-life in humans ($t_{1/2,Ke0}$), obtained from the literature, among the opioids examined in this study. The log-log correlation between clinical $t_{1/2,Ke0}$ and mouse $t_{1/2eq,brain}$ was excellent ($r^2 = 0.988$). With the exception of morphine, all of the opioids fell within a factor of 1.4-fold relative to the line of identity (Fig. 3.9).

DISCUSSION

An integrated pharmacokinetic/pharmacodynamic modeling strategy yielded an adequate description of the time course of antinociception, serum concentrations, and brain tissue concentrations for each of the opioids examined in this study. Differences in systemic pharmacokinetics among the opioids were relatively small (~10-fold for Cl) compared with differences in vivo potency measures (~30,000-fold) and brain pharmacokinetics (>70-fold for $K_{p,brain}$, $t_{1/2eq,brain}$, and Cl_{up}).

In Vitro-to-Preclinical Correlations.

Previous studies have established in vitro-to-preclinical correlations for opioid potency using K_i. Leysen et al. (1983) reported a correlation ($r^2 = 0.81$) between in vitro K_i (displacement of sufentanil in rat forebrain membranes) and ED_{50} (rat tail withdrawal reflex) for 35 opioids from five structural classes, with >100,000-fold difference in receptor affinity. However, no correlation existed between K_i and ED_{50} if only the seven opioids from this study were included in their analysis ($r^2 < 0.15$) (Niemegeers et al., 1979; Leysen et al., 1983). Results from this study show a similarly poor correlation ($r^2 = 0.167$) between in vitro K_i and mouse ED_{50}. This lack of correlation can be largely attributed to differences in pharmacokinetics and biophase distribution characteristics for the seven opioids. The opioids selected for this study come from four different structural classes and several are known P-gp substrates (Dagenais et al., 2004). Consequently, these opioids have different physiochemical properties and CNS (biophase) distribution characteristics. One would anticipate that K_i would be a better predictor of biophase EC_{50}, because the confounding influences of pharmacokinetics and biophase distribution are removed.

Total plasma, unbound plasma, and CSF concentrations have been used to estimate CNS biophase concentration for in vitro-to-in vivo correlations. Visser et al. (2003) demonstrated that, for nine $GABA_A$ modulators, in vitro-to-in vivo correlations could be made between K_i and either total or unbound plasma EC_{50}; however, the unbound plasma EC_{50} correlated better with K_i than total plasma EC_{50}. Another study demonstrated the in vitro K_i of alfentanil, fentanyl, and sufentanil correlated well with the in vivo EC_{50} determined from CSF concentrations (Cox et al., 1998).

In the present study, total plasma, total brain, unbound plasma, and unbound brain EC_{50} estimates were used to express opioid potency, and they were evaluated as potential surrogates for biophase EC_{50}. Unbound EC_{50} values were calculated by multiplying the total EC_{50} by the appropriate unbound fraction value ($f_{u,plasma}$ or $f_{u,brain}$) determined from equilibrium dialysis experiments conducted in accordance with the methods of Kalvass and Maurer (2002). The total serum and total brain EC_{50} values were weakly related to in vitro K_i ($r^2 < 0.5$). A modest improvement was observed with unbound serum $EC_{50,u}$ ($r^2 = 0.583$). However, the strongest relationship was observed between unbound brain $EC_{50,u}$ and K_i ($r^2 = 0.799$). These results, along with the hysteresis in the antinociception versus serum concentration relationship and the sigmoidal relationship between antinociception and brain concentration, suggest that unbound brain concentrations determined with $f_{u,brain}$, estimated from brain-homogenate equilibrium-dialysis approach, represent an optimal surrogate for CNS biophase concentrations. Furthermore, these results highlight the importance of using an appropriate surrogate for biophase concentration, presumably unbound concentration at the site of action, when making in vitro-to-in vivo correlations.

In this study, the in vitro parameter GTPγSEC_{50} was also used to construct in vitro-to-in vivo correlations. In every case, the correlation using K_i was stronger than the corresponding correlation using GTPγS EC_{50} (data not shown). It is unclear why in vivo EC_{50} values correlated better with receptor binding K_i values than with EC_{50} values obtained from [^{35}S]GTPγS experiments. Intuitively, one might expect an improved correlation between two functional measures of receptor activation than between in vivo function and receptor binding. However, differences in the intrinsic efficacy of agonists in the [^{35}S]GTPγS assay are generally observed as differences in maximal effect because receptor reserve for G protein activation in this assay is low, especially in native tissues such as brain (Selley et al., 1998). However, an attempt was made to adjust assay conditions to minimize E_{max} differences between full and partial agonists by decreasing both sodium and GDP concentrations relative to standard assay conditions (Selley et al., 1997, 2000) so that differences in intrinsic efficacy would be observed as potency differences. Nonetheless, under these optimized conditions, there were still slight E_{max} differences, which ranged from 73 to 85% of the full agonist [D-Ala^2,*N*-Me-Phe^4,Gly^5-ol]-enkephalin (data not shown). It should be noted that measurement of high-affinity agonist binding is also dependent on the formation of functional receptor-G protein complexes, so that these measurements when made in the absence of sodium and guanine nucleotides apparently provided slightly better correlation than EC_{50} values obtained from direct measurement of G protein activation with the [^{35}S]GTPγS assay.

Preclinical-to-Clinical Correlations.

Human efficacious plasma concentrations are often predicted from total plasma concentrations in preclinical efficacy models (Danhof et al., 1993; Ito et al., 1993). Assuming the drug has similar pharmacology and plasma protein binding in humans and preclinical

models, this prediction should be valid. In the present study, mouse total serum EC_{50} correlated well with human total plasma EC_{50} (r^2 = 0.949), consistent with similarities between mouse and human opioid pharmacology and plasma protein binding. However, the correlation improved when EC_{50} values were corrected for protein binding (r^2 = 0.995). On average, mouse unbound serum $EC_{50,u}$ overpredicted human unbound human plasma $EC_{50,u}$ by 2.8-fold. The murine model seems to be a remarkably effective predictor of relative human efficacious serum concentrations among a set of μ-opioids, even when those compounds are derived from different chemical classes.

The ability to predict human dose from in vitro and preclinical data are important. Clinical dose often correlates with ED_{50} obtained from animal models. For example, Niemegeers et al. (1979) demonstrated that rat ED_{50} determined for antidiarrheal and analgesic activity strongly correlated with clinical dose for 12 opioids. In the present study, the equipotent clinical i.v. dose and mouse ED_{50} correlated well for the seven opioids examined (r^2 = 0.932). Although efficacious dose is dependent on many factors, including systemic disposition, target-site pharmacokinetics, and intrinsic potency, the observed differences in efficacious dose for the examined opioids seem to be dominated by intrinsic potency. Therefore, any reliable measure of opioid in vivo intrinsic potency should correlate well with the clinical equipotent i.v. dose for these opioids.

Various in vitro and in vivo measures of opioid potency were correlated with clinical equipotent i.v. dose to evaluate predictive potential. The in vitro K_i was a weak predictor of equipotent clinical i.v. dose (r^2 = 0.677). Equipotent clinical dose correlated better with in vivo measures, including mouse ED_{50} (r^2 = 0.932) and total or unbound mouse serum EC_{50} (r^2 = 0.922 and r^2 = 0.937, respectively). It was surprising that equipotent clinical dose did

not correlate as well with total brain EC_{50} values (r^2 = 0.879) as with either serum concentration measure or murine effective dose, suggesting that nonspecific opioid binding in brain is substantial. As expected, the equipotent clinical dose correlated best with unbound brain $EC_{50,u}$ (r^2 = 0.982), consistent with unbound brain $EC_{50,u}$ being the best measure of in vivo intrinsic opioid potency.

It is interesting to note that the $t_{1/2eq,brain}$ determined in mice, derived from the kinetics of drug equilibration between brain tissue and serum (Fig. 3.5), was almost identical to the clinical $t_{1/2,Ke0}$, an inferred value from the kinetics of pharmacological response in the context of kinetics of systemic disposition (Fig. 3.9). Morphine evidenced the largest discrepancy between these metrics, with $t_{1/2,Ke0}$ being 2.4-fold larger than mouse $t_{1/2eq,brain}$. Morphine-6-glucuronide, an active metabolite of morphine in humans (Glare and Walsh, 1991) that is not formed extensively in mice, possesses a long $t_{1/2,Ke0}$ (>3600 min; Lötsch, 2005). Because morphine and its active metabolite exist in combination after morphine administration in humans, the $t_{1/2,Ke0}$ estimate obtained will reflect the contribution of both parent drug and metabolite. The remarkable relationship between $t_{1/2,Ke0}$ and $t_{1/2eq,brain}$, together with the strong interspecies correlation between unbound serum/plasma EC_{50}, suggests that the brain distribution characteristics are similar between humans and mice.

Relative Potency and $K_{p,brain}$.

Even though all seven opioids examined are μ-agonists, they do not have the same primary indication. The primary indication of a given opioid seems not to be related mainly to intrinsic opioid potency, but rather to differences in brain distribution characteristics and systemic pharmacokinetics. For example, the two anesthetic opioids, alfentanil and sufentanil, have the shortest mouse systemic half-life (8 and 14 min, respectively) and $t_{1/2eq,brain}$ (1 and 4

min, respectively) of the opioids examined. The short systemic half-life, combined with the short $t_{1/2eq,brain}$, results in a rapid onset and offset of action, allowing for rapid adjustment of response during i.v. infusion. Fentanyl, methadone, meperidine, and morphine, in contrast, have longer half-lives and $t_{1/2eq,brain}$, rendering them more suitable as analgesics. The brain distribution of loperamide is limited due to P-gp-mediated efflux (Schinkel et al., 1996), allowing it to act selectively on μ-opioid receptors in the intestinal tract versus the CNS and conferring ideal antidiarrheal properties. These relationships indicate that systemic pharmacokinetics and biophase distribution characteristics are more important than intrinsic potency for optimizing an opioid action toward a given indication (anesthetic, analgesic, or antidiarrheal). Undoubtedly, potency and biophase distribution characteristics must be balanced with other properties and considerations (i.e., solubility, permeability, bioavailability, systemic clearance, and half-life) to achieve compounds that will be useful clinical agents. However, the current data clearly indicate the importance of target-site pharmacokinetics and activity in determining qualitative, as well as quantitative, clinical response.

$K_{p,brain}$ often is used as a measure of CNS exposure, under the assumption that larger values of $K_{p,brain}$ equate with higher CNS exposure. CNS drug discovery programs have devoted much effort and resources to predicting and maximizing the $K_{p,brain}$ of drug candidates. Although not the main intent of this work, the results presented herein can be used to illustrate the fallacy of pursing this strategy. As demonstrated previously, K_i, ED_{50}, EC_{50}, and equipotent i.v. clinical doses are appropriate parameters for constructing in vitro-to-in vivo and preclinical-to-clinical correlations. The same cannot be said for $K_{p,brain}$. Even though $K_{p,brain}$ values differed by more than 50-fold among the opioids examined, there was

no correlation between $K_{p,brain}$ and any relevant pharmacodynamic parameter ($r^2 < 0.2$) for K_i, EC_{50}, $EC_{50,u}$, ED_{50}, equipotent i.v. clinical dose, $f_{u,plasma}$, $f_{u,brain}$, $t_{1/2eq,brain}$, and $t_{1/2,Ke0}$). With the exception of loperamide, all of the opioids examined are marketed as CNS-active drugs exhibiting $K_{p,brain}$ values ranging between 0.19 and 6.8. This large range of $K_{p,brain}$ values, which was not meaningfully correlated with any relevant measure of opioid action, indicates that $K_{p,brain}$ is not a useful parameter. In contrast to $K_{p,brain}$, the unbound brain and unbound plasma concentrations were useful for in vitro-to-in vivo and preclinical-to-clinical predictions, and the ratio of unbound brain to unbound plasma concentrations better reflects pharmacologically relevant brain exposure.

In summary, these results suggest that the mouse is a good model for opioid brain disposition and pharmacology and that superior in vitro-to-preclinical and preclinical-to-clinical correlations can be established when making comparisons between relevant unbound concentrations.

Table 3.1. Additional parameters used for correlation of i*n vitro*, preclinical, and clinical data.

Parameter	alfentanil	fentanyl	loperamide	meperidine	methadone	morphine	sufentanil
In Vitro Ki (nM) [a]	19	1.6	0.50 [b]	193	2.2	5.7	0.10
Mouse ED_{50} (mg/kg)	0.079	0.020	36	3.2	2.2	0.94	0.00041
Mouse $f_{u,plasma}$ [c]	0.26	0.17	0.029	0.36	0.15	0.50	0.054
Mouse $f_{u,brain}$ [c]	0.33	0.070	0.0047	0.13	0.029	0.41	0.034
Human Plasma EC_{50} (nM) [d]	1337	24	n.a.	6034 [e]	1151	195	1.8
Human Equipotent IV dose (mg) [f]	0.75	0.10	n.a.	90	8.75	10	0.015
Human $t_{1/2,Ke0}$ (min) [d]	1.0	5.8	n.a.	-	12	178	6.2
Human $f_{u,plasma}$	0.079 [g]	0.156 [g]	-	0.35 [e]	0.125 [h]	0.75 [i]	0.75 [g]

N.A., Not Available.

[a] (Leysen et al., 1983)

[b] (Terenius, 1975)

[c] (Kalvass and Pollack 2006).

[d] Average from EEG power spectrum analysis, analgesia (cancer pain), pain tolerance, and/or post operative analgesia; (Lotsch, 2005)

[e] Unbound potency of meperidine is 20 time less than alfentanil; (Kurz et al., 1997)

[f] (Wood and Alastair, 1990)

[g] (Meuldermans et al., 1982)

[h] (Inturrisi et al., 1987)

[i] (Glare and Walsh, 1991)

Table 3.2. Parameter estimates from PK-PD modeling.

Parameter	alfentanil	fentanyl	loperamide	meperidine	methadone	morphine	sufentanil
K_a (min^{-1})	0.35 ± 0.03	0.07 ± 0.07	0.063 ± 0.015	0.39 ± 0.18	0.55 ± 0.13	0.27 ± 0.04	0.32 ± 0.12
Cl ($ml \cdot min^{-1} \cdot kg^{-1}$)	82 ± 3	90 ± 40	58 ± 7	190 ± 40	127 ± 12	95 ± 5	19 ± 3
V_c ($ml \cdot kg^{-1}$)	1000 ± 60	3000 ± 3000	32000 ± 3000	6100 ± 1200	8800 ± 600	2900 ± 180	400 ± 80
Cl_d ($ml \cdot min^{-1} \cdot kg^{-1}$)	-	40 ± 30	-	-	-	-	-
V_p ($ml \cdot kg^{-1}$)	-	5000 ± 13000	-	-	-	-	-
Cl_{up} ($ml \cdot min^{-1} \cdot kg^{-1}$)	4 ± 3	8 ± 3	0.04 ± 0.06	100 ± 40	27 ± 4	9.5 ±0.5	37 ± 14
Cl_{efflux} ($ml \cdot min^{-1} \cdot kg^{-1}$)	22 ± 17	3.4 ± 1.4	0.3 ± 0.5	8 ± 4	5.1 ± 0.9	1.9 ± 1.4	12 ± 5
EC_{50} (ng/g)	9.2 ± 1.7	6.4 ± 1.1	100 ± 6	2200 ± 110	510 ± 60	38 ± 4	1.0 ± 0.2
γ	1.8 ± 0.4	1.4 ± 0.3	2.7 ± 0.5	7.8 ± 4.2	3.7 ± 1.1	2.3 ± 0.5	2.5 ± 1.3
$K_{p,brain}$	0.195 ± 0.0087	2.3 ± 0.2	0.115 ± 0.014	6.8 ± 0.5	3.3 ± 0.2	1.1 ± 0.6	2.1 ± 0.3
K_{eq} (min^{-1})	0.64 ± 0.09	0.14 ± 0.04	0.025 ± 0.010	0.13 ± 0.03	0.073 ± 0.014	0.009 ± 0.006	0.16 ± 0.06
$t_{1/2eq,brain}$ (min)	1.08 ± 0.16	4.9 ± 1.3	27 ± 11	5.4 ± 1.1	9.6 ± 1.8	74 ± 45	4.3 ± 1.6

Parameter estimate ± S.E. from non-linear regression analysis of pooled *mdr1a*(+/+) mouse data. $t_{1/2eq,brain}$ were calculated from $0.693/K_{eq,brain}$.

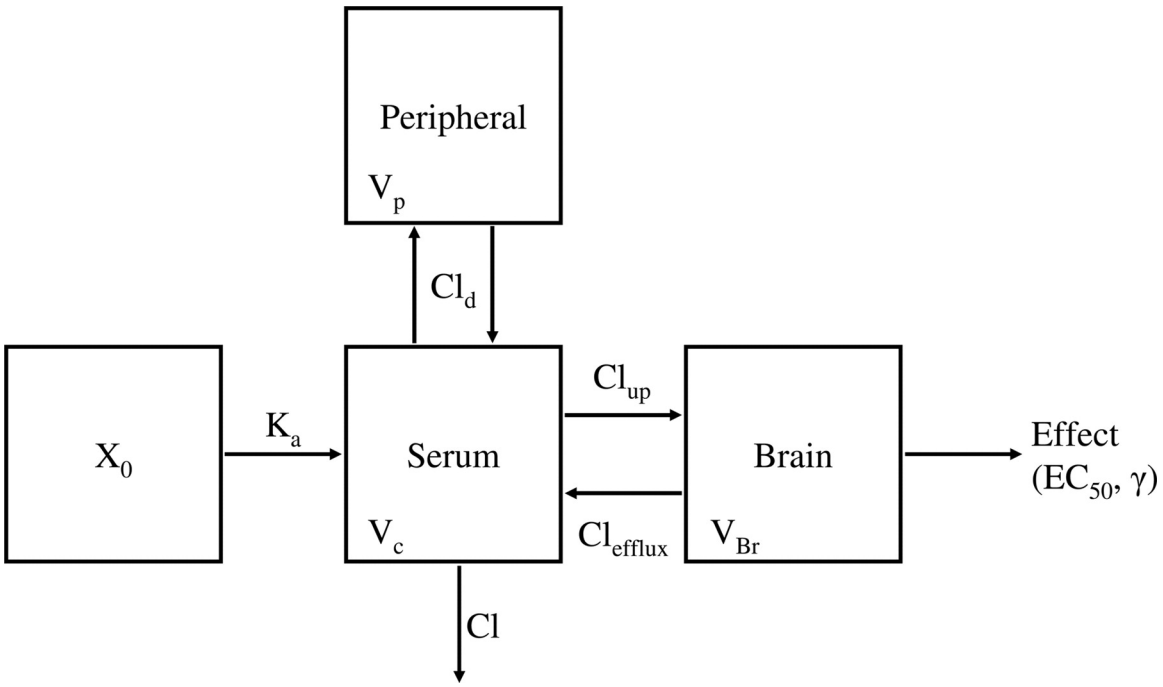

Figure 3.1. Pharmacokinetic/pharmacodynamic model for opioid disposition and antinociception in mice. Pharmacokinetic parameters were obtained by fitting the model to the time course of serum and brain concentrations in *mdr1a*(+/+) mice after subcutaneous administration. The absorption rate constant (K_a), central volume (V_c), systemic clearance (Cl), V_p, Cl_d, brain uptake clearance (Cl_{up}), and brain efflux clearance (Cl_{efflux}) were estimated for each opioid. The V_{Br} was fixed. The effect parameters EC_{50} and γ were obtained by fitting a sigmoidal E_{max} model to the brain concentration versus antinociception data. E_{max} was defined as 100%.

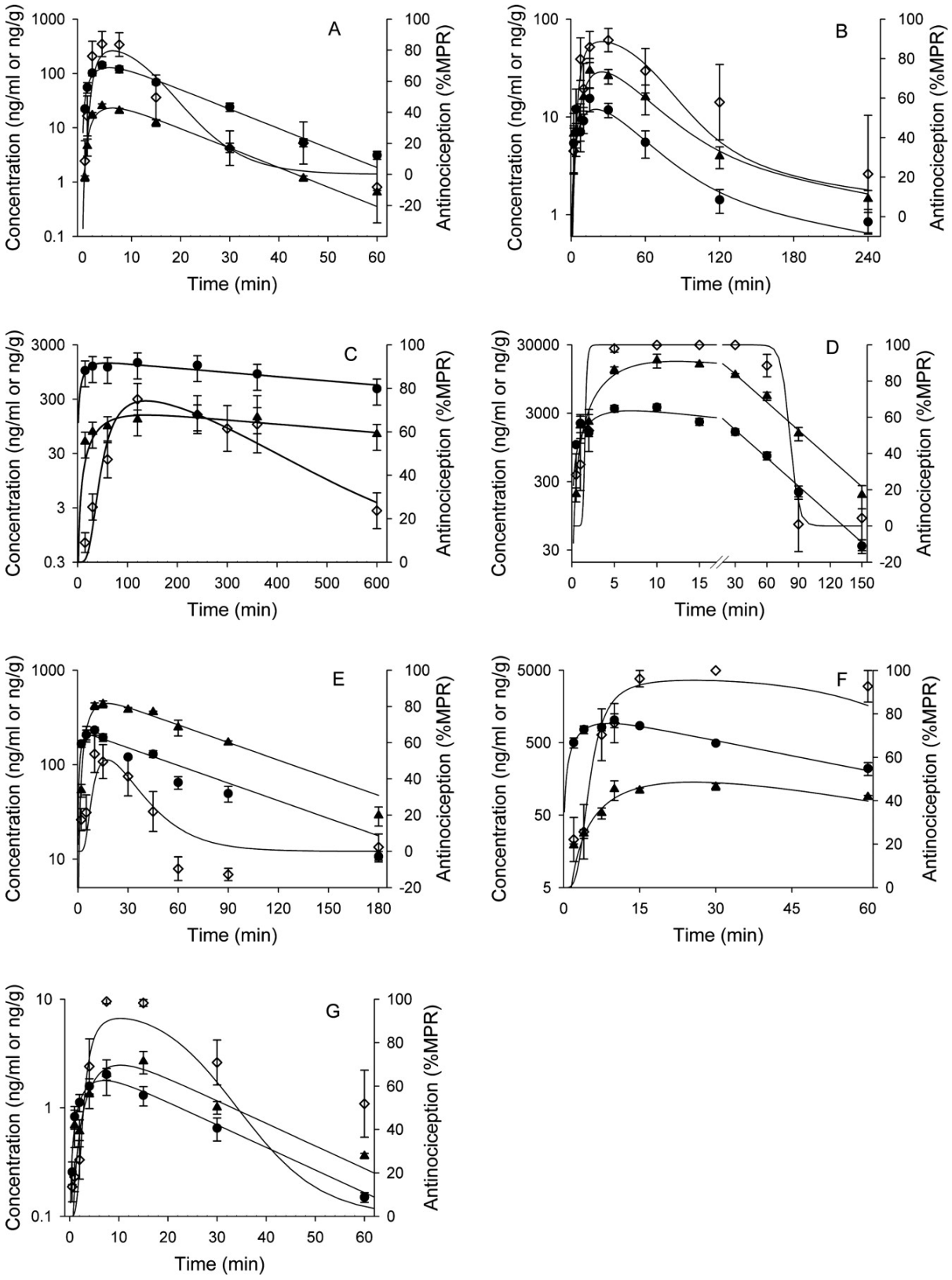
A
B
C
D
E
F
G
Concentration (ng/ml or ng/g)
Antinociception (%MPR)
Time (min)

Figure 3.2. Time course of antinociception (◇), serum (●) and brain (▲) concentrations after 0.2 mg/kg s.c. dose of alfentanil (A), 0.9 mg/kg s.c. dose of fentanyl (B), 50 mg/kg s.c. dose of loperamide (C), 25 mg/kg s.c. dose of meperidine (D), 2 mg/kg s.c. dose of methadone (E), 3.6 mg/kg s.c. dose of morphine (F), or 0.001-mg/kg s.c. dose of sufentanil (G) in CF-1 *mdr1a*(+/+) mice. Data are presented as mean ± S.E. [concentration data ($n \geq 3$); antinociception (n = 4–36)]. Lines represent the fit of the PK/PD model to the antinociception and concentration data.

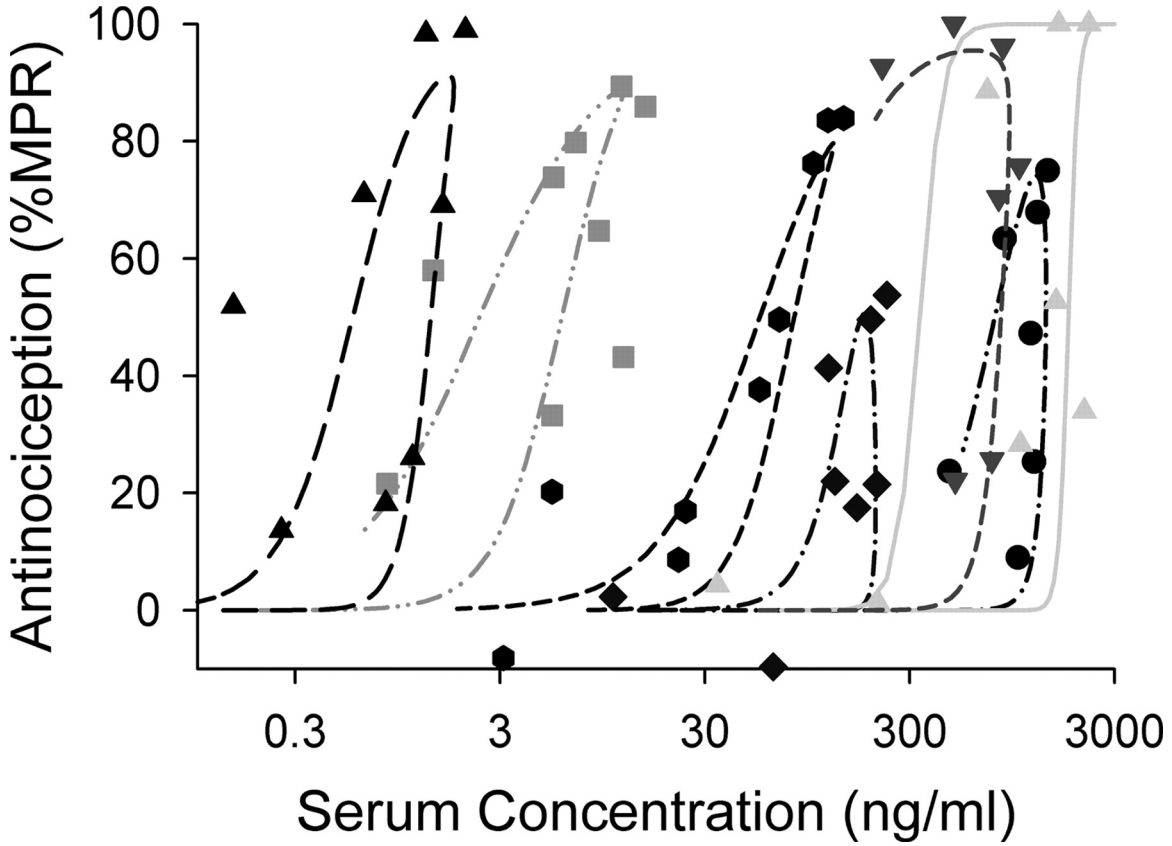

Figure 3.3. Relationship between plasma concentration and antinociception for μ-opioid agonists. Symbols represent data from CF-1 *mdr1a*(+/+) mice. Lines represent the fit of the PK/PD model to the antinociception-serum concentration data. Symbols are as follows: sufentanil (▲), fentanyl (■), alfentanil (⬢), methadone (◆), meperidine (▲), morphine (▼), and loperamide (●). All opioids exhibited a counter-clockwise hysteresis in the antinociception versus serum concentration relationship. Data are presented as means [serum concentration (n = 2–4); antinociception (n = 4–36)]

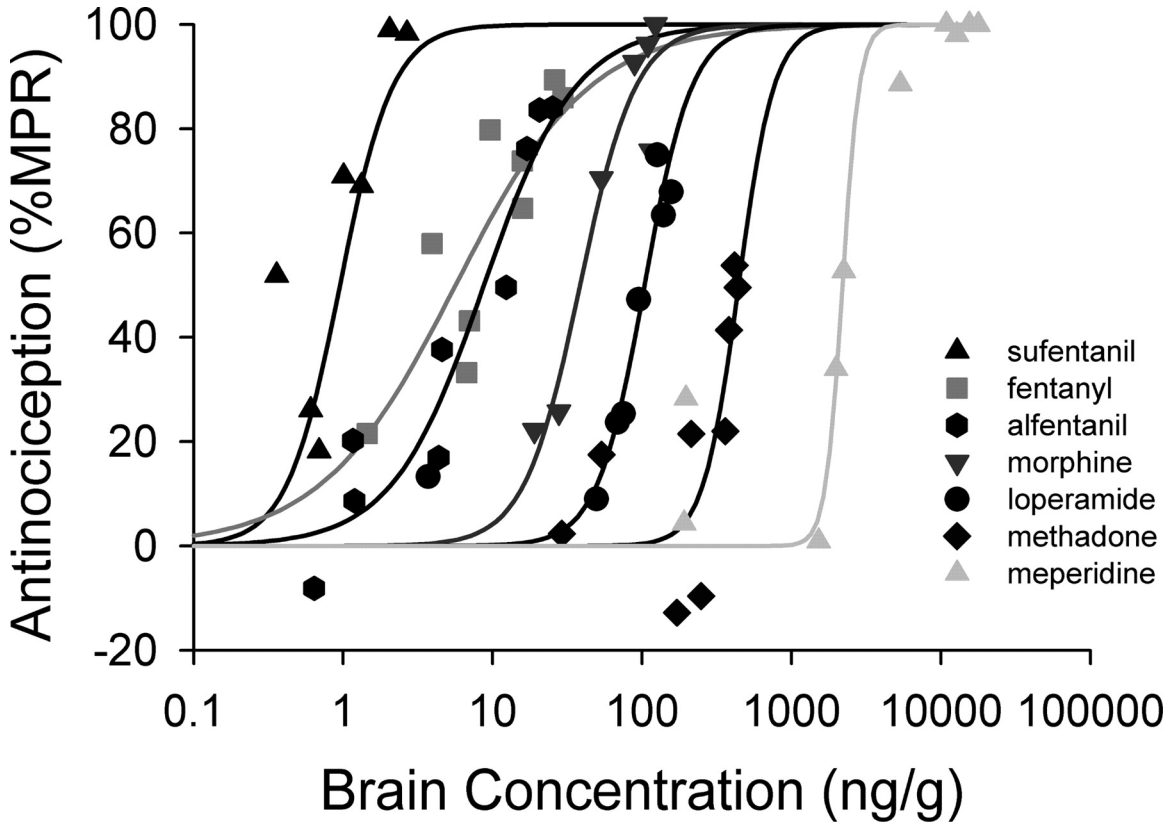

Figure 3.4. Relationship between brain concentration and antinociception for μ-opioid agonists. Symbols represent data from CF-1 *mdr1a*(+/+) mice. Lines represent the fit of a sigmoidal E_{max} model to the antinociception-brain concentration data. Data are presented as means [brain concentration (n = 2–4); antinociception (n = 4–36)].

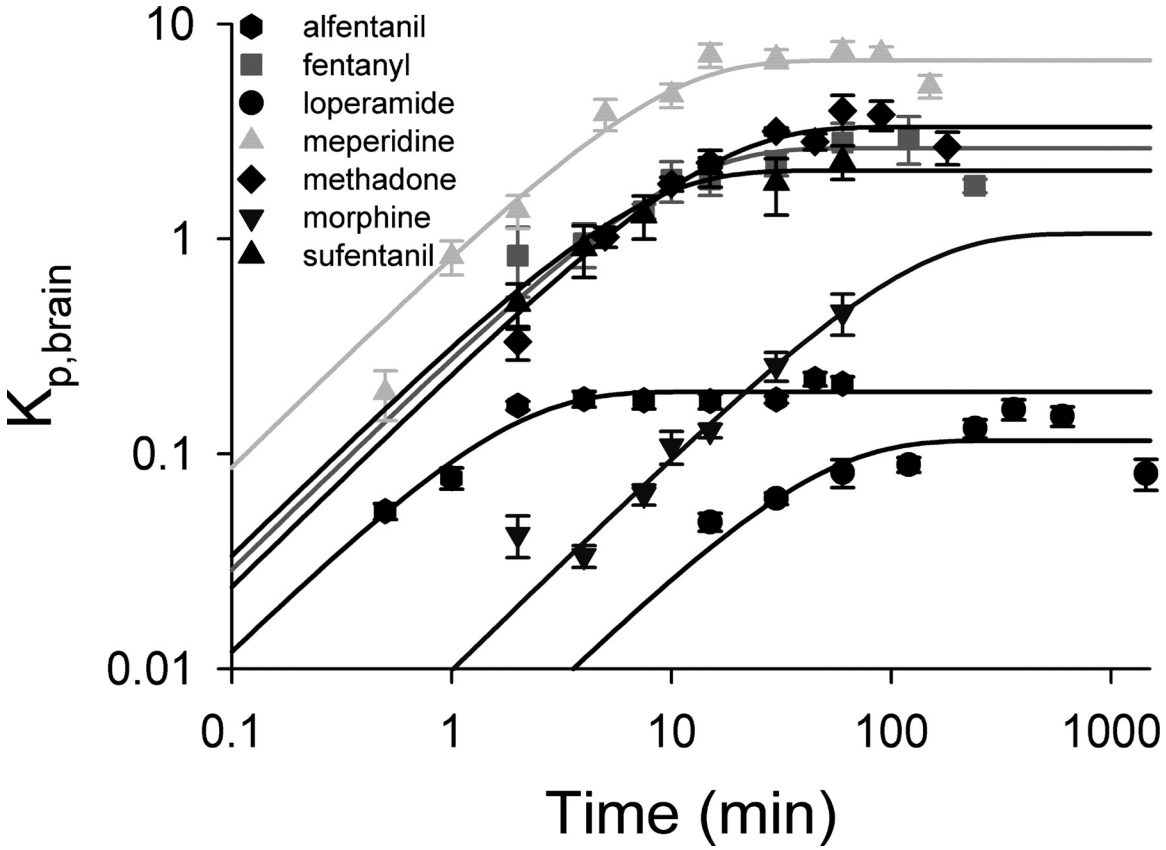

Figure 3.5. Time course of opioid $K_{p,brain}$ in CF-1 *mdr1a*(+/+). Solid lines represent the fit of a kinetic model to the data. Data are presented as mean ± S.E. ($n \geq 3$).

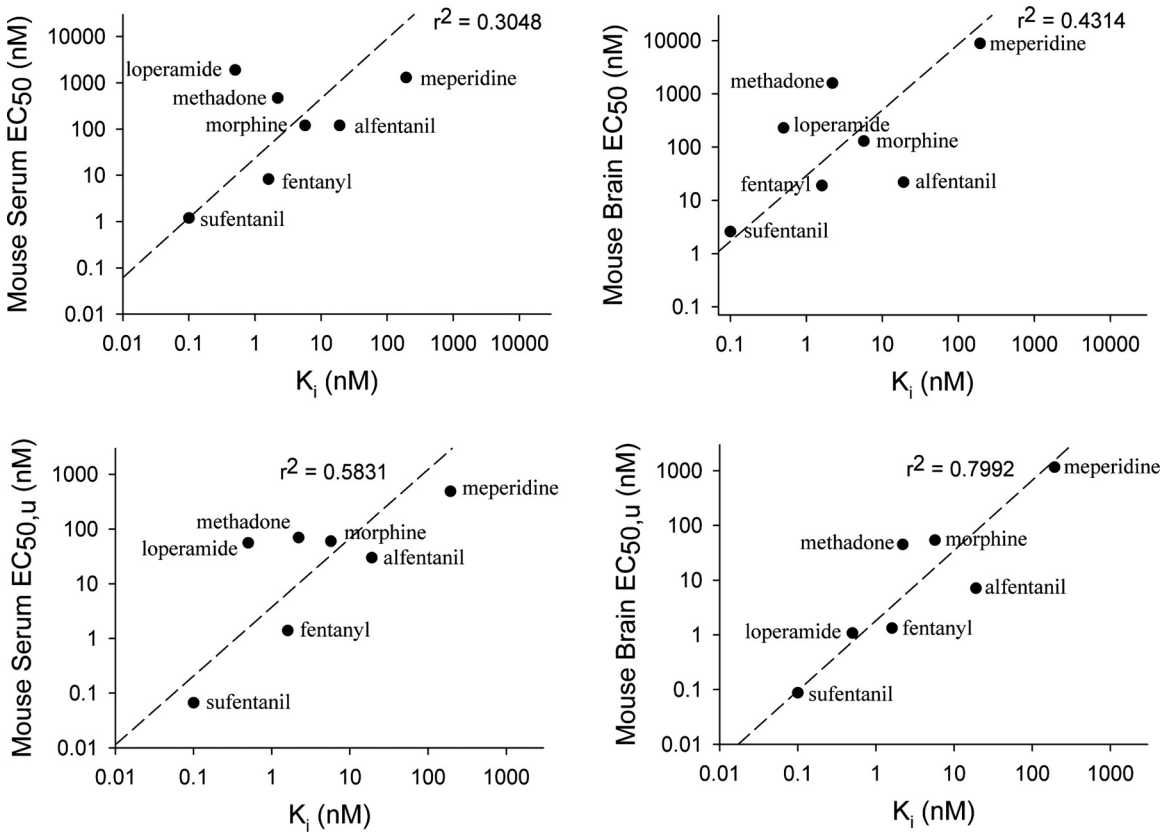

Figure 3.6. Correlation analysis for various in vivo measures relative to in vitro potency. The dashed line represents the line from log-log orthogonal regression analysis.

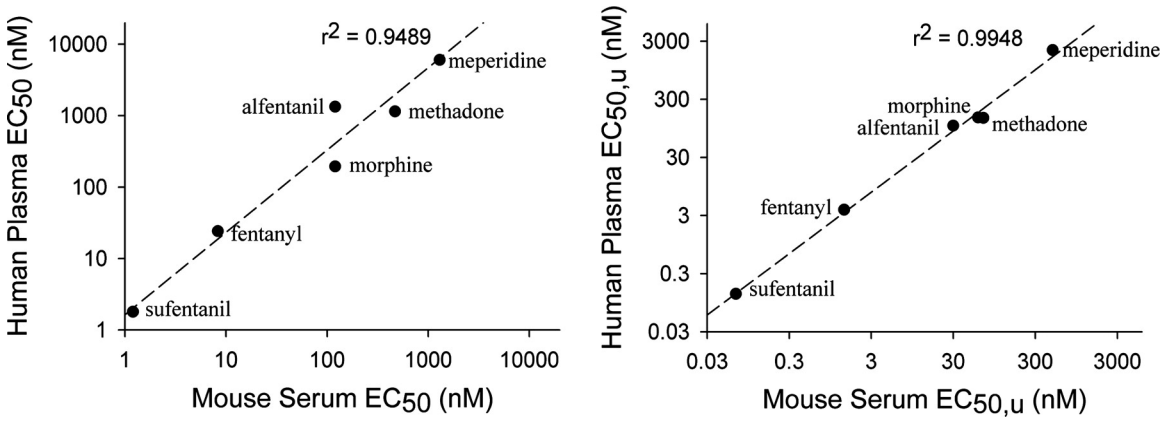

Figure 3.7. Correlation between mouse serum and human plasma EC_{50}s**.** The dashed line represents the line from log-log orthogonal regression analysis.

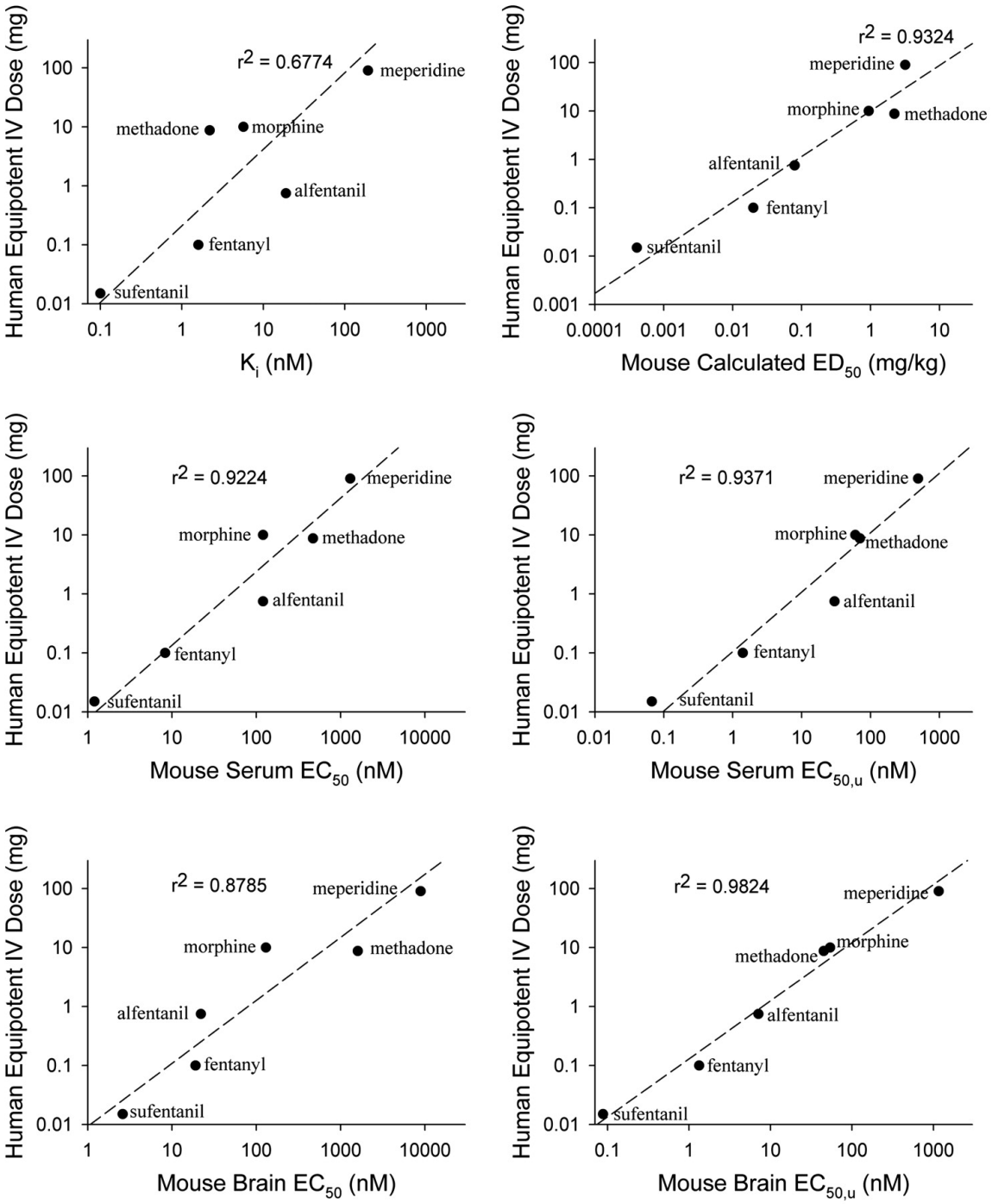

Figure 3.8. Correlation of equipotent clinical dose with in vitro K_i values, mouse ED_{50} values, and mouse EC_{50} values. The dashed line represents the line from log-log orthogonal regression analysis.

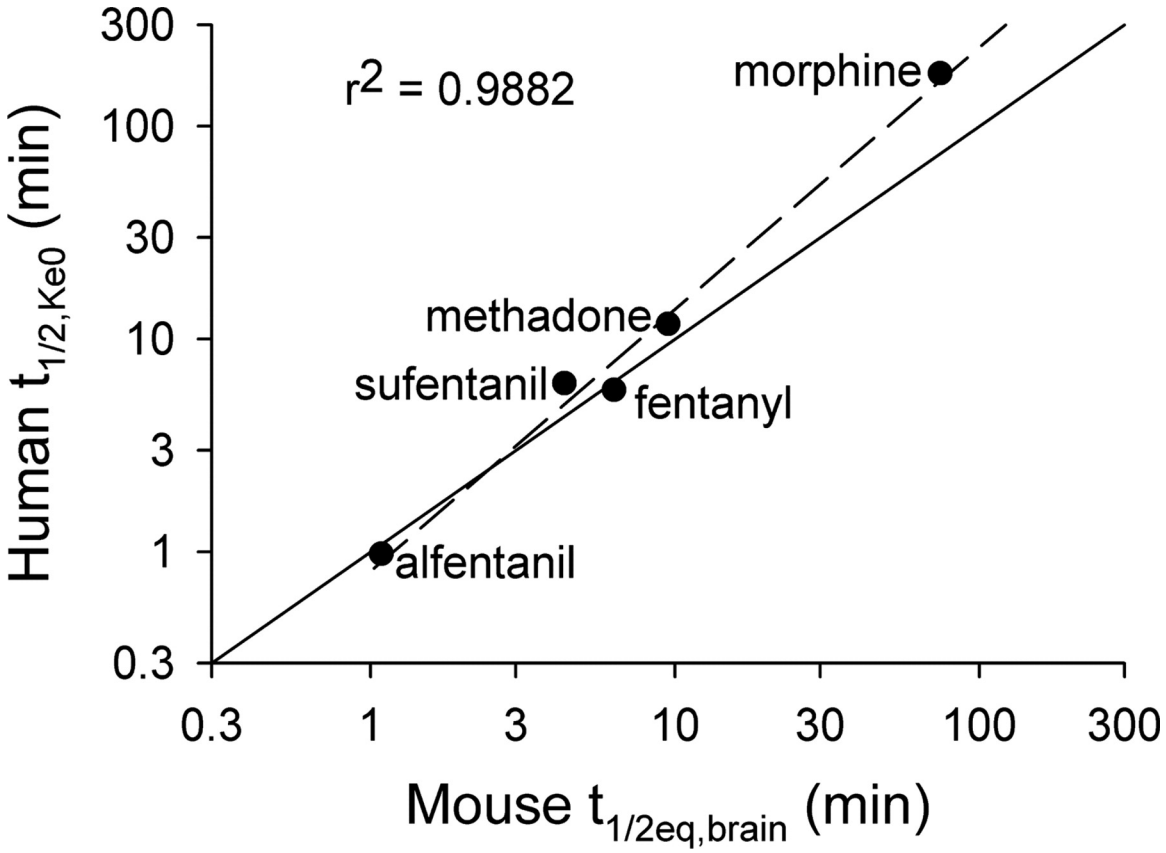

Figure 3.9. The log-log correlation between human plasma-biophase equilibration half-life ($t_{1/2,Ke0}$) and mouse brain equilibration half-life ($t_{1/2eq,brain}$). The solid line represents the line of unity; the dashed line represents the line from log-log orthogonal regression analysis. With the exception of morphine, all of the opioids fell within 1.4-fold of the line of unity.

REFERENCES

Bradford MM (1976) A rapid and sensitive method for the quantitation of microgram quantities of protein utilizing the principle of protein-dye binding. *Anal Biochem* **72:** 248–254.

Chen C and Pollack GM (1997) Blood-brain disposition and antinociceptive effects of -D-penicillamine2,5-enkephalin in the mouse. *J Pharmacol Exp Ther* **283:** 1151–1159.

Cox EH, Kerbusch T, Van der Graaf PH, and Danhof M (1998) Pharmacokinetic-pharmacodynamic modeling of the electroencephalogram effect of synthetic opioids in the rat: correlation with the interaction at the μ-opioid receptor. *J Pharmacol Exp Ther* **284:** 1095–1103.

Dagenais C, Graff CL, and Pollack GM (2004) Variable modulation of opioid brain uptake by P-glycoprotein in mice. *Biochem Pharmacol* **67:** 269–276.

Danhof M, Mandema JW, Hoogerkamp A, and Mathot RA (1993) Pharmacokinetic-pharmacodynamic modelling in pre-clinical investigations: principles and perspectives. *Eur J Drug Metab Pharmacokinet* **18:** 41–47.

Glare PA and Walsh TD (1991) Clinical pharmacokinetics of morphine. *Ther Drug Monit* **13:** 1–23.

Inturrisi CE, Colburn WA, Kaiko RF, Houde RW, and Foley KM (1987) Pharmacokinetics and pharmacodynamics of methadone in patients with chronic pain. *Clin Pharmacol Ther* **41:** 392–401.

Ito K, Yajima N, Ohtani H, Yamada Y, Nakamura K, Sawada Y, and Iga T (1993) Prediction of the therapeutic dose for beta-stimulants based on preclinical data: application of oral dosage forms and aerosols to asthmatic patients. *J Pharmacokinet Biopharm* **21:** 133–144.

Kalvass JC and Maurer TS (2002) Influence of nonspecific brain and plasma binding on CNS exposure: implications for rational drug discovery. *Biopharm Drug Dispos* **23:** 327–338.

Kalvass JC, Maurer TS, and Pollack GM (2007a) Use of plasma and brain unbound fractions to assess the extent of brain distribution of 34 drugs: comparison of unbound concentration ratios to in vivo p-glycoprotein efflux ratios. *Drug Metab Dispos* **35:** 660–666.

Kalvass JC, Olson ER, and Pollack GM (2007b) Pharmacokinetics and pharmacodynamics of alfentanil in P-glycoprotein-competent and P-glycoprotein-deficient mice: P-glycoprotein efflux alters alfentanil brain disposition and antinociception. *Drug Metab Dispos* **35:** 455–459.

Kurz A, Ikeda T, Sessler DI, Larson MD, Bjorksten AR, Dechert M, and Christensen R (1997) Meperidine decreases the shivering threshold twice as much as the vasoconstriction threshold. *Anesthesiology* **86:** 1046–1054.

Leysen JE, Gommeren W, and Niemegeers CJ (1983) [^{3}H]Sufentanil, a superior ligand for mu-opiate receptors: binding properties and regional distribution in rat brain and spinal cord. *Eur J Pharmacol* **87:** 209–225.

Lötsch J (2005) Pharmacokinetic-pharmacodynamic modeling of opioids. *J Pain Symptom Manage* **29:** S90–S103.

Meuldermans WE, Hurkmans RM, and Heykants JJ (1982) Plasma protein binding and distribution of fentanyl, sufentanil, alfentanil and lofentanil in blood. *Arch Int Pharmacodyn Ther* **257:** 4–19.

Niemegeers CJ, McGuire JL, Heykants JJ, and Janssen PA (1979) Dissociation between opiate-like and antidiarrheal activities of antidiarrheal drugs. *J Pharmacol Exp Ther* **210:** 327–333.

Schinkel AH, Wagenaar E, Mol CA, and van Deemter L (1996) P-glycoprotein in the blood-brain barrier of mice influences the brain penetration and pharmacological activity of many drugs. *J Clin Invest* **97:** 2517–2524.

Selley DE, Cao CC, Liu Q, and Childers SR (2000) Effects of sodium on agonist efficacy for G-protein activation in mu-opioid receptor-transfected CHO cells and rat thalamus. *Br J Pharmacol* **130:** 987–996.

Selley DE, Liu Q, and Childers SR (1998) Signal transduction correlates of μ opioid agonist intrinsic efficacy: receptor-stimulated [^{35}S]GTPγS binding in mMOR-CHO cells and rat thalamus. *J Pharmacol Exp Ther* **285:** 496–505.

Selley DE, Sim LJ, Xiao R, Liu Q, and Childers SR (1997) μ-Opioid receptor-stimulated guanosine-5'-*O*-(γ-thio)-triphosphate binding in rat thalamus and cultured cell lines: signal transduction mechanisms underlying agonist efficacy. *Mol Pharmacol* **51:** 87–96.

Terenius L (1975) Comparison between narcotic "receptors" in the guinea-pig ileum and the rat brain. *Acta Pharmacol Toxicol (Copenh)* **37:** 211–221.

Visser SA, Wolters FL, Gubbens-Stibbe JM, Tukker E, Van Der Graaf PH, Peletier LA, and Danhof M (2003) Mechanism-based pharmacokinetic/pharmacodynamic modeling of the electroencephalogram effects of $GABA_A$ receptor modulators: in vitro-in vivo correlations. *J Pharmacol Exp Ther* **304:** 88–101.

Wood M and Alastair JJ (1990) *Drugs and Anesthesia: Pharmacology for Anesthesiologist*, Williams & Wilkins, Baltimore, MD.

CHAPTER 4

INFLUENCE OF BLOOD-BRAIN BARRIER P-GLYCOPROTEIN ON BRAIN PENETRATION AND ANTINOCICEPTIVE EFFECTS OF MODEL OPIOIDS

This chapter has been submitted for publication in *Journal of Pharmacology and Experimental Therapeutics* and is presented in the style of that journal.

ABSTRACT

This study assessed the pharmacokinetic-pharmacodynamic (PK-PD) implications of variable substrate interactions with blood-brain barrier (BBB) P-glycoprotein (P-gp). Opioids were selected as model compounds because they elicit a readily-measured central effect (antinociception) and evidence a range of interactions with P-gp (loperamide: high; methadone: intermediate; fentanyl: low). P-gp-competent [*mdr1a*(+/+)] and P-gp-deficient [*mdr1a*(-/-)] CF-1 mice received equipotent subcutaneous doses of loperamide, methadone, or fentanyl. FVB [*mdr1a/b*(+/+)] and [*mdr1a/b*(-/-)] mice also received equipotent subcutaneous doses of loperamide in order to assess the potential influence of *mdr1b* on opioid brain penetration and antinociception. The time courses of antinociception and brain/serum concentrations were determined. Brain-to-plasma concentration ratios ($K_{p,brain}$), brain equilibration half-life ($t_{1/2eq,brain}$), and pharmacokinetic/pharmacodynamic parameters were estimated by fitting appropriate kinetic or kinetic/dynamic models to the data. *Mdr1a*(+/+) mice required 50- and 5-fold higher doses of loperamide and methadone, respectively, to produce antinociceptive activity similar to *mdr1a*(-/-) mice. P-gp efflux reduced the $K_{p,brain}$ of loperamide, methadone, and fentanyl by ~40-, ~7-, and ~2-fold, respectively. However, P-gp efflux had no effect on brain EC_{50}, indicating that the only

influence of P-gp on loperamide-, methadone-, and fentanyl-associated antinociception was through limiting CNS exposure across the BBB. P-gp efflux decreased brain uptake clearance, $K_{p,brain}$, and $t_{1/2eq,brain}$. The ~2-fold decrease in the time to brain/plasma equilibration for loperamide and methadone is consistent with theoretical considerations for BBB efflux transport, assuming that the egress rate from brain determines brain/plasma equilibration half-life.

INTRODUCTION

Several opioids, including fentanyl, methadone, and loperamide, are substrates for the efflux transporter P-glycoprotein (P-gp) (Dagenais et al., 2004). P-gp was first identified in tumor cells for its ability to confer multi-drug resistance against chemotherapy agents (Juliano, 1976; Gros et al., 1986). P-gp is also expressed in several normal organs and tissues, such as the intestine, liver, kidneys, testes, and brain. P-gp expression at these sites appears to serve a protective role by limiting absorption, facilitating excretion, and reducing tissue distribution of potentially harmful xenobiotics, including calcium channel blockers, HIV protease inhibitors, immunosuppressants, and opioids to sensitive tissues, including the brain (Matheny et al., 2001).

While human P-gp is encoded by the MDR1 gene, rodents encode the transporter through two distinct genes, *mdr1a* and *mdr1b*. Two strains of P-gp-deficient mice have been used in a variety of experimental protocols to study the influence of P-gp on the pharmacokinetic and pharmacodynamics of drugs: the CF-1 mouse strain, which naturally lacks the *mdr1a* gene product, and *mdr1a/b* double knockouts, which were developed in the FVB murine line (Schinkel et al., 1994; Chen et al., 2003). The *mdr1a* isoform is expressed on the apical membrane of capillary endothelial cells comprising the BBB, and is thought to

be the prominent isoform restricting the entry of P-gp substrates into the brain (Schinkel et al., 1994). In contrast, the *mdr1b* isoform has been reported to be expressed in brain parenchyma (Golden and Pardridge, 2000); the role of *mdr1b* P-gp in attenuating opioid-associated antinociception is unknown. Studies with P-gp-competent and P-gp-deficient mice of both strains have shown that P-gp is responsible for attenuating brain uptake, decreasing brain tissue concentrations, and reducing the antinociceptive action of some opioids (Schinkel et al., 1996; Chen and Pollack, 1998; Thompson et al., 2000; Dagenais et al., 2004).

It has been proposed that P-gp expression within brain parenchyma may serve as a tertiary barrier to substrate approach to pharmacologic targets such as opioid receptors (Golden and Pollack, 2003). Some experimental evidence supports this hypothesis. For example, the brain tissue EC_{50} of the metabolically stable cyclic opioid peptide [D-penicillamine^{2,5}]-enkephalin (DPDPE) was 10-fold lower in P-gp-deficient as compared to P-gp-competent mice (Chen and Pollack, 1998). It was proposed that the difference in brain tissue EC_{50} was due to P-gp within the brain parenchyma effluxing drug away from the receptor site. However, this explanation remains speculative.

The anti-diarrheal agent loperamide is devoid of central activity at therapeutic doses, despite being a potent *mu* opioid agonist, due to substantial P-gp-mediated efflux (Schinkel et al., 1996). Efflux by BBB P-gp decreases the loperamide brain-to-plasma ratio ($K_{p,brain}$) by ~60-fold (Kalvass et al., 2004). P-gp-mediated efflux also has been reported to decrease the $K_{p,brain}$ for methadone and to attenuate fentanyl-associated antinociception in mice (Thompson et al., 2000; Wang et al., 2004). The effect of P-gp on opioid flux is in the order loperamide > methadone > fentanyl, making this a useful compound set for comprehensive

evaluation of the role of P-gp in modulating central opioid response. A side-by-side comparison of the pharmacokinetics and pharmacodynamics of these compounds will allow a better understanding of the effect of on brain penetration and antinociception of opioids. The specific goal of the present study was to use a PK-PD modeling approach to assess the influence of P-gp-mediated BBB efflux on the pharmacokinetics, brain disposition, and antinociception of fentanyl, methadone, and loperamide.

MATERIAL AND METHODS

Materials

Fentanyl, methadone, and loperamide were purchased from Sigma-Aldrich (St. Louis, MO). All other reagents were obtained from common sources and were of reagent grade or better.

Animals

Male CF-1 [*mdr1a*(+/+) and *mdr1a*(-/-)] and FVB [*mdr1a/b(*+/+) and *mdr1a/b(*-/-)] mice (30-40 g; Charles River Laboratories, Inc. Wilmington, MA; and Taconic, Germantown, NY, respectively) were maintained on a 12-h light/dark cycle in a temperature- and humidity-controlled room with access to water and food ad libitum. All procedures involving mice were approved by The Institutional Animal Care and Use Committee of the University of North Carolina and were conducted in accordance with "Principles of Laboratory Animal Care" (NIH Publication No. 85-23, revised in 1985).

Opioid Pharmacokinetics and Pharmacodynamics

Based on the results of pilot studies, 36 *mdr1a*(-/-) and 36 *mdr1a*(+/+) CF-1 mice received equipotent subcutaneous doses of loperamide (1 or 50 mg/kg, respectively),

methadone (0.2 or 0.6 mg/kg, respectively), or fentanyl (0.09 mg/kg, respectively). The loperamide and fentanyl doses were prepared in 50/50 propylene glycol/water, whereas the methadone dose was prepared in 0.9% saline. In a separate experiment designed to assess the significance of *mdr1b* on opioid brain penetration and antinociception, 36 *mdr1a/b*(-/-) and 36 *mdr1a/b*(+/+) FVB mice received equipotent subcutaneous doses of loperamide (1 or 25 mg/kg, respectively). For both sets of experiments, antinociception was assessed; 4 *mdr1a*(-/-) and 4 *mdr1a*(+/+) mice were sacrificed by decapitation for collection of brain tissue and trunk blood at selected time points. Trunk blood was collected in 1.5-ml microcentrifuge tubes and was allowed to clot for ≥ 30 min at room temperature. Serum was harvested following centrifugation. Brain and serum samples were stored at -20°C until analysis by HPLC-MS/MS.

Assessment of Antinociception

Antinociception was assessed with the hot plate latency test as described elsewhere (Chen and Pollack, 1997). Prior to administration of opioids, baseline hotplate latency was determined for each animal in triplicate. Hotplate latency was defined as the time interval between placement on the hot plate (55°C; Columbus Instruments, Columbus, OH) and first observation of a jump or lick of the hind limb(s). Animals with an average baseline latency <25 sec were used in the study. A cut-off latency of 60 sec was used to avoid tissue damage. The degree of antinociception was calculated as:

$$\%MPR = \frac{Test\ latency - Control\ latency}{Maximum\ latency - Control\ latency} x\ 100\% \qquad \text{(Eqn. 4.1)}$$

Quantitation of Opioids in Serum and Brain Tissue Samples

Brain samples were homogenized in water (1:2 v/v) via sonic probe. A 25-µl aliquot of homogenate or serum was transferred to a HPLC vial, and protein was precipitated with 100 µl methanol containing internal standard (5 ng/ml loperamide for fentanyl and methadone; 20 ng/ml methadone for loperamide). The sample was vortex-mixed, centrifuged, and the supernatant was analyzed by HPLC-MS/MS. Samples were injected (3 µl; CTC Analytics autosampler, Zwingen, Switzerland) onto a Phenomenex 2.0 x 30 mm, 5 µm Gemini 110A column (Phenomenex, Torrance, CA) maintained at room temperature. The total run time was 3 min. Analytes were eluted with a linear gradient consisting of ammonium acetate (pH 6.8; 10 mM) ["A"] and methanol ["B"] produced by two Shimadzu LC-10ADVP binary pumps. An initial condition of 5% "B" was ramped to 95% "B" over 2 min, held for 0.5 min, and then returned initial condition of 5% "B" in a single step to re-equilibrate the column. During the run, the flow rate was increased from 750 to 1500 µl/min over the first 2 min, held at 1500 µl/min for 1 min, and then returned the initial flow rate of 750 µl/min in a single step. The entire column effluent was diverted from the source of the PE-Sciex API-4000 quadrupole mass spectrometer (Turbo V Ionspray source, 700˚C, PerkinElmerSciex Instruments, Boston, MA) for the first 1 min and last 0.5 min of the run. Fentanyl, loperamide, and methadone were measured in positive ionization mode using multiple reaction monitoring (337.1→188.3, 477.4→266.0 and 310.3→265.1, respectively). Standard curves were prepared in brain homogenate, serum, plasma, or buffer and were identical in composition to corresponding samples.

Pharmacokinetic-Pharmacodynamic Analysis

A compartmental modeling approach with distribution between serum and brain tissue was used to describe fentanyl, loperamide, and methadone pharmacokinetics. The pharmacokinetic model in Figure 4.1 was fit simultaneously to the serum and brain tissue concentration-time data using nonlinear least-squares regression analysis (WinNonlin 4.1; Pharsight Corporation, Mountain View, CA). The brain volume (V_b) was determined experimentally (0.47 ml) assuming a specific gravity of 1.0 ml. All other pharmacokinetic parameters were obtained from fitting the kinetic model to the data. The pharmacodynamic parameters, EC_{50} and γ, were determined from fitting a sigmoidal E_{max} model to the antinociception versus brain concentration (C) data.

$$\%MPR = \frac{E_{\max}\ x\ C^{\gamma}}{EC_{50} + C^{\gamma}} \qquad \text{(Eqn. 4.2)}$$

E_{max} was defined as 100%, and γ was constrained to the same value for P-gp-competent and P-gp-deficient mice. The time course of brain-to-serum ratio ($K_{p,brain}$) was used to estimate the brain equilibration rate constant (k_{eq}) and steady-state brain-to-serum ratio ($K_{p,brain,ss}$) according to:

$$K_{p,brain} = K_{p,brain,ss}\,(1 - e^{-k_{eq}\,t}) \qquad \text{(Eqn. 4.3)}$$

The brain equilibration half-life ($t_{1/2eq,brain}$) was obtained from k_{eq}:

$$t_{\frac{1}{2},eq,brain} = \frac{\ln(2)}{k_{eq}} \qquad \text{(Eqn. 4.4)}$$

RESULTS

In order to achieve similar antinociception between *mdr1a*(+/+) and *mdr1a*(-/-) mice, *mdr1a*(+/+) animals received 5- and 50-fold larger doses of methadone and loperamide,

respectively. Consistent with receiving a larger dose, the serum concentrations of methadone and loperamide in *mdr1a*(+/+) mice exceeded those in *mdr1a*(-/-) mice. However, brain tissue concentrations were similar between the two strains of mice. The time course of serum and brain tissue concentrations in the *mdr1a*(-/-) and *mdr1a*(+/+) mice following subcutaneous dose of loperamide, methadone, and fentanyl are reported in Figure 4.2. In general, the brain concentrations for each opioid were similar between the two mouse strains, consistent with the fact that equipotent doses were administered. However, because larger doses were administered to P-gp-competent mice, opioid concentrations in the systemic circulation were higher in these animals as compared to their P-gp-deficient counterparts, and were approximately dose-proportional. Again consistent with the administration of equipotent doses in the two mouse strains, the magnitude and duration of fentanyl-, methadone-, and loperamide-associated antinociception were similar between *mdr1a*(-/-) and *mdr1a*(+/+) mice (Figure 4.3). The fit of the PK/PD model to the concentration vs. time and antinociception vs. time data is shown in Figures 4.2 and 4.3, respectively. Corresponding estimates of pharmacokinetic and pharmacodynamic parameters obtained from the model are reported in Table 4.1.

The systemic pharmacokinetics of fentanyl and methadone did not differ substantially between *mdr1a*(-/-) and *mdr1a*(+/+) mice, so in the implementation of modeling estimates of systemic pharmacokinetic parameters were constrained to the same values for both *mdr1a*(-/-) and *mdr1a*(+/+) mice. However, differences in loperamide systemic pharmacokinetics between P-gp-deficient [*mdr1a*(-/-) and *mdr1a/b*(-/-)] and P-gp-competent [*mdr1a*(+/+) and *mdr1a/b*(+/+)] mice were apparent. Hence, independent estimates of pharmacokinetic parameters were obtained for P-gp-deficient and P-gp-competent mice for this agent. The

systemic pharmacokinetics of fentanyl were most consistent with a two-compartment model, whereas a one-compartment model best described the systemic pharmacokinetics of methadone and loperamide (Table 4.1 and 4.2).

The antinociception versus opioid serum and brain concentration relationships are shown in Figures 4.4 and 4.5, respectively. For each of the opioids, the antinociception versus serum concentration relationship evidenced a counterclockwise hysteresis, consistent with delayed distribution between serum and the biophase. Compared to *mdr1a*(-/-) mice, the antinociception versus serum concentration relationship in *mdr1a*(+/+) mice was shifted rightward 1.9-, 7-, and 44-fold for fentanyl, methadone, and loperamide, respectively. In contrast, no hysteresis or rightward shift was observed in the antinociception versus brain concentration relationships. A sigmoidal E_{max} model was capable of adequately describing the relationship between antinociception and brain concentrations. There was no difference in brain EC_{50} between *mdr1a*(-/-) and *mdr1a*(+/+) mice for any of the opioids examined. The brain EC_{50} estimates for loperamide in *mdr1a/b*(-/-) and *mdr1a/b*(+/+) mice were consistent with the brain EC_{50} from *mdr1a*(-/-) and *mdr1a*(+/+) mice (Table 4.1 and 4.2). The time course of $K_{p,brain}$, as well as the antinociception versus serum and brain tissue concentration relationships (Figure 4.7, panels C, D, and E, respectively), were similar between the P-gp-competent CF-1 *mdr1a*(+/+) and FVB *mdr1a/b*(+/+) mice, and between the P-gp-deficient CF-1 *mdr1a*(-/-) and FVB *mdr1a/b*(-/-) mice.

P-gp-mediated efflux reduced the $K_{p,brain}$ of fentanyl, methadone, and loperamide by 1.9-, 7.2-, and 44-fold, respectively (Figure 4.6 and Table 4.1). P-gp efflux did not prolong the brain equilibrium half-life. To the contrary, P-gp efflux decreased the time to brain/plasma equilibration of loperamide and methadone by ~2-fold.

DISCUSSION

Previous studies have indicated that P-gp-mediated efflux attenuates the brain uptake and antinociception of fentanyl, methadone, and loperamide. In this study, a PK/PD modeling approach was used to more fully elucidate the mechanism(s) by which P-gp attenuates brain penetration and antinociception. Multiple mechanisms may be involved in the attenuation of antinociception, including alteration in systemic pharmacokinetics (e.g., decreased bioavailability or increased clearance), reduction in brain penetration (e.g., decreased brain uptake and/or increased brain efflux), and alteration of drug distribution within the brain (e.g., increased brain EC_{50}).

Estimates of systemic pharmacokinetic parameters for fentanyl and methadone were similar between *mdr1a*(-/-) and *mdr1a*(+/+) mice, indicating no change in systemic pharmacokinetics due to P-gp-mediated efflux. However, different pharmacokinetic parameters were necessary to fit the model to the loperamide serum concentration vs. time data from the *mdr1a*(-/-), *mdr1a*(+/+), *mdr1a/b*(-/-), *mdr1a/b*(+/+) mice. This difference in loperamide pharmacokinetics between the different groups of mice may not be due to P-gp-mediated efflux, but rather to non-linear pharmacokinetics.

The loperamide serum concentrations in *mdr1a*(-/-) mice were poorly described by the pharmacokinetic model in Figure 4.1, regardless of whether the one- or two-compartment system was used. The estimate for K_a from the model consistently converged to the maximum valued allowed, and had a large associated variance. Since the K_a was large and could not be estimated with reasonable accuracy, the data set was treated as an i.v. bolus and K_a was removed as a fitted parameter. A two-compartment model with bolus input, consistent with this approximation, yielded parameter estimates with the lowest variance, and was best able to fit the serum concentration-time data in *mdr1a*(-/-) mice.

In order to avoid acute toxicity in the P-gp-competent FVB mice, it was necessary to reduce the dose of loperamide by half compared to the P-gp-competent CF-1 mice (25 vs. 50 mg/kg). The increased sensitivity towards loperamide toxicity in the FVB P-gp-competent mice is attributed to lower systemic clearance (28 vs 58 $ml \cdot min^{-1} \cdot kg^{-1}$), not to any innate difference in pharmacology or P-gp activity. Serum and brain tissue concentrations, as well as antinociception, were similar between the FVB *mdr1a/b*(+/+) and CF-1 *mdr1a*(+/+) mice at one-half the dose.

A counterclockwise hysteresis in the antinociceptive effect versus serum concentration relationship was observed for both *mdr1a*(+/+) and *mdr1a*(-/-) mouse strains, consistent with delayed distribution between the serum and the biophase. The antinociception versus serum concentration relationship shifted rightward in P-gp-competent animals, in proportion to the fold change in $K_{p,brain}$. Similarly, the ED_{50} of loperamide and methadone in P-gp-competent mice shifted rightward ~30-fold and ~5-fold compared to P-gp-deficient mice (data not shown). No hysteresis was observed in the antinociceptive effect versus brain concentration relationship. The brain EC_{50} was identical between P-gp-deficient and P-gp-competent mice. These results are consistent with the brain being the site of opioid action. The loperamide brain EC_{50} estimates for the *mdr1a*(+/+), *mdr1a*(-/-), *mdr1a/b*(+/+), and *mdr1a/b*(-/-) mice were similar suggesting that P-gp (neither the *mdr1a* nor the *mdr1b* gene product) had no effect on brain EC_{50} and that brain EC_{50} were similar between CF-1 and FVB mouse strains.

Previously, this laboratory demonstrated a 10-fold difference in brain tissue EC_{50} between *mdr1a/b*(-/-) and *mdr1a/b*(+/+) mice for the cyclic opioid peptide DPDPE (Chen and Pollack, 1998). This observation has been used to support the hypothesis that P-gp efflux

not only limits access to the brain via the BBB, but parenchymal expression of P-gp may also limit access of P-gp substrates to biophase once the P-gp substrates have crossed the BBB. Another study conducted with morphine indicated that P-gp-mediated efflux had no effect in brain tissue EC_{50} between *mdr1a*(-/-) and *mdr1a*(+/+), even though P-gp efflux increased the ED_{50} by reducing the $K_{p,brain,ss}$ (Zong and Pollack, 2000). Results from this study are consistent with the previous observations for morphine, as there was no difference in brain EC_{50} of fentanyl, methadone, and loperamide between *mdr1a*(-/-) and *mdr1a*(+/+) mice. However, it should be noted that DPDPE is specific agonist for the delta opioid receptor, whereas fentanyl, methadone, and loperamide are mu opioid agonists. Whether this difference has any bearing on P-gp related difference in brain EC_{50} requires further investigation.

P-gp-mediated efflux reduced the $K_{p,brain}$ of fentanyl, methadone, and loperamide by 1.9-, 7.2-, and 44-fold, respectively. These results are consistent with previously reported values for methadone and loperamide (16- and 65-fold, respectively) (Kalvass et al., 2004; Wang et al., 2004). The $K_{p,brain}$ was reduced through the attenuation of brain uptake and the enhancement of brain efflux. This is evident by the fact that the Cl_{up} was smaller, and the Cl_{efflux} was larger, in the P-gp-competent mice compared to P-gp-deficient mice. The effect of P-gp-mediated efflux on brain uptake was generally more significant than on brain efflux. The location of P-gp on the apical membrane of capillary endothelial cells allows it to more effectively attenuate brain uptake than enhance brain efflux (Thiebaut et al., 1989). This is consistent with the present observation that P-gp-mediated efflux attenuated the brain uptake clearance of loperamide by ~20-fold (0.8 vs 0.04 $ml \cdot min^{-1} \cdot kg^{-1}$) and enhanced brain efflux of loperamide only by ~1.5-fold (0.2 vs 0.3 $ml \cdot min^{-1} \cdot kg^{-1}$). Furthermore, the brain equilibration

rate constant was about 2-fold higher, and the brain equilibrium half-life was shorter, in P-gp-competent as compared to P-gp-deficient animals. Consistent with P-gp attenuating brain uptake and enhancing brain efflux, P-gp-mediated efflux reduced the extent ($K_{p,brain}$) but not the rate ($K_{eq,brain}$) of brain distribution.

An explanation for why P-gp efflux affects uptake to a larger extent than efflux can be achieved by considering the orientation of P-gp in the BBB, and by taking into account the diffusional barriers a molecule must traverse to cross the BBB. In order for a molecule to transverse the BBB, it must cross both the apical and basolateral membranes of the endothelial cell. P-gp is present on the apical membrane and pumps in the direction of the capillary lumen (Tsuji et al., 1992). During brain uptake, a drug first encounters the apical membrane followed by the basolateral membrane. The presence of P-gp on the apical membrane allows it to severely limit brain uptake. However, during egress from the brain the drug first encounters the basolateral membrane followed by the apical membrane. In the complete absence of P-gp, the basolateral and apical membranes equally dictate the rate of drug egress from the brain. When P-gp-mediated efflux is present and is sufficiently large, P-gp efflux reduces the resistance of the apical membrane to the point that it is no longer a diffusional barrier, and only the basolateral membrane is a barrier to movement out of the brain. In the absence of efflux, two barriers restrict drug egress from the brain. However, with efflux these two barriers can be effectively reduced to one barrier, resulting in an increase in drug efflux. If the membrane permeability is similar between the apical and basolateral membranes, then P-gp would be expected to increase efflux from the brain by no more than 2-fold. Further evidence supporting this hypothesis is that the brain equilibration half-life, which is inversely proportional to the rate of efflux from the brain, was about 2-fold

shorter in the P-gp-competent animals. Other studies indicate a similar effect of P-gp efflux on brain equilibration half-life (Letrent et al., 1999; Sugiyama et al., 2003).

In summary, this study demonstrated that P-gp-mediated efflux reduced antinociception of fentanyl, methadone, and loperamide by attenuating $K_{p,brain}$. This was evident by rightward-shifts in the antinociception versus serum concentration relationship, identical brain tissue EC_{50} between P-gp-competent and P-gp-deficient mice, and that brain Cl_{up} was increased while brain Cl_{efflux} was decreased in P-gp-competent mice. Although the extent of brain penetration ($K_{p,brain}$) was reduced by P-gp efflux, the rate of equilibration ($K_{eq,brain}$) of drug between serum and brain was increased by P-gp efflux. The effects of P-gp-mediated efflux on opioid brain penetration and antinociception appear to be due to the *mdr1*a isoform of P-gp.

Table 4.1. Parameter estimates from PK-PD modeling.

Parameter	fentanyl		methadone		loperamide	
	mdr1a(+/+)	*mdr1a*(-/-)	*mdr1a*(+/+)	*mdr1a*(-/-)	*mdr1a*(+/+)	*mdr1a*(-/-)
K_a (min^{-1})	0.07 ± 0.07		0.55 ± 0.13		0.063 ± 0.015	-
Cl ($ml \cdot min^{-1} \cdot kg^{-1}$)	90 ± 40		127 ± 12		58 ± 7	34 ± 8
V_c ($ml \cdot kg^{-1}$)	2900 ± 2800		8800 ± 600		32000 ± 3000	3000 ± 2000
Cl_d ($ml \cdot min^{-1} \cdot kg^{-1}$)	40 ± 30		-		-	130 ± 140
V_p ($ml \cdot kg^{-1}$)	5000 ± 13000		-		-	4300 ± 1600
Cl_{up} ($ml \cdot min^{-1} \cdot kg^{-1}$)	8 ± 3	10 ± 2	27 ± 4	43 ± 5	0.04 ± 0.06	0.8 ± 0.5
Cl_{efflux} ($ml \cdot min^{-1} \cdot kg^{-1}$)	3.4 ± 1.4	2.2 ± 0.7	5.1 ± 0.9	1.8 ± 0.2	0.3 ± 0.5	0.20 ± 0.11
EC_{50} (ng/g)	6.4 ± 1.1	8.7 ± 1.8	510 ± 60	480 ± 30	104 ± 6	73 ± 12
γ	1.4 ± 0.3		3.7 ± 1.1		2.7 ± 0.5	1.2 ± 0.2
$K_{p,brain}$	2.3 ± 0.2	4.5 ± 0.2	3.3 ± 0.2	24 ± 3	0.115 ± 0.014	5.1 ± 0.9
K_{eq} (min^{-1})	0.14 ± 0.04	0.13 ± 0.02	0.073 ± 0.014	0.029 ± 0.008	0.025 ± 0.010	0.015 ± 0.008
$t_{1/2eq,brain}$ (min)	4.9 ± 1.3	5.2 ± 0.0	9.6 ± 1.8	26 ± 6	27 ± 11	50 ± 20

Parameter estimate ± S.E. from non-linear regression analysis of pooled mouse data.
$t_{1/2eq,brain}$ were calculated from $0.693/K_{eq,brain}$.

Table 4.2. Parameter estimates for loperamide in FVB mice

Parameter	loperamide (FVB mice)	
	mdr1a/b(+/+)	*mdr1a/b*(-/-)
K_a (min^{-1})	0.12±0.04	0.24±0.11
Cl ($ml \cdot min^{-1} \cdot kg^{-1}$)	28±4	100±20
V_c ($ml \cdot kg^{-1}$)	13000±1000	15000±3000
Cl_d ($ml \cdot min^{-1} \cdot kg^{-1}$)	-	-
V_p ($ml \cdot kg^{-1}$)	-	-
Cl_{up} ($ml \cdot min^{-1} \cdot kg^{-1}$)	0.02±0.05	0.88±0.19
Cl_{efflux} ($ml \cdot min^{-1} \cdot kg^{-1}$)	0.2±0.7	0.27±0.06
EC_{50} (ng/g)	82±6	61±5
γ	2.9±0.6	
$K_{p,brain}$	0.13±0.02	18±3
K_{eq} (min^{-1})	0.009±0.003	0.0028±0.0008
$t_{1/2eq,brain}$ (min)	77±20	250±70

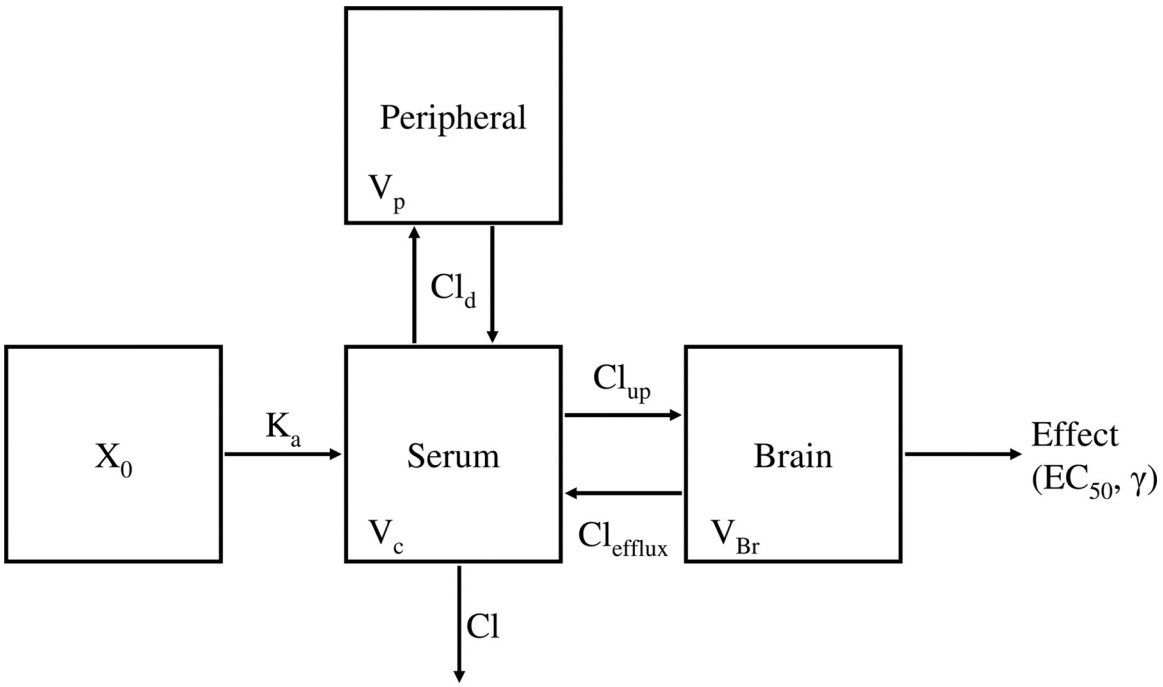

Figure 4.1. Pharmacokinetic-pharmacodynamic model for opioid disposition and antinociception in mice. Pharmacokinetic parameter were obtained by fitting the above model to the time course of serum and brain concentrations of *mdr1*a(-/-) and *mdr1a*(+/+) mice following subcutaneous administration of opioid. Except for loperamide, the absorption rate constant (K_a), central volume (V_c), and systemic clearance (Cl), peripheral volume (V_p), and distributional clearance (Cl_d) were held constant between *mdr1*a(-/-) and *mdr1a*(+/+) mice; whereas, the brain uptake (Cl_{up}) and brain efflux clearances (Cl_{efflux}) were allowed to vary between *mdr1*a(-/-) and *mdr1a*(+/+) mice**.** The brain volume (V_b) was fixed. The effect parameters, EC_{50} and γ, were obtained by fitting a sigmoidal E_{max} model to the brain concentration versus antinociception data. E_{max} was defined as 100%.

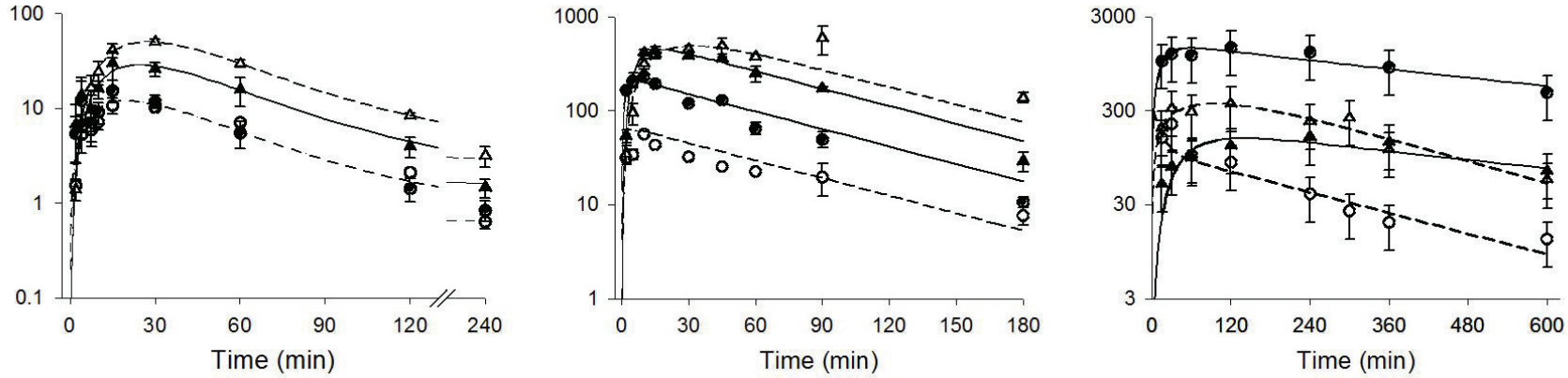

Figure 4.2. Time course of serum (●) and brain (□) concentrations following s.c. administration of opioids (from left to right: fentanyl [0.09-mg/kg], methadone [0.2- and 0.6-mg/kg], and [1- and 50-mg/kg]) in *mdr1a*(-/-) and *mdr1a*(+/+) mice (open and solid symbols, respectively). Data are presented as mean ± S.E. ($n \geq 3$). Note: At the given doses, nearly equivalent brain concentrations where achieved in *mdr1a*(-/-) and *mdr1a*(+/+) mice, however methadone and loperamide serum concentrations in the *mdr1a*(+/+) mice were much higher than in *mdr1a*(-/-) mice.

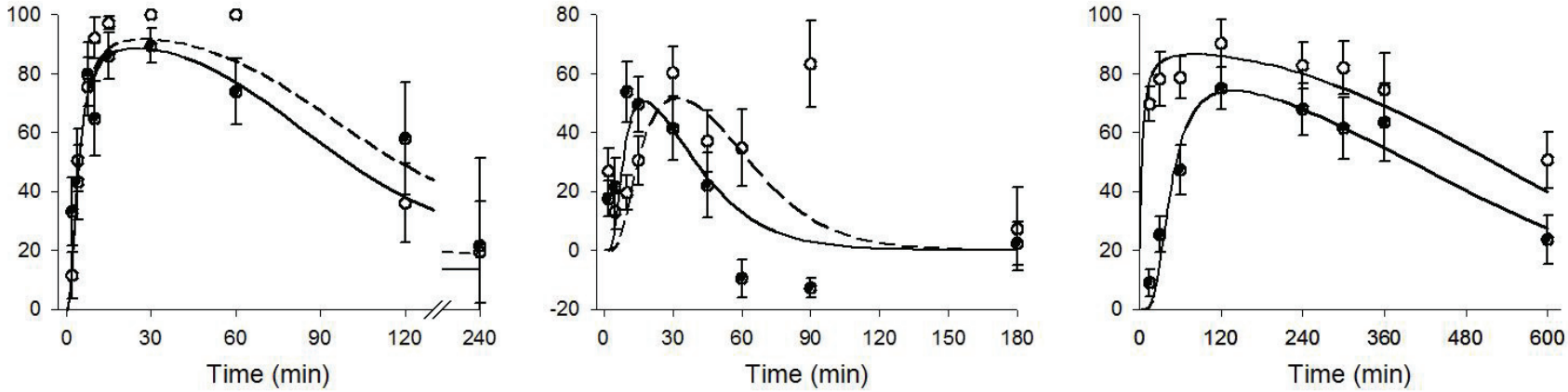

Figure 4.3. Time course of antinociception following s.c. administration of opioids (from left to right: fentanyl, methadone, and loperamide) in *mdr1a*(-/-) and *mdr1a*(+/+) mice (open and solid symbols, respectively). Data are presented as mean ± S.E. (n = 4 to 36).

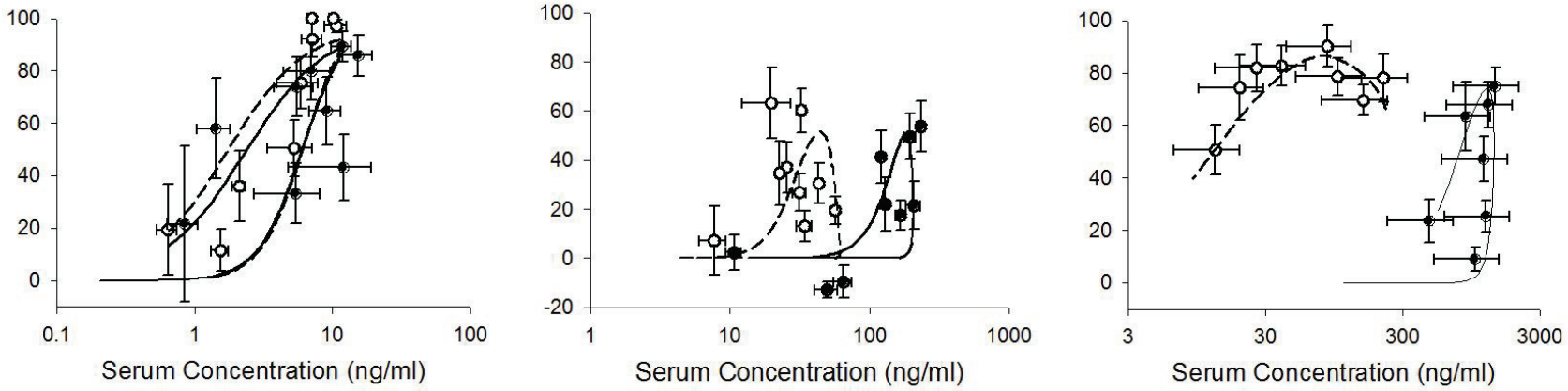

Figure 4.4. Relationship between antinociception and opioid serum concentration (from left to right: fentanyl, methadone, and loperamide) in *mdr1a*(-/-) and *mdr1a*(+/+) mice (open and solid symbols, respectively). Data are presented as mean ± S.E. (n = 4 to 36).

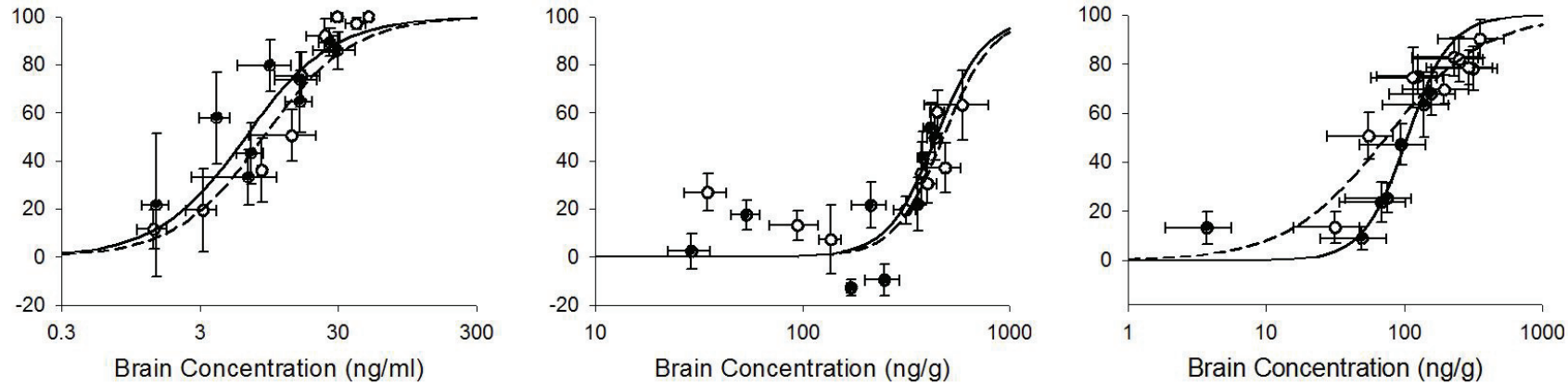

Figure 4.5. Relationship between antinociception and opioid brain concentration (from left to right: fentanyl, methadone, and loperamide) in *mdr1a*(-/-) and *mdr1a*(+/+) mice (open and solid symbols, respectively). Dashed and solid lines represent the fit of a kinetic model to the *mdr1a*(+/+) and *mdr1a*(-/-) data, respectively Data are presented as mean ± S.E. (n = 4 to 36).

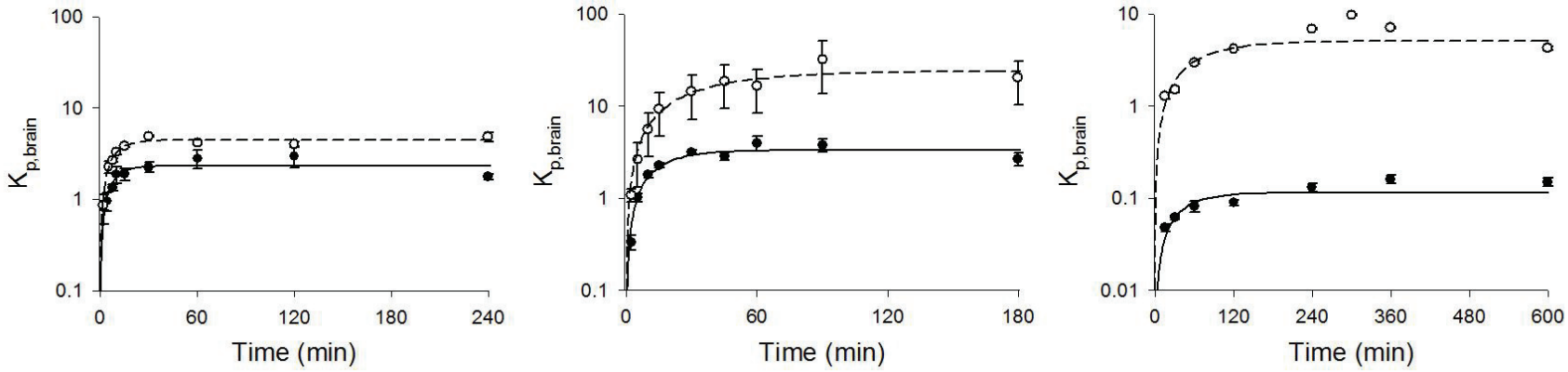

Figure 4.6. Time course of opioid (from left to right: fentanyl, methadone, and loperamide) $K_{p,brain}$ in *mdr1a*(-/-) and *mdr1a*(+/+) mice (open and solid symbols, respectively). Dashed and solid lines represent the fit of a kinetic model to the *mdr1a*(+/+) and *mdr1a*(-/-) data, respectively.

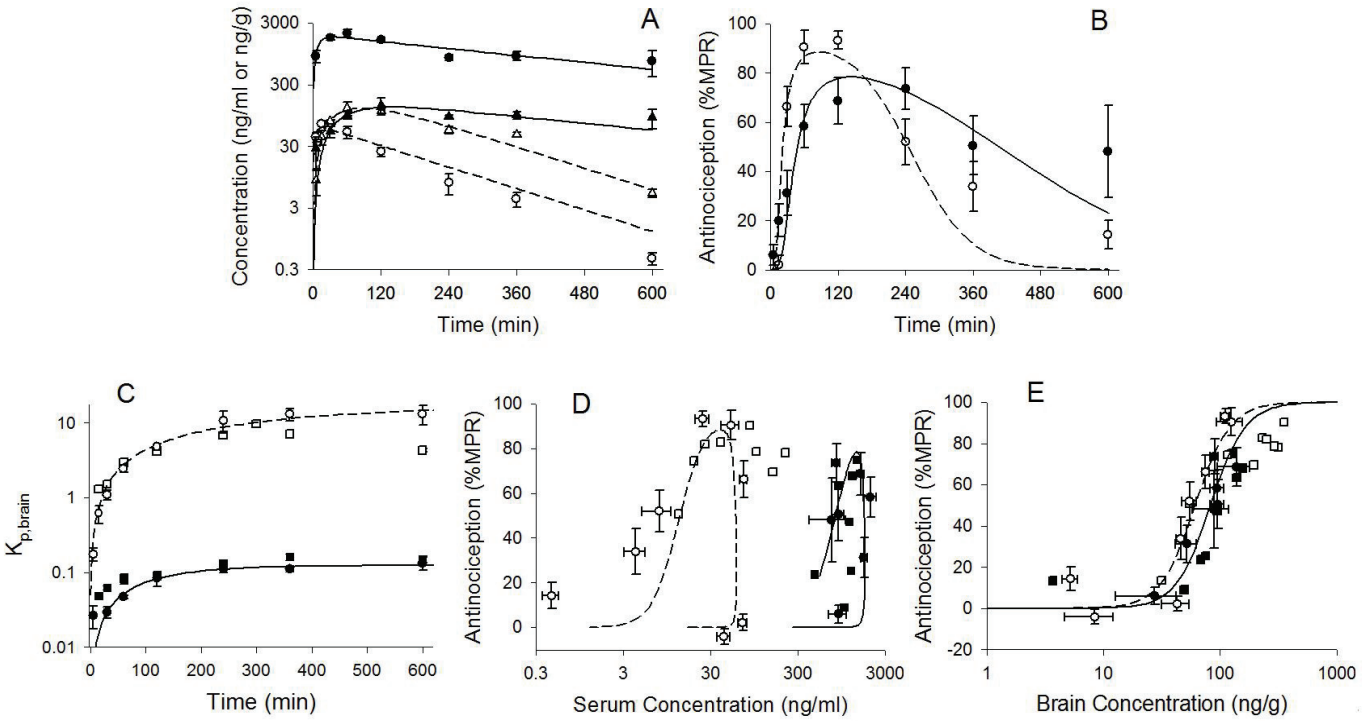

Figure 4.7. Pharmacokinetics/pharmacodynamics of loperamide in FVB mice. Time course of (A) serum (circle) and brain (triangle) concentrations, (B) antinociception, and (C) $K_{p,brain}$ following s.c. administration of 1- and 25-mg/kg dose of loperamide in FVB *mdr1a/b*(-/-) and *mdr1a/b*(+/+) mice, respectively. Antinociception versus serum and brain concentrations are depicted in panels D and E, respectively. Solid and open symbols represent mean data ± S.E. (n=?) from P-gp-competent and P-gp-deficient mice, respectively. Solid and dashed lines represent the fit of a PK/PD model to the FVB *mdr1a/b*(+/+) and *mdr1a/b*(-/-) mouse data, respectively. For comparison, squares symbols in panel C, D, and E represent the mean loperamide data obtained from CF-1 mice.

REFERENCES

Chen C, Liu X and Smith BJ (2003) Utility of Mdr1-gene deficient mice in assessing the impact of P-glyco-protein on pharmacokinetics and pharmacodynamics in drug discovery and development. *Curr Drug Metab* **4:**272-291.

Chen C and Pollack GM (1997) Blood-brain disposition and antinociceptive effects of -D-penicillamine2,5-enkephalin in the mouse. *J Pharmacol Exp Ther* **283:**1151-1159.

Chen C and Pollack GM (1998) Altered disposition and antinociception of [D-penicillamine(2,5)] enkephalin in mdr1a-gene-deficient mice. *J Pharmacol Exp Ther* **287:**545-552.

Dagenais C, Graff CL and Pollack GM (2004) Variable modulation of opioid brain uptake by P-glycoprotein in mice. *Biochem Pharmacol* **67:**269-276.

Golden PL and Pardridge WM (2000) Brain microvascular P-glycoprotein and a revised model of multidrug resistance in brain. *Cell Mol Neurobiol* **20:**165-181.

Golden PL and Pollack GM (2003) Blood-brain barrier efflux transport. *J Pharm Sci* **92:**1739-1753.

Gros P, Ben Neriah YB, Croop JM and Housman DE (1986) Isolation and expression of a complementary DNA that confers multidrug resistance. *Nature* **323:**728-731.

Juliano R (1976) Drug-resistant mutants of Chinese hamster ovary cells possess an altered cell surface carbohydrate component. *J Supramol Struct* **4:**521-526.

Kalvass JC, Graff CL and Pollack GM (2004) Use of loperamide as a phenotypic probe of mdr1a status in CF-1 mice. *Pharm Res* **21:**1867-1870.

Letrent SP, Pollack GM, Brouwer KR and Brouwer KL (1999) Effects of a potent and specific P-glycoprotein inhibitor on the blood-brain barrier distribution and antinociceptive effect of morphine in the rat. *Drug Metab Dispos* **27:**827-834.

Matheny CJ, Lamb MW, Brouwer KR and Pollack GM (2001) Pharmacokinetic and pharmacodynamic implications of P-glycoprotein modulation. *Pharmacotherapy* **21:**778-796.

Schinkel AH, Smit JJ, van Tellingen O, Beijnen JH, Wagenaar E, van Deemter L, Mol CA, van der Valk MA, Robanus-Maandag EC, te Riele HP and et al. (1994) Disruption of the mouse mdr1a P-glycoprotein gene leads to a deficiency in the blood-brain barrier and to increased sensitivity to drugs. *Cell* **77:**491-502.

Schinkel AH, Wagenaar E, Mol CA and van Deemter L (1996) P-glycoprotein in the blood-brain barrier of mice influences the brain penetration and pharmacological activity of many drugs. *J Clin Invest* **97:**2517-2524.

Sugiyama D, Kusuhara H, Lee YJ and Sugiyama Y (2003) Involvement of multidrug resistance associated protein 1 (Mrp1) in the efflux transport of 17beta estradiol-D-17beta-glucuronide (E217betaG) across the blood-brain barrier. *Pharm Res* **20:**1394-1400.

Thiebaut F, Tsuruo T, Hamada H, Gottesman MM, Pastan I and Willingham MC (1989) Immunohistochemical localization in normal tissues of different epitopes in the multidrug transport protein P170: evidence for localization in brain capillaries and crossreactivity of one antibody with a muscle protein. *J Histochem Cytochem* **37:**159-164.

Thompson SJ, Koszdin K and Bernards CM (2000) Opiate-induced analgesia is increased and prolonged in mice lacking P-glycoprotein. *Anesthesiology* **92:**1392-1399.

Tsuji A, Terasaki T, Takabatake Y, Tenda Y, Tamai I, Yamashima T, Moritani S, Tsuruo T and Yamashita J (1992) P-glycoprotein as the drug efflux pump in primary cultured bovine brain capillary endothelial cells. *Life Sci* **51:**1427-1437.

Wang JS, Ruan Y, Taylor RM, Donovan JL, Markowitz JS and DeVane CL (2004b) Brain penetration of methadone (R)- and (S)-enantiomers is greatly increased by P-glycoprotein deficiency in the blood-brain barrier of Abcb1a gene knockout mice. *Psychopharmacology (Berl)* **173:**132-138.

Zong J and Pollack GM (2000) Morphine antinociception is enhanced in *mdr1a* gene-deficient mice. *Pharm Res* **17:**749-75

CHAPTER 5

PHARAMCOKINETICS AND PHARMACODYNAMICS OF ALFENTANIL IN P-GLYCOPROTEIN-COMPETENT AND P-GLYCOPROTEIN-DEFICIENT MICE: P-GLYCOPROTEIN EFFLUX ALTERS ALFENTANIL BRAIN DISPOSITION AND ANTINOCICEPTION.

This chapter has been published in *Drug Metabolism and Disposition* and is presented in the style of that journal.

ABSTRACT

Previous studies have indicated that P-glycoprotein (P-gp) attenuates the central nervous system penetration and central activity of some opioids. The impact of P-gp-mediated efflux on the disposition and efficacy of the synthetic opioid alfentanil currently is unknown. In this study, P-gp-competent [*mdr1a*(+/+)] and P-gp-deficient [*mdr1a*(–/–)] mice were used to investigate the impact of P-gp-mediated efflux on the systemic pharmacokinetics, brain disposition, and central activity of alfentanil. Equipotent doses of alfentanil were administered to *mdr1a*(+/+) and *mdr1a*(–/–) mice (0.2 and 0.067 mg/kg, respectively), and the time course of brain and serum concentrations as well as antinociception were determined. A pharmacokinetic-pharmacodynamic (PK-PD) model was fit to the data and used to assess the impact of P-gp on parameters associated with alfentanil disposition and action. The *mdr1a*(+/+) mice were less sensitive to alfentanil than *mdr1a*(–/–) mice, requiring a 3-fold higher dose to produce similar antinociception. PK-PD modeling revealed no differences in alfentanil systemic pharmacokinetics between P-gp expressers and nonexpressers. However, the steady-state brain-to-serum concentration ratio ($K_{p,brain,ss}$) was ~3-fold lower in *mdr1a*(+/+) mice compared with *mdr1a*(–/–) mice (0.19 ± 0.01 versus 0.54 ±

0.04, respectively). Consistent with the ~3-fold lower $K_{p,brain,ss}$, the antinociception versus serum concentration relationship in *mdr1a*(+/+) mice was shifted ~3-fold rightward compared with *mdr1a*(–/–) mice. However, there was no difference in the antinociception versus brain concentration relationship, or in the brain tissue EC_{50} (11 ± 1.8 versus 9.2 ± 1.7 ng/g), between *mdr1a*(+/+) and *mdr1a*(–/–) mice. These results indicate 1) that alfentanil is an in vivo P-gp substrate and 2) are consistent with the hypothesis that P-gp-mediated efflux attenuates antinociception by reducing alfentanil $K_{p,brain,ss}$.

INTRODUCTION

P-glycoprotein (P-gp) is the 170-kDa protein product of the multidrug resistance gene (*mdr1*) first identified for its ability to confer multidrug resistance in tumor cells (Juliano, 1976; Gros et al., 1986). P-gp mediates excretory and barrier functions in several tissue (e.g., proximal tubular cells of the kidneys, the canalicular membrane of hepatocytes in the liver, the apical membrane of intestinal enterocytes, and the luminal membrane of brain capillary endothelial cells) (Thiebaut et al., 1987; Cordon-Cardo et al., 1989, 1990). P-gp seems to play a protective role in intact mammals by attenuating absorption, facilitating excretion, and restricting distribution to several tissue sites, including the central nervous system, of many structurally diverse xenobiotics, including calcium channel blockers, human immunodeficiency virus protease inhibitors, immunosuppressants, and opioids (Matheny et al., 2001).

Concomitant administration of P-gp inhibitors with P-gp substrates may lead to clinically significant drug interactions (Ho and Kim, 2005). For example, although the antidiarrheal agent loperamide is a potent opioid agonist, it is not centrally active due, in part, to P-gp-mediated efflux at the blood-brain barrier (BBB) (Schinkel et al., 1996). However,

when loperamide and the P-gp inhibitor quinidine were coadministered to subjects, respiratory depression was observed, which was attributed to an increase in loperamide brain concentration caused by P-gp inhibition (Sadeque et al., 2000). Although the precise mechanism of this interaction has not been verified, the potential for enhanced central effects of P-gp substrates due to P-gp inhibition is nonetheless clear.

Studies have demonstrated that P-gp attenuates the brain distribution and central activity of several opioids. For example, Thompson et al. (2000) showed that fentanyl, morphine, and methadone resulted in increased and prolonged antinociception in *mdr1a*(–/–) mice compared with *mdr1a*(+/+) mice. Likewise, the cyclic peptide opioid [D-Pen^2,D-Pen^5]-enkephalin produced increased antinociception in *mdr1a*(–/–) mice as opposed to their P-gp-expressing counterparts (Chen and Pollack, 1998). The P-gp inhibitor GF120918 was able to restore [D-Pen^2,D-Pen^5]-enkephalin-mediated antinociception in *mdr1a*(+/+) mice to levels observed in the *mdr1a*(–/–) mice (Chen and Pollack, 1999). The P-gp inhibitor verapamil also was capable of increasing morphine brain concentrations and morphine-associated antinociception in *mdr1a*(+/+) mice (Zong and Pollack, 2000).

Alfentanil is a synthetic opioid used for the induction of surgical anesthesia and the management of postsurgical pain. The alfentanil dose needs to be individualized based on numerous factors, including pathological condition, use of other medicines, and the type and duration of the surgical procedure (Scholz et al., 1996). Because alfentanil is a CYP3A4 substrate, CYP3A4 activity is another important determinant of the required alfentanil dose (Kharasch and Thummel, 1993). Many compounds are substrates of both CYP3A4 and P-gp. If alfentanil is a P-gp substrate, P-gp may be a determinant of the required alfentanil dose, a possible a source of interpatient variability, and a potential locus of drug-drug interactions.

The impact of P-gp-mediated efflux on the pharmacokinetics and central pharmacodynamics of alfentanil is unknown. Initial pilot experiments in this laboratory indicated P-gp-mediated efflux reduces alfentanil-associated antinociception. To investigate these observations further, and to evaluate whether P-gp efflux activity may contribute to interpatient variability in alfentanil response or serve as a locus of drug-drug interactions, the present study was undertaken to determine the impact of P-gp-mediated efflux on the systemic pharmacokinetics, brain disposition, and central activity of alfentanil. A PK-PD modeling approach was used to assess the mechanism(s) by which P-gp-mediated efflux influences alfentanil-associated antinociception.

MATERIALS AND METHODS

Materials.

Alfentanil was obtained from Taylor Pharmaceuticals (Decatur, IL), and loperamide was purchased from Sigma-Aldrich (St. Louis, MO). All other reagents were obtained from common sources and were of reagent grade or better.

Animals.

Male CF-1 *mdr1a*(+/+) and *mdr1a*(–/–) mice (30–40 g; Charles River Laboratories, Inc., Wilmington, MA) were maintained on a 12-h light/dark cycle in a temperature- and humidity-controlled room with access to water and food ad libitum. All procedures involving mice were approved by The Institutional Animal Care and Use Committee of the University of North Carolina and were conducted in accordance with *Principles of Laboratory Animal Care* (National Institutes of Health Publication 85-23, revised in 1985).

PK-PD Study.

Based on the results of pilot studies, 36 *mdr1a*(–/–) and 36 *mdr1a*(+/+) mice received equipotent subcutaneous doses of alfentanil in physiological saline (0.067 and 0.2 mg/kg, respectively). At 0.5, 1, 2, 4, 8, 15, 30, 45, and 60 min postadministration, antinociception was assessed, and four *mdr1a*(–/–) and four *mdr1a*(+/+) mice were sacrificed by decapitation for collection of brain tissue and trunk blood. Trunk blood was collected in 1.5-ml microcentrifuge tubes and was allowed to clot for ≥30 min at room temperature. Serum was harvested following centrifugation. Brain and serum samples were stored at –20°C until analysis by HPLC-tandem mass spectrometry.

Assessment of Antinociception.

Antinociception was assessed with the hot-plate latency test as described previously (Chen and Pollack, 1997). Before administration of alfentanil, baseline hot-plate latency was determined for each animal in triplicate. Hot-plate latency was defined as the time interval between placement on the hot-plate (55°C; Columbus Instruments, Columbus, OH) and first observation of a jump or lick of the hind limb(s). Animals with an average baseline latency <25 s were used in the study. A cut-off latency of 60 s was used to avoid tissue damage. The degree of antinociception was calculated as follows:

$$\%MPR = \frac{Test\ latency - Control\ latency}{60 - Control\ latency} x\ 100\% \qquad \text{(Eqn. 5.1)}$$

Quantitation of Alfentanil in Serum and Brain.

Brain samples were homogenized in water (1:2, v/v) with a sonic probe. A 25-µl aliquot of homogenate or serum was transferred to an HPLC vial, and protein was precipitated with 100 µl of methanol containing internal standard (5 ng/ml loperamide). The

sample was vortex-mixed and centrifuged, and the supernatant was analyzed by HPLC-tandem mass spectrometry. Samples (3 µl) were injected (autosampler; CTC Analytics, Zwingen, Switzerland) onto a Gemini 110A column (2.0 by 30 mm, 5 µm; Phenomenex, Torrance, CA) maintained at room temperature. The total run time was 3 min. Analytes were eluted with a linear gradient consisting of 10 mM ammonium acetate, pH 6.8 (A) and methanol (B) produced by two Shimadzu LC-10ADVP binary pumps. An initial condition of 5% B was ramped to 95% B over 2 min, held for 0.5 min, and then returned initial condition of 5% B in a single step to re-equilibrate the column. During the run, the flow rate was increased from 750 to 1500 µl/min over the first 2 min, held at 1500 µl/min for 1 min, and then returned to the initial flow rate of 750 µl/min in a single step. The entire column effluent was diverted from the source of the API-4000 quadrupole mass spectrometer (Turbo V Ionspray source, 700°C; PerkinElmerSciex Instruments, Boston, MA) for the first 1 min and last 0.5 min of the run. Alfentanil and loperamide were measured in positive ionization mode using multiple reaction monitoring (417.3 → 268.3 and 477.4 → 266.0, respectively). Standards were prepared in brain homogenate and serum and fitted with a quadratic equation with 1/y weighting (0.1–500 ng/ml). Accuracy of standards was within ± 15%.

Pharmacokinetic-Pharmacodynamic Analysis.

A compartmental modeling approach with distribution between serum and brain tissue was used to describe alfentanil pharmacokinetics. The pharmacokinetic model shown schematically in Fig. 5.1 was fit simultaneously to the serum and brain concentration data from both *mdr1a*(–/–) and *mdr1a*(+/+) mice using nonlinear least-squares regression (WinNonlin 4.1; Pharsight, Mountain View, CA). The absorption rate constant (K_a), central volume (V_c), and systemic clearance (Cl) did not differ between *mdr1a*(–/–) and *mdr1a* (+/+)

mice; therefore, they were assumed to be identical when fitting the model to the data from both mouse strains simultaneously. The brain uptake (Cl_{up}) and brain efflux (Cl_{efflux}) clearances were allowed to vary between *mdr1a*(–/–) and *mdr1a*(+/+) mice. The brain volume (V_b) was determined experimentally as 13.4 ml · kg^{-1}, assuming a specific gravity of 1.0 ml. The pharmacodynamic parameters EC_{50} and γ were determined directly from fitting a sigmoidal E_{max} model to the antinociception versus brain concentration (C) data:

$$\%MPR = \frac{E_{\max}\ x\ C^{\gamma}}{EC_{50} + C^{\gamma}} \qquad \text{(Eqn. 5.2)}$$

E_{max} was defined as 100%, and γ was constrained to the same value for *mdr1a*(–/–) and *mdr1a*(+/+) mice. The time course of the brain-to-serum concentration ratio ($K_{p,brain}$) was used to estimate the brain equilibration rate constant (k_{eq}) and steady-state brain-to-serum ratio ($K_{p,brain,ss}$) according to the following:

$$K_{p,brain} = K_{p,brain,ss}\ (1 - e^{-k_{eq}\ x\ t}) \qquad \text{(Eqn. 5.3)}$$

The brain equilibration half-life ($t_{1/2eq,brain}$) was obtained from k_{eq}:

$$t_{\frac{1}{2},eq,brain} = \frac{0.693}{k_{eq}} \qquad \text{(Eqn. 5.4)}$$

RESULTS

Alfentanil Pharmacokinetics.

Alfentanil was absorbed rapidly following subcutaneous administration, with peak serum and brain concentrations achieved in less than 10 min (Fig. 5.2). Alfentanil clearance was high (approximately equivalent to hepatic blood flow), assuming complete absorption from the subcutaneous site, and half-life was short ($t_{1/2}$ < 15 min). Alfentanil serum

concentrations were 3-fold lower in the *mdr1a*(–/–) mice, consistent with those animals receiving a 3-fold lower dose than their transporter-competent counterparts. However, the time course of brain concentrations in the *mdr1a*(–/–) and *mdr1a*(+/+) mice were nearly superimposable (Fig. 5.2). Both the systemic and brain tissue pharmacokinetics were capable of being described by the pharmacokinetic model (Fig. 5.2; Table 5.1). Parameter estimates obtained from the pharmacokinetic model are reported in Table 5.1.

Alfentanil Pharmacodynamics.

Pilot experiments indicated that, at equivalent doses, antinociceptive activity was lower in *mdr1a*(+/+) mice than in *mdr1a*(–/–) mice (data not shown). However, at a 3-fold higher dose (0.20 versus 0.067 mg/kg), the magnitude and duration of antinociception in *mdr1a*(+/+) were identical to those in *mdr1a*(–/–) mice (Fig. 5.3). In both *mdr1a*(+/+) and *mdr1a*(–/–) mice, alfentanil had a rapid onset of antinociception, a peak effect of ~85% MPR, and a rapid offset of action with nociceptive response returning to baseline within 60 min of administration. Consistent with a lower alfentanil potency in *mdr1a*(+/+) mice (due to P-gp-mediated efflux from the brain), there was a 3-fold rightward shift in the serum concentration-effect relationship in transporter-competent versus transporter-deficient mice (Fig. 5.4). There was no difference in the brain concentration-effect relationship or brain EC_{50} values between the *mdr1a*(+/+) and *mdr1a*(–/–) mice (Fig. 5.5; Table 5.1). The PK-PD model adequately described the time course of antinociception, the serum concentration-effect relationships, and the brain concentration-effect relationships in both mouse strains (Figs. 5.3, 5.4, 5.5, respectively). The PK-PD model indicated the presence of a slight counterclockwise hysteresis in the antinociceptive effect versus serum concentration relationship (Fig. 5.4). However, there was no hysteresis in the antinociceptive effect versus

brain concentration relationship (Fig. 5.5). Pharmacodynamic parameter estimates obtained from the PK-PD model are reported in Table 5.1.

Alfentanil Brain Disposition.

Equilibration of alfentanil between brain and serum occurred rapidly, with state-steady $K_{p,brain}$ reached within approximately 4 min. The time course of alfentanil $K_{p,brain}$ is shown in Fig. 5.6. The $K_{p,brain,ss}$ was less than unity for both *mdr1a*(+/+) and *mdr1a*(–/–) mice, and the $K_{p,brain,ss}$ in *mdr1a*(–/–) mice was 3-fold higher than in *mdr1a*(+/+) mice (Table 5.1; Fig. 5.6). Estimates of Cl_{up} and Cl_{efflux} differed between *mdr1a*(+/+) and *mdr1a*(–/–) mice, with Cl_{up} increased (1.6-fold) and Cl_{efflux} decreased (1.6-fold) in *mdr1a*(–/–) mice. The $t_{1/2eq,brain}$ was short (≤1.5 min) in both *mdr1a*(+/+) and *mdr1a*(–/–) mice. However, $t_{1/2eq,brain}$ was ~1.5-fold longer in *mdr1a*(–/–) mice (Table 5.1). Consistent with implicit assumptions of the PK model, the ratios of Cl_{up}/Cl_{efflux} [0.18 and 0.47 in *mdr1a*(+/+) and *mdr1a*(–/–) mice, respectively) were comparable with the respective $K_{p,brain,ss}$ values (Table 5.1).

DISCUSSION

The ATP-dependent efflux transporter P-gp is the protein product of the *mdr1* gene, and it is expressed in variety of tissues, including the luminal membrane of the BBB (Cordon-Cardo et al., 1989, 1990). Several studies have indicated that some opioids have reduced brain penetration and attenuated central activity due to P-gp-mediated efflux (Chen and Pollack, 1998; Thompson et al., 2000; Zong and Pollack, 2000; Dagenais et al., 2004). The influence of P-gp on the pharmacokinetics and central pharmacodynamics of the synthetic opioid alfentanil had not been explored previously. Pilot experiments in this laboratory indicated that alfentanil produced less antinociception in *mdr1a*(+/+) mice than in *mdr1a*(–/–) mice, consistent with P-gp-mediated efflux at the BBB. In this study, the time

course of antinociception as well as serum and brain concentrations of alfentanil were evaluated in *mdr1a*(+/+) and *mdr1a*(–/–) mice to investigate the impact of P-gp-mediated efflux on the systemic pharmacokinetics, brain disposition, and central activity of alfentanil.

To achieve a similar degree of antinociception in both *mdr1a*(+/+) and *mdr1a*(–/–) mice, the dose administered to *mdr1a*(+/+) mice was 3-fold higher than that in transporter-deficient animals. Even though the doses were different, pharmacokinetic modeling indicated no difference in systemic pharmacokinetics between *mdr1a*(+/+) and *mdr1a*(–/–) mice (Table 5.1). This result was not unexpected, because P-gp often has minimal impact on systemic pharmacokinetics following subcutaneous or intravenous administration (Chen et al., 2003).

In contrast to the serum pharmacokinetics, P-gp had a pronounced effect on alfentanil brain pharmacokinetics. The $K_{p,brain,ss}$ of *mdr1a*(+/+) mice was ~3-fold lower compared with *mdr1a*(–/–) mice (0.19 versus 0.54). The decrease in $K_{p,brain,ss}$ was accompanied by a ~1.6-fold decrease in Cl_{up} and ~1.6-fold increase in Cl_{efflux}. These observations are consistent with the hypothesis that P-gp decreases $K_{p,brain,ss}$ by both attenuating brain uptake and enhancing brain efflux. Similar observations have been reported for other P-gp substrates (Kusuhara et al., 1997). The brain and serum concentrations of alfentanil equilibrated rapidly, with a $t_{1/2,eq,,brain}$ ≦1.5 min. This value is similar to previously reported estimates from humans (Lotsch, 2005). Unexpectedly, the $t_{1/2,eq,,brain}$ was shorter in the *mdr1a*(+/+) mice (Table 5.1). This observation may be explained by the fact that $t_{1/2,eq,,brain}$ is inversely proportional to Cl_{efflux} and that P-gp increased Cl_{efflux} (~1.6-fold), thereby causing a proportional decrease in the $t_{1/2,eq,,brain}$ in *mdr1a*(+/+) mice (~1.4-fold). Interestingly, this result implies that P-gp-mediated efflux may reduce equilibration time between brain and systemic concentrations. Previously, the short $t_{1/2,eq,,brain}$ of alfentanil had been attributed in part to a small $K_{p,brain,ss}$

(Upton et al., 1997). In this study, the $K_{p,brain,ss}$ of alfentanil was less than unity for both *mdr1a*(+/+) and *mdr1a*(–/–) mice, indicating two important points: first, that a small $K_{p,brain,ss}$ may indeed facilitate rapid equilibrium between systemic and brain concentration, and second, that a $K_{p,brain,ss}$ greater than unity may not be needed, or even desirable, for a central nervous system drug with rapid onset and offset of action.

PK-PD modeling indicated an ~3-fold rightward shift in the antinociception versus serum concentration relationship for *mdr1a*(+/+) mice compared with *mdr1a*(–/–) mice. PK-PD modeling also revealed a slight counterclockwise hysteresis in the antinociception versus serum concentration relationship for both *mdr1a*(+/+) and *mdr1a*(–/–) mice. However, there was no hysteresis in the antinociception versus brain concentration relationship, and the brain tissue EC_{50} values between *mdr1a*(+/+) and *mdr1a*(–/–) mice were not different. These observations are consistent with brain concentrations driving antinociception, and they provide compelling evidence that P-gp efflux attenuates alfentanil antinociception by reducing $K_{p,brain,ss}$.

This study is the first to show that alfentanil is a P-gp substrate. In contrast, an earlier study that examined the transcellular flux of alfentanil across L-MDR1 (expressing P-gp) and LLC-PK1 cell monolayers concluded alfentanil was not a P-gp substrate and had low affinity toward P-gp (IC_{50} > 50 μM) (Wandel et al., 2002). There are at least two possible explanations for the difference in results between these two studies. First, even though murine-human differences in P-gp substrate recognition and transport seem modest for most substrates (Yamazaki et al., 2001; Hochman et al., 2002; Takeuchi et al., 2006), there might be species differences in the P-gp-mediated transport of alfentanil. This study evaluated the in vivo effects of murine P-gp (*mdr1a*), whereas the previous work studied the human form

of P-gp (*MDR1*) in vitro. Second, in vitro systems often are less sensitive than intact animal models for identifying weak P-gp substrates (Polli et al., 2001). In the Wandel et al. (2002) study, the basal activity of endogenous efflux transporter(s) in the LLC-PK1 and L-MDR1 cell lines may have masked P-gp-mediated transport of alfentanil, because flux was higher in the basolateral-to-apical direction in both the P-gp-expressing L-MDR1 and control LLC-PK1 cell monolayers.

Alfentanil is a CYP3A4 substrate in humans, and it has been used as a noninvasive clinical probe to evaluate CYP3A4 activity (Kharasch et al., 2005). The degree of miosis produced by alfentanil has been shown to correlate well with alfentanil plasma concentrations, and as such alfentanil-pupillometry studies have been used to evaluate CYP3A4 activity and to conduct drug-drug interaction studies. An assumption of such studies is that any increase or decrease in alfentanil-induced miosis is due primarily to changes in CYP3A4 activity (inhibition or induction). The present results showing that alfentanil is a P-gp substrate indicate that alfentanil-pupillometry studies may have the potential to detect alterations in P-gp activity. Previous pupillometry studies conducted with the P-gp substrates morphine, fentanyl, methadone, and loperamide have shown that inhibition of P-gp at the BBB by the P-gp inhibitor quinidine is modest (Kharasch et al., 2003, 2004ab; Skarke et al., 2003). Because quinidine is one of the most potent compounds capable of inhibiting P-gp that is in clinical use, the likelihood of significant inhibition of P-gp at the BBB seems remote. However, future drug-drug interaction studies conducted with alfentanil should be assessed carefully to ensure that any observed drug-drug interaction is not caused by P-gp inhibition. The clinical significance of alfentanil being a P-gp substrate is not known, but it may be modest considering that only a 3-fold P-gp effect was observed in mice, that all human *MDR1*

polymorphisms identified to date retain most functional activity, and that clinically significant inhibition of P-gp at the BBB has not been well documented (Ho and Kim, 2005; Kerb, 2006).

In summary, the present study indicated that alfentanil is a P-gp substrate, and that P-gp-mediated efflux attenuates alfentanil antinociception by reducing $K_{p,brain,ss}$. These observations may have important implications regarding interindividual differences in alfentanil pharmacodynamics and for the risk of drug-drug interactions. Additional studies may be warranted to assess the clinical relevance of P-gp efflux as a determinant of alfentanil pharmacotherapy.

Table 5.1. PK-PD parameters for alfentanil in *mdr1a*(-/-) and *mdr1a*(+/+) mice

Parameter[a]	Weighting	*mdr1a*(-/-)	*mdr1a*(+/+)
K_a (min^{-1})		0.35 ± 0.03	0.35 ± 0.03
Cl ($ml \cdot min^{-1} \cdot kg^{-1}$)	1/y	82 ± 3	82 ± 3
V_c ($ml \cdot kg^{-1}$)	1/y	1000 ± 60	1000 ± 60
$t_{1/2}$ (min)		12 ± 0.6[b]	12 ± 0.6[b]
Cl_{up} ($ml \cdot min^{-1} \cdot kg^{-1}$)	1/y	7 ± 5	4 ± 3
Cl_{efflux} ($ml \cdot min^{-1} \cdot kg^{-1}$)	1/y	13 ± 12	22 ± 17
V_b ($ml \cdot kg^{-1}$)		13.4 (fixed)	13.4 (fixed)
EC_{50} (ng/g)	Uniform	9.2 ± 1.7	11 ± 1.8
γ	Uniform	1.8 ± 0.4	1.8 ± 0.4
$K_{p,brain}$	1/y	0.54 ± 0.04	0.195 ± 0.008
K_{eq} (min^{-1})	1/y	0.46 ± 0.10	0.64 ± 0.09
$t_{1/2eq,brain}$ (min)		1.5 ± 0.3	1.08 ± 0.16

[a] Parameter estimate ± S.E. from nonlinear least-squares regression analysis of pooled *mdr1a*(-/-) or *mdr1a*(+/+) mouse data. K_a, Cl, V_c, V_b, and γ were constrained to the same value for *mdr1a*(-/-) or *mdr1a*(+/+) mice. $t_{1/2}$ and $t_{1/2eq,brain}$ were calculated from $0.693/(V_c/Cl)$ and $0.693/K_{eq,brain}$, respectively.
[b] Propagation of error was used to calculated S.E.

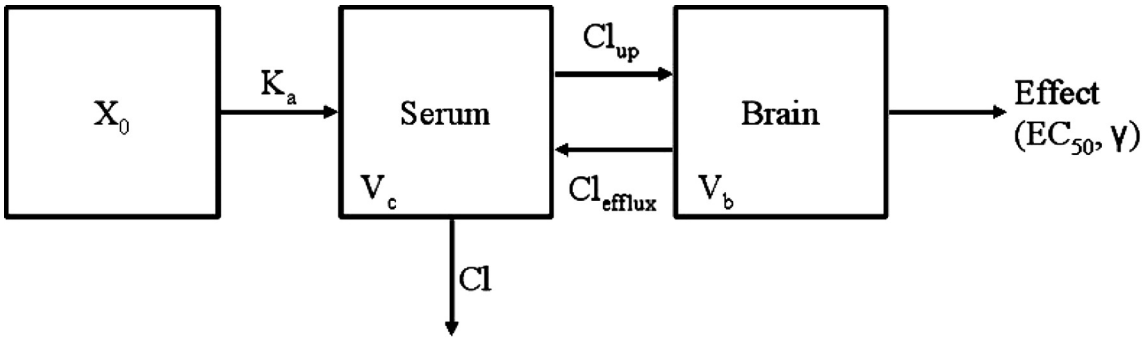

Figure 5.1. Pharmacokinetic-pharmacodynamic model for alfentanil disposition and antinociception in mice. Pharmacokinetic parameters were obtained by fitting the above-mentioned model to the time course of serum and brain concentrations of *mdr1a*(–/–) and *mdr1a*(+/+) mice following subcutaneous administration of alfentanil. k_a, V_c, and systemic Cl were held constant between *mdr1a*(–/–) and *mdr1a*(+/+) mice, whereas Cl_{up} and Cl_{efflux} were allowed to vary between *mdr1a*(–/–) and *mdr1a*(+/+) mice. The brain volume (V_b) was fixed. The effect parameters EC_{50} and γ were obtained by fitting a sigmoidal E_{max} model to the brain concentration versus antinociception data. E_{max} was defined as 100%, and γ was constrained to the same value for *mdr1a*(–/–) and *mdr1a*(+/+) mice.

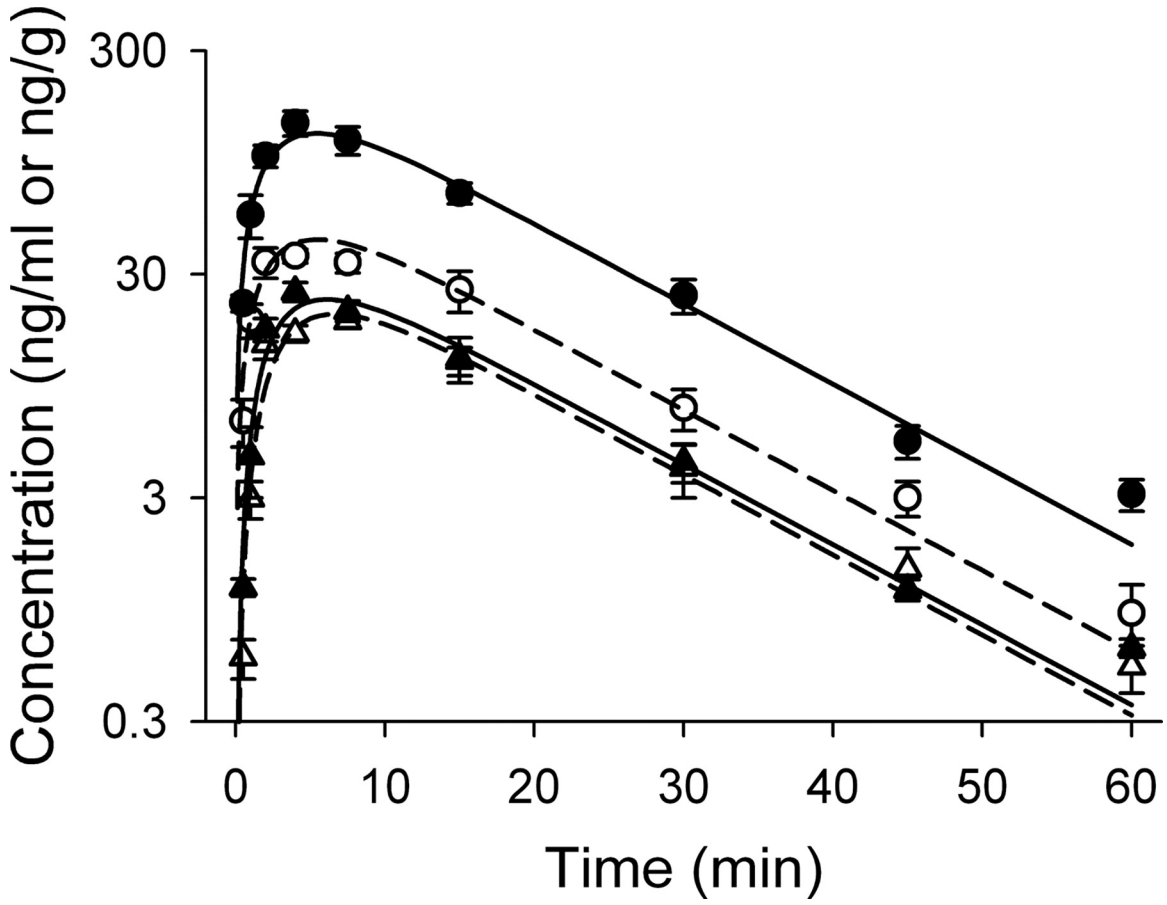

Figure 5.2. Time course of serum (●) and brain (▲) concentrations following a 0.067- or 0.2-mg/kg s.c. dose of alfentanil in *mdr1a*(–/–) (open symbols) or *mdr1a*(+/+) (solid symbols) mice, respectively. Data are presented as mean ± S.E. (n ≥3). Dashed and solid lines represent the fit of the PK model to the concentration data for *mdr1a*(–/–) and *mdr1a*(+/+) mice, respectively.

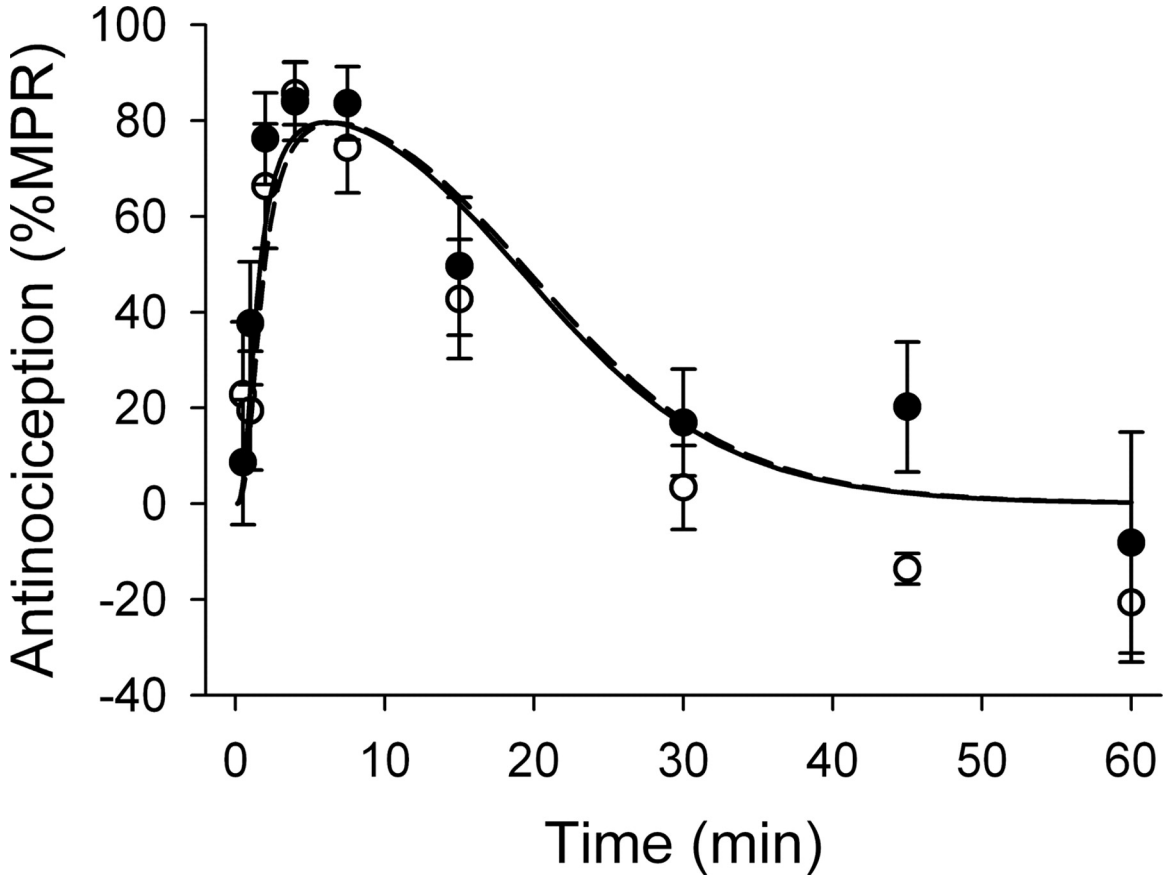

Figure 5.3. Time course of antinociception following a 0.067- or 0.2-mg/kg s.c. dose of alfentanil in *mdr1a*(–/–) (open symbols) or *mdr1a*(+/+) (solid symbols) mice, respectively. Data are presented as mean ± S.E. ($n \geq 3$). Dashed and solid lines represent the fit of the PK-PD model to the antinociception data for *mdr1a*(–/–) and *mdr1a*(+/+) mice, respectively.

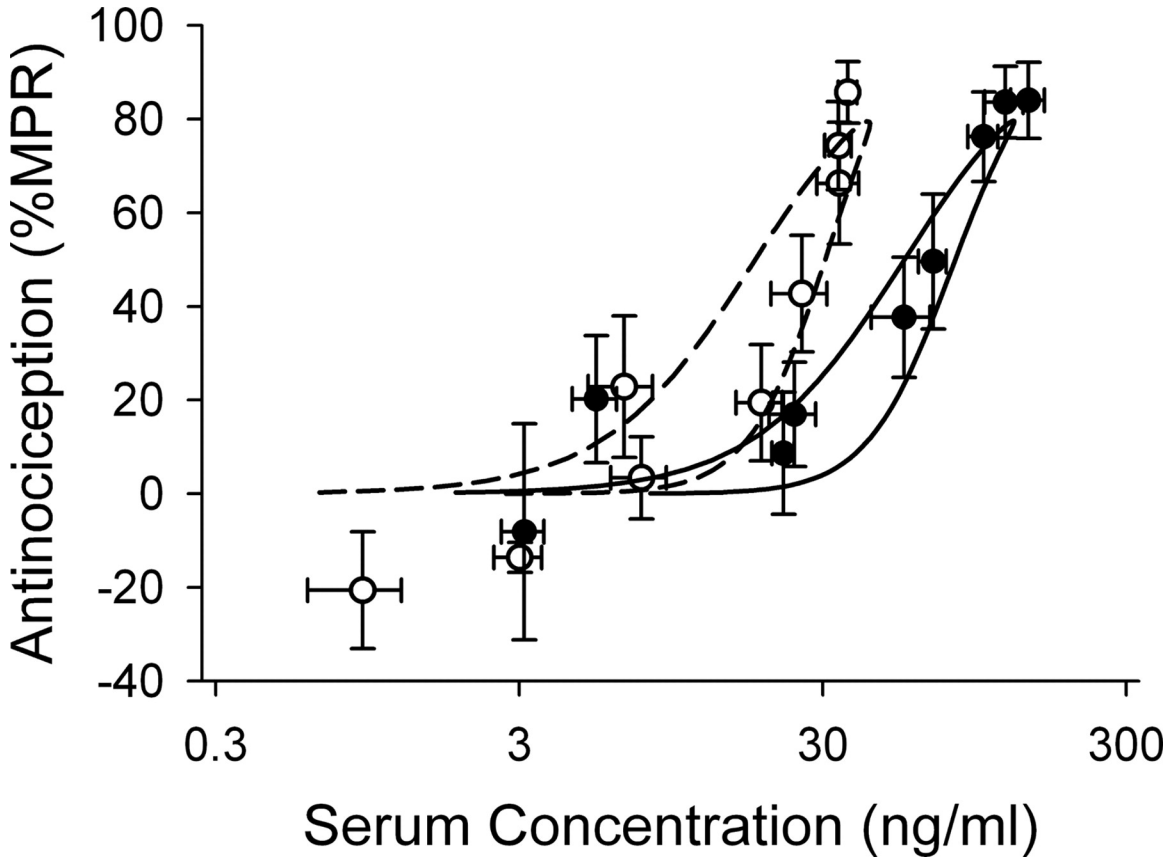

Figure 5.4. Relationship between antinociception and serum concentration of alfentanil following a 0.067-mg/kg s.c. dose [*mdr1a*(–/–); ○] or 0.2-mg/kg s.c. dose [*mdr1a*(+/+); ●]. Data are presented as mean ± S.E. [concentration data ($n \geq 3$); a ntinociception ($n = 4–33$)]. Dashed and solid lines represent the fit of the PK-PD model to the antinociception and serum concentration data for *mdr1a*(–/–) and *mdr1a*(+/+) mice, respectively. A slight counterclockwise hysteresis is present for both *mdr1a*(–/–) and *mdr1a*(+/+) mouse strains.

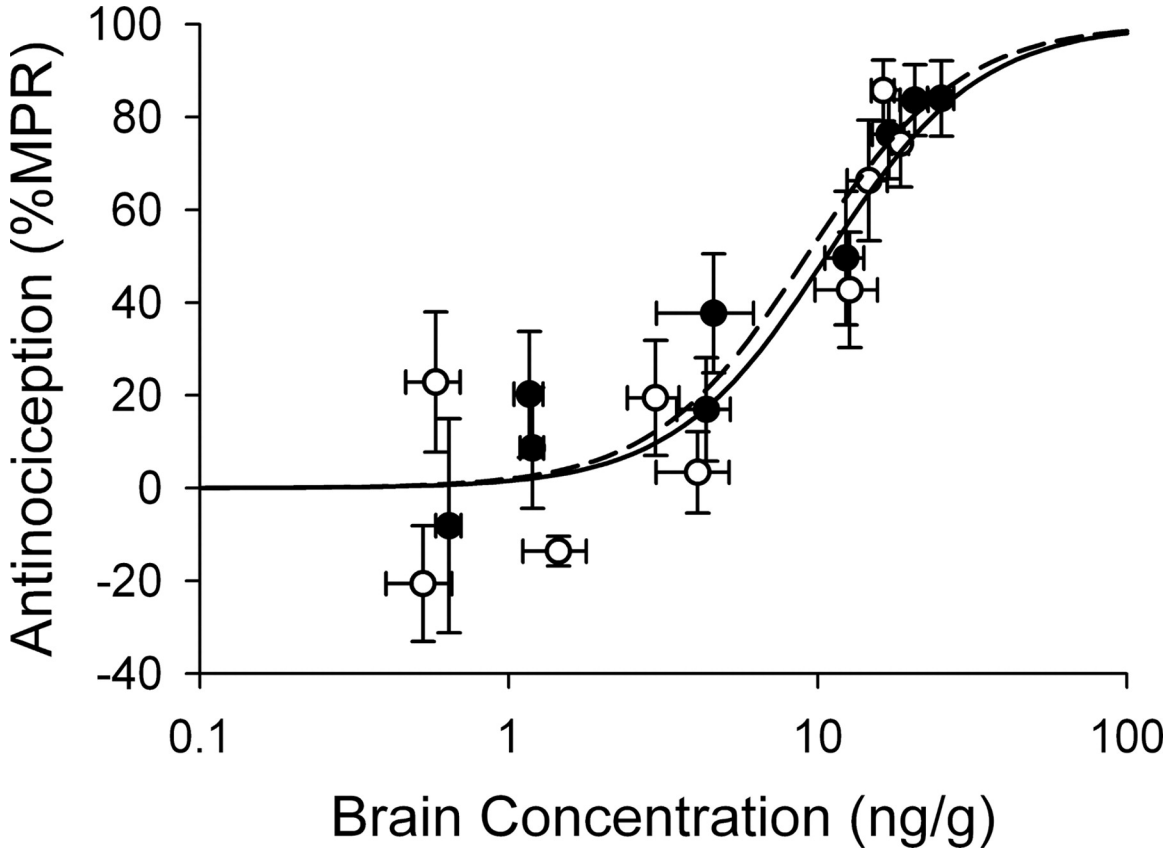

Figure 5.5. Relationship between antinociception and brain concentration of alfentanil following a 0.067-mg/kg s.c. dose [*mdr1a*(–/–);○] or 0.2-mg/kg s.c. dose [*mdr1a*(+/+);●]. Data are presented as mean ± S.E. [concentration data ($n \geq 3$); antinociception (n = 4–33)]. Dashed and solid lines represent the fit of a sigmoidal E_{max} model to the effect data obtained from *mdr1a*(–/–) and *mdr1a*(+/+) mice, respectively. Gamma was constrained to the same value for both mouse strains.

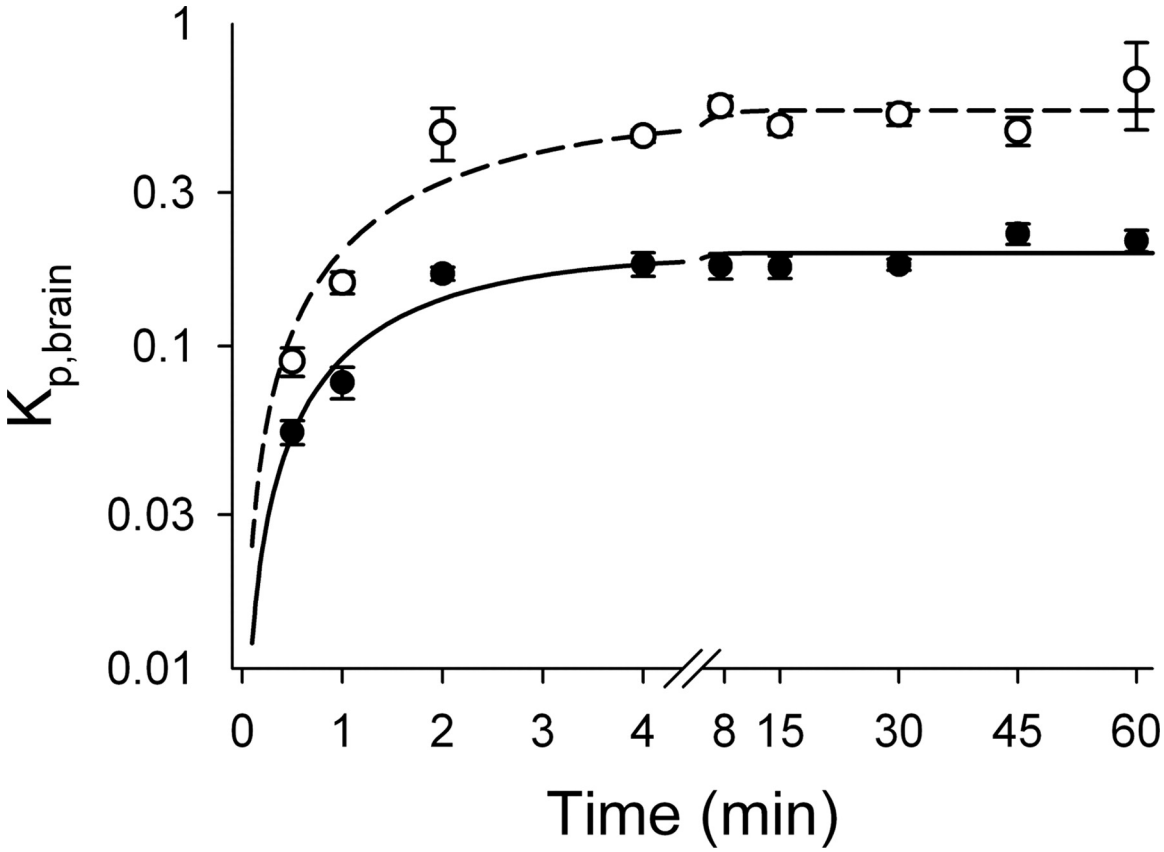

Figure 5.6. Time course of alfentanil $K_{p,brain}$ in mice following a 0.067-mg/kg s.c. dose [*mdr1a*(–/–);○] or 0.2-mg/kg s.c. dose [*mdr1a*(+/+);●]. Data are presented as mean ± S.E. ($n \geq 3$). Dashed and solid lines represent the fit of a kinetic model to the *mdr1a*(–/–) and *mdr1a*(+/+) data, respectively.

REFERENCES

Chen C, Liu X, and Smith BJ (2003) Utility of Mdr1-gene deficient mice in assessing the impact of P-glyco-protein on pharmacokinetics and pharmacodynamics in drug discovery and development. Curr Drug Metab 4: 272–291.

Chen C and Pollack GM (1997) Blood-brain disposition and antinociceptive effects of -D-penicillamine2,5-enkephalin in the mouse. J Pharmacol Exp Ther 283: 1151–1159.

Chen C and Pollack GM (1998) Altered disposition and antinociception of [D-penicillamine(2,5)] enkephalin in mdr1a-gene-deficient mice. J Pharmacol Exp Ther 287: 545–552.

Chen C and Pollack GM (1999) Enhanced antinociception of the model opioid peptide [D-penicillamine] enkephalin by P-glycoprotein modulation. *Pharm Res (NY)* **16:** 296–301.

Cordon-Cardo C, O'Brien JP, Boccia J, Casals D, Bertino JR, and Melamed MR (1990) Expression of the multidrug resistance gene product (P-glycoprotein) in human normal and tumor tissues. *J Histochem Cytochem* **38:** 1277–1287.

Cordon-Cardo C, O'Brien JP, Casals D, Rittman-Grauer L, Biedler JL, Melamed MR, and Bertino JR (1989) Multidrug-resistance gene (P-glycoprotein) is expressed by endothelial cells at blood-brain barrier sites. *Proc Natl Acad Sci USA* **86:** 695–698.

Dagenais C, Graff CL, and Pollack GM (2004) Variable modulation of opioid brain uptake by P-glycoprotein in mice. *Biochem Pharmacol* **67:** 269–276.

Gros P, Ben Neriah YB, Croop JM, and Housman DE (1986) Isolation and expression of a complementary DNA that confers multidrug resistance. *Nature (Lond)* **323:** 728–731.

Ho RH and Kim RB (2005) Transporters and drug therapy: implications for drug disposition and disease. *Clin Pharmacol Ther* **78:** 260–277.

Hochman JH, Yamazaki M, Ohe T, and Lin JH (2002) Evaluation of drug interactions with P-glycoprotein in drug discovery: in vitro assessment of the potential for drug-drug interactions with P-glycoprotein. *Curr Drug Metab* **3:** 257–273.

Juliano R (1976) Drug-resistant mutants of Chinese hamster ovary cells possess an altered cell surface carbohydrate component. *J Supramol Struct* **4:** 521–526.

Kerb R (2006) Implications of genetic polymorphisms in drug transporters for pharmacotherapy. *Cancer Lett* **234:** 4–33.

Kharasch ED, Hoffer C, Altuntas TG, and Whittington D (2004a) Quinidine as a probe for the role of P-glycoprotein in the intestinal absorption and clinical effects of fentanyl. *J Clin Pharmacol* **44:** 224–233.

Kharasch ED, Hoffer C, and Whittington D (2004b) The effect of quinidine, used as a probe for the involvement of P-glycoprotein, on the intestinal absorption and pharmacodynamics of methadone. *Br J Clin Pharmacol* **57:** 600–610.

Kharasch ED, Hoffer C, Whittington D, and Sheffels P (2003) Role of P-glycoprotein in the intestinal absorption and clinical effects of morphine. *Clin Pharmacol Ther* **74:** 543–554.

Kharasch ED and Thummel KE (1993) Human alfentanil metabolism by cytochrome P450 3A3/4. An explanation for the interindividual variability in alfentanil clearance? *Anesth Analg* **76:** 1033–1039.

Kharasch ED, Walker A, Hoffer C, and Sheffels P (2005) Sensitivity of intravenous and oral alfentanil and pupillary miosis as minimally invasive and noninvasive probes for hepatic and first-pass CYP3A activity. *J Clin Pharmacol* **45:** 1187–1197.

Kusuhara H, Suzuki H, Terasaki T, Kakee A, Lemaire M, and Sugiyama Y (1997) P-Glycoprotein mediates the efflux of quinidine across the blood-brain barrier. *J Pharmacol Exp Ther* **283:** 574–580.

Lotsch J (2005) Pharmacokinetic-pharmacodynamic modeling of opioids. *J Pain Symptom Manage* **29:** S90–S103.

Matheny CJ, Lamb MW, Brouwer KR, and Pollack GM (2001) Pharmacokinetic and pharmacodynamic implications of P-glycoprotein modulation. *Pharmacotherapy* **21:** 778–796.

Polli JW, Wring SA, Humphreys JE, Huang L, Morgan JB, Webster LO, and Serabjit-Singh CS (2001) Rational use of in vitro P-glycoprotein assays in drug discovery. *J Pharmacol Exp Ther* **299:** 620–628.

Sadeque AJ, Wandel C, He H, Shah S, and Wood AJ (2000) Increased drug delivery to the brain by P-glycoprotein inhibition. *Clin Pharmacol Ther* **68:** 231–237.

Schinkel AH, Wagenaar E, Mol CA, and van Deemter L (1996) P-glycoprotein in the blood-brain barrier of mice influences the brain penetration and pharmacological activity of many drugs. *J Clin Investig* **97:** 2517–2524.

Scholz J, Steinfath M, and Schulz M (1996) Clinical pharmacokinetics of alfentanil, fentanyl and sufentanil. An update. *Clin Pharmacokinet* **31:** 275–292.

Skarke C, Jarrar M, Schmidt H, Kauert G, Langer M, Geisslinger G, and Lotsch J (2003) Effects of ABCB1 (multidrug resistance transporter) gene mutations on disposition and central nervous effects of loperamide in healthy volunteers. *Pharmacogenetics* **13:** 651–660.

Takeuchi T, Yoshitomi S, Higuchi T, Ikemoto K, Niwa S, Ebihara T, Katoh M, Yokoi T, and Asahi S (2006) Establishment and characterization of the transformants stably-

expressing MDR1 derived from various animal species in LLC-PK1. *Pharm Res (NY)* **23:** 1460–1472.

Thiebaut F, Tsuruo T, Hamada H, Gottesman MM, Pastan I, and Willingham MC (1987) Cellular localization of the multidrug-resistance gene product P-glycoprotein in normal human tissues. *Proc Natl Acad Sci USA* **84:** 7735–7738.

Thompson SJ, Koszdin K, and Bernards CM (2000) Opiate-induced analgesia is increased and prolonged in mice lacking P-glycoprotein. *Anesthesiology* **92:** 1392–1399.

Upton RN, Ludbrook GL, Gray EC, and Grant C (1997) The cerebral pharmacokinetics of meperidine and alfentanil in conscious sheep. Anesthesiology 86: 1317–1325.

Wandel C, Kim R, Wood M, and Wood A (2002) Interaction of morphine, fentanyl, sufentanil, alfentanil, and loperamide with the efflux drug transporter P-glycoprotein. Anesthesiology 96: 913–920.

Yamazaki M, Neway WE, Ohe T, Chen I, Rowe JF, Hochman JH, Chiba M, and Lin JH (2001) In vitro substrate identification studies for p-glycoprotein-mediated transport: species difference and predictability of in vivo results. J Pharmacol Exp Ther 296: 723–735.

Zong J and Pollack GM (2000) Morphine antinociception is enhanced in mdr1a gene-deficient mice. Pharm Res (NY) 17: 749–753.

PART II

NOVEL APPROACHES TO CHARACTERIZING PHARMACOKINETICS AND PHARMACODYNAMICS

CHAPTER 6

USE OF A PHARMACOKINETIC-PHARMACODYNAMIC (PK-PD) MODEL INCORPORATING SERUM AND BRAIN CONCENTRATIONS TO EXAMINE CENTRAL AND PERIPHERAL CONTRIBUTIONS TO ANTINOCICEPTION

This chapter will be submitted for publication in *Journal of Pharmacology and Experimental Therapeutics* and is presented in the style of that journal.

ABSTRACT

The purpose of this study was to characterize the influence of behavioral endpoints on measures of antinociception assessed using the hot plate latency assay. The time course of opioid antinociception, together with serum and brain tissue concentrations, was determined for equipotent doses of loperamide (50 mg/kg), methadone (2 mg/kg), and sufentanil (0.001 mg/kg). Antinociception was assessed with two sets of behavioral measures: "standard criteria" defined hot plate latency as the time interval between placement on the hotplate and the observation of a jump or hind paw lick; "modified criteria" defined latency as the interval between placement and observation of a lick, shake or withdrawl of the hind limb(s) or a jump. A PK-PD model was fit to the concentration- and effect- time course, and estimates of relevant parameters were recovered. Loperamide, methadone and sufentanil serum and brain concentration time data were best fit by a two-compartment model with first-order absorption into the serum, brain tissue residing in a peripheral compartment, and clearance from the central (serum) compartment. A sigmoidal E_{max} model driven by brain concentrations was capable of describing the standard antinociceptive effect, while the modified effect data were best fit by an additive sigmoidal E_{max} model, with components driven separately by serum

and brain concentration. The PD parameter estimates recovered in this analysis were used to simulate the individual contributions of serum and brain concentrations to the observed modified criteria expression of antinociceptive effect over time. These simulations revealed that serum-mediated antinociception predominates at early timepoints and that as drug distributes to central locales, the contribution of brain-driven antinociception to the modified effect increases. This study is the first example of a hot plate latency assay that concomitantly assesses central and peripheral opioid antinociception. The implication of these observations is that behavioral endpoint criterion influences measures of hot plate latency antinociception, and should be considered when selecting a nociceptive assay.

INTRODUCTION

The analgesic effect mediated by opioid receptor binding is a result of the signal transduction pathway that induces membrane hyperpolarization, ultimately reducing pain transmission. The three major mammalian types of opioid receptors are designated as μ, δ, and κ (Evans et al., 1992; Chen et al., 1993; Li et al., 1993). Pharmacologic studies using opioid receptor ligands and receptor knockout mice identified centrally-located μ-opioid receptors (MOR) as the primary mediators of the therapeutic effects associated with traditional, alkaloid-derived opioids such as morphine (Matthes et al., 1996; Kieffer, 1999). While centrally-mediated antinociception has been the primary focus of opioid research, less is known about the role of peripheral opioid receptors as mediators of antinociception.

The potential for peripherally-mediated antinociception is, in part, supported by the broad distribution of opioid receptors on sensory neurons. The MOR is present in a number of peripheral tissues, including the small and large intestines, kidney, lung, spleen, testis, ovaries and uterus (Wittert et al., 1996). The μ, δ, and κ-opioid receptors are present in the

peritoneum, on cutaneous nerves and unmyelinated cutaneous sensory axons in both normal and inflammatory states (Stein et al., 1990; Coggeshall et al., 1997; Labuz et al., 2007). Moreover, these peripheral opioid receptors are functional mediators of antinociception. The co-administration of centrally-acting opioids with a peripherally-restricted opioid receptor antagonist, naloxone methiodide, significantly decreased antinociception, nearly approaching pre-drug baseline responses (Labuz et al., 2007). Clinically, local morphine administration has proven to be efficacious in producing analgesia when injected intraarticularly, in situations of chronic tooth inflammation, or into the intraligamentary space following arthroscopic knee surgery (Stein et al., 1991; Dionne et al., 2001). Topical application of the opioids, morphine, [D-Ala^2-MePhe^4-Gly(ol)^5]enkephalin (DAMGO) and morphine-6-glucuronide (M6G) to mouse tails produces antinociception that, following repeated exposures, displays tolerance that can be reversed by application of an NMDA receptor antagonist (Kolesnikov and Pasternak, 1999). While the classic opioid paradigm recognizes the supraspinal and spinal contributions of opioids, contemporary research also has focused on the functionality of peripherally-mediated antinociception.

A diverse set of assays, incorporating chemical, mechanical, thermal and electrical stimuli, have been developed to assess antinociception. A survey of primary articles published between 1970 and 1999 identified chemical and thermal stimuli as the most common tests of antinociception (Le Bars et al., 2001). Depending on the methodology, one advantage of thermal stimulus models is the ability to assess antinociception mediated by peripheral, spinal and supraspinal sites. For example, the hot plate latency assay is considered an assay of supraspinally-mediated antinociception because it requires central-processing of the nociceptive input before a response is observed (Le Bars et al., 2001). In

contrast, the radiant heat tail-flick assay is most commonly considered a measure of spinally-mediated antinociception in that the tail flick response remains, and is sensitive to opioid administration, in spinalized animals (Irwin et al., 1951).

Peripheral antinociception can be assessed with a modified tail flick assay in which a segment of the tail is exposed to a low-dose, topical opioid solution that produces antinociception in the exposed portions of the tail but not in the surrounding regions; the use of radiolabelled drug confirms that the opioid has not distributed to other receptor populations to contribute to the effect. Overall, there are a variety of thermal assays that, depending on the methodology, can be used to determine supraspinal, spinal and peripheral contributions to antinociception.

One drawback to thermal assays is the absence of a consistent methodology. In particular, methods for the hot plate latency assay vary markedly between studies, employing a range of temperatures, cut-off times and behavioral endpoints. One rationale for this variability is that mice exhibit a range of sensitivity to thermal stimuli (Mogil et al., 1999b; Mogil et al., 1999a). While ethical considerations dictate minimizing hot plate exposure temperatures and times, it is imperative that the influence of assay methodology on measures of antinociception be understood. For example, a variety of behavioral endpoints, including any combination of jumping, licking or lifting of the paws, has been used with the hot plate assay; while limiting thermal exposure through study endpoint selection is desirable, it is difficult to compare antinociception measured by different methodologies. The experiments reported herein were conducted to test the hypothesis that behavioral endpoint criteria influences measures of antinociception, and that simultaneously assessing reflexive

responses, such as lifting and shaking of the paw, and processed responses, such as jumping and licking, will permit differentiation between central and peripheral antinociception.

METHODS

Materials

Methadone and loperamide were purchased from Sigma-Aldrich (St. Louis, MO). Sufentanil was purchased from Abbott Laboratories (North Chicago, IL). All other chemicals and reagents were of the highest grade available from commercial sources.

Animals

Adult male CF-1 mice (30-40 g; Charles River Laboratories, Raleigh, NC) were housed in a temperature- and humidity-controlled room with a 12-h light cycle (7 a.m. to 7 p.m) and free access to food and water. The experimental protocol was approved by the Institutional Animal Care and Use Committee of the University of North Carolina and was in accordance with the Guide for the Care and Use of Laboratory Animals (Institute of Laboratory Animal Resources, Commission on Life Sciences, National Research Council, Washington, DC, 1996).

Study Design

Loperamide (50 mg/kg), methadone (2 mg/kg), sufentanil (0.001 mg/kg) prepared in 50:50 propylene glycol:water (loperamide) or 0.9% saline (methadone and sufentanil), was administered (0.1-0.2 ml per 30g) as a single subcutaneous dose to mice (n= 4 per time point, 8-9 time points per drug).

Antinociception was determined at timed intervals (n=8-9 per drug) post-dose using the hot plate (55°C) latency assay. Latency to respond to the thermal stimulus was defined

using two sets of behavioral endpoints, referred to as the standard and modified criteria. "Standard criteria" defined latency as the time interval between placement on the hotplate and observation of a jump or hind paw lick. "Modified criteria" defined latency as the interval between placement on the hotplate and observation of a lick, shake or withdrawal of the hind limb(s), or a jump. Pre-drug baseline latency was determined in triplicate, and animals with pre-drug latencies >15 sec (modified criteria) or >25 sec (standard criteria) were excluded from the study. Post-drug latency was determined at designated time points, with a maximum latency of 30 or 60 sec for the modified and standard criteria, respectively. Antinociceptive response was calculated as the percent maximum possible response (%MPR) with negative values set to zero.

$$\%\,MPR = \frac{Test\ latency - Control\ latency}{Maximum\ latency - Control\ latency} \times 100\% \qquad \text{(Eqn. 6.1)}$$

Immediately following post-drug latency testing, animals (n=4 per time point) were sacrificed by decapitation, and brain tissue and trunk blood were collected. Blood samples were allowed to clot at room temperature for at least 30 min, and serum was harvested following centrifugation. Whole brain tissue was homogenized in HPLC quality water (1:2 v/v) using an ultrasonic probe. Samples were prepared for analysis in an HPLC vial using a protein precipitation method. An aliquot of sample (2 to 25 µl of serum or brain homogenate) was precipitated with methanol (100-250 µl) containing an appropriate internal standard. Loperamide (20 ng/ml) was used as the internal standard for methadone and sufentanil and methadone (20 ng/ml) served as the internal standard for loperamide. Following methanol addition, samples were vortex-mixed and centrifuged, and an aliquot of supernatant was injected on-column for analysis

The concentration of loperamide, methadone, or sufentanil in brain and serum was determined by LC-MS/MS (PE-Sciex API-4000 triple quadrupole mass spectrometer). Samples (3 µl; CTC Analytics autosampler, Zwingen, Switzerland) were injected onto a Phenomenex 2.0 x 30 mm, 5 µm Gemini 110A column (Phenomenex, Torrance, CA). Analytes were eluted by ramping the initial gradient of 5% "B" to 95% "B" and increasing flow rate from 750 to 1500 µl/min and over the first 2 min, holding "B" at 95% for 0.5 min and maintaining flow at 1500 µl/min for 1 min, and finally returning mobile phase composition and flow rate to initial conditions, for a total run time of 3 min. Column effluent was sent to the source of the mass spectrometer (Turbo V Ionspray source, 700˚C, PerkinElmerSciex Instruments, Boston, MA) from 1 to 2.5 min. Positive ionization mode with multiple reaction monitoring was used to measure loperamide (477.4→266.0), methadone (310.3→265.2) and sufentanil (387.2→238.4).

Pharmacokinetic-Pharmacodynamic Modeling

Loperamide, methadone and sufentanil serum and brain concentration-time profiles were fit with a two-compartment model (Figure 6.1) incorporating first-order absorption (k_a) of the dose (X_0) into the serum, uptake and efflux clearance (Cl_{up}, Cl_{ef}) between serum and brain, and systemic clearance (Cl) from the serum compartment. Opioid disposition at the absorption site (X_A), serum (X_S), and brain (X_B) was characterized with the following differential equations:

$$\frac{dX_A}{dt} = -k_a \cdot X_0 \qquad \text{(Eqn. 6.2)}$$

$$\frac{dX_S}{dt} \cdot V_C = k_a \cdot X_A - Cl \cdot X_S - Cl_{up} \cdot X_S + Cl_{ef} \cdot X_B \qquad \text{(Eqn. 6.3)}$$

$$\frac{dX_B}{dt} \cdot V_B = Cl_{up} \cdot X_S - Cl_{ef} \cdot X_B \qquad \text{(Eqn. 6.4)}$$

where V_S and V_B are the apparent volume of distribution for the serum (central compartment) and the physiologic volume of brain, respectively. Brain volume was fixed as 13.4 ml/kg, based on an experimentally determined volume of 0.47 ml, assuming a specific gravity of 1.0 ml, and an average mouse body weight of 35 g (Kalvass et al., 2006).

Two pharmacodynamic models were employed to describe the standard and modified effect-time profiles. A sigmoidal E_{max} model characterized the relationship between drug concentration in the brain and the standard antinociceptive effect (Figure 6.1, Model 1) with the following equation:

$$E_S = \frac{E_{max} \cdot C_B^{\gamma}}{EC_{50}^{\gamma} + C_B^{\gamma}} \qquad \text{(Eqn. 6.5)}$$

where E_s is the effect based on standard criteria, E_{max} is the maximum effect, defined as 100%, C_B is the brain concentration, EC_{50} is the brain concentration at 50% of the maximum effect and γ is the Hill factor.

The antinociceptive effect based on modified criteria was characterized by fitting an additive sigmoidal E_{max} model incorporating serum and brain concentrations as contributors to pharmacologic response (Figure 6.1, Model 2):

$$E_M = \frac{E_{max} \cdot C_S^{\gamma,S}}{EC_{50,S}^{\gamma,S} + C_S^{\gamma,S}} + \frac{E_{max} \cdot C_B^{\gamma,B}}{EC_{50,B}^{\gamma,B} + C_B^{\gamma,B}} \qquad \text{(Eqn. 6.6)}$$

where E_M is the modified effect, E_{max} is the maximum effect, defined as 100%, C_S is the serum concentration, C_B is the brain concentration, $EC_{50,S}$ is the serum concentration at 50%

of the maximum effect, $EC_{50,B}$ is the brain concentration at 50% of the maximum effect, and $\gamma_{,S}$ and $\gamma_{,B}$ are the Hill factors for serum and brain, respectively. . Due to the additive nature of the modified effect model, the overall maximum effect is 200% MPR, 100% from each matrix.

Nonlinear least-squares regression was used to fit pharmacokinetic and pharmacodynamic models to the concentration and effect data using WinNonlin software (Pharsight Corporation, Mountain View, CA). The model schemes were selected based on Aikike's Information Criteria (AIC), the goodness of fit using the coefficients of variation (% CV) and visual inspection of the distribution of residual error.

RESULTS

Estimates of key pharmacokinetic/pharmacodynamic parameters for loperamide, methadone and sufentanil were recovered with stepwise nonlinear least-squares regression. Opioid pharmacokinetics (the time course of serum and brain tissue concentrations) were best described with a two-compartment model (Figure 6.1) with first-order absorption into the central compartment. The ability of the model to describe the disposition of each drug is displayed in Figure 6.2. The best numerical estimates for each pharmacokinetic parameter (Table 6.1), obtained in this step of the analysis, were held constant for subsequent modeling of the time course of pharmacologic response.

Antinociceptive response based on standard criteria was characterized by fitting a sigmoidal E_{max} model (Figure 6.1, Model 1) to the effect vs. brain concentration data. In general, this model described the standard criteria effect data well (Figure 6.3), and provided final parameter estimates with reasonable apparent precision (Table 6.2). Pilot studies were conducted to determine equipotent doses of loperamide, methadone and sufentanil. Although

loperamide has a ~4.5-fold lower brain EC_{50} compared to methadone (Table 6.2), a 50-fold higher loperamide dose was administered to achieve an antinociceptive effect similar to that produced by methadone. This difference is attributed primarily to P-glycoprotein (P-gp)-mediated efflux at the blood-brain barrier (BBB); loperamide exhibits a 40-fold P-gp effect (attenuation of brain uptake attributable to P-gp) compared to only a 7-fold effect for methadone (Kalvass et al., Submitted). The rank order of BBB penetration is further confirmed with Cl_{up} parameter estimates of 0.039-, 5.2- and 8.6-ml/min·kg for loperamide, methadone, and sufentanil, respectively. Rapid onset of effect was observed for sufentanil and methadone, with a time of maximal effect (T_{max}) of 7.5- and 10-min, respectively. In contrast, loperamide exhibited a gradual onset of effect, with an E_{max} of 75% MPR at 120 min.

A sigmoidal E_{max} model incorporating both serum and brain opioid concentrations as mediators of overall antinociceptive response was fit to the effect data based on the modified criteria (Figure 6.1, Model 2). This analytical approach recovered estimates of four pharmacodynamic parameters for each opioid: $EC_{50,S}$, γ_S, $EC_{50,B}$, and γ_B (Table 6.3). Reflexive behaviors (hind paw lifting and shaking) generally preceded the observation of processed behaviors (jumping and licking) and resulted in a lower % MPR over time for the modified compared to standard effect profiles. Furthermore, the modified criteria exhibited earlier onset and offset of effect compared to the standard antinociception time course (Figure 6.3).

A counterclockwise hysteresis in the relationship between standard criteria effect versus serum concentrations was observed, whereas standard criteria effect versus brain concentrations exhibited a sigmoidal relationship with no evidence of hysteresis behavior

(Figure 6.4). These observations suggest that opioid concentrations in serum are not in rapid equilibrium with concentrations in brain tissue, and that antinociceptive effect based on the standard criteria is driven by brain concentrations for loperamide, methadone and sufentanil. In contrast, the relationship between effect based on modified criteria and serum concentrations evidenced a slight degree of hysteresis, with a more substantial hysteresis behavior observed for the relationship between modified criteria effect versus brain concentrations (Figure 6.5).

The pharmacodynamic parameters recovered from the modified criteria effect data (Table 6.3) were used to simulate the apparent individual contributions of serum and brain concentrations to overall modified effect (Figure 6.6). The initial effect was driven predominantly by serum concentrations; as time progressed, the contribution of effect driven by brain tissue concentrations to the overall modified effect increased. These changes in fractional contribution to overall effect paralleled the time course of brain:serum concentration ratios. The contribution of serum concentration-driven response to the modified effect exceeded the contribution associated with brain concentrations at all time points.

Figure 6.7 presents the simulated effect vs. concentration relationships for the apparent serum and brain contributions to the modified criteria effect. These effect-concentration relationships suggest the possibility that an opioid can exhibit substantial antinociceptive response that appears to be mediated by serum, as opposed to brain, concentrations.

DISCUSSION

The hot plate latency assay is a common method of assessing antinociception in preclinical species, particularly mice. One disadvantage of this assay is an inability to detect antinociception in some drug classes (e.g. NSAIDS) that are recognized clinically as analgesics (Hammond, 1989). Thus, this model can be used only to ascertain antinociception for specific drug classes, such as opioids. An additional complication associated with the hot plate latency model, as well as with other thermal stimulus assays, is poor predictability of clinical analgesia, which can be attributed in part to a diversity of assay methodologies used to generate data sets subjected to correlative analysis. Some of the inter-study differences can be attributed to the high degree of variability in rodent thermal sensitivities, where higher temperatures or longer exposure times may be required for heat-insensitive strains, whereas heat-sensitive strains exhibit shorter response latencies, often at lower temperatures (Mogil et al., 1999a).

While these different methodologies often are selected in order to minimize nociceptive input, difficulties are encountered when trying to interpret results from different studies. Furthermore, the hot plate latency behavioral endpoint criteria are highly variable, including various combinations of lifting and shaking of the hind paw, jumping or hindpaw licking, and to some extent may be subjective. While each of these responses represent a reasonable endpoint, little is known about the mechanistic aspects of antinociception that are assessed by each combination of behavioral endpoints. Ultimately, the ideal assay would minimize thermal exposure, assess a specific and known component of antinociception (e.g., spinal versus supraspinal), and be transferable between different strains within a given rodent species.

In the present study, the influence of hot plate behavioral endpoints on measures of antinociception was examined. As would be predicted, reflexive endpoints such as lifting and shaking of the hind paw resulted in shorter response latencies compared to centrally-processed behaviors such as jumping and licking of the hind paws (Figure 6.3). This observation is in agreement with previous work describing two distinct behavioral responses following exposure of the shaved back of a rat to a light beam; an initial twitch of the exposed skin followed shortly thereafter by a retraction of the entire body (Ercoli and Lewis, 1945). Results of this study revealed that both the twitching and escape response were sensitive to opioid-associated antinociception, with the latter response more sensitive to modulation by opioids (Ercoli and Lewis, 1945). While the different nociceptor populations, Aδ fibers (which produce early, pricking sensations) and C-fibers (which cause a second, persistent pain state) likely play a role in these observations, the two distinct antinociceptive responses suggest the possibility that opioid receptor populations in multiple physiologic locales mediate antinociception separately (Yeomans and Proudfit, 1996), with the overall response measurement resulting from the combination of all contributing locales.

The hypothesis that centrally-located opioid receptors play a primary role in mediating antinociception is supported in the present study by the sigmoidal relationship between the standard criteria effect and brain concentrations (Figure 6.4B). The distributional delay in equilibration of opioid concentrations between serum and brain tissue results in a counterclockwise hysteresis behavior in the relationship between the standard criteria effect and serum opioid concentrations (Figure 6.4A).

While central opioid receptors are important mediators of antinociception, recent results have implicated peripheral opioid receptors in mediation of antinociception (Reichert

et al., 2001; Shannon and Lutz, 2002; Kolesnikov et al., 2004; Labuz et al., 2007). While some of these studies have suggested that peripheral receptors function predominantly in states of inflammatory pain, the hypothesis that opioid antinociception is mediated through a combination of central and peripheral receptor populations is now broadly accepted.

One challenge in isolating the contribution of central versus peripheral opioid receptors to net antinociceptive response is the absence of an assay that teases apart each contribution from the overall effect profile. While assays that characterize supraspinal, spinal and peripheral antinociception have been developed and are well-characterized, they often fail to assess the comprehensive physiologic response. A relevant example of this point is provided by the current data. When describing antinociceptive pharmacodynamics when response was expressed with the modified behavioral criteria, neither serum opioid concentrations nor brain opioid concentrations alone could adequately describe the magnitude and time course of pharmacologic activity. The ability to describe the time course of antinociception was improved (Figure 6.6) by a model that allowed both serum and brain tissue concentrations to drive separate but additive antinociceptive responses (Figure 6.1, Model 2).

The relationship between modified criteria effect and serum concentrations was characterized by a slight hysteresis (Figure 6.5A), a consequence of the contribution of brain receptor occupancy to the net effect. The large hysteresis behavior observed when the modified criteria effect was related to brain tissue concentrations supports the premise that opioid receptor occupancy in the brain is a relatively minor contributor to net antinociception as expressed by the modified criteria (Figure 6.5B).

The pharmacodynamic parameters recovered from fitting Model 2 (Figure 6.1) to the modified criteria effect data were used to isolate the peripherally- and centrally-mediated contributions to effect over time (Figure 6.6). All opioids exhibited an early, rapid onset of effect that appeared to be mediated by serum concentrations. As time progressed and drug distributed to central sites, the contribution of brain tissue concentrations to overall antinociceptive response increased. Despite this time-dependent increase in the apparent contribution of central activity to net effect, in all cases the predicted central response contributed less than the peripheral response (driven by serum concentrations) to the overall effect based on modified criteria (Figure 6.6).

The fractional contributions of peripheral (based on serum concentrations) and central (based on brain concentrations) antinociception to overall modified criteria effect reveal that, while it is possible to achieve 100% serum- or brain-mediated effect (Figure 6.7), in practice this may be difficult due to the high doses required and potential for side effects. Loperamide serves as an excellent example of this principle, as a 50-mg/kg dose resulted in a 55% overall effect based on the modified criteria; a 2-fold increase in dose (to 100 mg/kg) resulted in 100% mortality (data not shown). Overall, the additive response that comprises the modified effect reveals the importance of opioid receptor populations throughout the body.

The interaction between supraspinal, spinal and peripheral contributions to antinociception has been characterized as being synergistic (Kolesnikov et al., 1996). In contrast, the present study utilized an additive model to describe brain- and serum-mediated antinociception. This result may provide insight into mechanisms underlying opioid tolerance. For example, if two distinct opioids are administered, one at a low dose that

primarily targets central tissues, and the other at a medium to high dose that targets peripheral tissues, effective analgesia may be accomplished, with a delay in tolerance onset, because the receptor populations are not working synergistically in tolerance development. In fact, the effectiveness and increasing popularity of co-administering multiple low-dose opioids may in part be attributed to the additive relationship observed in this study.

One consequence of using different behavioral endpoint criteria is the inability to recover consistent pharmacodynamic parameters. This study used preliminary dose ranging strategies to determine the ED_{50} for loperamide, methadone and sufentanil. These pilot data were used to select a dose that elicited approximately 80% MPR with respect to the standard criteria endpoint. In comparison, an ED_{50} calculated using the modified criteria endpoint would be much higher because of the lower response latency compared to the standard criteria. An additional consideration is that fitting both sets of effect measurements with Model 1 (Figure 6.1) would recover two very different EC_{50} values, with the value for the modified criteria effect being much higher compared to the standard criteria effect. Furthermore, selecting the modified criteria as a measure of centrally-mediated antinociception would result in a poor fit of the pharmacodynamic model to the observed effect. Loperamide and sufentanil brain EC_{50}s are 2- and 6-fold greater when calculated when recovered using the standard (Eqn. 6.1) versus the modified criteria (Eqn. 6.2; Tables 6.2 and 6.2). In contrast, methadone is more potent in the brain when effect is assessed using the modified criteria, evidenced by a 1.5-fold decrease in brain $EC_{50,}$ compared to the standard criteria. These EC_{50} observations suggest that some opioids may have a more substantial central contribution than others, and that characterizing the peripheral contributions with the modified criteria may reveal unique opioid characteristics. The

differences in EC_{50} values highlight one source of the inter-laboratory variability in recovered PD parameter values for a single compound.

This study is the first example of an assay that appears to concurrently assess central and peripheral opioid antinociception. Results indicate that when performing the hot plate latency assay, reflexive behaviors of hind limb licking and shaking are representative of a combination of peripheral and central contributions to antinociception, inferred by the correspondence to both serum and brain opioid concentrations, whereas the centrally-processed behaviors of jumping and licking of the hind paw are more reflective of central receptor occupancy (driven solely by opioid concentration in brain tissue). Future work will be required to assess the sensitivity of the modified criteria by perturbing central and peripheral contributions to antinociception. Overall, this study highlights the importance of selecting suitable hot plate latency assay methodology based on what type of antinociceptive response is to be characterized.

Table 6.1. Pharmacokinetic parameter estimates [mean (% CV)] derived using non-linear regression analysis.

Parameter	loperamide	methadone	sufentanil
K_a (min^{-1})	0.064 (25)	0.57 (23)	0.30 (37)
Cl ($ml \cdot min^{-1} \cdot kg^{-1}$)	58 (12)	140 (8.7)	19 (16)
V_c ($ml \cdot kg^{-1}$)	32000 (8.1)	8300 (5.8)	380 (22)
Cl_{up} ($ml \cdot min^{-1} \cdot kg^{-1}$)	0.039 (140)	5.2 (12)	8.6 (40)
Cl_{efflux} ($ml \cdot min^{-1} \cdot kg^{-1}$)	0.31 (160)	2.1 (15)	6.0 (48)

Table 6.2. Pharmacodynamic parameter estimates [mean (% CV)] by fitting Model 1 to the standard effect data using non-linear regression analysis.

Parameter	loperamide	methadone	sufentanil
EC_{50} (ng/g)	100 (6.1)	430 (7.5)	0.50 (30)
γ	2.4 (20)	3.1 (30)	1.1 (32)

Table 6.3. Pharmacodynamic parameter estimates [mean (% CV)] derived by fitting Model 2 to the modified effect data using non-linear regression analysis.

Parameter	loperamide	methadone	sufentanil
$EC_{50,S}$ (ng/ml)	1800 (12)	520 (5.9)	1.8 (30)
γ_S	2.2 (55)	8.8 (35)	1.8 (37)
$EC_{50,B}$ (ng/g)	190 (11)	270 (6.8)	2.9 (26)
γ_B	7.0 (55)	2.7 (16)	5.0 (135)

Model 1

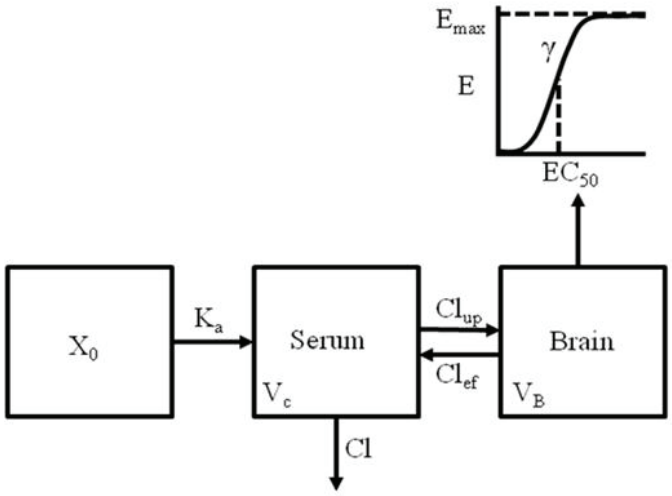

Model 2

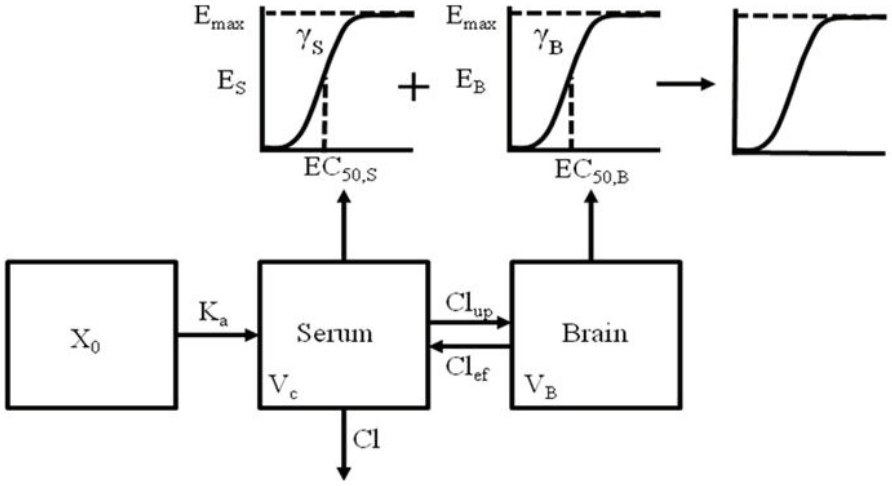

Figure 6.1. Pharmacokinetic-pharmacodynamic models characterizing opioid disposition and antinociception. Model 1 and 2 used to recover key PK-PD parameters by fitting a two-compartment model to the time course of opioid serum and brain concentrations. Model 1 recovered pharmacodynamic parameters by fitting a sigmoidal E_{max} model to the brain concentration versus standard antinociception time profile. Model 2 recovered key pharmacodynamic parameters by fitting sigmoidal E_{max} model to the serum- and brain-concentration versus modified antinociceptive effect profile.

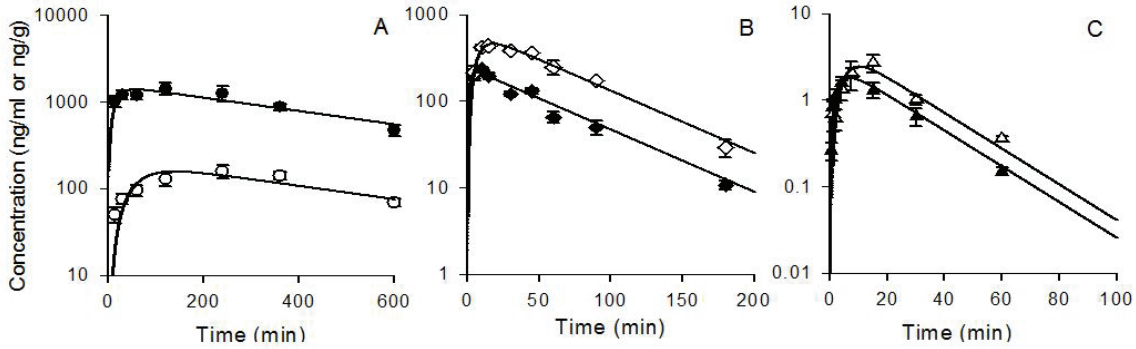

Figure 6.2. Time course of observed and predicted (solid lines) opioid serum (closed symbols) and brain (open symbols) concentrations (mean ± S.E; n ≥ 3) following subcutaneous administration of 50-mg/kg loperamide (A), 2-mg/kg methadone (B) and 0.001-mg/kg sufentanil (C).

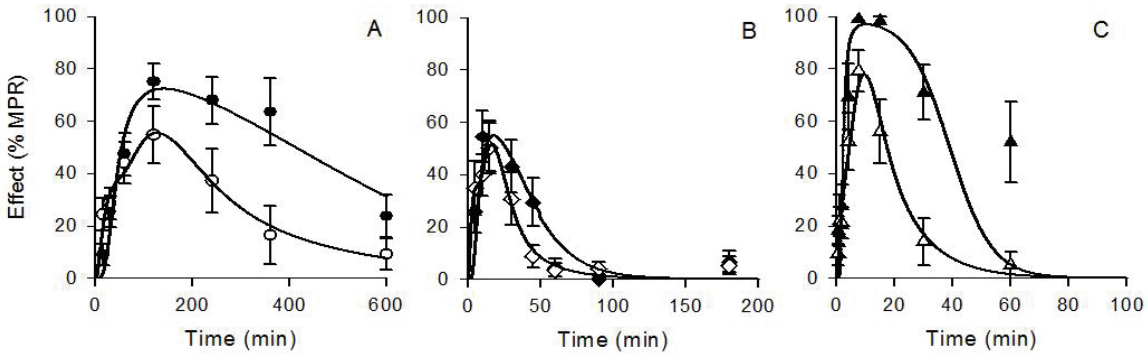

Figure 6.3. Time course of observed and predicted (solid lines) opioid standard (solid symbols) and modified (closed symbols) antinociceptive effect (mean ± S.E; n = 4 to 36) following administration of loperamide (A), methadone (B) and sufentanil (C).

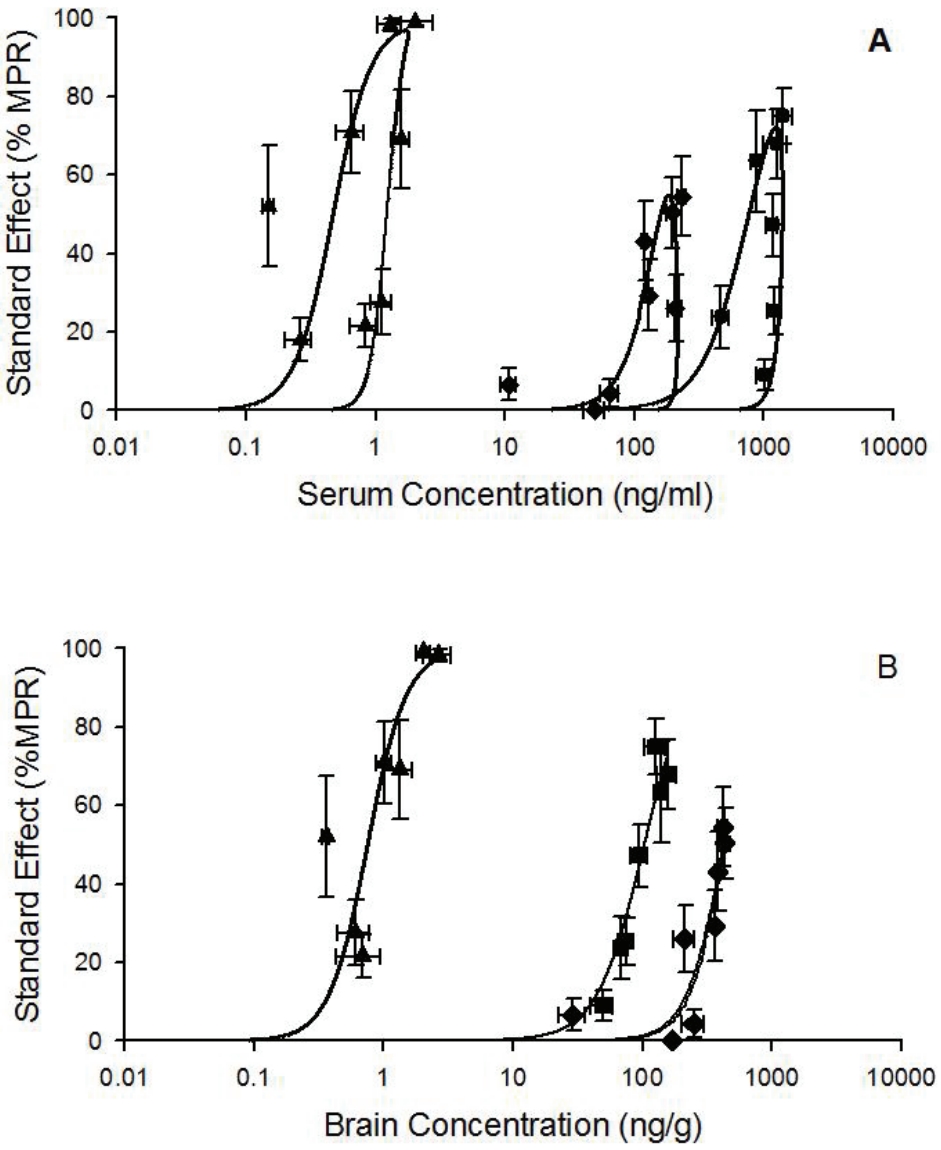

Figure 6.4. Relationship between standard antinociceptive effect and concentration for loperamide (●), methadone (◆) and sufentanil (▲). A) The counterclockwise hysteresis between the standard effect and serum concentrations. B) The sigmoidal relationship between standard effect and brain concentration. Symbols represent observed data [mean ± S.E for concentration ($n \geq 3$) and effect ($n = 4$ to 36)] and solid lines represent the fit of Model 1 to the standard antinociceptive effect and concentration data.

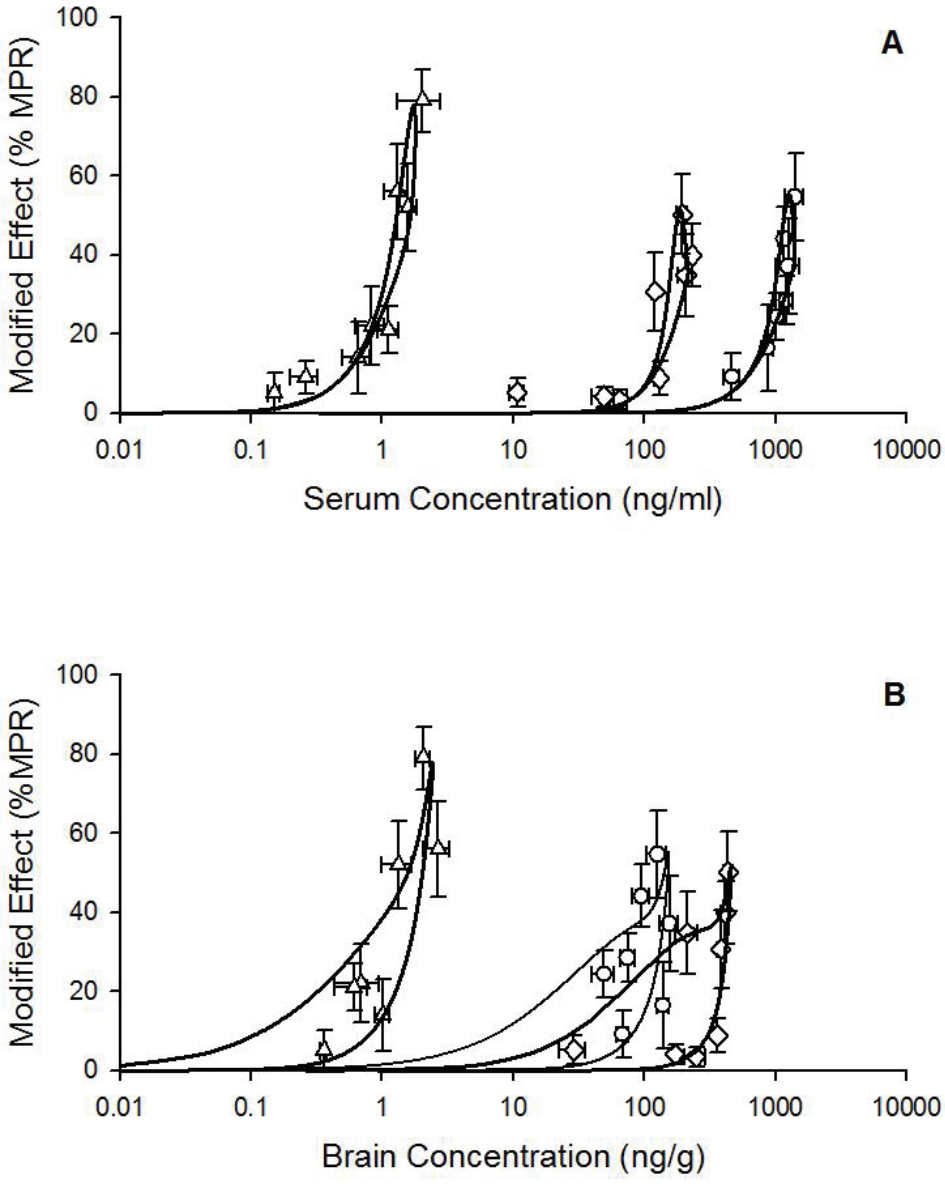

Figure 6.5. Relationship between modified antinociceptive effect and serum (A) or brain (B) concentrations for loperamide (○), methadone (◇) and sufentanil (△). Symbols represent observed data [mean ± S.E for concentration (n ≥ 3) and effect (n = 4 to 36)] and solid lines represent the fit of Model 2 to the modified antinociceptive effect and concentration data.

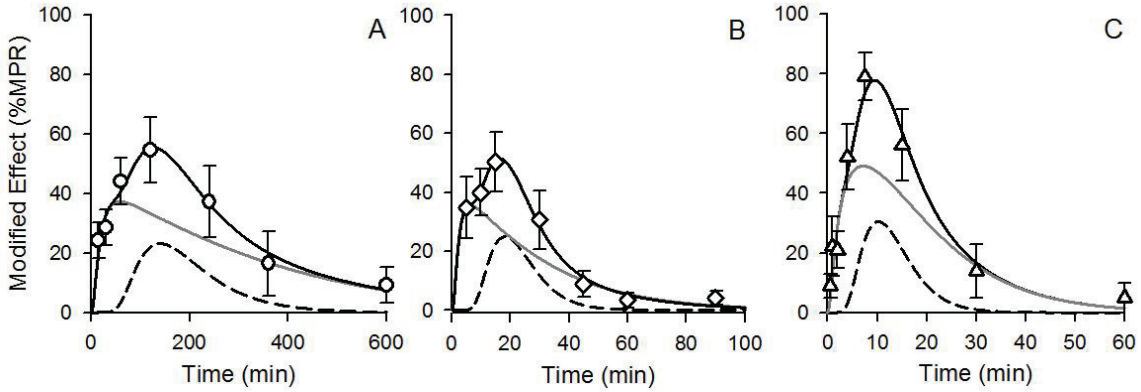

Figure 6.6. Contribution of serum (solid gray line) and brain (dashed black line) to overall observed (symbols; n = 4 to 36) and predicted (solid black line) modified antinociceptive effect for loperamide (○), methadone (◇) and sufentanil (△).

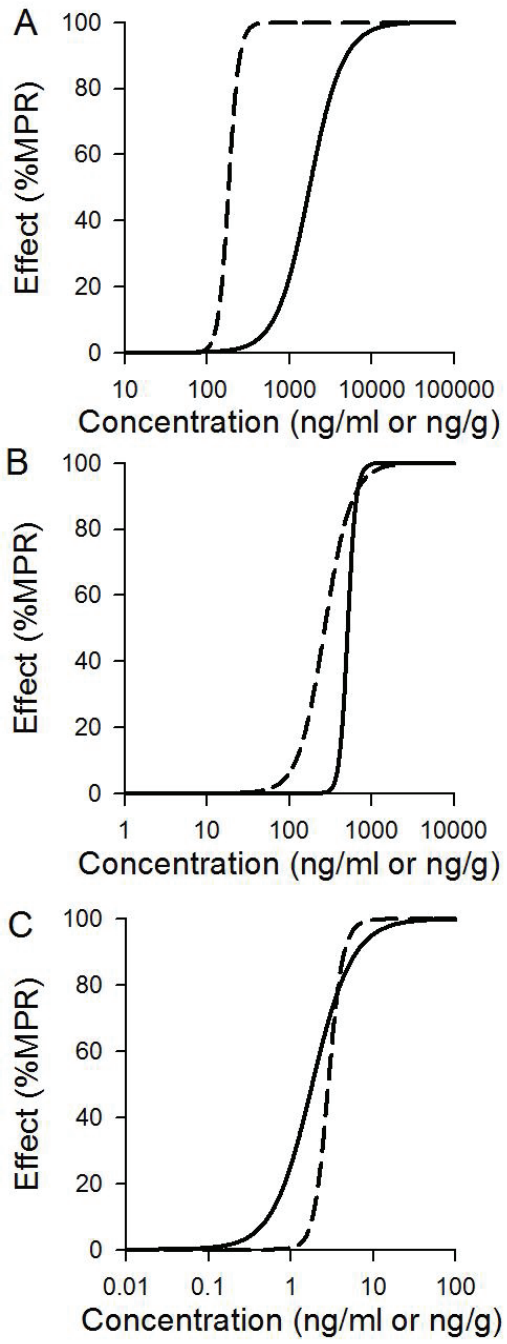

Figure 6.7. Pharmacodynamic parameter estimates for modified antinociceptive effect were used to simulate serum (solid black line)- and brain (dashed black line)-mediated contributions to modified effect for loperamide (A), methadone (B) and sufentanil (C).

REFERENCES

Chen Y, Mestek A, Liu J, Hurley JA and Yu L (1993) Molecular cloning and functional expression of a mu-opioid receptor from rat brain. Mol Pharmacol 44:8-12.

Coggeshall RE, Zhou S and Carlton SM (1997) Opioid receptors on peripheral sensory axons. Brain Res 764:126-132.

Dionne RA, Lepinski AM, Gordon SM, Jaber L, Brahim JS and Hargreaves KM (2001) Analgesic effects of peripherally administered opioids in clinical models of acute and chronic inflammation. Clin Pharmacol Ther 70:66-73.

Ercoli N and Lewis MN (1945) Studies on Analgesics. Journal of Pharmacology and Experimental Therapeutics 84:301-317.

Evans CJ, Keith DE, Jr., Morrison H, Magendzo K and Edwards RH (1992) Cloning of a delta opioid receptor by functional expression. Science 258:1952-1955.

Hammond DL (1989) Inference of Pain and Its Modulation from Simple Behaviors, in Issues in Pain Management (Chapman CRL, J.D. ed) pp 69-89, Raven Press, Ltd., New York.

Irwin S, Houde RW, Bennett DR, Hendershot LC and Seevers MH (1951) The effects of morphine methadone and meperidine on some reflex responses of spinal animals to nociceptive stimulation. J Pharmacol Exp Ther 101:132-143.

Kalvass JC, Olson EO and Pollack GM (Submitted) Influence of Blood-Brain Barrier P-glycoprotein on Brain Penetration and Antinociceptive Effects of Model Opioids. Drug Metabolism and Disposition.

Kalvass JC, Olson ER and Pollack GM (2006) Pharmacokinetics and Pharmacodynamics of Alfentanil in P-glycoprotein-Competent and P-glycoprotein-Deficient Mice: P-glycoprotein Efflux Alters Alfentanil Brain Disposition and Antinociception. Drug Metab Dispos.

Kieffer BL (1999) Opioids: first lessons from knockout mice. Trends Pharmacol Sci 20:19-26.

Kolesnikov Y, Cristea M, Oksman G, Torosjan A and Wilson R (2004) Evaluation of the tail formalin test in mice as a new model to assess local analgesic effects. Brain Res 1029:217-223.

Kolesnikov Y and Pasternak GW (1999) Topical opioids in mice: analgesia and reversal of tolerance by a topical N-methyl-D-aspartate antagonist. J Pharmacol Exp Ther 290:247-252.

Kolesnikov YA, Jain S, Wilson R and Pasternak GW (1996) Peripheral morphine analgesia: synergy with central sites and a target of morphine tolerance. J Pharmacol Exp Ther 279:502-506.

Labuz D, Mousa SA, Schafer M, Stein C and Machelska H (2007) Relative contribution of peripheral versus central opioid receptors to antinociception. Brain Res 1160:30-38.

Le Bars D, Gozariu M and Cadden SW (2001) Animal Models of Nociception. Pharmacol Rev 53:597-652.

Li S, Zhu J, Chen C, Chen YW, Deriel JK, Ashby B and Liu-Chen LY (1993) Molecular cloning and expression of a rat kappa opioid receptor. Biochem J 295 (Pt 3):629-633.

Matthes HW, Maldonado R, Simonin F, Valverde O, Slowe S, Kitchen I, Befort K, Dierich A, Le Meur M, Dolle P, Tzavara E, Hanoune J, Roques BP and Kieffer BL (1996) Loss of morphine-induced analgesia, reward effect and withdrawal symptoms in mice lacking the mu-opioid-receptor gene. Nature 383:819-823.

Mogil JS, Wilson SG, Bon K, Lee SE, Chung K, Raber P, Pieper JO, Hain HS, Belknap JK, Hubert L, Elmer GI, Chung JM and Devor M (1999a) Heritability of nociception I: responses of 11 inbred mouse strains on 12 measures of nociception. Pain 80:67-82.

Mogil JS, Wilson SG, Bon K, Lee SE, Chung K, Raber P, Pieper JO, Hain HS, Belknap JK, Hubert L, Elmer GI, Chung JM and Devor M (1999b) Heritability of nociception II. 'Types' of nociception revealed by genetic correlation analysis. Pain 80:83-93.

Reichert JA, Daughters RS, Rivard R and Simone DA (2001) Peripheral and preemptive opioid antinociception in a mouse visceral pain model. Pain 89:221-227.

Shannon HE and Lutz EA (2002) Comparison of the peripheral and central effects of the opioid agonists loperamide and morphine in the formalin test in rats. Neuropharmacology 42:253-261.

Stein C, Comisel K, Haimerl E, Yassouridis A, Lehrberger K, Herz A and Peter K (1991) Analgesic effect of intraarticular morphine after arthroscopic knee surgery. N Engl J Med 325:1123-1126.

Stein C, Hassan AH, Przewlocki R, Gramsch C, Peter K and Herz A (1990) Opioids from immunocytes interact with receptors on sensory nerves to inhibit nociception in inflammation. Proc Natl Acad Sci U S A 87:5935-5939.

Wittert G, Hope P and Pyle D (1996) Tissue distribution of opioid receptor gene expression in the rat. Biochem Biophys Res Commun 218:877-881.

Yeomans DC and Proudfit HK (1996) Nociceptive responses to high and low rates of noxious cutaneous heating are mediated by different nociceptors in the rat: electrophysiological evidence. Pain 68:141-150.

CHAPTER 7

INFLUENCE OF TRUNCATING THE DYNAMIC RANGE OF PHARMACOLOGIC EFFECT MEASUREMENTS ON PHARMACODYNAMIC PARAMETER ESTIMATES

This chapter will be submitted for publication in *Drug Metabolism Letters* and is presented in the style of that journal.

ABSTRACT

Hotplate latency is commonly used to assess drug-associated antinociception in rodents. Analysis of data generated by this assay often is confounded by the artificial ceiling imposed by cut-off times (e.g. censoring) for exposure to the thermal stimulus implemented to prevent tissue damage. This study was conducted to examine the feasibility of estimating the true maximum effect (E_{max}) in the absence of an artificial ceiling in the analysis of typical pharmacodynamic data. This approach was evaluated by fitting a linked pharmacokinetic-pharmacodynamic model, including a sigmoidal relationship between effect and hypothetical effect-compartment concentrations, to the time course of drug disposition and antinociception after subcutaneous administration of fentanyl (0.09 mg/kg) or morphine (3.6 mg/kg) to mice. Recovering an estimate of the true E_{max}, rather than truncating the dynamic range of effect, improved the fit of the model for both drugs, dynamic range of effect increased from 65% to 100% of the theoretical maximum effect, and estimates of k_{e0}, EC_{50} and γ more closely approximated previously-reported values. Simulations were performed to examine the influence of effect-range truncation on estimates of EC_{50}. Increasing degrees of truncation resulted in increased underprediction of EC_{50}; the magnitude of underprediction was modulated by sigmoidicity in the relationship between effect and concentration. In

summary, inclusion of E_{max} as an estimated parameter, rather than a fixed arbitrary ceiling value, represents an alternative method for analyzing antinociceptive effect data. The principles communicated herein are applicable to analysis of pharmacodynamic data generated by any pharmacologic model in which an arbitrary maximum response is implemented or assumed.

INTRODUCTION

Characterization of pharmacologic response requires the use of specific and sensitive assays that are validated and reproducible. Quantifying antinociception in animal models is particularly challenging, and a diverse set of assays that utilize chemical, electrical, mechanical or thermal stimuli has been developed to evaluate alterations in rate, frequency, extent or time to response following opioid administration (D'Amour and Smith, 1941; Ercoli and Lewis, 1945; Collier et al., 1961; Paalzow, 1969b; Paalzow, 1969a; Hunskaar et al., 1985). In the hotplate assay, one of the more common systems utilized, an animal is placed on a metallic surface heated to a specified temperature (50 to 60°C) and the time interval until observation of a jump or hind paw lick is recorded (Woolfe and Macdonald, 1944). Data analysis can be quantal, presented as a percentage of animals that respond over a designated time period, or more often as a graded metric of response (Woolfe and Macdonald, 1944; O'Callaghan and Holtzman, 1975). While quantal analysis avoids some of the methodological limitations imposed by graded analysis, it fails to utilize all available data and more crude estimation of efficacy.

Graded analysis utilizes individual time-to-response data, and presents those data as absolute latency or as a percentage response. When graded analysis is utilized, maximum exposure cut-off times, typically between 30 and 60 sec for the hotplate assay, are

implemented to prevent or minimize damage to tissues exposed directly to the thermal stimulus (Le Bars et al., 2001). While an ethical necessity, exposure cut-off times can skew data and hinder the use of parametric statistical and pharmacodynamics analyses when subjects approach or reach the cut off time. Use of cut-off times typically involves establishing individualized dynamic ranges for drug response ranging from 0% (i.e., pre-drug latency) to "100%" (i.e., the established cut-off time) of maximum possible response (% MPR).

One disadvantage associated with this method of analysis is its sensitivity to experimental manipulations. For example, by increasing cut-off time from 30 to 60 sec, a 25-sec response time with a 5-sec pre-drug latency decreases the apparent response from 80 to 36% MPR. While a higher cut-off time may be justifiable, for example if a thermally-insensitive strain of mice is used, the same absolute response time can impact the calculation of % MPR, and in turn will be reflected in estimates of EC_{50} and γ when relating response to metrics of drug exposure (Mogil et al., 1999). Further complications associated with % MPR calculations in the presence of a ceiling effect occur when multiple subjects exhibit responses at or greater than the imposed cut-off time. In this case, subjects will demonstrate identical apparent responses, while the actual biologic responses could be quite different. While various methods of data analysis have been proposed for this experimental situation, alternative approaches to data analysis are needed, particularly when performing integrated PK-PD analysis. In this specific case, the failure to produce elevations in antinociception commensurate with increases in drug concentration can significantly impede the ability to recover estimates of key pharmacodynamics parameters (Kitchen and Crowder, 1985).

The present study was conducted to investigate the influence of E_{max} truncation on the ability to analyze antinociceptive data with traditional PK-PD paradigms. To this end, an integrated PK-PD model was fit to effect vs. time and concentration vs. time data for fentanyl and morphine in the mouse hotplate model. Two analysis approaches were evaluated: effect referenced to an arbitrary E_{max} of 100% MPR, or effect referenced to an E_{max} that was recovered as a parameter in the overall analysis scheme. The effect of E_{max} truncation on PD parameter estimates was examined further by simulating earlier cutoff times, thereby increasing degrees of truncation compared to the hypothetical value of E_{max} recovered by PK-PD modeling. The influence of E_{max} truncation on estimates of EC_{50}, and the potential modulation of this effect by the degree of sigmoidicity in the effect vs. concentration relationship, also was explored through simulation experiments.

MATERIALS AND METHODS

Materials

Fentanyl, loperamide, morphine, and oxycodone were purchased from Sigma-Aldrich (St. Louis, MO). All other reagents were obtained from common sources, and they were of reagent grade or better.

Animals

Adult male CF-1 *mdr1a*(+/+) and *mdr1a*(-/-) mice (30–40 g; Charles River Laboratories, Inc., Wilmington, MA) were maintained on a 12-h light/dark cycle in a temperature- and humidity-controlled room with access to water and food ad libitum. The experimental protocol was approved by the Institutional Animal Care and Use Committee of the University of North Carolina and was in accordance with the Guide for the Care and Use

of Laboratory Animals (Institute of Laboratory Animal Resources, Commission on Life Sciences, National Research Council, Washington, DC, 1996).

Pharmacokinetic-Pharmacodynamic Study.

Based on the results of pilot experiments, *mdr1a*(-/-) or *mdr1a*(+/+) CF-1 mice received a single equipotent subcutaneous dose of fentanyl (0.09 mg/kg) or morphine (3.6 mg/kg), respectively. Fentanyl was prepared in 50:50 propylene glycol/water, and morphine was prepared in 0.9% saline. Antinociception was assessed using the hot plate latency assay as described previously (Kalvass et al., 2007). Latency was defined as the time interval between placement on the hotplate (55°C; Columbus Instruments, Columbus, OH) and observation of a jump or hind paw lick. Pre-drug baseline latency was determined in triplicate. A maximum latency time of 60 sec was used to avoid tissue damage and animals with pre-drug latencies >25 sec were excluded from the study. Post-drug latency was determined at designated time points and antinociceptive response was calculated as the percent maximum possible response (%MPR; Eqn. 7.1) with negative values set to zero.

$$\%MPR = \frac{Test\ latency - Control\ latency}{Maximum\ latency - Control\ latency} x\ 100\% \qquad \text{(Eqn. 7.1)}$$

Immediately following the terminal post-drug latency test, trunk blood was collected (n=4 animals per time point), allowed to clot for at least 30 min at room temperature and serum was harvested after centrifugation. Serum samples were stored at –20°C until analysis by HPLC-MS/MS.

Bioanalysis Methodology

Samples were prepared for analysis in an HPLC vial using a protein precipitation method, where an aliquot of serum (25 µl) was precipitated following the addition of 4- or 10-volumes of methanol containing loperamide (5 ng/ml) or oxycodone (100 ng/ml) as an internal standard for fentanyl and morphine, respectively. Prior to undergoing LC-MS/MS (PE-Sciex API-4000 triple quadrupole mass spectrometer) analysis, samples were vortex-mixed and centrifuged. Sample supernatant (3 µl; CTC Analytics autosampler, Zwingen, Switzerland) was injected onto a Phenomenex 2.0 x 30 mm, 5 µm Gemini 110A column (Phenomenex, Torrance, CA). The initial column condition of 5 % methanol: 95 % ammonium acetate (pH 6.8; 10 mM) was immediately (fentanyl), or following 0.5 min (morphine), ramped to 95 % methanol over 2 min and held for 0.5 min before being returned to starting conditions in a single step. The flow rate was concurrently increased from 750 to 1500 µl/min over 2 min, held at 1500 µl/min for 1 min, and returned the initial flow rate of 750 µl/min in a single step. Column effluent was sent to the source of the mass spectrometer (Turbo V Ionspray source, 700˚C, PerkinElmerSciex Instruments, Boston, MA) from 1 to 2.5 min. Multiple reaction monitoring in the positive mode was used to measure fentanyl (337.1→188.3), loperamide (477.4→266.0), morphine (286.1→201.1) or oxycodone (316.0 → 298.0). Standard curves were prepared in serum or buffer and were identical in composition to corresponding samples. Accuracy of standards and interassay variability was within ± 20%.

Pharmacokinetic-Pharmacodynamic Modeling

Fentanyl and morphine serum concentration-time profiles were fit with a one-compartment model (Figure 7.1) incorporating first-order absorption (k_{01}) of the dose (X_0)

into the systemic circulation, contained in a central compartment of apparent volume V_c, with first-order elimination (k_{10}) from the compartment. Opioid disposition in the absorption site (X_A) and in the central, serum compartment (X_C) was characterized (Eqns. 2 and 3) using nonlinear least-squares regression (WinNonlin, Pharsight Corporation, Mountain View, CA).

$$\frac{dX_A}{dt} = -k_{01} \cdot X_0 \qquad \text{(Eqn. 7.2)}$$

$$\frac{dX_C}{dt} \cdot V_C = k_{01} \cdot X_A - k_{01} \cdot X_C \qquad \text{(Eqn. 7.3)}$$

The dissociation between the time course of antinociception and serum concentrations was addressed by linking a hypothetical effect site with the central pharmacokinetic compartment, assuming a rate of equilibration governed by a first-order rate constant k_{e0} (Figure 7.1; Eqn. 7.4). The relationship between antinociceptive effect and drug concentration in the hypothetical effect compartment was assumed to be sigmoidal (Eqn. 7.5). The PD parameters k_{e0}, EC_{50}, and γ were estimated in a stepwise approach by fitting these equations to the observed antinociceptive response vs. time data, with E_{max} fixed at 100 % or recovered as a parameter with no theoretical limit.

$$\frac{dC_e}{dt} = k_{e0} \cdot (C_c - C_e) \qquad \text{(Eqn. 7.4)}$$

$$E = \frac{E_{max} \cdot C_e^{\gamma}}{EC_{50}^{\gamma} + C_e^{\gamma}} \qquad \text{(Eqn. 7.5)}$$

Pharmacodynamic Simulations of E_{max} Truncation

The influence of E_{max} truncation on estimates of k_{e0}, EC_{50} and γ was examined using fentanyl and morphine data sets. Varying degrees of E_{max} truncation were simulated by fixing E_{max} between 60% and 150%, in 10% increments, and recovering estimates of the key PD parameters incorporated in the model equations. Fentanyl and morphine PK parameter estimates recovered from nonlinear least-squares regression were held constant during all simulations.

In a second set of simulations, the effect versus concentration relationship was simulated based on the sigmoidal E_{max} function (Eqn. 7.5) at three different degrees of sigmoidicity: $\gamma = 1$, $\gamma = 2$, or $\gamma = 4$. In all cases, EC_{50} was set at 100 concentration units, and effect was allowed to range from 0 to 100%. The effect versus concentration relationships then were truncated under five different maximum allowable response (MAR) scenarios: 100% of the theoretical maximum (i.e., no truncation), or 80%, 60%, 40%, or 20% of the theoretical maximum. Under each truncation scenario, the effect data were transformed relative to the MAR. The apparent EC_{50} recovered from each %MAR versus concentration relationship was obtained by inspection (n=1000 simulated data points per profile).

RESULTS

The fentanyl and morphine doses administered to mice produced robust antinociception with at least one time point at which effect reached the pre-defined cut-off (100 % MPR), as assessed using the hotplate latency assay. For both drugs, the time course of serum concentrations was adequately described with a one compartment system incorporating first-order absorption from the site of administration and drug elimination from the serum compartment (Figures 7.2 and 7.3). Drug distribution from serum to the site of

action was characterized using a biophase distribution model incorporating the first-order equilibrium rate constant k_{e0}.

The time course of antinociception was described by a sigmoidal E_{max} model with E_{max} fixed at 100% or as determined as a model parameter. Estimates of relevant PK-PD parameters for the fixed and variable E_{max} models are presented in Tables 7.1 and 7.2, respectively. The observed peak effect was underpredicted when E_{max} was fixed at 100% (Figure 7.2), whereas the inclusion of E_{max} as a variable parameter improved the fit (Figure 7.3).

The influence of E_{max} truncation on fentanyl and morphine parameter estimates and associated variability was assessed with simulation experiments by fixing E_{max} between 60% (representing the maximum degree of truncation) and 150% (no truncation). As the value of E_{max} approached the theoretical maximum of 150%, the PD parameter estimates become more representative of the true parameter values. The PD parameter that was most sensitive to E_{max} truncation was EC_{50}, evidenced by a 1.8- and 3.3-fold increase in estimated parameter value for fentanyl and morphine, respectively, when E_{max} was increased from 100 to 150% (Figure 7.4). The sigmoidicity factor of both opioids decreased in concert with increasing values of E_{max}, whereas decreasing truncation moved estimates of k_{e0} in opposing directions.

Additional simulations examined three effect versus concentration relationships representing varying degrees of sigmoidicity: $\gamma = 1$, $\gamma = 2$, or $\gamma = 4$. As effect data were increasingly truncated (i.e., as MAR decreased from 100% to 20 %; Panel A in Figures 7.5-7.7), the EC_{50} recovered from the %MAR versus concentration relationship decreased (Panel B in Figures 7.5-7.7). The influence of truncation on the EC_{50} was modulated by the degree

of sigmoidicity in the relationship between the actual response and concentration (Figure 7.8). As γ increased, the perturbation of EC_{50} associated with data truncation decreased.

DISCUSSION

The present study presents a modified approach to modeling antinociceptive effect data that are skewed by the presence of one or more data points at or near a pre-defined maximum degree of response. The serum- and effect-time courses were described by a one-compartment PK model linking serum concentrations to antinociception with a hypothetical effect compartment. A sigmoidal E_{max} model, with E_{max} fixed at 100% MPR, was applied to the time course of fentanyl and morphine antinociception. While this traditional modeling approach adequately described the onset of effect, peak response was underpredicted (Figure 7.2). The inclusion of E_{max} as a variable in the PD model, as opposed to a fixed ceiling, improved the fit. The associated parameter estimates (Table 7.2) were used to predict the observed time course of antinociception as well as the time course of antinociception in the absence of a 60-sec cut-off (Figure 7.3). As the extent of E_{max} truncation decreased, the dynamic range of effect increased from 65 to 100% of the theoretical range. Consequently, the estimates of fentanyl and morphine EC_{50} increased, whereas the apparent degree of sigmoidicity decreased (Figure 7.4). In contrast, the value of k_{e0}, the rate constant of equilibrium between serum and the hypothetical effect compartment, increased for fentanyl but decreased for morphine (Figure 7.4). This seemingly contradictory observation may be explained, in part, by differences in the time delay between serum concentrations and onset of effect. As the value of E_{max} approached the theoretical estimate, the dissociation between concentration and effect increased for fentanyl, as evidenced by a decrease in the value of k_{e0}. In contrast, the estimate for morphine, a drug with a modest degree of dissociation

between the time course of drug action and drug disposition, increased as the value of E_{max} increased. The hypothesis that k_{e0} is better approximated as E_{max} approaches its hypothetical value is supported by the observed shift of predicted values towards previously-reported estimates of k_{e0} as 0.31 and 0.02 min^{-1} for fentanyl and morphine, respectively (Gardmark et al., 1993; Cox et al., 1998). Determining whether PD parameter estimates are better approximated when E_{max} approaches its theoretical value could be assessed further by administering lower opioid doses that do not reach or exceed the 60-sec threshold and comparing the recovered parameter values.

The use of exposure cut-off times imposes an artificial ceiling on responsivity, which can result in the underestimation of EC_{50}. While the disagreement between predicted and theoretical parameter estimates is mitigated as the degree of sigmoidicity increases, drugs with small γ values are more common than those with large values, primarily because the all-or-none, switch-like effects associated with large γ values present challenges in dose titration, particularly for drugs with a narrow therapeutic window (Dutta et al., 1996). The present simulations demonstrate that E_{max} truncation influences parameter estimates and should be considered when translating estimates between species or into a clinical population. While hotplate exposure cut-off times are emphasized in this study, the principles highlighted in these simulations can be extended to other methodological issues associated with the characterization of pharmacologic response.

The opposing situation, of a theoretical maximum effect that exceeds the range of observable effects, presents similar complications in recovering parameter estimates by PK-PD data analysis. This situation may arise for a number of reasons, including the desire to achieve a minimal effect compared to a theoretical maximum, such as the antipyretic effects

of paracetamol, or the existence of intolerable side effects that limit characterization of the entire range of responsivity (Anderson et al., 1998). In situations in which the entire range of effect cannot be examined, the relationship between maximum allowable response (expressed as a percentage of the theoretical maximum response) and the recovered EC_{50} (expressed as a percentage of the true EC_{50}) presented in Figure 7.8 can be used to extrapolate the theoretical value of E_{max} and EC_{50}. Previous studies characterizing the relationship between parameter estimates and observed effect found that the closer the observed response to E_{max}, the greater the reliability of recovered estimates (Dutta et al., 1996; Schoemaker et al., 1998). Because achieving 95% effect is not always feasibility, an alternative parameter, S_0, has been proposed to represent the ratio of E_{max}/EC_{50} when a portion of the sigmoidal E_{max} curve is known (Schoemaker et al., 1998). Continued examination of the relationship between observed and theoretical response in relation to maximum effect will ultimately improve pharmacodynamic characterization of diverse effects, over both large and small ranges.

Table 7.1. Final parameter estimates from traditional PK-PD modeling.

	fentanyl ***mdr1a*(-/-)**		**morphine** ***mdr1a*(+/+)**	
Parameter	**Estimate**	**CV%**	**Estimate**	**CV%**
k_{01} (min^{-1})	0.02	30.5	0.25	24
k_{10} (min^{-1})	100	12.4	96	13
V (ml/kg)	1500	38	2800	12
k_{e0} (min^{-1})	0.79	35	0.012	68
EC_{50} (ng/ml)	2.8	9.7	29	84
γ	2.3	14	1	83

Table 7.2. Final parameter estimates from traditional PK-PD modeling.

	fentanyl ***mdr1a*****(-/-)**		**morphine** ***mdr1a*****(+/+)**	
Parameter	**Estimate**	**CV%**	**Estimate**	**CV%**
k_{01} (min^{-1})	0.02	31	0.25	24
k_{10} (min^{-1})	100	12	96	13
V (ml/kg)	1500	38	2800	12
k_{e0} (min^{-1})	0.57	35	0.014	62
EC_{50} (ng/ml)	5.2	62	96	58
γ [a]	1.0	-	1.0	-
E_{max} (%) [a]	155	-	150	-

[a] A stepwise approach was used to fit γ and $E_{max,}$. The value of E_{max} was fixed as the estimate and γ was set as 1.0 prior to fitting k_{e0} and EC_{50}.

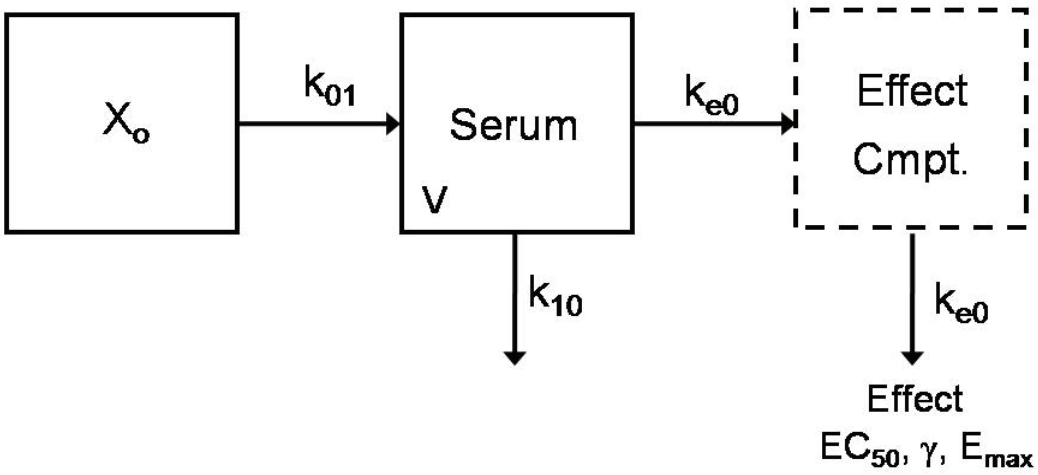

Figure 7.1. Scheme of the pharmacokinetic-pharmacodynamic model for opioid disposition and antinociception in mice. Pharmacokinetic parameters were obtained by fitting the model to the time course of group averaged serum concentrations and estimates were obtained for the absorption rate constant (k_{01}), central volume (V) and first-order elimination rate constant (k_{10}). The effect parameters k_{01}, EC_{50}, γ, and E_{max} were obtained by fitting an effect compartment model to the time course of serum concentrations and antinociception.

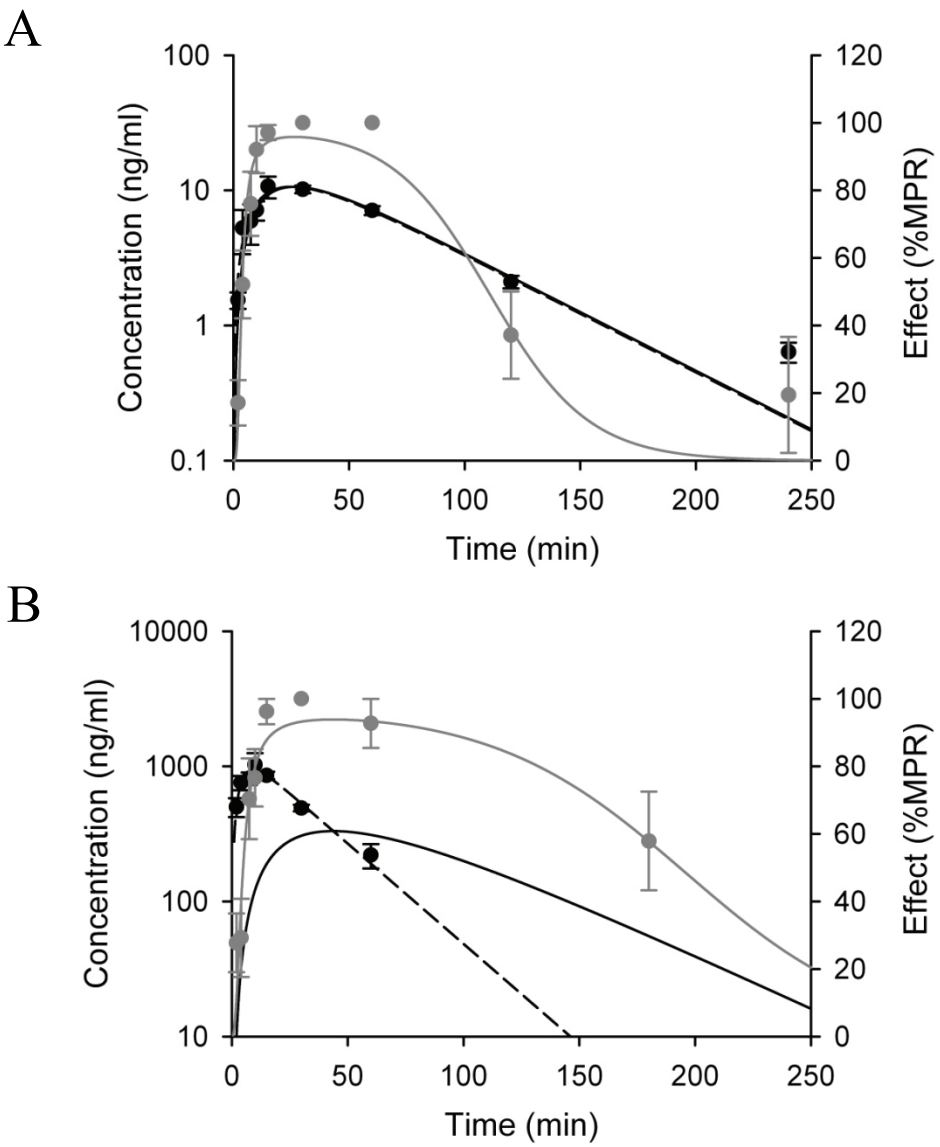

Figure 7.2. Influence of E_{max} fixed at 100% on the time course of antinociception. Data points represent observed antinociception (▲) and serum (●) concentrations following subcutaneous administration of 0.9 mg/kg fentanyl (A) or 3.6 mg/kg s.c. morphine (B) to mice. Data are presented as mean ± S.E. ($n \geq 3$, serum concentration; $n = 4$ to 18, antinociception). Lines represent the fit of the model to the time course of antinociception (solid gray), serum (dashed black), and effect (solid black) compartment concentration data.

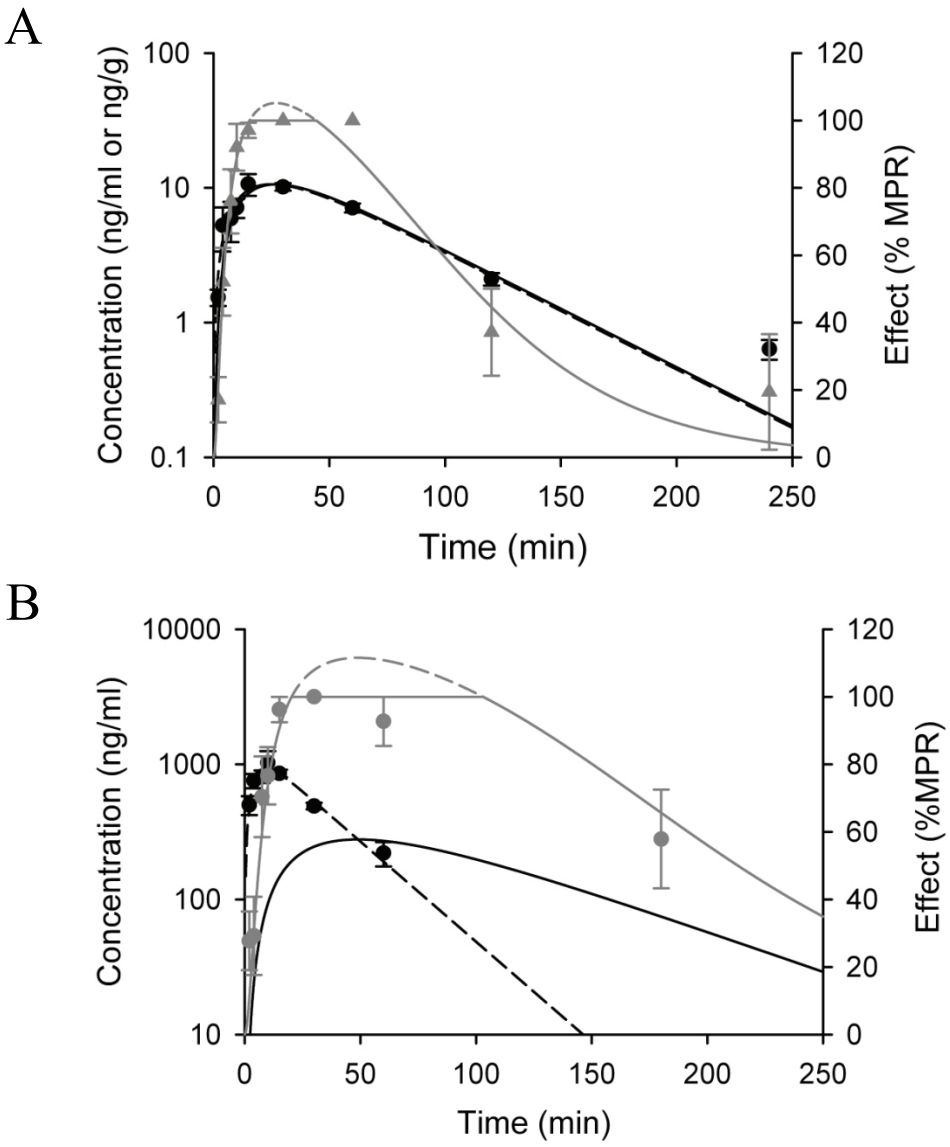

Figure 7.3. Influence of a variable E_{max} on the predicted time course of antinociception. Data points represent observed antinociception (▲) and serum (●) concentrations following subcutaneous administration of 0.9 mg/kg fentanyl (A) or 3.6 mg/kg s.c. morphine (B) to mice. Data are presented as mean ± S.E. ($n \geq 3$, serum concentration; n = 4 to 18, antinociception). Lines represent the fit of the model to the time course of antinociception (solid gray), serum (dashed black), and effect (solid black) compartment concentration data.

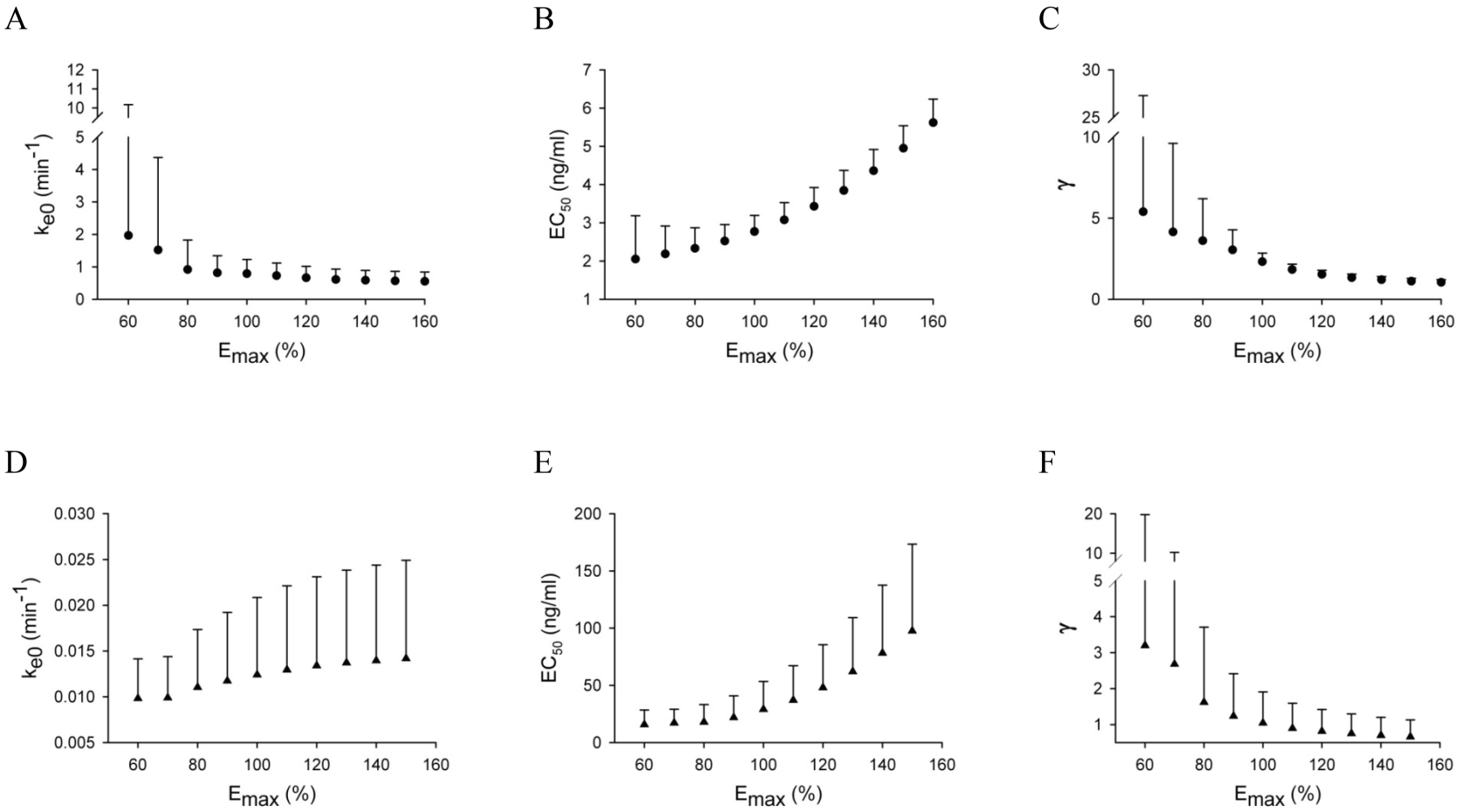

Figure 7.4. Influence of E_{max} truncation on estimates of (A and D) k_{e0}, (B and E) EC_{50} and (C and F) γ for fentanyl (●) and morphine (▲). Data are presented as parameter estimate ± S.E.

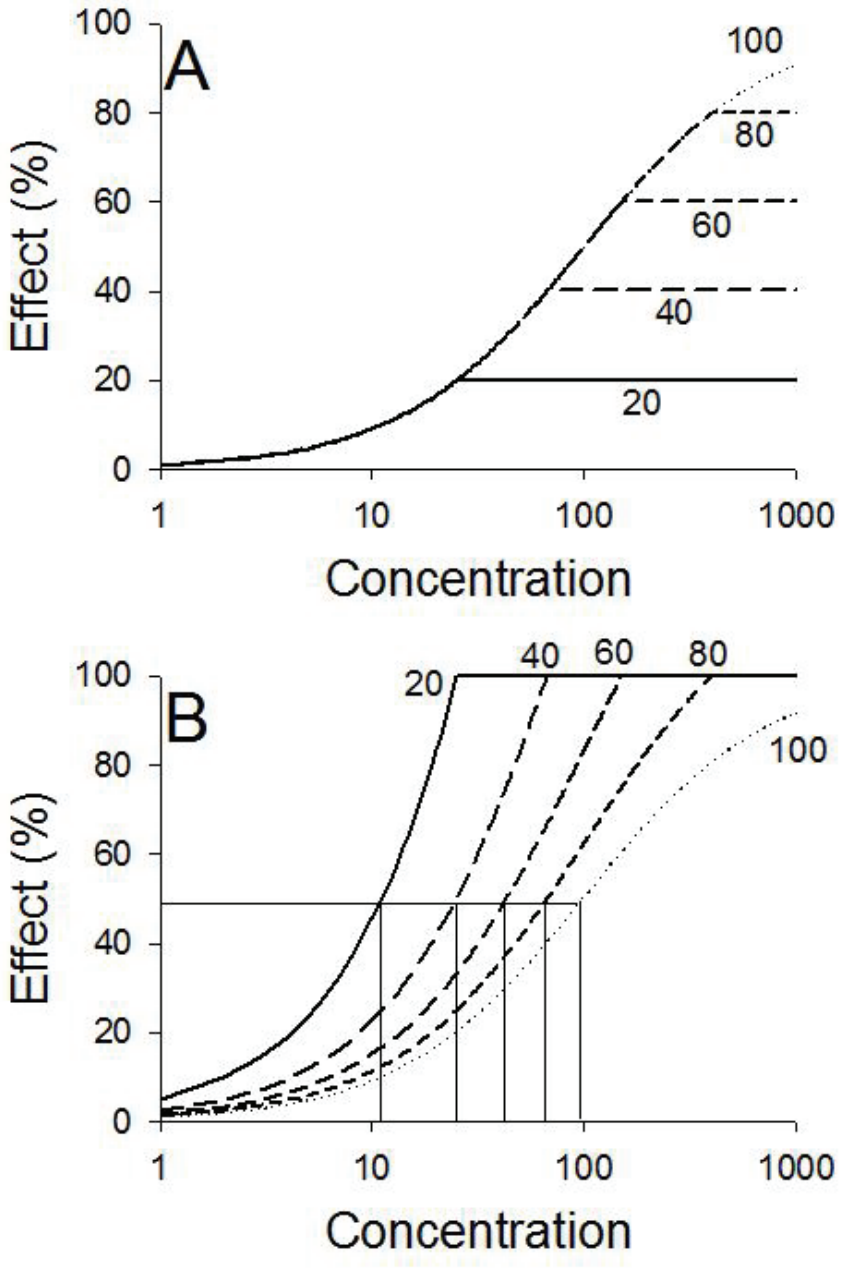

Figure 7.5. Effect versus concentration relationships expressed as actual response (A) or relative to the maximum allowable response (MAR; B) when MAR was 100%, 80%, 60%, 40%, or 20% of the theoretical maximum. Relationships were generated with a sigmoidal E_{max} model, γ=1.

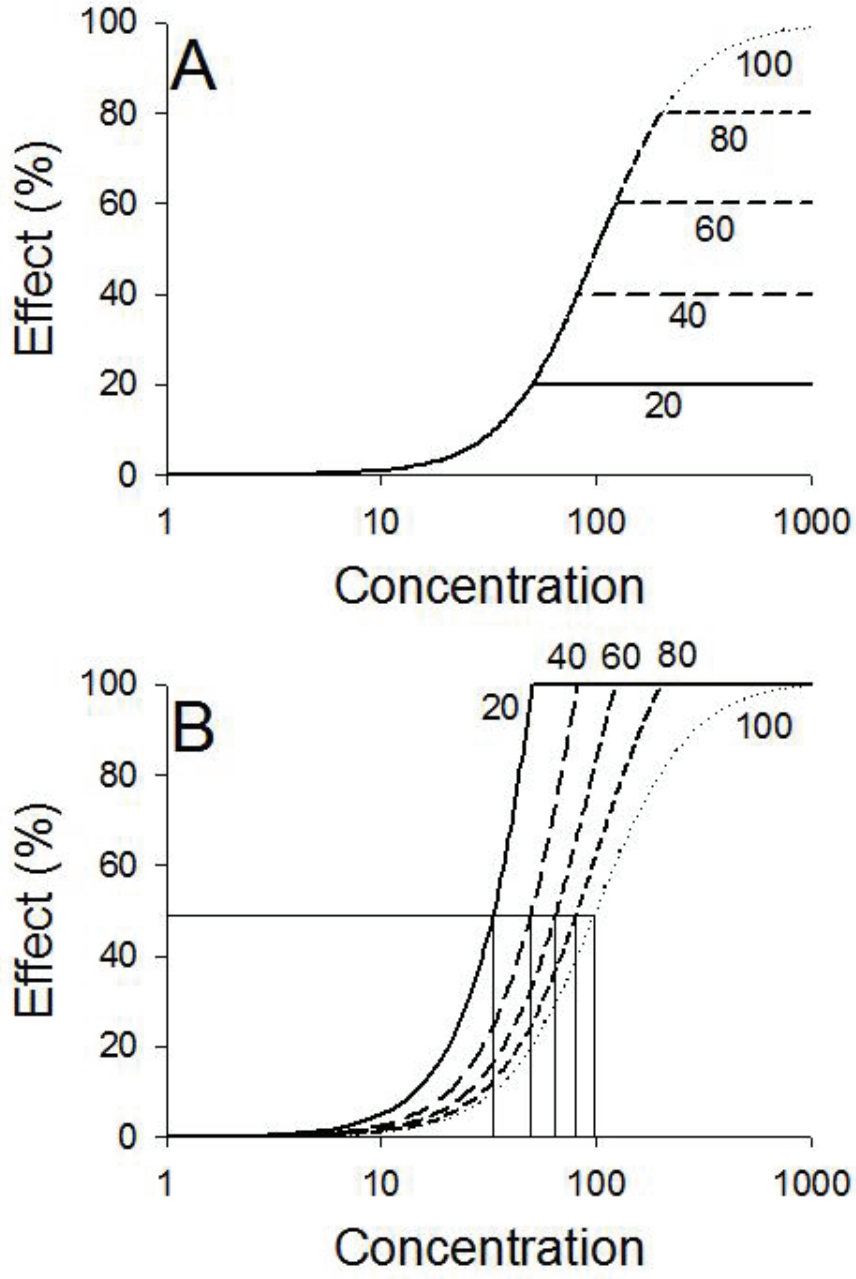

Figure 7.6. Effect versus concentration relationships expressed as actual response (A) or relative to the maximum allowable response (MAR; B) when MAR was 100%, 80%, 60%, 40%, or 20% of the theoretical maximum. Relationships were generated with a sigmoidal E_{max} model, γ=2.

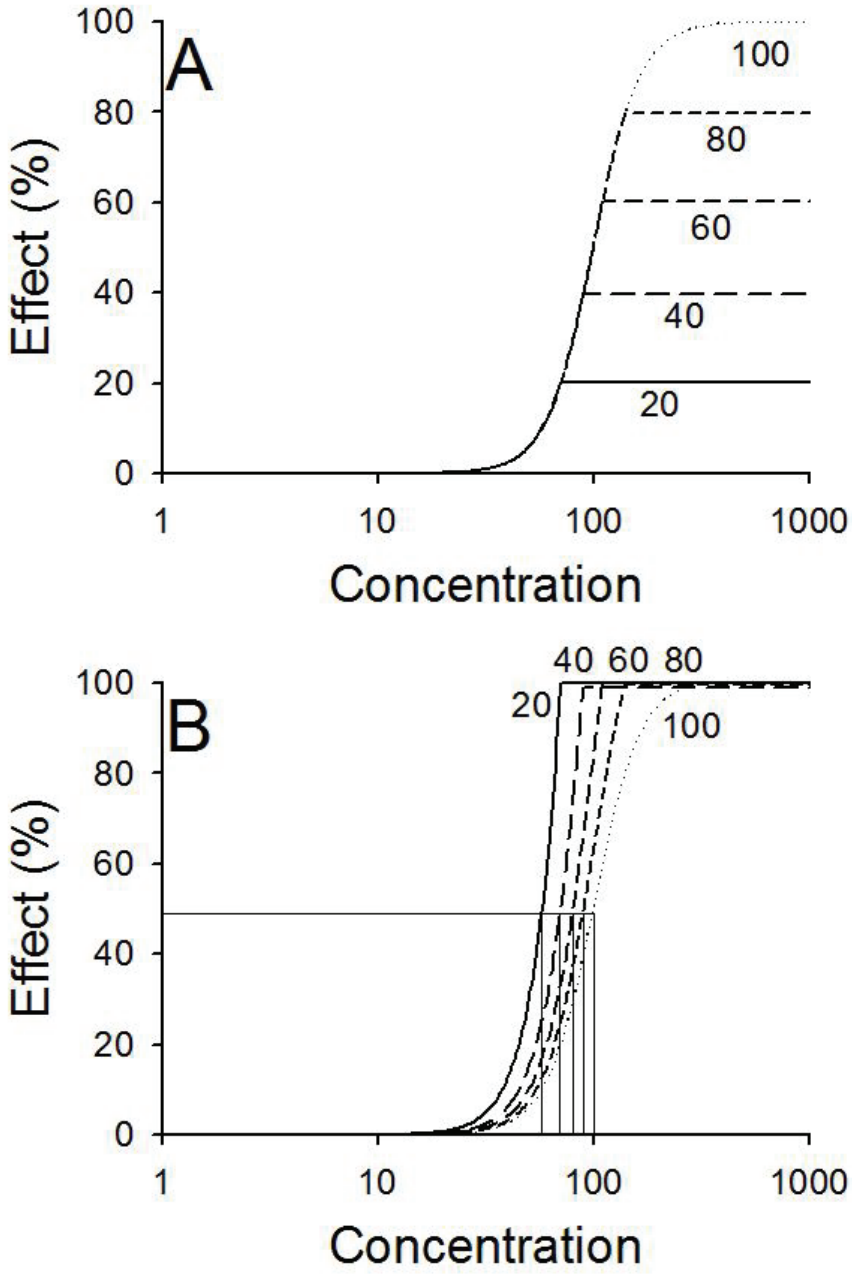

Figure 7.7. Effect versus concentration relationships expressed as actual response (A) or relative to the maximum allowable response (MAR; B) when MAR was 100%, 80%, 60%, 40%, or 20% of the theoretical maximum. Relationships were generated with a sigmoidal E_{max} model, γ=4.

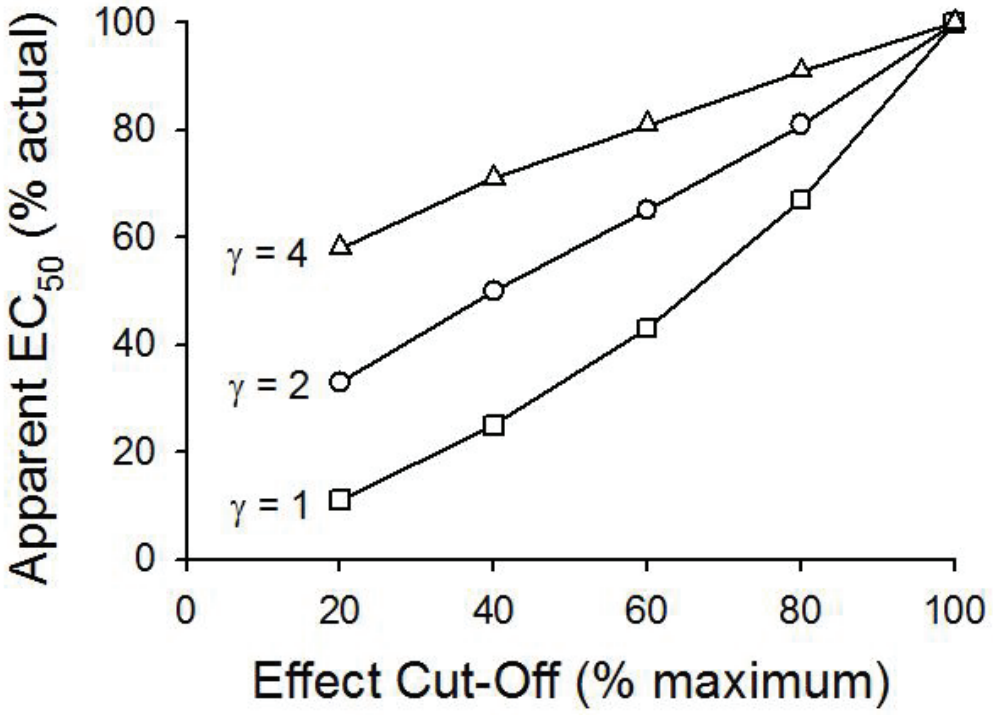

Figure 7.8. Relationship between the apparent EC_{50} (expressed as a percentage of the true EC_{50}) and the maximum allowable response (expressed as a percentage of the theoretical maximum response) for truncated effect data. Effect versus concentration data were simulated with a sigmoidal E_{max} model, with $\gamma=1$, $\gamma=2$, or $\gamma=4$.

REFERENCES

Anderson BJ, Holford NH, Woollard GA and Chan PL (1998) Paracetamol plasma and cerebrospinal fluid pharmacokinetics in children. *Br J Clin Pharmacol* **46**:237-243.

Collier HO, Warner BT and Skerry R (1961) Multiple toe-pinch method for testing analgesic drugs. *Br J Pharmacol Chemother* **17**:28-40.

Cox EH, Kerbusch T, Van der Graaf PH and Danhof M (1998) Pharmacokinetic-pharmacodynamic modeling of the electroencephalogram effect of synthetic opioids in the rat: correlation with the interaction at the mu-opioid receptor. *J Pharmacol Exp Ther* **284**:1095-1103.

D'Amour FE and Smith DL (1941) A method for determining loss of pain sensation. *J Pharmacol Exp Ther* **72**:74-79.

Dutta S, Matsumoto Y and Ebling WF (1996) Is it possible to estimate the parameters of the sigmoid Emax model with truncated data typical of clinical studies? *J Pharm Sci* **85**:232-239.

Ercoli N and Lewis MN (1945) Studies on Analgesics. *Journal of Pharmacology and Experimental Therapeutics* **84**:301-317.

Gardmark M, Ekblom M, Bouw R and Hammarlund-Udenaes M (1993) Quantification of effect delay and acute tolerance development to morphine in the rat. *J Pharmacol Exp Ther* **267**:1061-1067.

Hunskaar S, Fasmer OB and Hole K (1985) Formalin test in mice, a useful technique for evaluating mild analgesics. *J Neurosci Methods* **14**:69-76.

Kalvass JC, Olson ER, Cassidy MP, Selley DE and Pollack GM (2007) Pharmacokinetics and pharmacodynamics of seven opioids in P-glycoprotein-competent mice: assessment of unbound brain EC50,u and correlation of in vitro, preclinical, and clinical data. *J Pharmacol Exp Ther* **323**:346-355.

Kitchen I and Crowder M (1985) Assessment of the hot-plate antinociceptive test in mice. A new method for the statistical treatment of graded data. *J Pharmacol Methods* **13**:1-7.

Le Bars D, Gozariu M and Cadden SW (2001) Animal Models of Nociception. *Pharmacol Rev* **53**:597-652.

Mogil JS, Wilson SG, Bon K, Lee SE, Chung K, Raber P, Pieper JO, Hain HS, Belknap JK, Hubert L, Elmer GI, Chung JM and Devor M (1999) Heritability of nociception I: responses of 11 inbred mouse strains on 12 measures of nociception. *Pain* **80**:67-82.

O'Callaghan JP and Holtzman SG (1975) Quantification of the analgesic activity of narcotic antagonists by a modified hot-plate procedure. *J Pharmacol Exp Ther* **192**:497-505.

Paalzow L (1969a) An electrical method for estimation of analgesic activity in mice. I. Methodological investigations. *Acta Pharm Suec* **6**:193-206.

Paalzow L (1969b) An electrical method for estimation of analgesic activity in mice. II. Application of the method in investigations of some analgesic drugs. *Acta Pharm Suec* **6**:207-226.

Schoemaker RC, van Gerven JM and Cohen AF (1998) Estimating potency for the Emax-model without attaining maximal effects. *J Pharmacokinet Biopharm* **26**:581-593.

Woolfe G and Macdonald AD (1944) The evaluation of the analgesic action of pethidine hydrochloride (Demerol). *J Pharmacol Exp Ther* **80**:300-307.

CHAPTER 8

THE INFLUENCE OF PHARMACOKINETIC AND PHARMACODYNAMIC PARAMETERS ON HYSTERESIS LOOP AREA

ABSTRACT

Purpose: The objective of this study was to develop a computational method to quantitate the area bounded by a hysteresis loop (ABH) and to utilize this METHOD to determine the influence of pharmacokinetic (PK) and pharmacodynamic (PD) parameters on ABH.

Methods: An effect-compartment (sigmoidal E_{max}) PK/PD model was used to simulate blood (C_B) and biophase (C_E) concentration- and effect-time profiles. The influence of PK/PD parameters on the effect vs. concentration relationships was examined by varying parameter values. ABH was calculated in Matlab by subtracting the area under the ascending curve was subtracted from the area of the descending curve. An image processing program was used to validate measurements of ABH.

Results: Good agreement was observed between ABH measurements using Matlab and ImageJ (r^2>0.99), suggesting that the computational approach returned a precise measure of the hysteresis area. The technique then was used to explore fundamental relationships between ABH and PK/PD parameters. The ABH for the effect vs. C_B hysteresis increased linearly with dose, was inversely related to Cl and V, and asymptotically approached a limiting value as the value of K_a increased. A biphasic relationship was observed between ABH and PD parameters, k_{e0} and EC_{50}.

Conclusions: The approach for calculating ABH provided reliable estimates of the effect-C_B ABH. Simulations indicated that the ABH is sensitive to changes in PK/PD parameters, and that the relationship between ABH and PK/PD parameters would be amenable to laboratory investigation.

INTRODUCTION

In situations of receptor-mediated pharmacologic responses, the magnitude of response is assumed to be proportional to the fraction of the receptor population occupied at a particular drug concentration. In this case, if concentrations in the biophase (C_E) are in immediate equilibrium with concentrations in blood (C_B), and the effect (E) is elicited instantaneously, reversible, and time-invariant, the relationship between E and C_B can be described with a sigmoidal E_{max} model. A classic example of this simple pharmacodynamics case is the neuromuscular blocker turbocurarine, for which the relationship between degree of paralysis and blood concentrations is sigmoidal (Gibaldi and Levy, 1972). In contrast to this simple time-independent relationship, a time-dependent dissociation between systemic drug disposition and the time course of pharmacologic effect produces a more complicated effect versus concentration relationship, often referred to as a hysteresis loop. Hysteresis loops that progress chronologically in a counterclockwise direction are indicative of delays in effect elaboration compared to presentation of the agent to the systemic circulation, whereas hysteresis loops that progress in a clockwise direction, also known as proteresis, are most commonly observed in the presence of acute tolerance development.

The prevalence of counterclockwise hysteresis loops in the effect versus systemic concentration relationship can be attributed in part to the diverse physiologic processes that mediate pharmacologic response. Many different mechanisms or factors can result in

hysteresis behavior. One such example is the formation of an active metabolite from a prodrug, for which the degree of dissociation between E and C_B is related to the rate of metabolite formation and elimination (Gupta et al., 1993). Hysteresis loops can also be a consequence of delayed effect elaboration after drug-receptor binding, e.g., when a signal transduction cascade is initiated and a series of events are required before an effect is realized. Finally, if the receptor biophase is pharmacokinetically distinct from the systemic circulation, a delay in drug equilibration between the target organ and/or biophase and blood will result in a temporal dissociation between E and C_B. This situation was addressed by Shiner et al. (Sheiner et al., 1979) with the indirect-link PK/PD model, a parametric analysis approach that utilizes C_B and E data to generate a time course for substrate concentrations in a hypothetical effect compartment (C_E). A sigmoidal relationship between E and C_E then is used to recover the primary PD parameters: EC_{50}, the concentration resulting in 50% of maximum drug effect, and E_{max}, the maximal drug effect, in addition to a rate constant governing the time course of concentrations at the putative effect site, k_{e0}, and a sigmoidicity factor, γ. An alternative method of hysteresis minimization addresses the influence of sampling locales by including the rate of equilibration between arterial (C_A) and venous (C_V) concentrations, as well as between C_A and C_E. If C_A and C_V equilibrate rapidly, but distribution from C_A to C_E is slow, sampling C_A will yield a counterclockwise hysteresis for the E vs. C_A relationship, whereas sampling C_E will yield a sigmoidal curve in the relationship between E and C_E (Verotta et al., 1989; Tuk et al., 1997). Overall, a number of processes contribute to the observation of hysteresis loops and a variety of mathematical and experimental techniques have been developed to minimize the presence of hysteresis loops.

There is a relative lack of information regarding the degree to which the area bounded by a hysteresis loop (ABH) can be used as a meaningful system descriptor. For example, Gastonguay and Schwartz simulated multiple IV dosing for a drug that exhibits distributional delays to the effect site and acute tolerance (Gastonguay and Schwartz, 1994). These authors utilized a computational technique that minimized the distributional hysteresis in order to reveal the true extent of tolerance. A more quantitative approach developed by Upton and Doolette (Upton and Doolette, 2002) involved calculating drug transit time through an organ by examining the differential between the amount of drug entering and exiting organ, with the presence of a hysteresis loop between the efferent (C_{out}) vs. afferent (C_{in}) concentrations signifying a transport delay. The mean transit time of transport delay was determined by calculating the difference in the area fractions between C_{out} and C_{in} area under the curve (AUC) at each time point normalized to total AUC. While these techniques are valuable, alternative assessments of hysteresis behavior are likely to reveal important information regarding effect vs. concentration relationships.

An alternative approach to understanding hysteresis behavior is to assess the area of the effect versus concentration profile that is associated with the hysteresis, and to use this information to make meaningful inferences about a particular drug. These simulations were based on a sigmoidal E_{max} relationship embedded in an effect-compartment model of drug presentation to the effector to simulate concentration- and effect-time profiles. ABH was assessed quantitatively in a manner analogous to calculating the area under the systemic concentration-time profile (AUC). The fundamental influence of PK/PD parameters on ABH was investigated by sequentially varying these model parameters and assessing the resultant size of the hysteresis loop.

MATERIALS AND METHODS

Blood and biophase concentrations, as well as pharmacologic responses, were simulated using a standard effect-compartment model with a sigmoidal E_{max} relationship between effect and effect-site concentrations (Figure 8.1). All simulations were performed assuming first-order input of a dose X_0 with first-order elimination, first-order distribution to the effect site, and an immediately-elaborated pharmacologic response.

The pharmacokinetic simulations of mass or drug concentrations in the absorption (Eqn. 8.1), central (Eqn. 8.2) and effect (Eqn. 8.3) compartments using the following equations:

$$\frac{dX_A}{dt} = -k_A \cdot X_0 \qquad \text{(Eqn. 8.1)}$$

$$\frac{dC_B}{dt} = (k_a \cdot X_A - k_{el} \cdot X_B)/V_C \qquad \text{(Eqn. 8.2)}$$

$$\frac{dC_E}{dt} = k_{e0} \cdot X_B - k_{e0} \cdot X_E \qquad \text{(Eqn. 8.3)}$$

where X_A is mass in the absorption compartment, C_B is the concentration in the central, blood compartment and C_E is the concentration in the effect compartment, V_c is the apparent volume of the central compartment, and k_a, k_{el}, and k_{e0} are the first-order rate constants for absorption, elimination, and effect offset, respectively.

A sigmoidal E_{max} model was used to simulate the relationship between pharmacologic effect and drug concentration at the effect site (Eqn. 8.4).

$$E = \frac{E_{max} \cdot C_E^{\gamma}}{EC_{50}^{\gamma} + C_E^{\gamma}} \qquad \text{(Eqn. 8.4)}$$

where E is the effect, E_{max} is the maximum effect, C_E is the effect compartment concentration, EC_{50} is the effect compartment concentration associated with 50% of the maximum effect, and γ is the sigmoidicity factor.

Initial parameter values were selected in order to achieve a moderately-sized hysteresis (Table 8.1, Simulation 1). Blood and biophase concentration-time and effect-time profiles were simulated in WinNonlin (version 5.0.1, Pharsight Corporation, Cary, NC) by systematically varying the PK/PD parameters, X_0, V, k_a, k_{el}, k_{e0} and EC_{50} (15 values per parameter). The influence of parameters on the size of the E vs. C_B hysteresis was determined using Matlab (Release 12, The MathWorks, Natick, MA). In all simulations, the E vs. C_E relationship served as a negative control for the absence of hysteresis (i.e., statistically insignificant ABH) because the kinetic-dynamic dissociation in this model was due to equilibration delays between the effect site and the central compartment, as opposed to delay in elaboration of response after presentation of the drug to the effect site.

Analysis of the concentration- and effect-time profile data files was completed using a program written in Matlab (Appendix). This program was written to read the data file format and calculate the ABH for the polygon created by the effect vs. concentration relationship. Similar to methods for calculating AUC, the program calculates the area under the ascending effect-concentration profile and subtracts this value from the area under the descending effect-concentration profile to generate the ABH (Figure 8.2). Following this principle, this program is capable of distinguishing a clockwise from a counterclockwise

hysteresis loop such that a positive value is representative of a proteresis and a negative value for a counterclockwise hysteresis.

In order to validate the Matlab analysis, ten hysteresis loops of differing sizes were generated by sequentially varying the value of X_0 (25-500 mg), while holding the remaining parameters constant as listed in Table 8.1, Simulation 1. Matlab was used to determine the ABH for each loop, and the image processing program ImageJ (NIH, Bethesda, Maryland, USA) was used to calculate the number of pixels in the hysteresis normalized to the number of pixels per unit area in the plot (n=3 per hysteresis).

RESULTS

The blood and biophase concentration- and effect-time profiles for a one-compartment model (Figure 8.1) with first-order input (Table 8.1, Simulation 1) are shown in Figure 8.3a. The lag in t_{max} for concentrations at the receptor biophase compared to blood is evidence of the distributional delay between the two compartments. The sigmoidal relationship between effect and biophase concentration reflects the time-independent nature of the E vs. C_E relationship. In contrast, the counterclockwise hysteresis in the relationship between E and C_B is indicative of time dependency due to distributional delay at the hypothetical effect site (Figure 8.3b). The hysteresis is characterized by increasing blood concentrations at early time points with a delay in effect onset because drug is distributing to the biophase. At late time points, blood concentrations are decreasing but effect persists because of the lag in drug elimination from the biophase.

The ABH values generated using Matlab were verified using ImageJ. Excellent agreement ($r^2 \geq 0.99$) was observed for ABH (%*mg/L) calculated by these two methods

(Figure 8.4), validating the precision of the novel computational approach. Matlab therefore was used to calculate ABH in subsequent simulations.

To examine the influence of parameter values on ABH, each parameter in the PK/PD model was varied at least 5-fold from the value in the original parameter space, and the resulting ABH was calculated. ABH was proportional to the administered dose (Figure 8.5a), whereas an inverse hyperbolic relationship between ABH and either k_{el} or V was observed (Figure 8.5b-c). In contrast, ABH asymptotically approached a limiting value as the value of k_a increased (Figure 8.5d). The relationship between ABH and the PD parameters k_{e0} and EC_{50} was biphasic; the ABH increased, reached a maximum, and then decreased with increasing values of k_{e0} or EC_{50} (Figure 8.5e-f).

The cause of the differences in shape between ABH and PK parameters (monophasic), or between ABH and PD parameters (biphasic), was investigated by examining the effect-blood concentration relationship for all parameter values. Three representative values for each parameter (high, moderate, and low) were selected; the influence of changing these parameters on ABH is shown in Table 8.1. The moderate values in each case represent the initial parameter space (Table 8.1, Simulation 1). The corresponding effect-blood concentration profiles are presented in Figures 8.6 and 8.7 for the PK and PD parameters, respectively. Figure 8.6 demonstrates that the relative shape of the hysteresis was independent of the PK parameter value. In contrast, both the size and the shape of the hysteresis were dependent on the PD parameter value (Figure 8.7). These changes in hysteresis shape may, at least in part, explain the biphasic relationship between ABH and the PD parameters. As depicted in Figure 8.3, the blood concentration time course was independent of the PD parameters k_{e0} and EC_{50}, whereas these parameters play a distinct

role in determining the extent and time course of effect. A 5-fold decrease in the value of k_{e0} (1 to 0.2 hr^{-1}) or a 5-fold increase in EC_{50} (5 to 25 mg/L) altered the effect-time profile such that an overall reduction in effect was observed, characterized by a decrease in E_{max} from 62 to 44 % and 25 % and a decrease in ABH from 954.8 to 927.0 %*mg/L and 386.0 %*mg/L for k_{e0} and EC_{50}, respectively (Figure 8.7). In contrast, allowing greater sensitivity of the system to the drug, by increasing the value of k_{e0} or decreasing the EC_{50}, resulted in further decreases in ABH attributable to collapse of the hysteresis (Figure 8.7).

DISCUSSION

The fundamental goal of PK/PD analysis is to characterize the relationship between pharmacologic effect and drug concentrations, allowing estimation of an EC_{50} value. The simplest relationships are developed when blood concentrations are directly linked to pharmacologic response. A number of criteria must be met for this to occur: equilibrium between biophase and blood concentrations and receptor mediated pharmacologic response that is instantaneous, reversible, and time-independent. If these criteria are met, then the relationship between effect and blood concentration can be described using a sigmoidal E_{max} model. However, a violation of any of these limiting assumptions can result in a hysteresis in the relationship between effect and blood concentration.

The inclusion of a hypothetical effect compartment that drives effect is a common method of collapsing hysteresis loops (Holford and Sheiner, 1982). Simulating drug concentrations in a hypothetical effect compartment allows for the recovery of EC_{50} and E_{max} from the sigmoidal curve in the E-C_E relationship rather than the hysteresis between E-C_B. In the present simulations, a one-compartment link model was employed to generate concentration and effect data. The selection of this model was based on the frequency with

which experimental data are fit with a blood and biophase compartment (Kalvass et al., 2006; Kalvass et al., submitted). While this method is a useful approach in PK modeling and simulation, it results in a "collapsed" hysteresis loop. An important hypothesis underlying the present study was that the shape and size of the hysteresis loop may reveal meaningful information about the disposition of a particular drug.

A program written for Matlab was used to accurately and reproducibly measure ABH with a method analogous to calculating AUC, where subtracting the area of the ascending curve from the descending curve yielded the area bound by the data points. ImageJ was used to demonstrate that the measurements obtained using Matlab were reliable. HysQuant offers greater accuracy, due to the elimination of user error, and improved throughput compared to an image analysis approach. HysQuant is amenable to calculating ABH for experimentally derived data, in part because of its ability to calculate both clockwise and counterclockwise ABH. The ability to calculate clockwise ABH would be valuable in experiments designed to assess the influence of acute PD tolerance on hysteresis area. One limitation of this program is that it calculates the area of a polygon of a finite number of data points and not of a continuous loop. However, this aspect actually may prove to be advantageous and the ABH could be a model-independent method of characterizing the system.

It was expected that increasing or decreasing a particular parameter value would alter the blood and biophase concentration- and effect-time profiles, thereby influencing the ABH. A more interesting result was that there was a critical region over which small changes in PK/PD parameter values led to large changes in ABH. Incremental increases in the values of k_{el}, V, or k_a affected ABH to a larger extent when the values were low compared to those same increases in the higher ranges (Figure 8.5b-d). The critical regions for the PD

parameters, k_{e0} and EC_{50}, were also at low ranges but led to sharp increases in ABH followed by sharp decreases (Figure 8.5e-f). The locations of these critical regions may be important when fitting models to experimental data. Models could be assessed for their sensitivity to a particular parameter, depending on where the parameter value fell on the ABH curve. For example, Figure 8.5d reveals minimal increases in ABH when the value of k_a is 25 hr^{-1} or greater. Therefore, if a model estimates a parameter to be within this region, the significance of the parameter may be minimal because absorption is nearly instantaneous.

A particularly intriguing aspect of these simulations was the biphasic relationship between ABH and the PD parameters. This relationship can, in part, be attributed to the shifting nature of the shape of the hysteresis on each side of the ABH maximum. When k_{e0} or EC_{50} deviate from the values that yield the ABH maximum, the hysteresis begins to collapse (Figure 8.7). While this behavior is demonstrated within this series of simulations, it would not be evident in experimental data, which yield only one effect-concentration profile. For example, if a drug exhibits a low percent effect, as is the case with the antihypertensives, a full blood concentration-time profile will be obtained but the small changes in the effect-time profile will resulting in a low ABH value. In contrast, a drug that is administered at doses that achieve near 100% effect will cover a full effect range and a large hysteresis will be formed between the effect-blood concentration profile. The ratio of the effect-blood concentration ABH to effect-biophase concentration ABH for these two types of drugs will be small and large, respectively. Therefore, caution must be exercised so as to not falsely identify a drug with a small effect range as a hysteresis simply because it has a small E-C_B hysteresis to negative control E-C_E ratio. These simulations reveal that when

designating a particular effect-concentration relationship as a hysteresis, it is important to consider the concentration and effect ranges in addition to the ABH.

The influence of sampling schedule on measures of ABH is an interesting aspect of hysteresis behavior that was identified in this and previous studies (Levy et al., 1994). The present work revealed that time point selection plays a role in dictating measures of ABH. For example, if 15 concentration-effect measurements are simulated, an equal distribution of sampling time points would yield different ABH values compared to a sampling scheme that concentrates half of the time points at the beginning of the absorption and the remaining half during the elimination phase. The evenly distributed time points typically will yield a greater ABH compared to the latter scheme because the full shape of the curve is missed when sampling at the beginning and end of the profile. Previous work examining the practicality of sparse sampling schemes in clinical trials found that adequate effect-concentration relationships could be made for drugs exhibiting pharmacodynamic hysteresis when sampling was performed near the end of the dosing interval (Ebling et al., 1996). These simulations demonstrated the feasibility of sparse sampling when data are best fit by the indirect link model, although the inherent intra- and inter-individual subject variability is likely to produce parameter estimates that are less reliable than those produced by sampling a full concentration-effect profile. Furthermore, sampling at the end of the dosing interval may provide the best initial parameter estimates, but may fail to fully characterize the hysteresis. Considering the observations made by Ebling et al. in light of the present simulations, the most useful clinical sampling scheme for drugs exhibiting pharmacodynamic hysteresis may be to preliminarily obtain a full concentration-effect data within a limited population in order to characterize the shape and size of the hysteresis studies and use these model independent

observations to identify critical time points for subsequent sparse sampling in a fully powered trial (Ebling et al., 1996).

The present simulations are relevant to clinical research because blood concentration and effect are frequently the only data reported. Biophase concentrations are rarely known, largely due to physiologic isolation and the cost associated with precise methods of quantitation. By initially characterizing the effect-blood concentration hysteresis it is hoped that the relationship between effect and biophase concentrations will be better understood. Future work in this area will assess the influence of population variability on measures of hysteresis area and be used to develop a comprehensive definition of how large a hysteresis must be to differentiate it from a sigmoidal curve. A quantitative definition of a hysteresis loop and a method to calculate ABH will allow identification in a manner more objective than the current approach of visual inspection. An *in vivo* study by Cox et al. examined the relationship between effect, measured using an EEG, and blood concentrations for three opioids; results of this study revealed that alfentanil rapidly arrived at the receptor biophase and the effect-blood concentration relationship was sigmoidal whereas fentanyl and sufentanil exhibited moderate hysteresis behavior (Cox et al., 1998). A comprehensive definition of hysteresis loops would allow effect-concentration relationships such as these to be definitively classified as sigmoidal or a hysteresis. One critical component in developing this definition will be the incorporation of inter-individual variability, which is not always reported (Chen and Pollack, 1998; Cox et al., 1998; Kharasch et al., 2003). The magnitude of variability compared to the magnitude of effect and concentration will be important in determining the presence of a hysteresis in the data, e.g. overlapping error bars yield a questionable hysteresis. A final aspect that will be incorporated into future work is the

presence of indirect pharmacologic effects and other time-dependent processes into models of hysteresis behavior. These investigations will rely significantly on models developed by Jusko and colleagues (Krzyzanski and Jusko, 1997a; Krzyzanski and Jusko, 1997b). Ultimately, a number of factors contribute to hysteresis behavior and should be investigated. This paper presents a preliminary sense of the influence of PK/PD parameters on hysteresis loop area.

Table 8.1. Influence of model parameters on ABH.

Simulation	X_0 (mg)	K_{el} (L/hr)	V (L)	K_a (hr^{-1})	k_{e0} (hr^{-1})	E_{max} (%)	EC_{50} (mg/L)	H	ABH (%*mg/L)
1	100	1	2.5	2	1	100	5	1	954.8
2	**20**	1	2.5	2	1	100	5	1	77.20
3	**500**	1	2.5	2	1	100	5	1	5798
4	100	**0.2**	2.5	2	1	100	5	1	1116
5	100	**5**	2.5	2	1	100	5	1	427.0
6	100	1	**0. 5**	2	1	100	5	1	3535
7	100	1	**12.5**	2	1	100	5	1	27.84
8	100	1	2.5	**0.4**	1	100	5	1	313.1
9	100	1	2.5	**10**	1	100	5	1	1559
10	100	1	2.5	2	**0.2**	100	5	1	927.0
11	100	1	2.5	2	**5**	100	5	1	461.1
12	100	1	2.5	2	1	100	**1**	1	1159
13	100	1	2.5	2	1	100	**25**	1	386.0

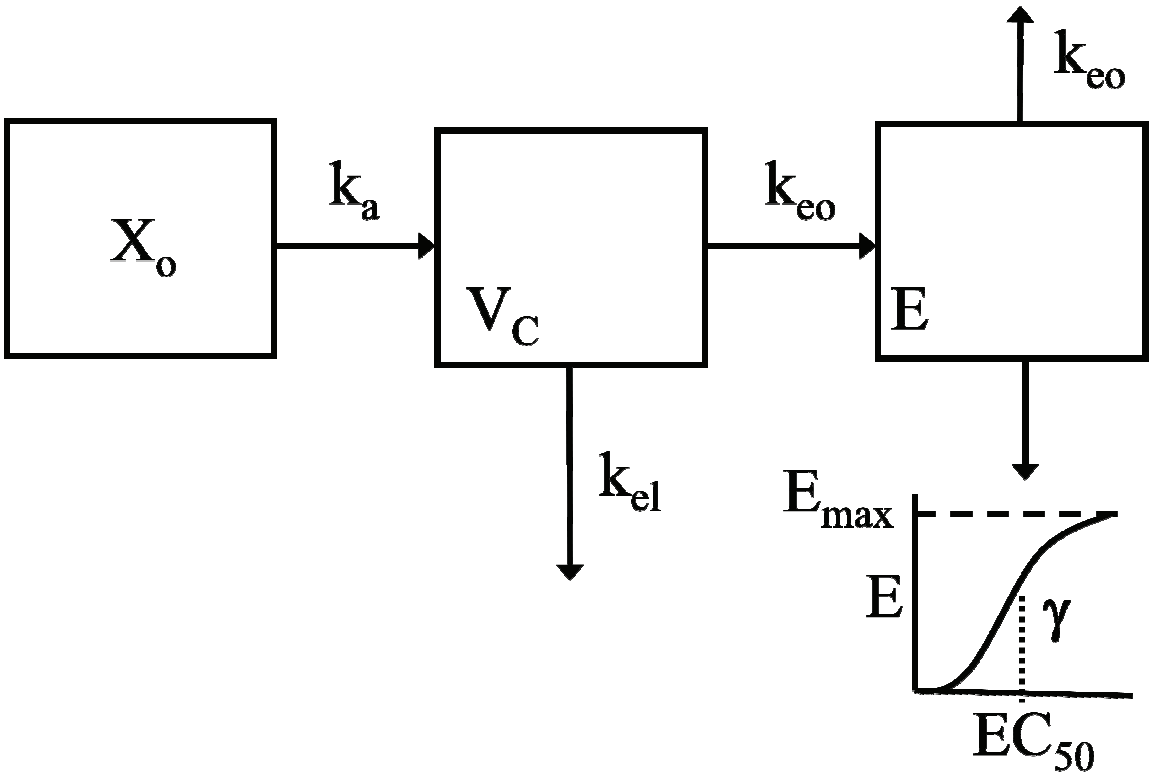

Figure 8.1. Scheme of the model used to generate concentration and effect profiles. Parameter values are defined in the methods section.

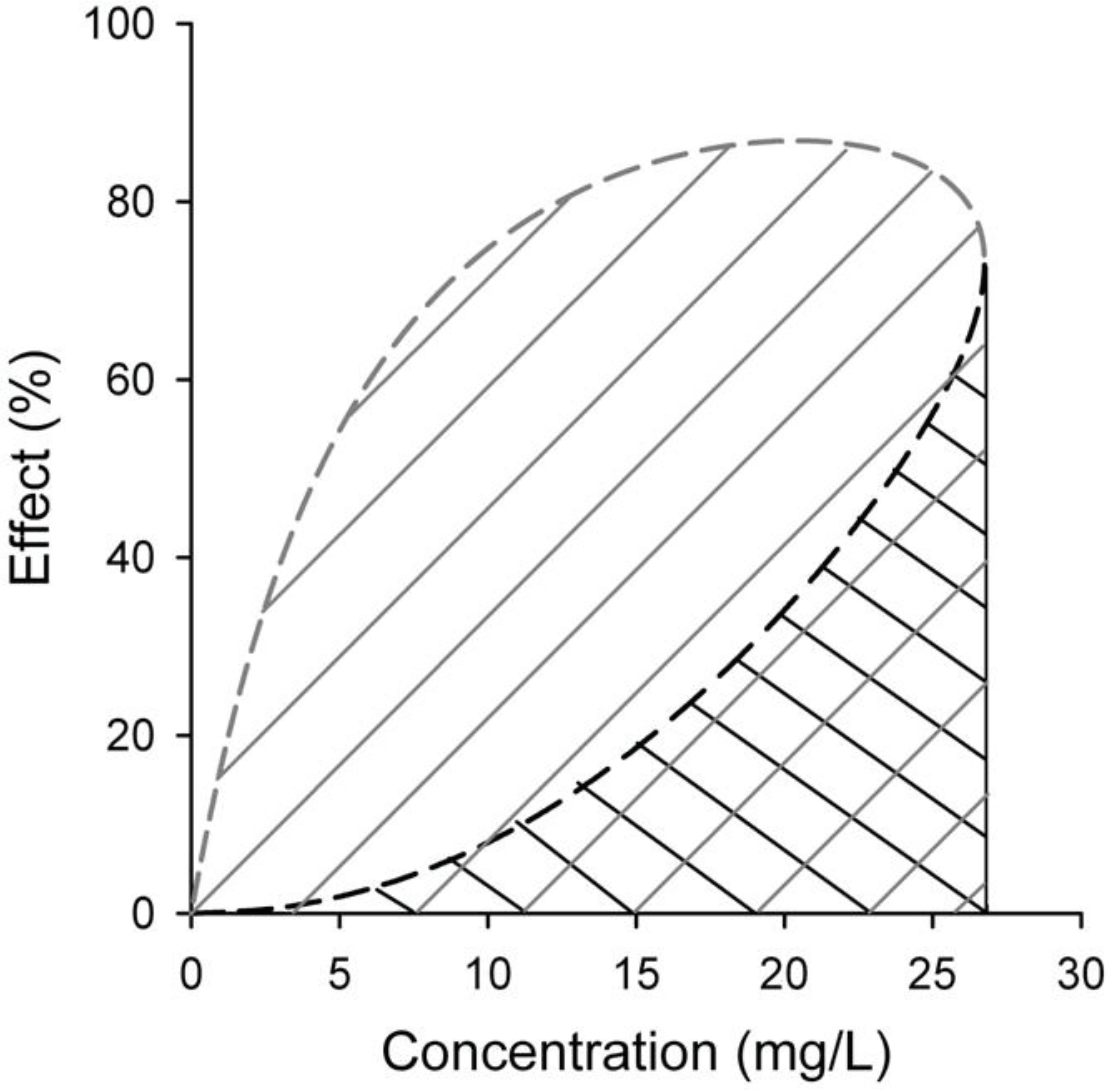

Figure 8.2. Method of calculating ABH utilized by Matlab. The hysteresis is divided into two segments at the C_{max}, the ascending curve (dashed black line) and the descending curve (dashed gray line). The area under the ascending curve (solid black lines) is subtracted from the area under the descending curve (solid gray lines).

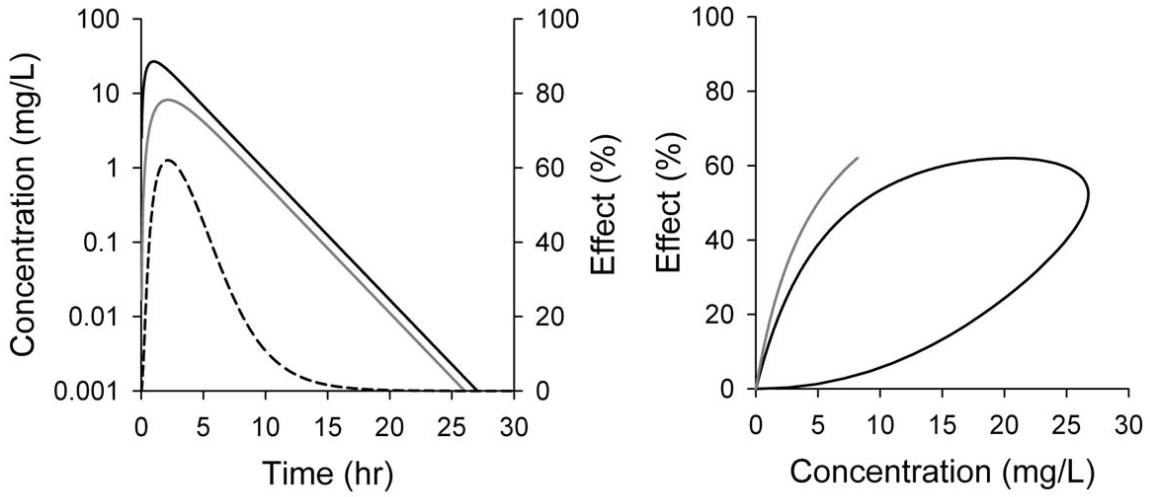

Figure 8.3. Representative pharmacokinetic and pharmacodynamic model output. The left panel depicts blood (———) and biophase (———) concentration- and effect- (– – –) time profiles were simulated using the PK-PD model (Figure 8.1) and the parameters in Table 8.1, Simulation 1. The right panel depicts the relationship between effect intensity and blood (———) or biophase (———) concentrations.

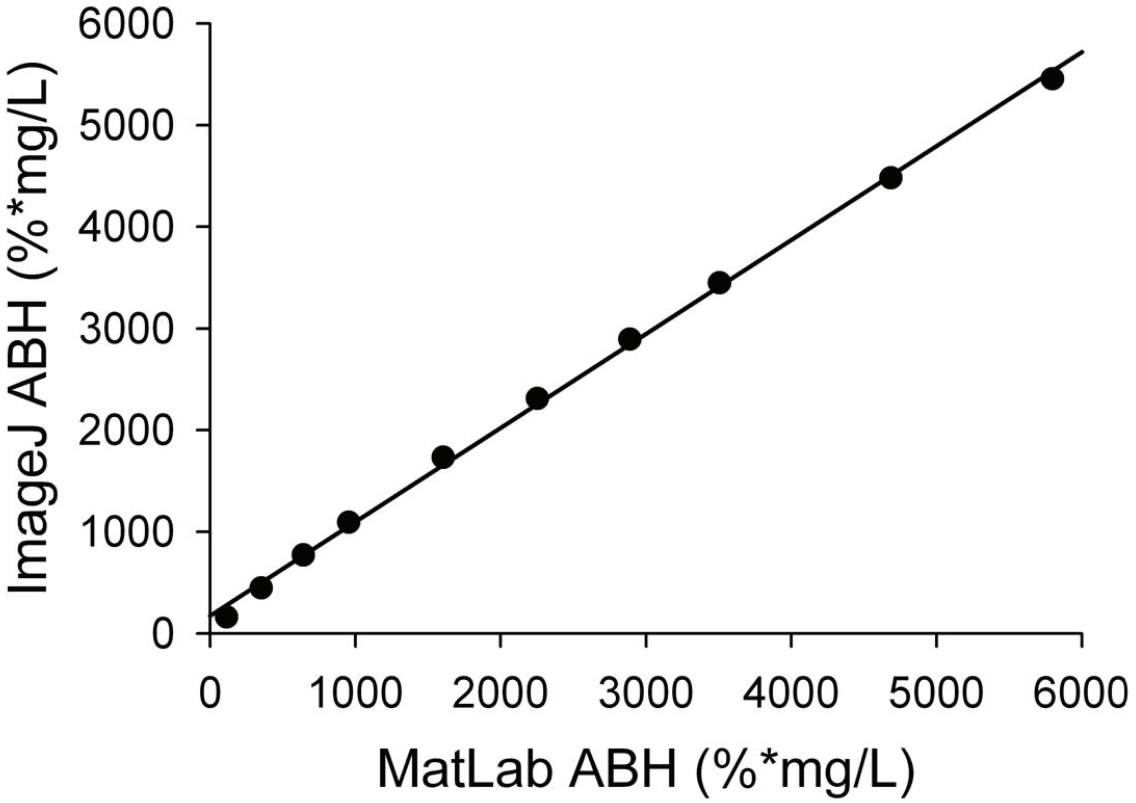

Figure 8.4. Relationship between ABH calculated using ImageJ and Matlab. The line represents the linear regression through the points ($r^2 > 0.99$).

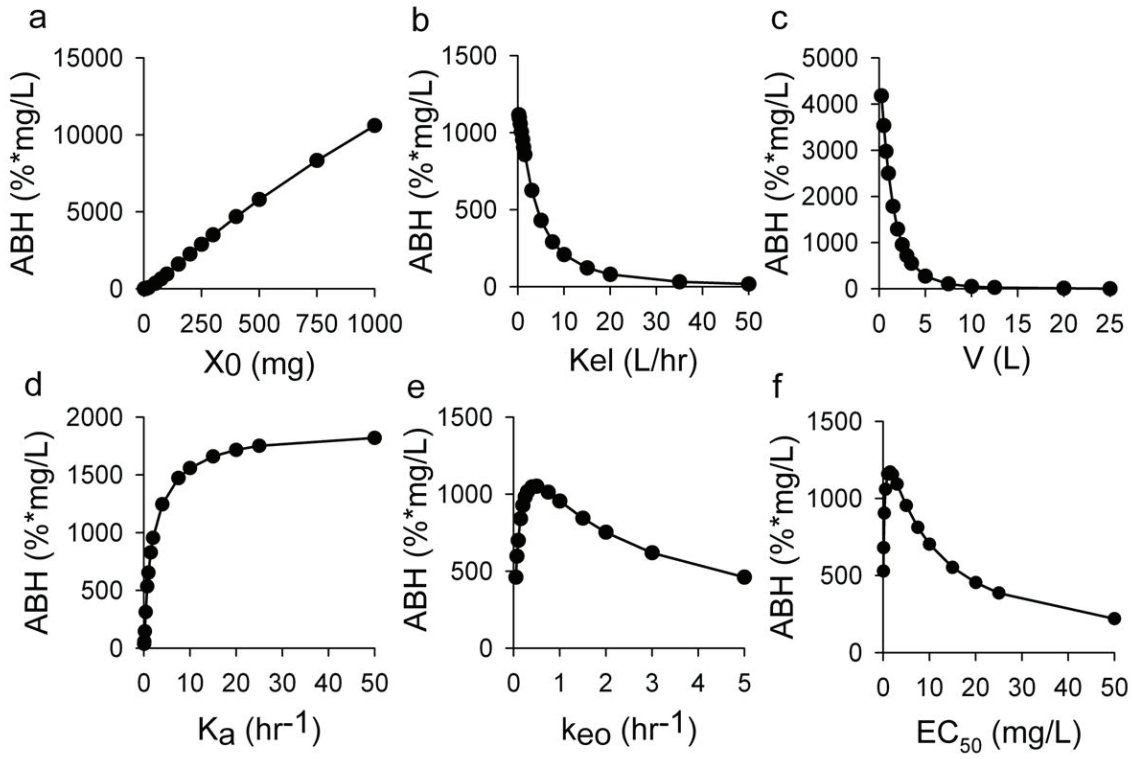

Figure 8.5. The influence of PK-PD parameter values on measures of ABH. The value of each parameter was sequentially varied (a) X_0, 2.5-1000 mg; (b) k_{el}, 0.2-50 hr^{-1}; (c) V, 0.25-25 L; (d) k_a, 0.075 – 50 hr^{-1}; (e) k_{e0}, 0.05-5 hr^{-1}; (f) EC_{50}, 0.05-50 mg and the remaining model parameters were held constant. The ABH was calculated for the simulated effect vs. blood concentration hysteresis.

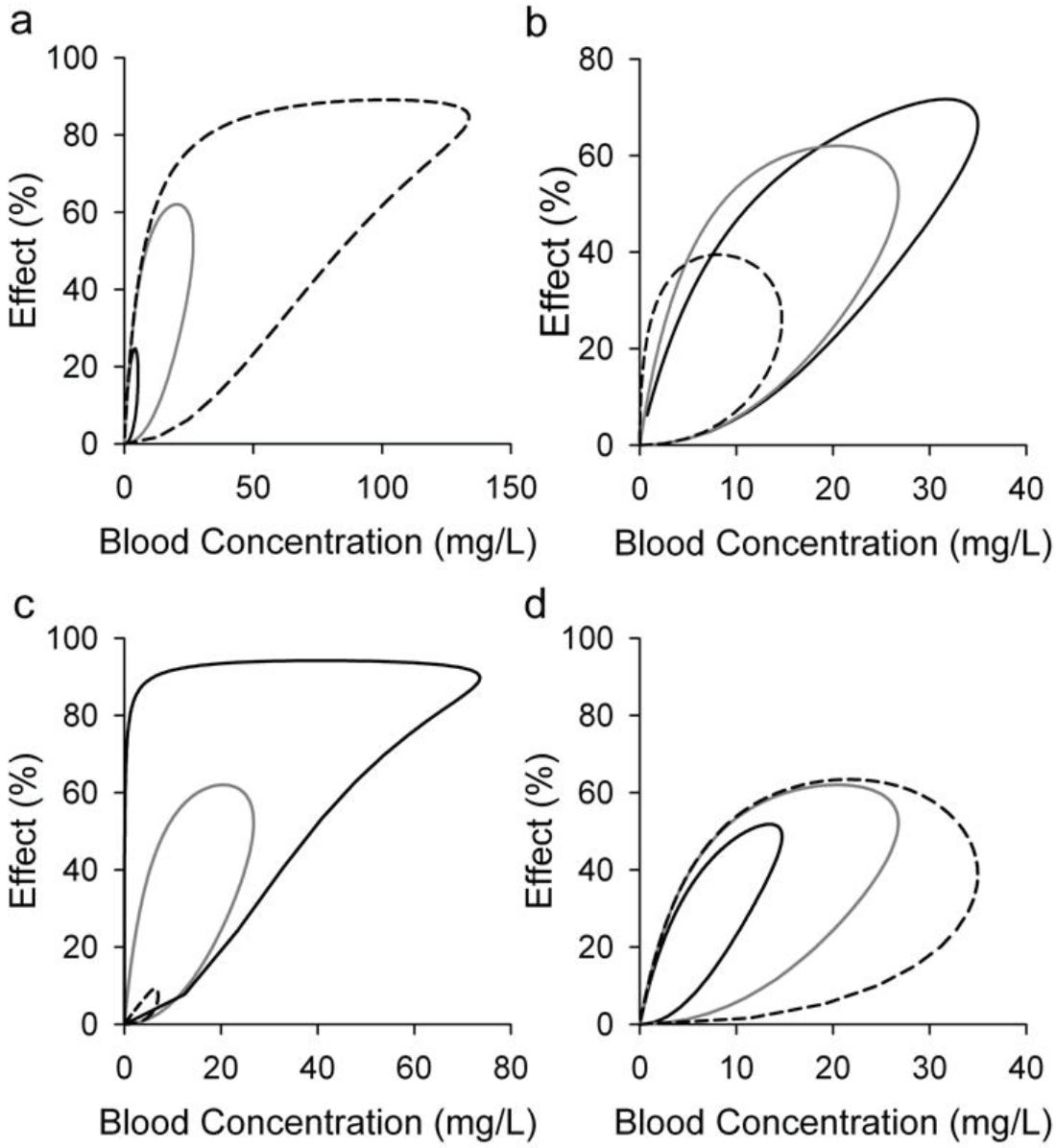

Figure 8.6. Influence of PK parameter values on the effect versus blood concentration hysteresis. The parameters (a) X_0; (b) k_{el}; (c) V and (d) k_a were increased (— — —) or decreased (———) by 5-fold compared to the core parameter value (———), corresponding with the parameter values listed in Table 8.1, Simulations 1-9.

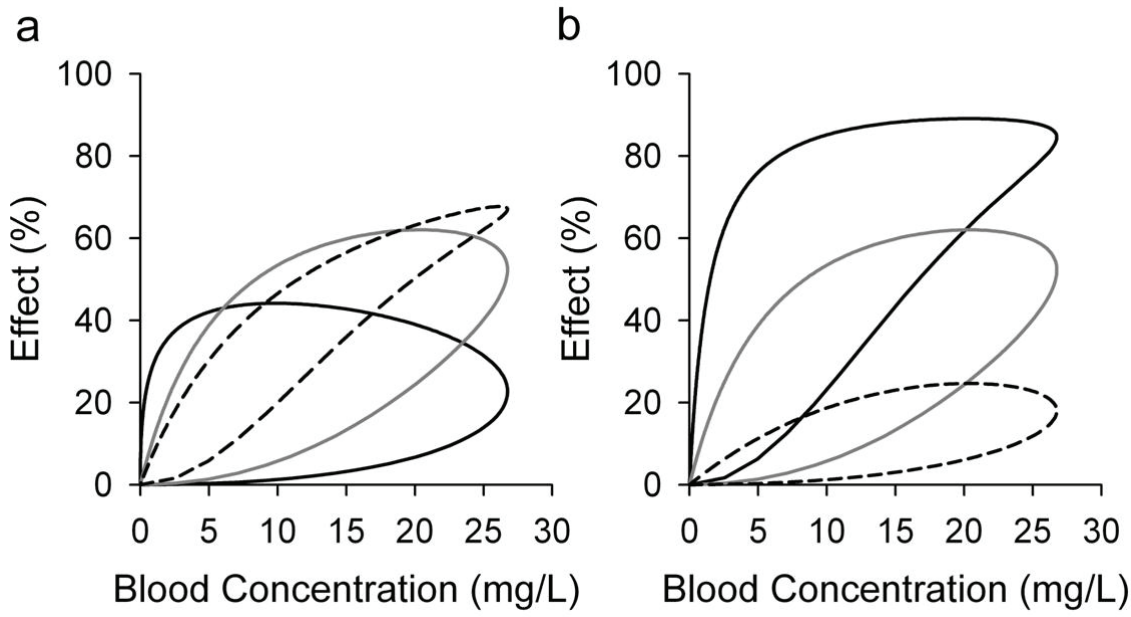

Figure 8.7. The influence of PD parameter values on the effect versus blood concentration hysteresis. The parameters k_{e0} (a) and EC_{50} (b) were increased (— — —) or decreased (———) by 5-fold compared to the core parameter value (———), corresponding with the parameter values listed in Table 8.1, Simulations 1 and 10-13.

REFERENCES

Chen C and Pollack GM (1998) Altered disposition and antinociception of [D-penicillamine(2,5)] enkephalin in mdr1a-gene-deficient mice. *J Pharmacol Exp Ther* **287**:545-552.

Cox EH, Kerbusch T, Van der Graaf PH and Danhof M (1998) Pharmacokinetic-pharmacodynamic modeling of the electroencephalogram effect of synthetic opioids in the rat: correlation with the interaction at the mu-opioid receptor. *J Pharmacol Exp Ther* **284**:1095-1103.

Ebling WF, Matsumoto Y and Levy G (1996) Feasibility of effect-controlled clinical trials of drugs with pharmacodynamic hysteresis using sparse data. *Pharm Res* **13**:1804-1810.

Gastonguay MR and Schwartz SL (1994) The use of multiple doses and pharmacodynamic system analysis to distinguish between dispositional delays and time-variant pharmacodynamics. *Pharm Res* **11**:1825-1828.

Gibaldi M and Levy G (1972) Dose-dependent decline of pharmacologic effects of drugs with linear pharmacokinetic characteristics. *J Pharm Sci* **61**:567-569.

Gupta SK, Hwang SS, Benet LZ and Gumbleton M (1993) Interpretation and utilization of effect and concentration data collected in an in vivo pharmacokinetic and in vitro pharmacodynamic study. *Pharm Res* **10**:889-894.

Holford NH and Sheiner LB (1982) Kinetics of pharmacologic response. *Pharmacol Ther* **16**:143-166.

Kalvass JC, Olson ER and Pollack GM (2006) Pharmacokinetics and Pharmacodynamics of Alfentanil in P-glycoprotein-Competent and P-glycoprotein-Deficient Mice: P-glycoprotein Efflux Alters Alfentanil Brain Disposition and Antinociception. *Drug Metab Dispos*.

Kalvass JC, Olson ER and Pollack GM (submitted) Pharmacokinetics and Pharmacodynamics of Seven Opioids in P-gp-Competent Mice: Assessment of Unbound Brain EC50s and Correlation of In Vitro, Preclinical, and Clinical Data *J Pharmacol Exp Ther*.

Kharasch ED, Hoffer C, Whittington D and Sheffels P (2003) Role of P-glycoprotein in the intestinal absorption and clinical effects of morphine. *Clin Pharmacol Ther* **74**:543-554.

Krzyzanski W and Jusko WJ (1997a) Application of moment analysis to the sigmoid effect model for drug administered intravenously. *Pharm Res* **14**:949-952.

Krzyzanski W and Jusko WJ (1997b) Mathematical formalism for the properties of four basic models of indirect pharmacodynamic responses. *J Pharmacokinet Biopharm* **25**:107-123.

Levy G, Ebling WF and Forrest A (1994) Concentration- or effect-controlled clinical trials with sparse data. *Clin Pharmacol Ther* **56**:1-8.

Sheiner LB, Stanski DR, Vozeh S, Miller RD and Ham J (1979) Simultaneous modeling of pharmacokinetics and pharmacodynamics: application to d-tubocurarine. *Clin Pharmacol Ther* **25**:358-371.

Tuk B, Danhof M and Mandema JW (1997) The impact of arteriovenous concentration differences on pharmacodynamic parameter estimates. *J Pharmacokinet Biopharm* **25**:39-62.

Upton RN and Doolette DJ (2002) A quantitative alternative to the hysteresis plot for measurement of drug transit time. *J Pharmacol Toxicol Methods* **47**:45-51.

Verotta D, Beal SL and Sheiner LB (1989) Semiparametric approach to pharmacokinetic-pharmacodynamic data. *Am J Physiol* **256**:R1005-1010.

CHAPTER 9

RELATIONSHIP BETWEEN AREA BOUNDED BY THE ANTINOCICEPTION-SERUM CONCENTRATION HYSTERESIS AND PHARMACOKINETIC-PHARMACODYNAMIC PARAMETER ESTIMATES FOR A SERIES OF OPIOIDS

This chapter will be submitted for publication in *Pharmaceutical Research* and is presented in the style of that journal.

ABSTRACT

Purpose: The objective of this study was to evaluate the relationship between pharmacokinetic-pharmacodynamic (PK-PD) parameters and the area bounded by the hysteresis loop (ABH) characterizing the antinociception versus serum concentration function for a series of opioid agonists. The potential modulation of this relationship by P-glycoprotein (P-gp) expression in the blood-brain barrier (BBB) also was evaluated.

Methods: Five mu-opioid receptor agonists (alfentanil, fentanyl, loperamide, methadone and morphine) were administered at equipotent doses to P-gp-competent and P-gp-deficient mice. The time course of serum concentrations and antinociception, assessed using the hotplate latency assay, was determined. An effect-compartment (sigmoidal E_{max}) PK-PD model was fit to the time course of serum concentrations and antinociception, and relevant parameter estimates were obtained. Matlab was used to calculate the observed and predicted ABH.

Results: A pronounced hysteresis was observed in the relationship between antinociception and serum concentrations, with the exception of alfentanil in P-gp-deficient mice. Good agreement was observed between ABH measurements for observed versus model-predicted data (r^2>0.95). The ABH correlated with area under the concentration curve

(AUC), the rate constant governing opioid distribution between serum and the hypothetical effect compartment (k_{e0}), and serum EC_{50}. Correcting for unbound concentrations improved the latter relationship. The normalized difference between the time at which opioid maximum serum concentrations occurred and the time to peak observed effect served as an alternative predictive metric of the value of k_{e0}.

Conclusions: The present results indicate that ABH is a novel, nonparametric metric for expressing distributional delays that result in a hysteresis loop in the relationship between opioid antinociceptive effect and serum concentrations.

INTRODUCTION

Describing the link between pharmacologic effect and drug concentrations is particularly challenging for drugs with central nervous system (CNS) activity. CNS concentrations, and consequently pharmacologic effect, are dictated by systemic concentrations of drug, and can be modulated by a variety of factors, including protein binding, blood-brain barrier (BBB) permeability, active transport, local metabolism, and cerebrospinal fluid (CSF) turnover. The BBB is an anatomical, biochemical, and functional barrier situated between the CNS and systemic circulation that serves to supply the brain with essential nutrients, regulate entry of endogenous and exogenous substances, and to efflux potential neurotoxins.

The predominant transmembrane efflux transporter expressed at the BBB is P-glycoprotein (P-gp; *ABCB1*), a member of the ABC superfamily (Golden and Pollack, 2003). Two strains of mice deficient in P-gp are commonly used to characterize the impact of P-gp efflux: the CF-1 strain, which possess a naturally occurring mutation in the *mdr1a(*-/-) gene and the FVB strain, which serves as the platform for creating knockout mice deficient in both

mdr1 isoforms expressed in brain, *mdr1a* and *mdr1b* (Schinkel et al., 1996; Lankas et al., 1997; Schinkel, 1997; Umbenhauer et al., 1997). The collection of whole tissues from intact animals in P-gp-competent and P-gp-deficient mice is a frequently-used method of determining net distribution across the BBB (Chen and Pollack, 1998). The use of knockout mice or naturally-occurring mutants has been instrumental in assessing the role of P-gp in attenuating brain uptake and antinociception of loperamide, methadone, DPDPE ([D-penicillamine(2,5)] enkephalin) (Chen and Pollack, 1998; Thompson et al., 2000; Dagenais et al., 2004). The diversity in chemical structure, BBB penetration, physicochemical properties, potency and duration of effect, make opioids an ideal group of compounds for probing a multiplicity of phenomena that determine CNS pharmacokinetics and pharmacodynamics. Moreover, the opioids are an ideal class of drugs to use for characterizing the counterclockwise hysteresis loop that results from the distributional-mediated dissociation between pharmacologic response and serum concentrations.

Recovering pharmacodynamic parameter estimates from the relationship between antinociception and opioid serum concentrations is not feasible in the presence of hysteresis behavior because two distinct concentrations correspond with the same effect. This effect-concentration disconnect is commonly addressed with the application of an effect compartment PK-PD model, which uses the temporal relationships between effect and blood concentrations to predict the time course of drug concentrations in a hypothetical effect compartment (Holford and Sheiner, 1982). Estimates of fundamental pharmacodynamic parameters (EC_{50} and γ) then can be recovered from the effect versus effect compartment concentration relationship. This analytical process is referred to as “collapsing the hysteresis loop”.

Alternative approaches to addressing hysteresis behavior have been examined in an effort to improve characterization of complex PK-PD systems. The influence of sampling locales on the dissociation between arterial and venous concentrations and effect has been addressed by a number of groups (Verotta et al., 1989; Tuk et al., 1997; Hermann et al., 1999). Quantitative approaches have been developed to characterize lidocaine tissue transit time through and antibiotic tissue distribution (Ganzinger and Neumann, 1992; Upton and Doolette, 2002). In addition, Cheng and Jusko identified an adaptation of disposition decomposition analysis that characterizes the biophase drug concentration-time function. Despite an understanding of the processes that contribute to hysteresis behavior and the mathematical and experimental techniques that have been developed to minimize the presence of hysteresis loops, there is a relative lack of information relating the area bounded by a hysteresis loop (ABH) to a meaningful system descriptor.

A method of calculating ABH was developed in Matlab with which, in a manner analogous to calculating AUC, the area under the ascending curve was subtracted from the area under the descending curve (Chapter 8). This aforementioned approach was utilized to assess the relationship between PK-PD parameter values of simulated effect-serum concentration and the corresponding ABH. The present study utilized a PK-PD modeling approach to describe the time-course of serum concentrations and opioid antinociception using a hotplate latency assay. Moreover, CNS penetration and pharmacologic effect was further modulated by characterizing the time course of response and concentrations in P-gp-competent and P-gp-deficient mice. The ABH of the antinociception-serum concentration hysteresis was calculated and related to estimates of PK-PD parameters.

METHODS

Materials

Fentanyl, loperamide, methadone, morphine, and oxycodone were purchased from Sigma-Aldrich (St. Louis, MO). Alfentanil was obtained from Taylor Pharmaceuticals (Decatur, IL). All other reagents were obtained from common sources, and they were of reagent grade or better.

Animals

Male CF-1 [*mdr1a*(+/+) and *mdr1a*(-/-)] and FVB [*mdr1a/b(*+/+) and *mdr1a/b(*-/-)] mice (30-40 g; Charles River Laboratories, Inc. Wilmington, MA; and Taconic, Germantown, NY, respectively) were maintained on a 12-h light/dark cycle in a temperature- and humidity-controlled room with free access to food and water. All procedures involving mice were approved by The Institutional Animal Care and Use Committee of the University of North Carolina and were conducted in accordance with "Principles of Laboratory Animal Care" (NIH Publication No. 85-23, revised in 1985).

Pharmacokinetic-Pharmacodynamic Experiments

Based on the results of pilot studies, 36 *mdr1a*(+/+) and 36 *mdr1a*(-/-) CF-1 mice received a single equipotent subcutaneous dose of alfentanil (0.2- or 0.067-mg/kg), fentanyl (0.09-mg/kg), loperamide (50- or 1-mg/kg), methadone (2- or 0.6 mg/kg), or morphine (only *mdr1a*(+/+); 3.6-mg/kg). In a separate experiment, 36 *mdr1a/b(*+/+) and 36 *mdr1a/b(*-/-) FVB mice received an equipotent subcutaneous dose of loperamide (25- or 1-mg/kg). The loperamide and fentanyl doses were prepared in 50/50 propylene glycol/water, whereas the remaining opioids were prepared in 0.9% saline. Antinociception was assessed at selected time points, and four mice of each strain per opioid were sacrificed by decapitation for

collection of blood samples. Serum was harvested after blood was allowed to clot for ~30 min at room temperature and following centrifugation. Serum samples were stored at –20°C until analysis by HPLC-MS/MS.

Assessment of Antinociception

Antinociception was assessed with the hotplate latency test as described elsewhere (Kalvass et al., 2007). Before opioid administration, baseline hotplate latency was determined for each animal in triplicate. Hotplate latency was defined as the time interval between placement on the hot plate (55°C; Columbus Instruments, Columbus, OH) and first observation of a jump or lick of the hind limb. Animals with an average baseline latency < 25 s were used in the study. A cut-off latency of 60 s was used to avoid tissue damage. The degree of antinociception, expressed as percent maximum possible response (% MPR) was calculated as:

$$\%MPR = \frac{Test\ latency - Control\ latency}{60 - Control\ latency} x\ 100\% \qquad \text{(Eqn. 9.1)}$$

Bioanalysis Methodology

An aliquot (2-25 µl) of serum was transferred to a HPLC vial, and protein was precipitated with 4 to 125 volumes methanol containing internal standard (5 ng/ml loperamide for alfentanil, fentanyl, and methadone; 20 ng/ml methadone for loperamide; and 100 ng/ml oxycodone for morphine). The samples were vortex-mixed and centrifuged, and supernatant was analyzed by HPLC-MS/MS. Samples were injected (2–10 µl; autosampler, CTC Analytics, Zwingen, Switzerland) onto a Phenomenex Gemini 110A column (2.0 x 30 mm, 5 µm; Phenomenex, Torrance, CA) maintained at room temperature. The total run time

was 3 min. Analytes were eluted with a linear gradient consisting of "A," ammonium acetate (pH 6.8; 10 mM) and "B" methanol produced by two Shimadzu LC-10ADVP binary pumps (Kyoto, Japan). An initial condition of 5% "B" was ramped to 95% "B" over 2 min, held for 0.5 min, and then returned initial condition of 5% B in a single step to re-equilibrate the column. During the run, the flow rate was increased from 750 to 1500 µl/min over the first 2 min, held at 1500 µl/min for 1 min, and then returned the initial flow rate of 750 µl/min in a single step. For the morphine samples, the initial conditions were held for 0.5 min before ramping the gradient and flow rate. The entire column effluent was diverted from the source of the PE Sciex API-4000 quadrupole mass spectrometer (Turbo V Ionspray source, 700°C; PerkinElmerSciex Instruments, Boston, MA) for the first 1 min and last 0.5 min of the run. Alfentanil, fentanyl, loperamide, methadone, meperidine, morphine, oxycodone, and sufentanil were measured in positive ionization mode using multiple reaction monitoring (417.3→268.3, 337.1→188.3, 477.4→266.0, 248.3→220.3, 286.1→201.1, and 316.0→298.0, respectively). Standard curves were prepared in serum, plasma, or buffer, and were identical in composition to corresponding samples. Accuracy of standards and interassay variability was within ± 20%.

Pharmacokinetic-Pharmacodynamic Analysis

The pharmacokinetic model depicted schematically in Fig. 9.1 was fit to the serum-concentration-time data using nonlinear least-squares regression (WinNonlin 4.1; Pharsight Corporation, Mountain View, CA). The dose (X_0) was assumed to exhibit first-order absorption (k_{01}) into the systemic circulation, contained in a central compartment of apparent volume V_c, with first-order elimination (k_{10}) from the compartment. Opioid disposition in

the absorption site (X_A) and in the central, serum compartment (X_C) was characterized (Eqns. 2 and 3).

$$\frac{dX_A}{dt} = -k_{01} \cdot X_0 \qquad \text{(Eqn. 9.2)}$$

$$\frac{dX_C}{dt} \cdot V_C = k_{01} \cdot X_A - k_{01} \cdot X_C \qquad \text{(Eqn. 9.3)}$$

The dissociation between the time course of antinociception and serum concentrations was addressed by linking a hypothetical effect site with the central pharmacokinetic compartment, assuming a rate of equilibration governed by a first-order rate constant k_{e0} (Figure 9.1; Eqn. 9.4). The relationship between antinociceptive effect and drug concentration in the hypothetical effect compartment was assumed to be sigmoidal (Eqn. 5).

$$\frac{dC_e}{dt} = k_{e0} \cdot (C_c - C_e) \qquad \text{(Eqn. 9.4)}$$

$$E = \frac{E_{max} \cdot C_e^{\gamma}}{EC_{50}^{\gamma} + C_e^{\gamma}} \qquad \text{(Eqn. 9.5)}$$

The pharmacodynamic parameters k_{e0}, EC_{50}, and γ were estimated in a stepwise approach by fitting these equations to the observed antinociceptive response vs. time data, with E_{max} fixed at 100 % or recovered as a parameter with no theoretical limit.

Calculation of Area Bound by the Hysteresis

The size of the model-derived antinociception-serum concentration hysteresis loop was determined for each opioid using a Matlab (Release 12, The MathWorks, Natick, MA) as described in Chapter 8. Briefly, the program written in Matlab was read the data file format and calculate the ABH for the dissociation between effect and concentration. Similar to methods of calculating AUC, the program calculated the area under the ascending effect-concentration profile and subtracted this value from the area under the descending effect-concentration profile to generate the ABH in units of %*mg/ml. The program is capable of distinguishing clockwise and counterclockwise hysteresis loops such that a positive value is representative of a proteresis and a negative value for a counterclockwise hysteresis. The antinociception versus effect compartment concentration relationship served as a negative control for the absence of hysteresis (i.e., statistically insignificant ABH). The ABH was calculated for the observed and predicted hysteresis between antinociception and serum concentrations.

Recovery of Fentanyl and Sufentanil Concentration-Effect Data from Literature

An earlier investigation on the PK-PD relationship between fentanyl and sufentanil serum concentrations and the electroencephalogram (EEG) effect in rats was identified and estimates of the relationship between concentration and effect were obtained graphically (Cox et al., 1998). The fentanyl and sufentanil ABH was calculated as previously described with Matlab (Release 12, The MathWorks, Natick, MA) and the correlation between ABH and estimates of PK-PD parameters was investigated.

RESULTS

Results of preliminary dose-response experiments were used to select opioid doses that elicited 80-90% MPR on the hotplate latency assay. Administered doses scaled four orders of magnitude, from 0.0067 for alfentanil [*mdr1a*(-/-)] to 50 mg/kg for loperamide [*mdr1a*(+/+)]. While the role of P-gp-mediated efflux in attenuating opioid CNS penetration was not explicitly characterized in this study, *mdr1a*(-/-) mice required 3-, 3.3- and 50-fold lower doses of alfentanil, methadone, and loperamide in order to elicit comparable antinociception. Preliminary experiments revealed dose-limiting toxicities associated with administration of 50 mg/kg loperamide to *mdr1a/b*(+/+) FVB mice that led to the substitution of a 25-mg/kg dose.

The time course of opioid systemic concentrations was described adequately by a one-compartment pharmacokinetic model (Figures 9.1 and 9.2). Estimates of k_{01}, k_{10}, and V_c are presented in Table 9.1. The time course of antinociception and serum concentrations was linked by k_{e0}, the first-order rate constant of distribution between serum and the hypothetical effect compartment (Figure 9.1). A sigmoidal E_{max} model was fit to the relationship between antinociception and hypothetical effect compartment concentrations (Figure 9.2). A fixed value of E_{max} at 100% adequately described the time course of opioid antinociception with two exceptions. By arbitrarily fixing E_{max} at 100%, fentanyl [*mdr1a*(-/-)] peak effect for morphine [*mdr1a(*+/+)] was underpredicted. Inclusion of E_{max} as a variable model parameter improved the description of the data (Figure 9.2). The rate of drug distribution between the serum and hypothetical effect compartments varied extensively, evidenced by k_{e0} values of 0.004 to 36 min^{-1} for loperamide and alfentanil in *mdr1a*(-/-) mice, respectively. A high degree of uncertainty was associated with alfentanil [*mdr1a*(-/-)] and loperamide

[*mdr1a*(+/+), *mdr1a* (-/-), and *mdr1a/b*(+/+)] pharmacodynamic estimates, particularly the value of $k_{e0,}$ as evidenced by CV% > 100 (Table 9.1).

The relationship between antinociception and hypothetical effect compartment oncentrations was sigmoidal (Figure 9.3). With the exception of alfentanil in *mdr1a*(-/-) mice, the relationship between opioid antinociception and serum concentrations evidenced a hysteresis loop progressing temporally in a counterclockwise direction (Figure 9.3). The rapid distribution between serum and effect compartment concentrations, as described by a k_{e0} of 36 min^{-1}, explains the absence of hysteresis behavior for alfentanil in *mdr1a*(-/-) mice. Moreover, the area calculations for alfentanil [*mdr1a*(+/+) and (-/-)] and fentanyl [*mdr1a*(-/-)] indicated low values of ABH and a high degree of variability around the observed effect-concentration hysteresis, a consequence of overlap in the ascending and descending curves for the observed points compared to the predicted fit. The remaining calculations of ABH for observed effect-concentration data were within 2-fold of the values calculated for the predicted fit to the antinociception-serum concentration data (Figure 9.4).

The degree of systemic exposure is commonly expressed as area under the concentration-time curve (AUC); the magnitude of pharmacologic response is, in part, dictated by the value of k_{e0} when a hypothetical effect compartment is utilized. As it is a product of effect (% MPR) and concentrations (ng/ml), the area bounded by the antinociception-serum concentration hysteresis would be expected to correspond with PK-PD parameters. The ABH is correlated with AUC and k_{e0}, the latter relationship dictated in part by P-gp expression (Figures 9.5 and 9.6). An alternative metric of effect and concentration that potentially correlates with ABH is EC_{50} (Figure 9.7A). Figure 9.7B presents the modest improvement in the correlation when EC_{50} is corrected for protein binding. Moreover, the

data points associated with the hysteresis between fentanyl and sufentanil EEG effect and serum concentrations were obtained graphically and used to calculate the ABH. The literature-derived estimate of ABH correlated well with estimates of EC_{50} and $EC_{50,u}$ (Figure 9.7). In a final step, the reciprocal value of k_{e0} was observed to correlate with the normalized difference between time to maximum concentrations and time to maximum effect.

DISCUSSION

The opioids characterized in this study are diverse with respect to structural classes, physicochemical properties, BBB penetration, P-gp-mediated efflux, and receptor potency. The influence of these properties on systemic disposition is reflected in pharmacokinetic parameter estimates. For example, the $f_{u,plasma}$ ranged from 0.03 to 0.5 for loperamide and morphine, respectively, and a ~30-fold difference in estimates of k_{10} was observed (Table 9.1). A one compartmental model adequately described the time-course of serum concentrations (Figure 9.2).

A hypothetical effect compartment containing the receptor biophase was used to link serum concentrations and antinociception. The inclusion of a hypothetical effect compartment was effective in describing the time-course of antinociception (Figure 9.2). Distribution between serum and the hypothetical effect compartment was slowest for loperamide in *mdr1a*(-/-) and *mdr1a/b*(-/-) mice, 0.0097 and 0.004 min^{-1}, respectively, and fastest for alfentanil in *mdr1a*(-/-) mice, 36 min^{-1} (Table 9.1). The sigmoidal relationship between alfentanil [*mdr1a*(-/-)] antinociception and serum concentrations (Figure 9.3B) yielded a negligible ABH value (28 %*mg/ml). The absence of a hysteresis between alfentanil [*mdr1a*(-/-)] antinociception and serum concentrations suggests that a value of k_{eo} equal to or greater than 36 min^{-1} reflects a collapse in the separation of serum and

hypothetical effect compartment concentrations. The remaining opioids exhibited a hysteresis between antinociception and serum concentrations (Figure 9.3).

The ABH was best predicted for observed versus predicted data for large hysteresis loops (Figure 9.4). With the exception of alfentanil [*mdr1a*(+/+) and *mdr1a*(-/-)] and fentanyl [*mdr1a*(+/+)], the use of 9 data points recovered ABH values within a 2-fold range of the predicted ABH calculation. A bootstrap technique could be utilized in future investigations to characterize the reliability of ABH calculated for sparsely sampled data and to identify portions of the hysteresis that contribute to reliable estimates of ABH, although such an approach was beyond the scope of the current investigation. The utility of ABH as a nonparametric parameter that characterizes the dissociation between concentration and pharmacologic effect will be strengthened if these studies identify sparse sampling schemes that reliably estimate the value of ABH.

Preliminary experiments were performed to identify doses that elicit 80-90% MPR in the hotplate latency assay. While systemic exposure is largely dictated by the absorption, distribution, metabolism and excretion (ADME) properties of a drug, pharmacologic effect is a function of both pharmacokinetic and pharmacodynamic processes. It is therefore logical that the size of the hysteresis is related to metrics of systemic exposure and biophase distribution (Figures 9.5 and 9.6). However, the relationship between ABH and the reciprocal of k_{e0} differs based on P-gp expression (Figure 9.6). It is possible that decreasing the dose of alfentanil, methadone or loperamide administered to mice deficient in P-gp diminished the dynamic range of serum concentrations since greater CNS distribution enabled lower doses. P-gp-competent mice receiving fentanyl were an outlier, a potential consequence of P-gp efflux that was addressed with a higher dose concentration compared to

the P-gp-deficient mice. This observation is consistent with previous observations of fentanyl as substrate, albeit to a physiologically negligible extent, of P-gp at the BBB (Dagenais et al., 2004).

A number of metrics, including ED_{50} and EC_{50}, the effective dose and effective concentration that elicits a 50% response, are commonly utilized to characterize pharmacodynamics. While ED_{50} is a straightforward, robust and easily-obtainable metric of potency, EC_{50} is preferred when a compound set exhibits pharmacokinetic diversity. As a measurement of potency, the serum EC_{50} directly relates concentration to effect; as such, it is not surprising that this parameter is correlated with ABH (Figure 9.7A). Correcting the serum EC_{50} for protein binding provides a more direct expression of the biologically-relevant concentration of drug, i.e., the substrate pool that can penetrate membranes (e.g., the BBB) or bind to receptors (e.g., the opioid receptor). The serum EC_{50} corrected for protein binding improved the correlation with ABH (Figure 9.7B). Similarly, Kalvass et al. (2007) identified brain $EC_{50,u}$ as the best correlate to clinical equipotent opioid dose, followed by brain EC_{50}, serum $EC_{50,u}$ and lastly, serum EC_{50}. Considering the results presented by Kalvass et al. (2007), the correlations with ABH may be improved further by comparing this metric to brain EC_{50} and $EC_{50,u}$, surrogates of biophase concentrations.

Results obtained by Cox et al. (1998) were used to characterize the effect-serum concentration hysteresis of fentanyl and sufentanil. Similar to observations in the present study, alfentanil did not exhibit a substantial dissociation between EEG effect expressed as a function of amplitude and serum concentrations. The value of ABH for the extracted data was calculated and, using the published PK-PD parameter estimates, was found to correlate with the previously-established relationship between ABH and EC_{50} or $EC_{50,u}$ (Figure 9.7).

The posterior validation of the relationship between ABH and EC_{50} strengthens the conclusions of the present study, in part due to the different route of opioid administration via an IV-infusion and the characterization of effect using electroencephalography rather than the hotplate assay. Further work relating ABH to EC_{50} that includes drugs from therapeutic classes other than opioids should be performed to test the generalizability of the approach described herein.

While the relationship between the normalized difference in time to C_{max} and E_{max} versus the reciprocal value of k_{e0} was not linear, it could be a useful and straightforward method of approximating the value of k_{e0} (Figure 9.8). As evidenced in Table 9.1, k_{e0} is a poor estimator of the distributional relationship between serum and the hypothetical effect compartment. Estimates of k_{e0} are often sensitive to minor changes in observed values or model parameters. While eliminating the need to use k_{e0} is the optimal solution, characterizing biophase concentrations often requires the use of intensive and costly experimental approaches. Thus, the ability to narrow the range of initial estimates of k_{e0} using the time of maximum observed concentration and effect would be ideal.

In summary, the present study presents the relevant PK-PD parameter estimates obtained from the time course of opioid antinociception and serum concentrations in P-gp-competent and P-gp-deficient mice. The area bounded by the hysteresis loop resulting from distributional dissociation between antinociception and serum concentrations was calculated and correlated with area under the curve or the rate constant of distribution between serum and the hypothetical effect compartment was observed. A strong correlation was observed between ABH and EC50 and a modest improvement resulted when EC_{50} was corrected for

protein binding. Finally, the relationship between the time difference in C_{max} and E_{max} may be used as an initial representation of the value of k_{e0}.

Table 9.1. Parameter estimates from PK-PD modeling.

Parameter	alfentanil		fentanyl		loperamide		loperamide	
	mdr1a(+/+)	*mdr1a*(-/-)	*mdr1a*(+/+)	*mdr1a*(-/-)	*mdr1a*(+/+)	*mdr1a*(-/-)	*mdr1a/b*(+/+)	*mdr1a/b*(-/-)
k_{01} (min^{-1})	0.36 (21)	0.48 (20)	0.021 (65)	0.020 (31)	0.067 (38)	0.12 (79)	0.11 (42)	0.011 (5.7)
k_{10} (min^{-1})	85 (9.0)	82 (11)	1000 (36)	1000 (12)	52 (26)	40 (27)	29 (21)	120 (3.6)
V (ml/kg)	930 (14)	1300 (11)	7500 (90)	15000 (38)	33000 (12)	4500 (22)	12000 (11)	880 (9.1)
k_{e0} (min^{-1})	1.8 (56)	36 (420)	0.087 (30)	0.57 (35)	0.028 (330)	0.004 (150)	0.0156 (710)	0.0097 (12)
EC_{50} (ng/ml)	41 (20)	23 (5.9)	0.84 (22)	5.3 (62)	870 (100)	1 (440)	690 (370)	13 (8.7)
γ [a]	1.1 (19)	2.6 (16)	0.60 (12)	1[b]	2.2 (230)	0.43 (140)	0.88 (470)	2.3
E_{max} (%) [a]	-	-	-	150[b]	-	-	-	-

Cont. Parameter	methadone		morphine
	mdr1a(+/+)	*mdr1a*(-/-)	*mdr1a*(+/+)
k_{01} (min^{-1})	0.52 (23)	0.38 (37)	0.25 (24)
k_{10} (min^{-1})	48 (10)	160 (20)	96 (13)
V (ml/kg)	2400 (6.7)	11000 (12)	2800 (12)
k_{e0} (min^{-1})	0.27 (48)	0.035 (63)	0.014 (62)
EC_{50} (ng/ml)	190 (15)	30 (41)	96 (58)
γ [a]	2.2 (40)	0.67 (41)	1[b]
E_{max} (%) [a]	-	-	150[b]

[a] Unless otherwise noted, E_{max} was fixed at 100% MPR.

[b] A stepwise approach was used to fit γ and $E_{max,}$. The value of E_{max} was fixed as the estimate and γ was set as 1.0 prior to fitting k_{e0} and EC_{50}.

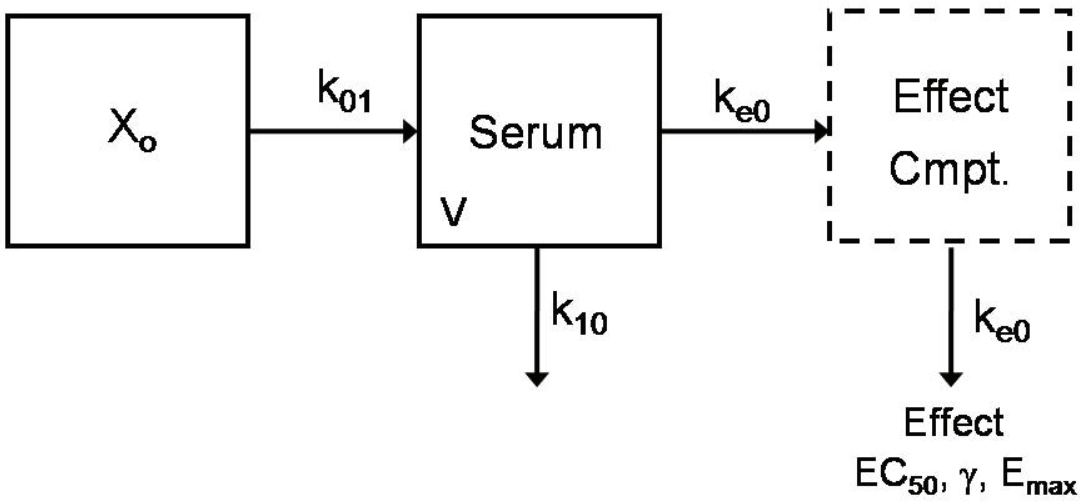

Figure 9.1. Scheme of the pharmacokinetic-pharmacodynamic model for opioid disposition and antinociception in mice. A stepwise approach was used to recover pharmacokinetic parameter estimates by fitting a one-compartment model to the time course of group averaged serum concentrations. Estimates were obtained for the absorption rate constant (k_{01}), central volume (V) and first-order elimination rate constant (k_{10}). An effect-compartment, sigmoidal Emax model was used to describe the time course of antinociception. PK parameter estimates were fixed and the values of k_{e0}, EC_{50}, and γ were recovered. The value of E_{max} was fixed at 100% MPR or, in the case of fentanyl *mdr1a*(-/-) and morphine, fit as a model parameter.

A

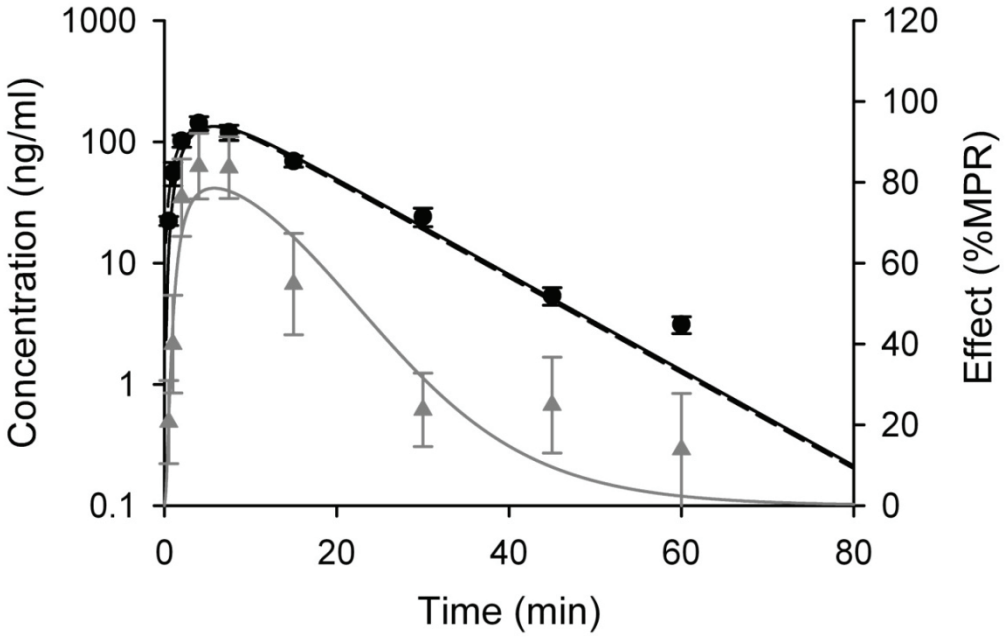
1000
100
10
1
0.1
Concentration (ng/ml)
120
100
80
60
40
20
0
Effect (%MPR)
0
20
40
60
80
Time (min)

B

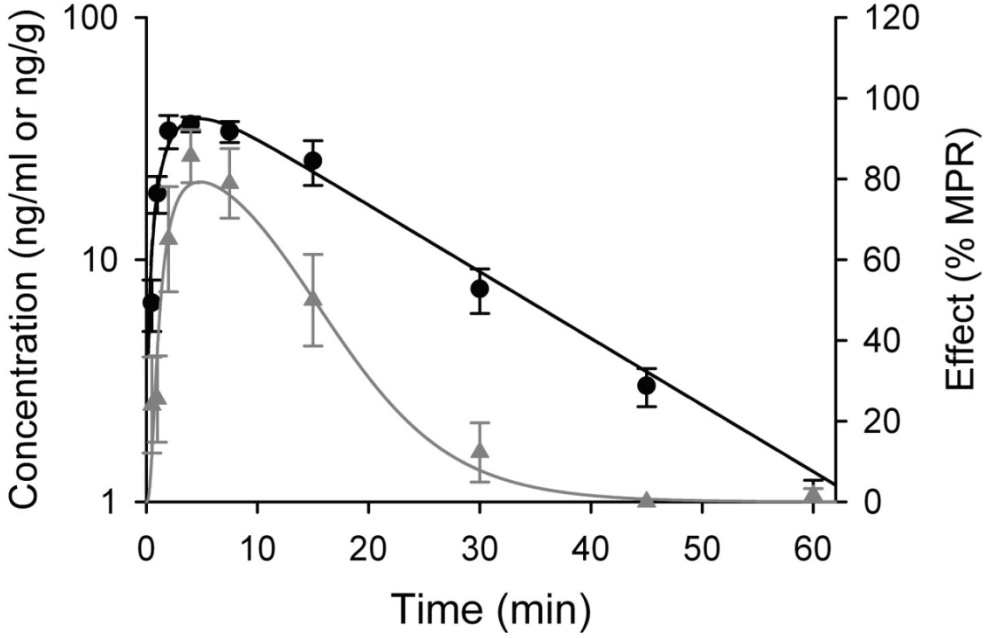
100
10
1
Concentration (ng/ml or ng/g)
120
100
80
60
40
20
0
Effect (% MPR)
0
10
20
30
40
50
60
Time (min)

C

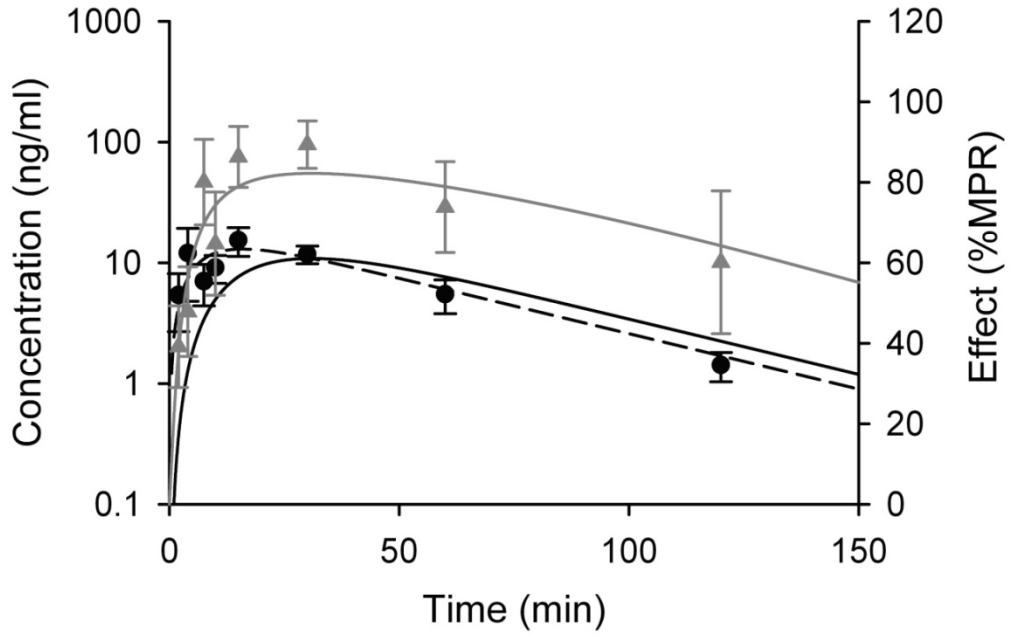
Concentration (ng/ml)
1000
100
10
1
0.1
0
50
100
150
Time (min)
120
100
80
60
40
20
0
Effect (%MPR)

D

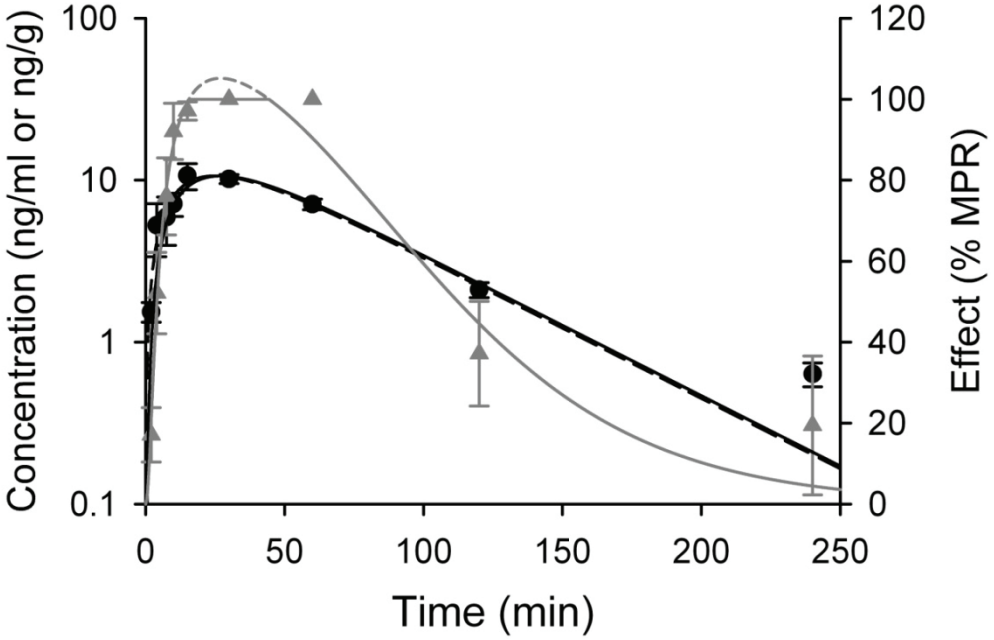
Concentration (ng/ml or ng/g)
100
10
1
0.1
0
50
100
150
200
250
Time (min)
120
100
80
60
40
20
0
Effect (% MPR)

E

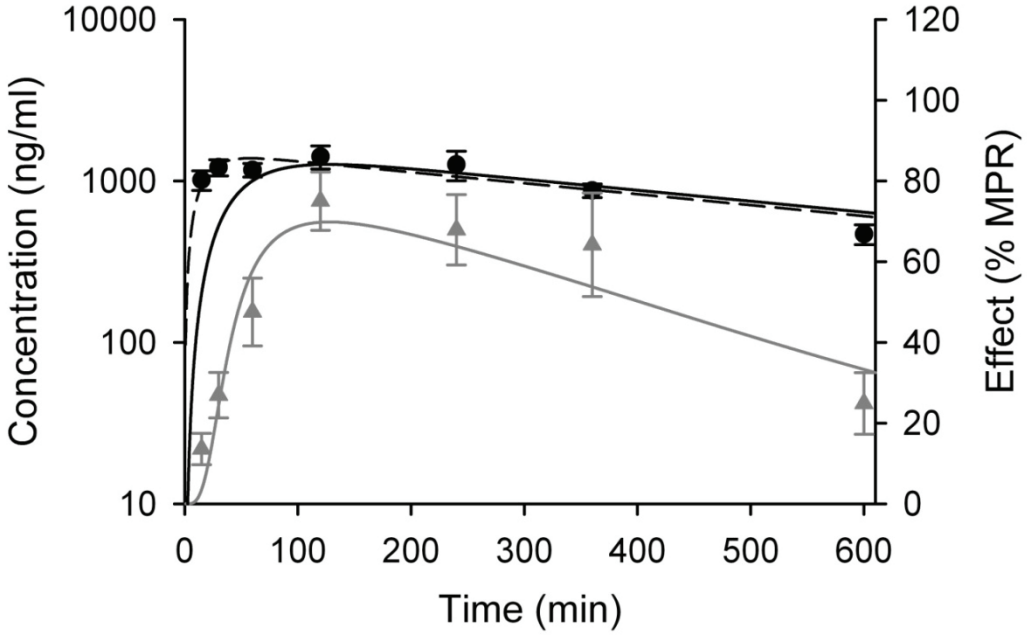
10000
1000
100
10
Concentration (ng/ml)
120
100
80
60
40
20
0
Effect (% MPR)
0
100
200
300
400
500
600
Time (min)

F

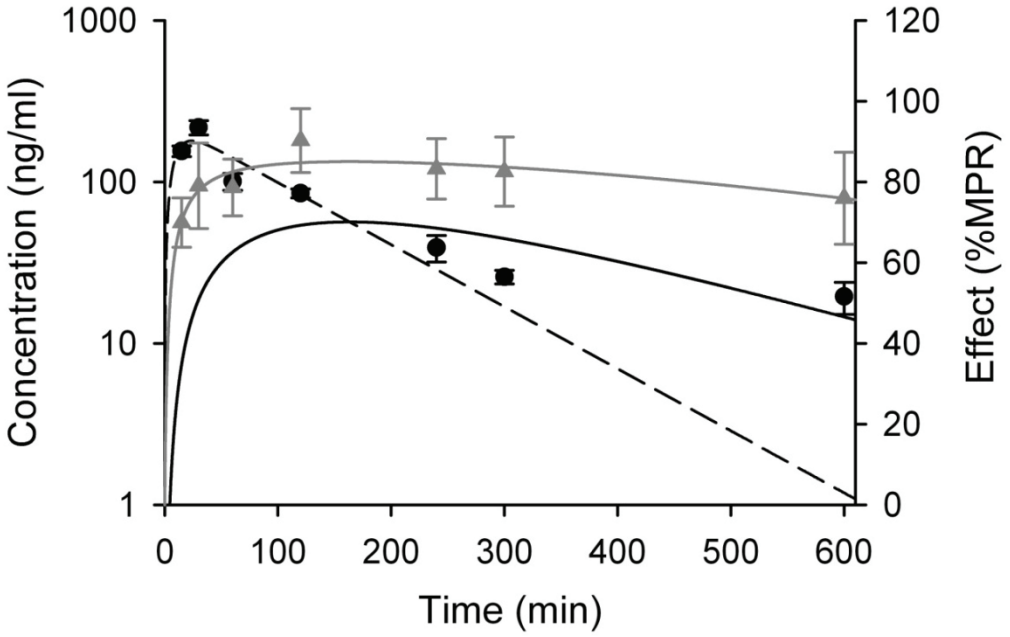
1000
100
10
1
Concentration (ng/ml)
120
100
80
60
40
20
0
Effect (%MPR)
0
100
200
300
400
500
600
Time (min)

G

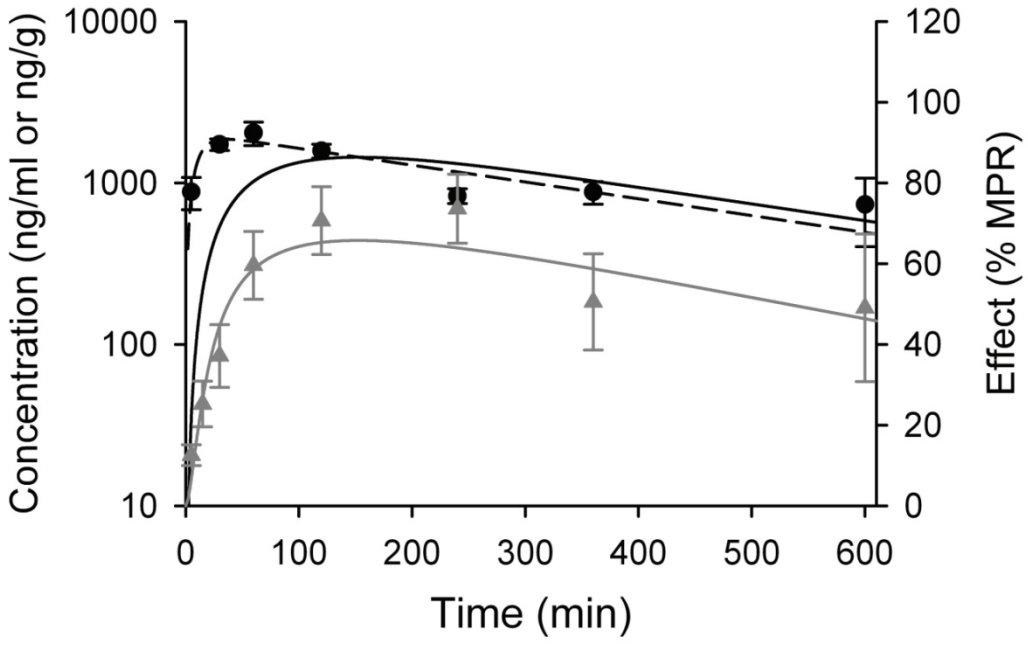
Concentration (ng/ml or ng/g)
10000
1000
100
10
Effect (% MPR)
120
100
80
60
40
20
0
0
100
200
300
400
500
600
Time (min)

H

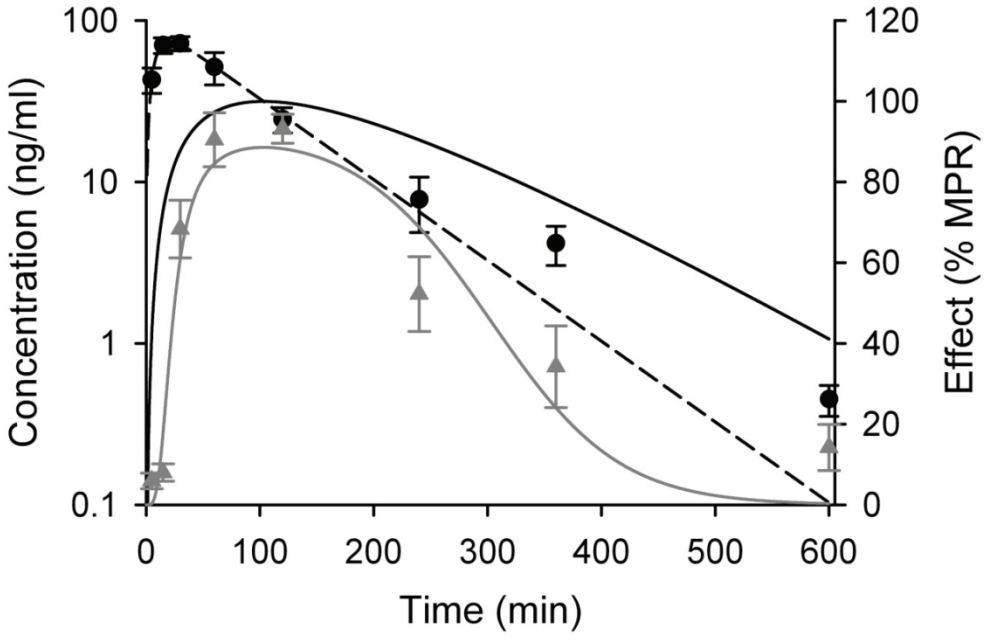
Concentration (ng/ml)
100
10
1
0.1
Effect (% MPR)
120
100
80
60
40
20
0
0
100
200
300
400
500
600
Time (min)

I

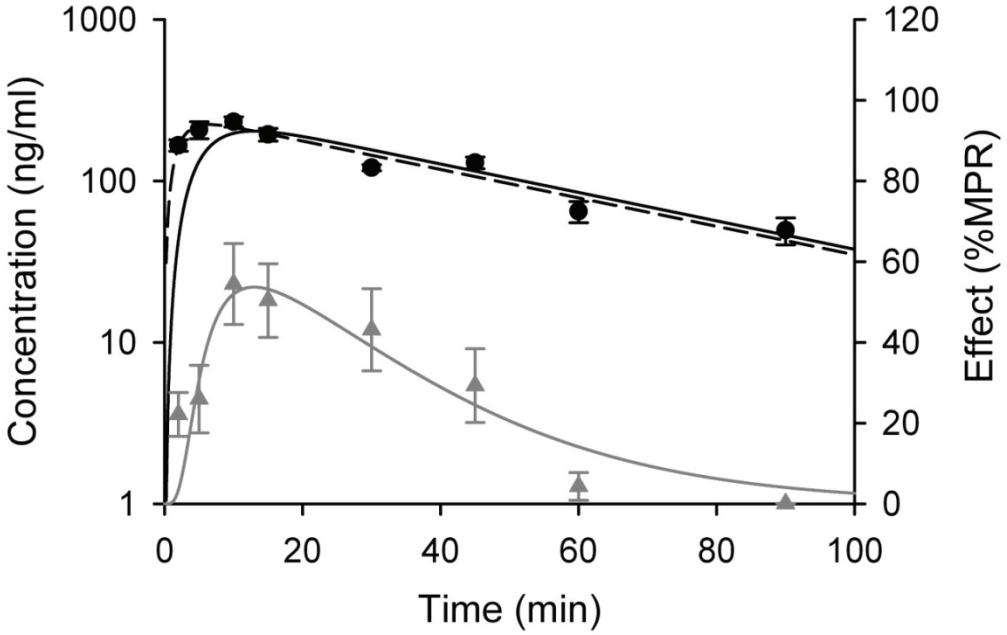
Concentration (ng/ml)
1000
100
10
1
0
20
40
60
80
100
Time (min)
120
100
80
60
40
20
0
Effect (%MPR)

J

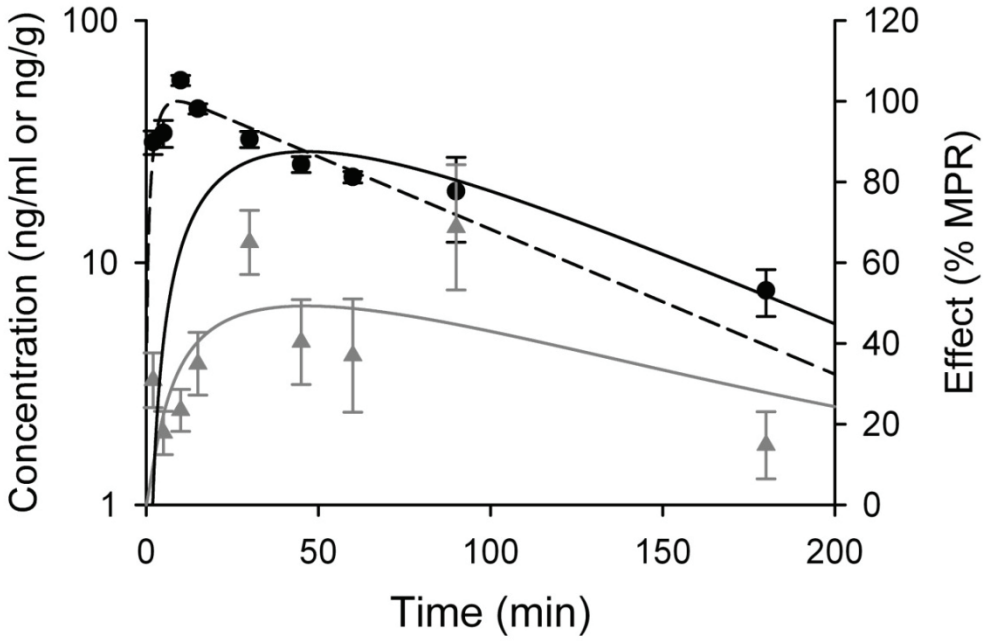
Concentration (ng/ml or ng/g)
100
10
1
0
50
100
150
200
Time (min)
120
100
80
60
40
20
0
Effect (% MPR)

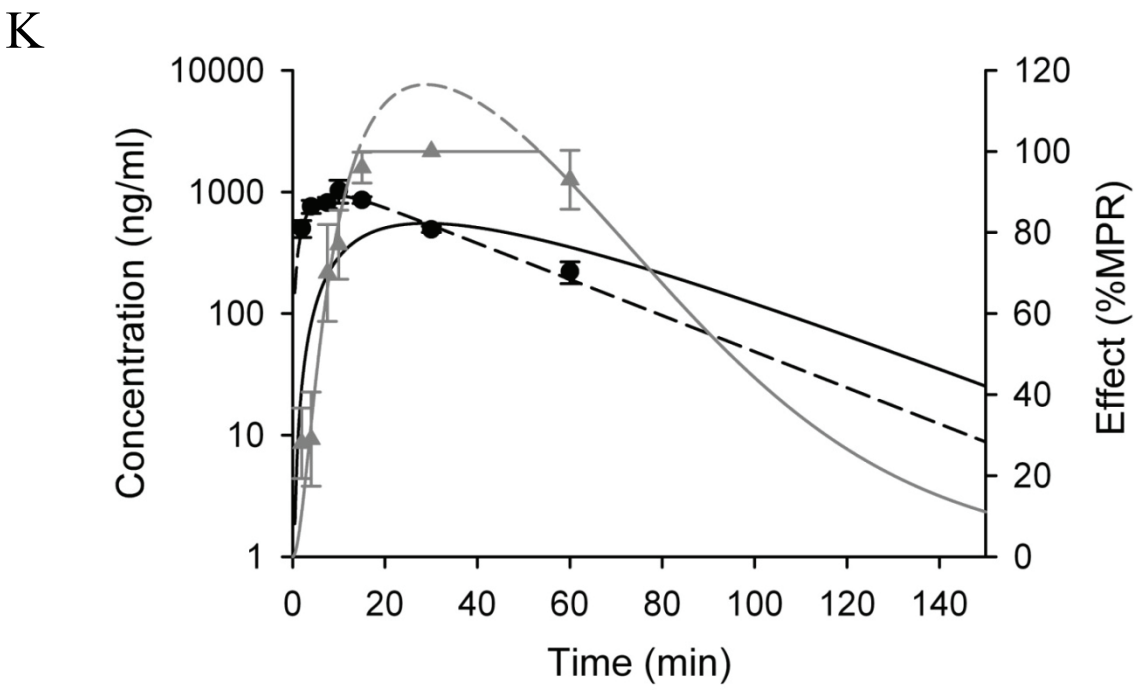

Figure 9.2. Time course of antinociception (▲), serum (●), and effect compartment concentrations following subcutaneous administration of (A) 0.2-mg/kg alfentanil to *mdr1a*(+/+) mice; (B) 0.067-mg/kg alfentanil to *mdr1a*(-/-) mice; (C) 0.9-mg/kg fentanyl to *mdr1a*(+/+) mice; (D) 0.9-mg/kg fentanyl to *mdr1a*(-/-) mice; (E) 50-mg/kg loperamide to *mdr1a*(+/+) mice; (F) 1-mg/kg loperamide to *mdr1a*(-/-) mice; (G) 25-mg/kg loperamide to *mdr1a/b*(+/+) mice; (H) 1-mg/kg loperamide *mdr1a/b*(+/+) mice; (I) 2-mg/kg methadone to *mdr1a*(+/+) mice; (J) 0.6-mg/kg methadone to *mdr1a*(-/-) mice; or (K) 3.6-mg/kg morphine to *mdr1a*(+/+) mice. Data are presented as mean ± S.E. ($n \geq 3$, serum concentrations; $n = 4$ to 36, antinociception). Lines represent the fit of the model to the time course of antinociception (solid gray), serum (dashed black), and effect (solid black) compartment concentration data.

A

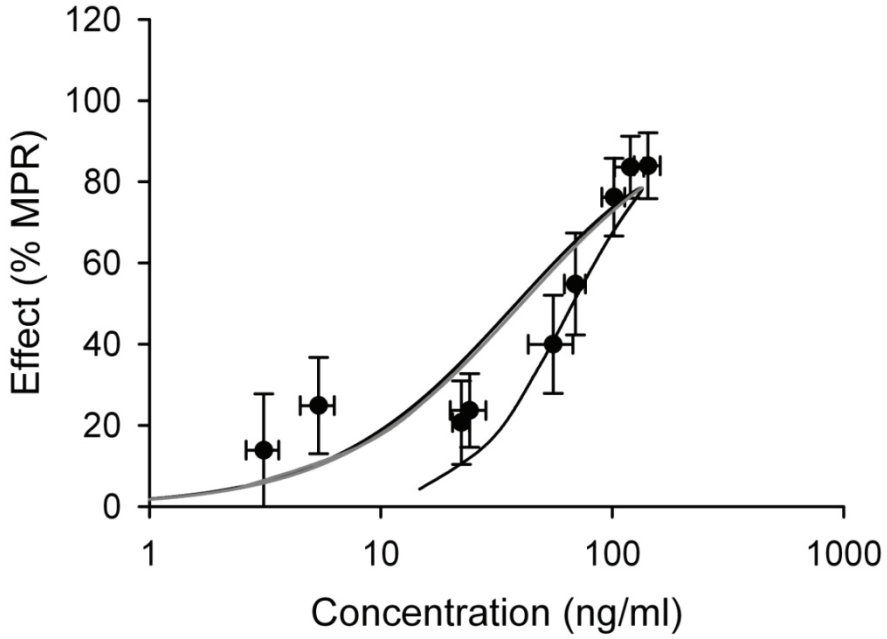
120
100
80
60
40
20
0
Effect (% MPR)
1
10
100
1000
Concentration (ng/ml)

B

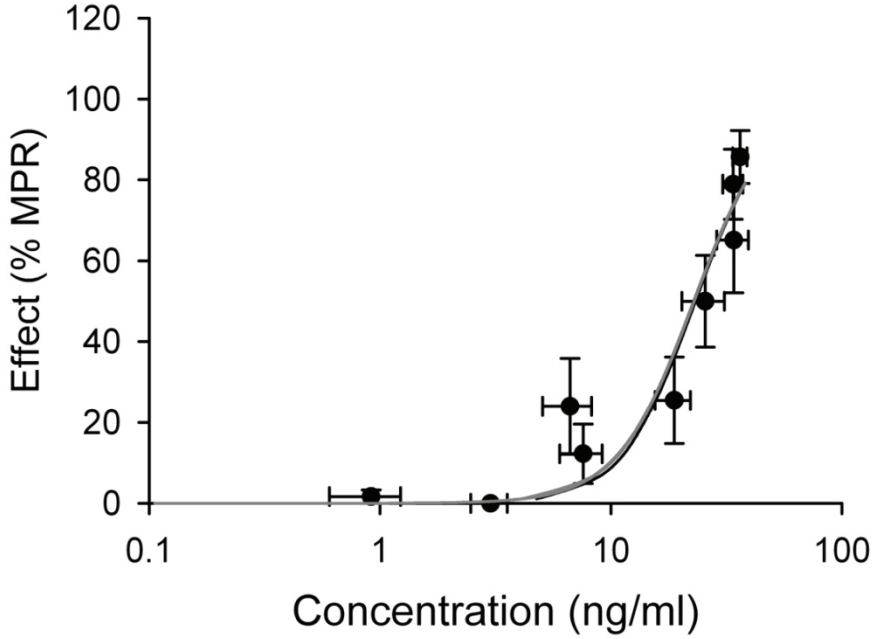
120
100
80
60
40
20
0
Effect (% MPR)
0.1
1
10
100
Concentration (ng/ml)

C

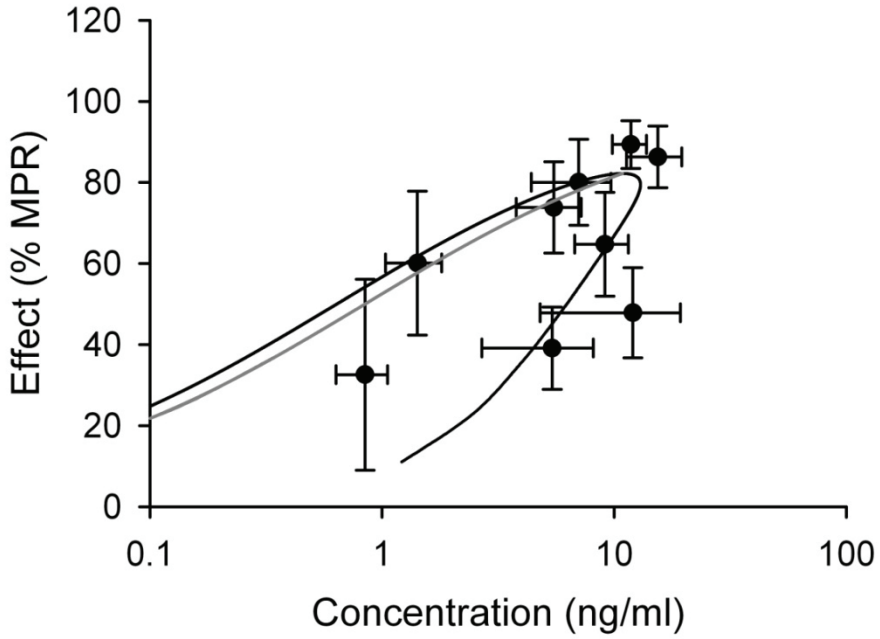
120
100
80
60
40
20
0
Effect (% MPR)
0.1
1
10
100
Concentration (ng/ml)

D

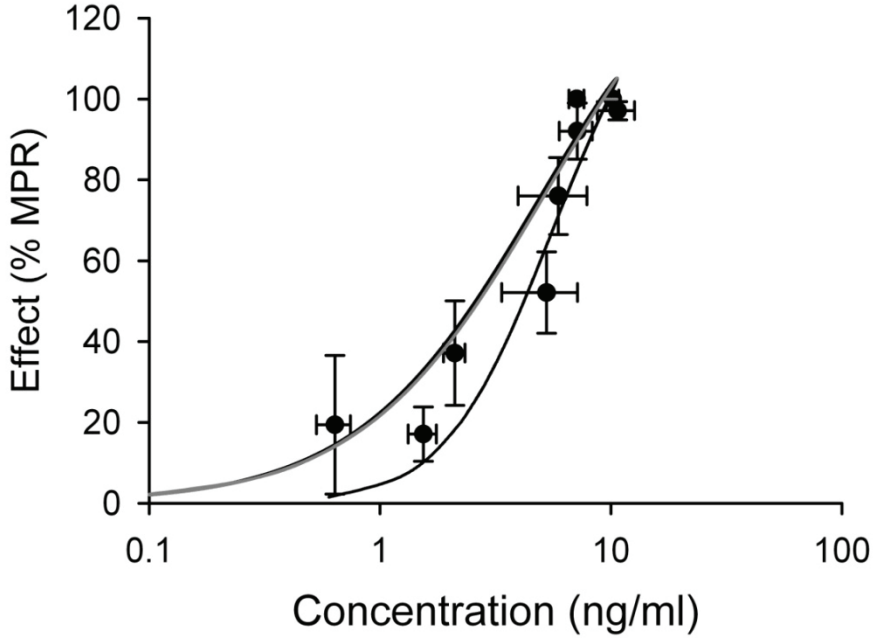
120
100
80
60
40
20
0
Effect (% MPR)
0.1
1
10
100
Concentration (ng/ml)

E

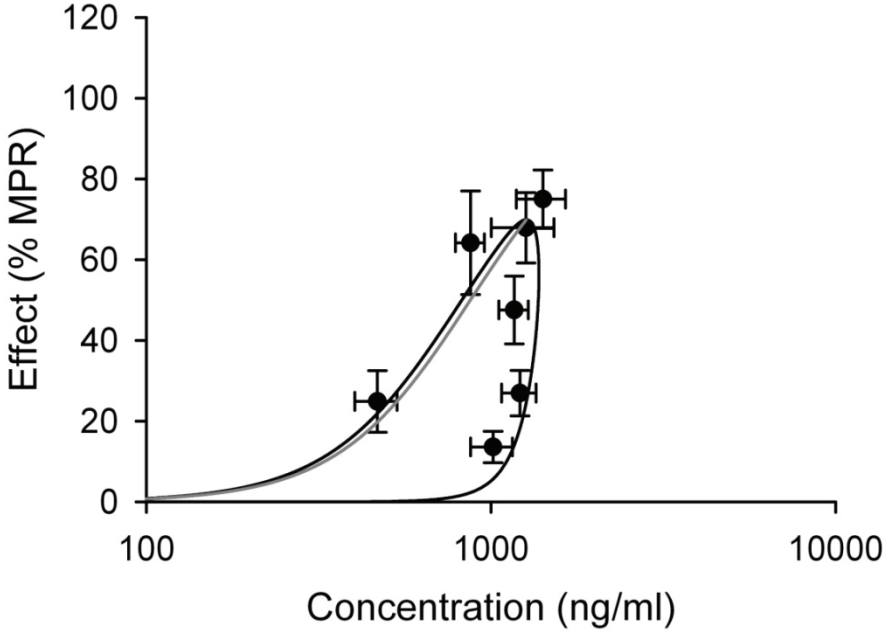
120
100
80
60
40
20
0
Effect (% MPR)
100
1000
10000
Concentration (ng/ml)

F

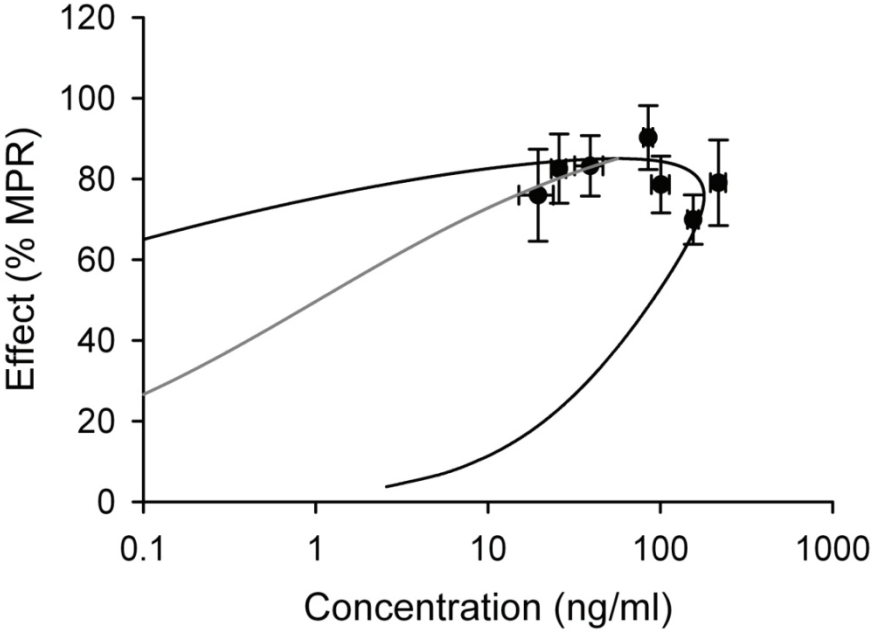
120
100
80
60
40
20
0
Effect (% MPR)
0.1
1
10
100
1000
Concentration (ng/ml)

G

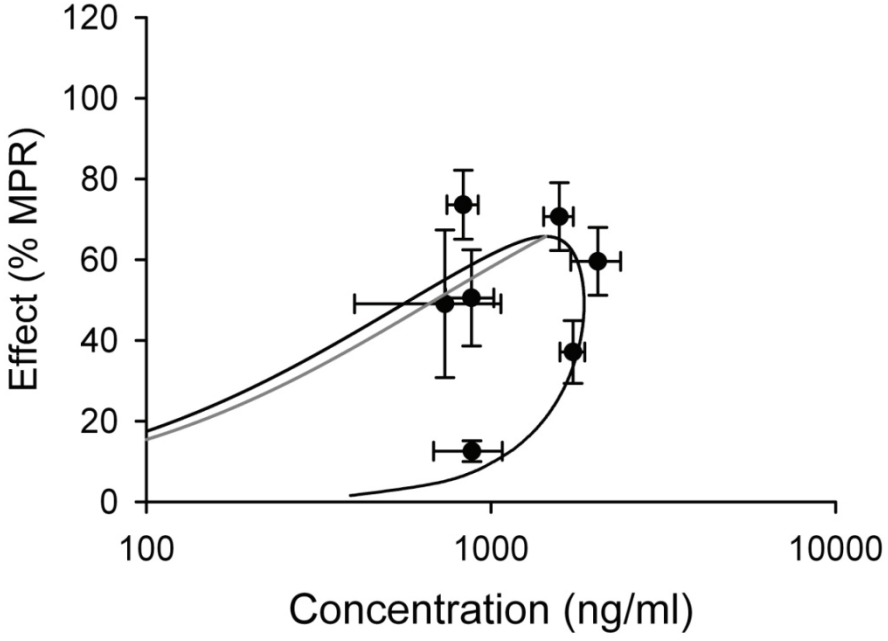
120
100
80
60
40
20
0
Effect (% MPR)
100
1000
10000
Concentration (ng/ml)

H

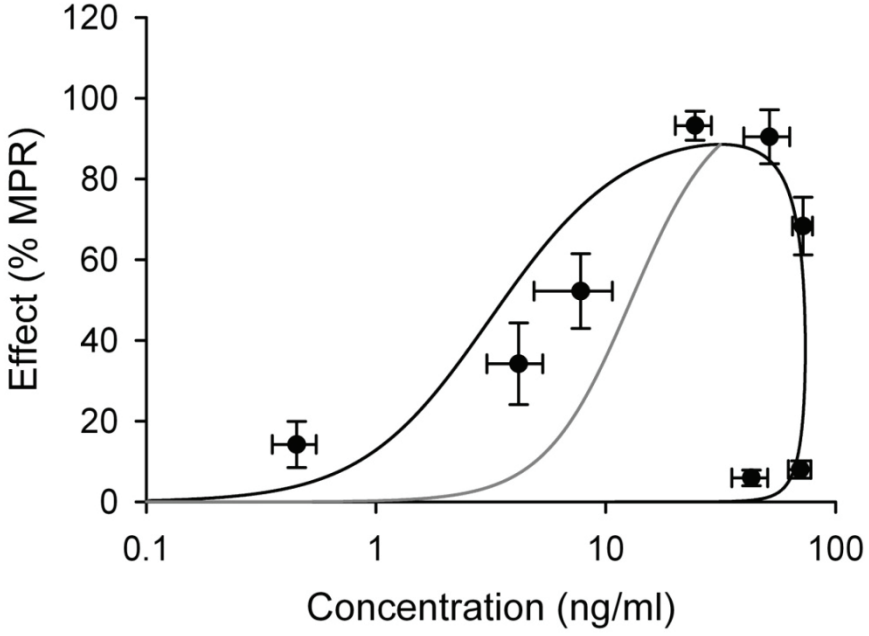
120
100
80
60
40
20
0
Effect (% MPR)
0.1
1
10
100
Concentration (ng/ml)

I

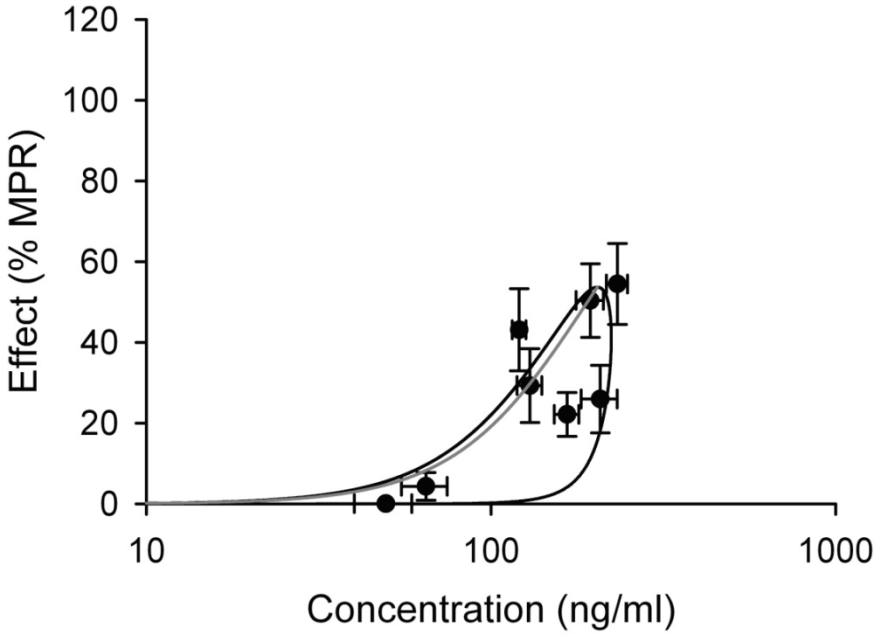
120
100
80
60
40
20
0
Effect (% MPR)
10
100
1000
Concentration (ng/ml)

J

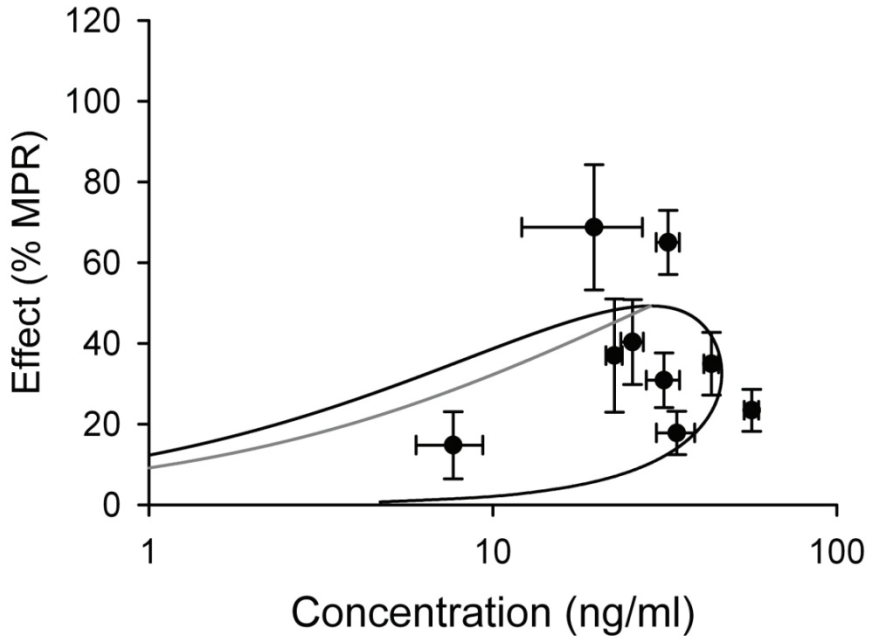
120
100
80
60
40
20
0
Effect (% MPR)
1
10
100
Concentration (ng/ml)

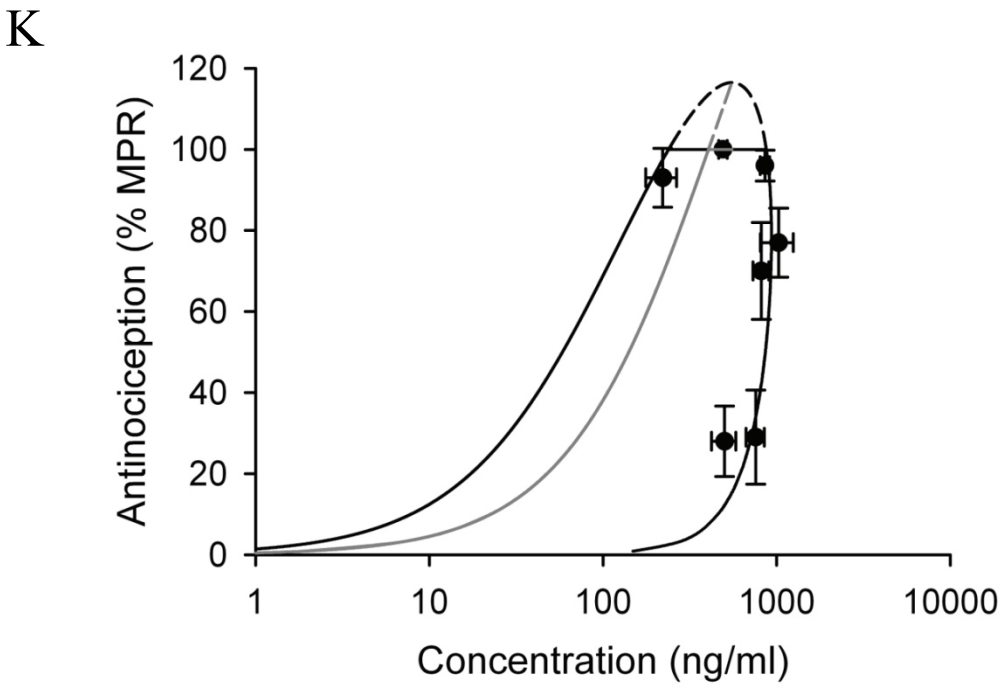

Figure 9.3. Relationship between opioid antinociception and serum or effect compartment concentrations of (A) alfentanil [*mdr1a*(+/+) mice]; (B) alfentanil [*mdr1a*(-/-) mice]; (C) fentanyl [*mdr1a*(+/+) mice]; (D) fentanyl [*mdr1a*(-/-) mice]; (E) loperamide [*mdr1a*(+/+) mice]; (F) loperamide [*mdr1a*(-/-) mice]; (G) loperamide [*mdr1a/b*(+/+) mice]; (H) loperamide [*mdr1a/b*(+/+) mice]; (I) methadone [*mdr1a*(+/+) mice]; (J) methadone [*mdr1a*(-/-) mice]; or (K) morphine [*mdr1a*(+/+) mice]. Symbols represent the mean ± S.E. of observed antinociception (n = 4 to 36) and serum concentrations (n ≥ 3). Lines represent the fit of the model to the time course of antinociception (solid gray), serum (dashed black), and effect (solid black) compartment concentration data.

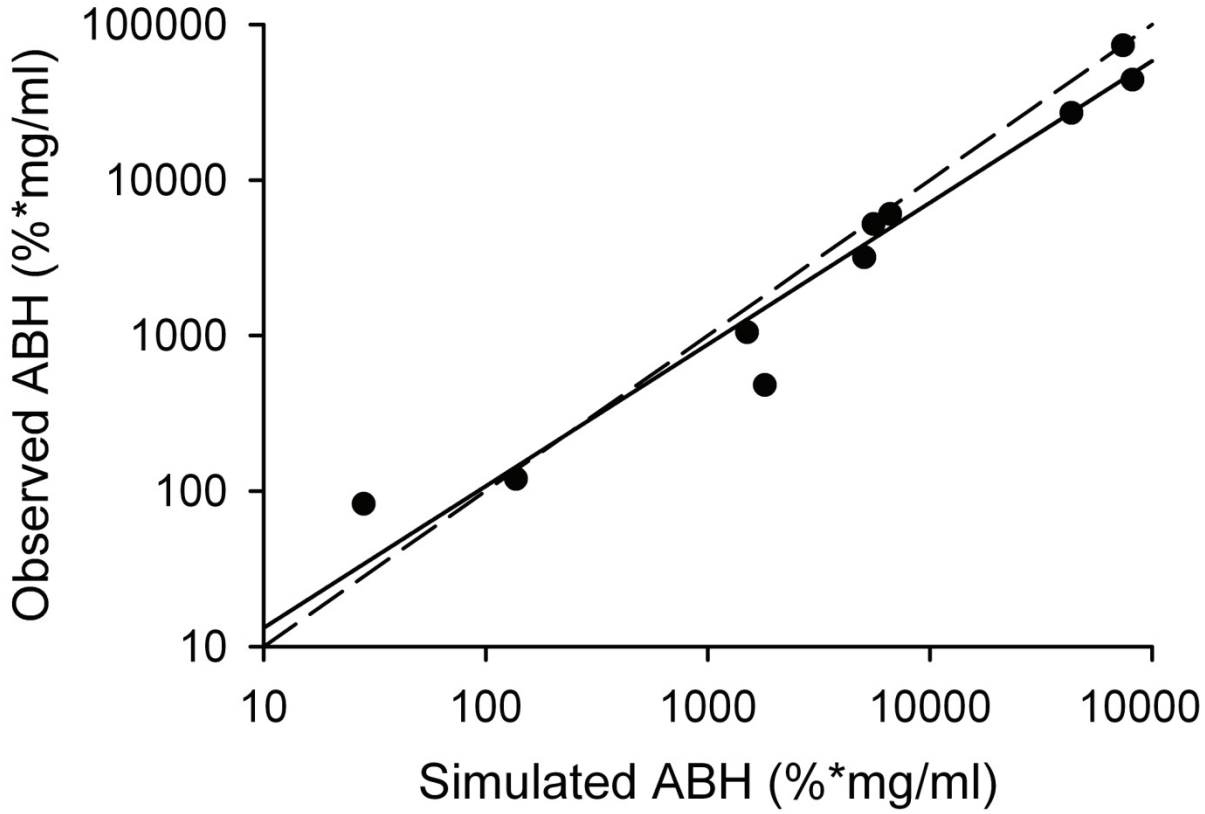

Figure 9.4. Relationship between ABH calculated using observed data versus predicted fit of the model for a series of opioids (r^2=0.95).

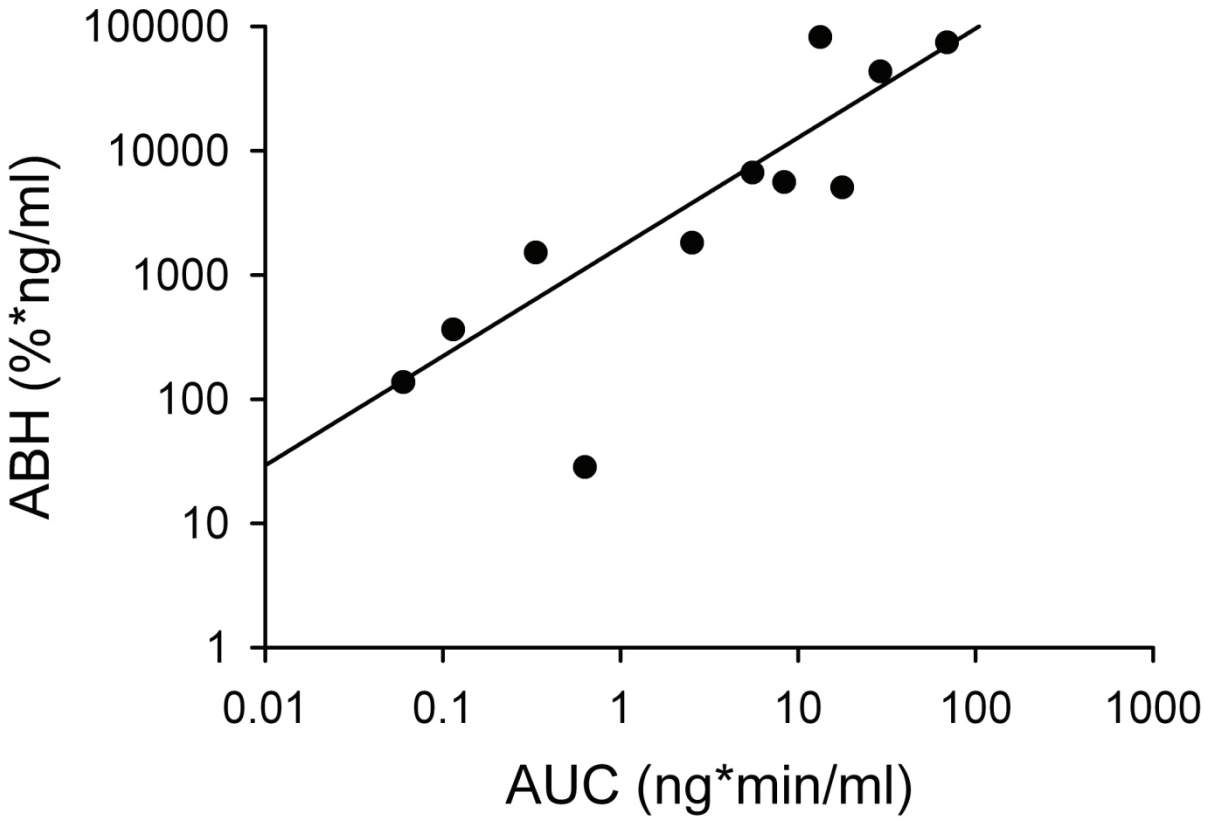

Figure 9.5. Relationship between ABH and AUC for a series of opioids (r^2=0.85).

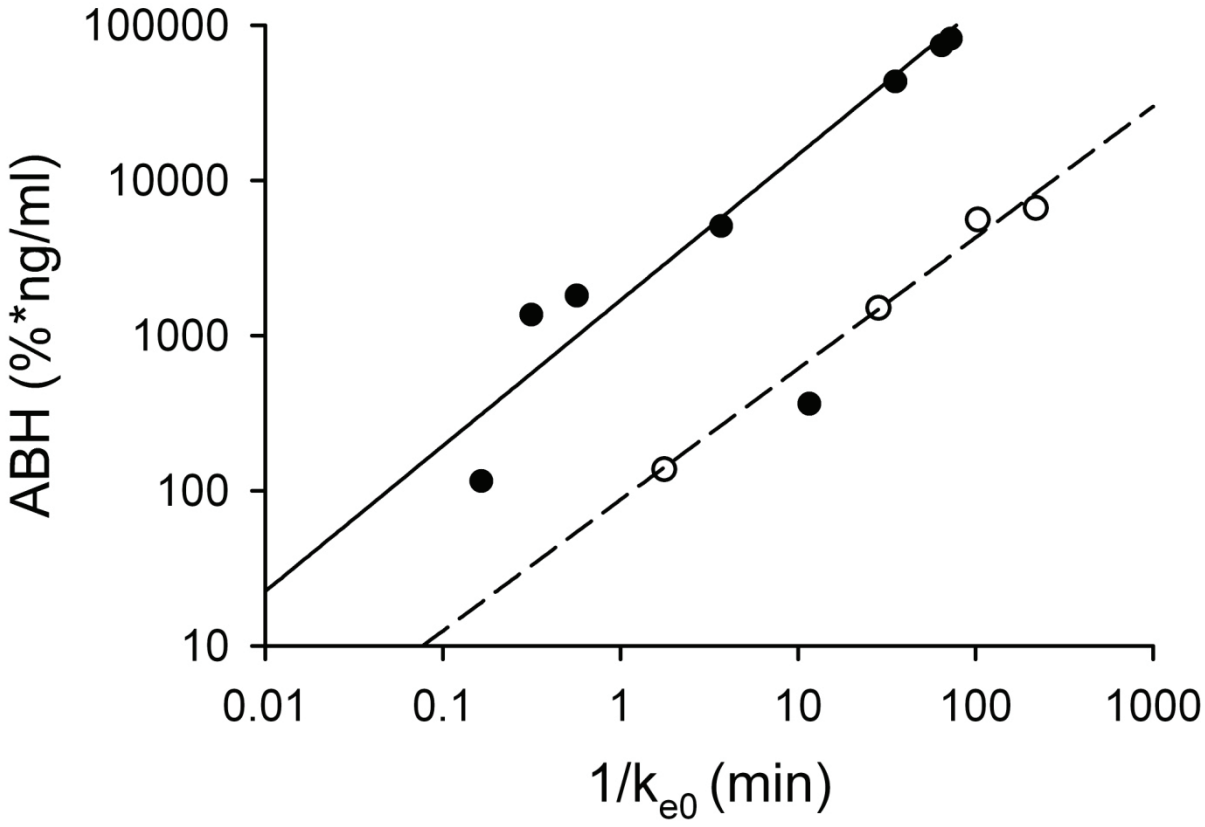

Figure 9.6. Relationship between ABH and $1/k_{e0}$ for a series of opioids in P-gp competent (●; r^2=0.94) and deficient (○: r^2=0.99) mice.

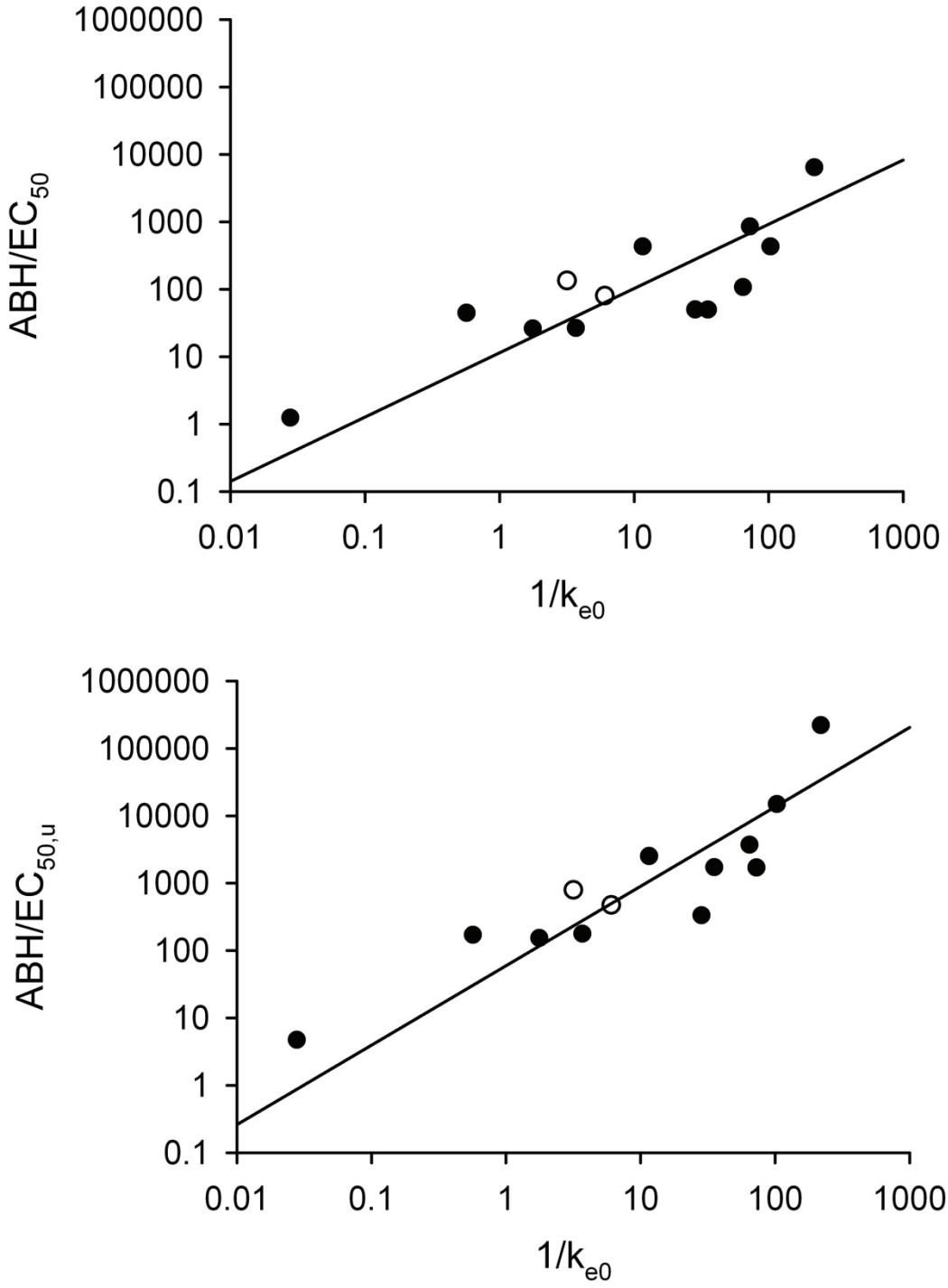

Figure 9.7. Correlation between ABH normalized by EC_{50} (top; r^2=0.49) or $EC_{50,u}$ (bottom; 0.67) and $1/k_{e0}$ for data obtained experimentally (●) or adapted from literature (○) (Cox et al., 1998).

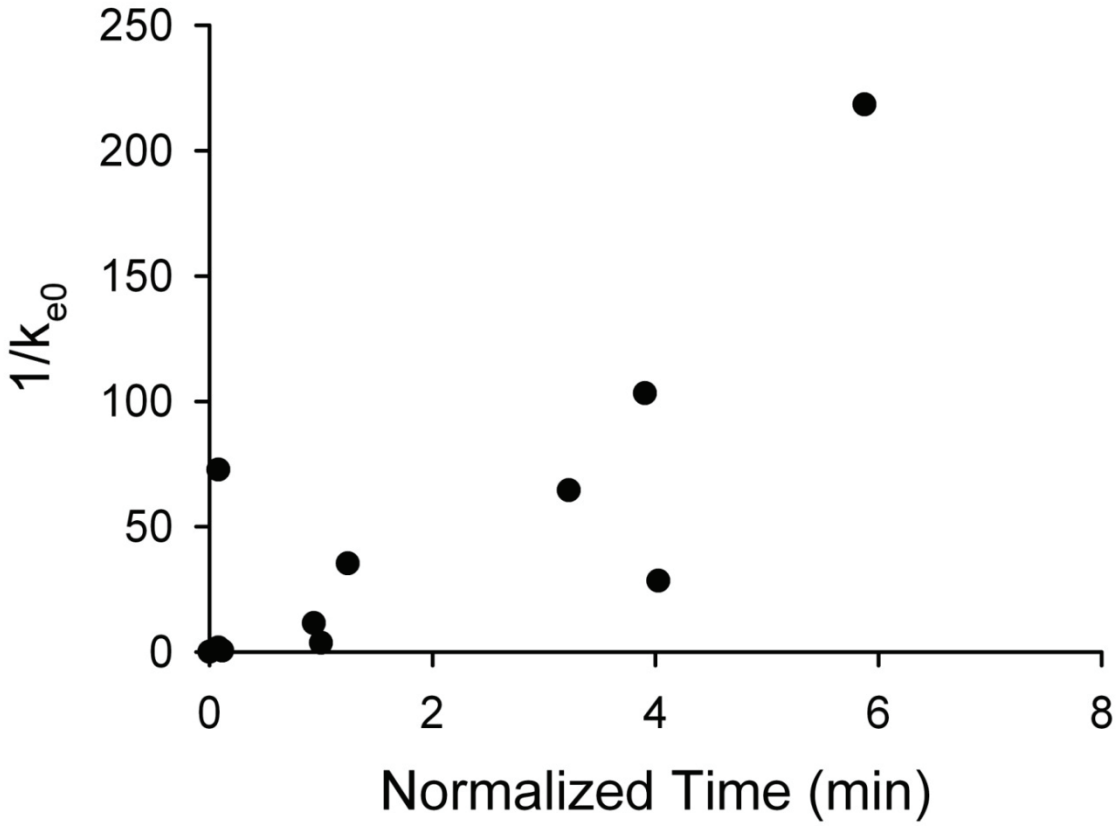

Figure 9.8. Relationship between $1/k_{e0}$ and the normalized time between maximum serum and effect compartment concentrations.

REFERENCES

Chen C and Pollack GM (1998) Altered disposition and antinociception of [D-penicillamine(2,5)] enkephalin in mdr1a-gene-deficient mice. *J Pharmacol Exp Ther* 287:545-552.

Cox EH, Kerbusch T, Van der Graaf PH and Danhof M (1998) Pharmacokinetic-pharmacodynamic modeling of the electroencephalogram effect of synthetic opioids in the rat: correlation with the interaction at the mu-opioid receptor. *J Pharmacol Exp Ther* 284:1095-1103.

Dagenais C, Graff CL and Pollack GM (2004) Variable modulation of opioid brain uptake by P-glycoprotein in mice. *Biochem Pharmacol* 67:269-276.

Ebling WF, Matsumoto Y and Levy G (1996) Feasibility of effect-controlled clinical trials of drugs with pharmacodynamic hysteresis using sparse data. *Pharm Res* 13:1804-1810.

Ganzinger U and Neumann K (1992) Quantification of tissue distribution of antibiotics by kinetic hysteresis analysis. *Eur J Clin Pharmacol* 43:517-522.

Golden PL and Pollack GM (2003) Blood-brain barrier efflux transport. *J Pharm Sci* 92:1739-1753.

Hermann DJ, Egan TD and Muir KT (1999) Influence of arteriovenous sampling on remifentanil pharmacokinetics and pharmacodynamics. *Clin Pharmacol Ther* 65:511-518.

Holford NH and Sheiner LB (1982) Kinetics of pharmacologic response. *Pharmacol Ther* 16:143-166.

Kalvass JC, Olson ER, Cassidy MP, Selley DE and Pollack GM (2007) Pharmacokinetics and pharmacodynamics of seven opioids in P-glycoprotein-competent mice: assessment of unbound brain EC50,u and correlation of in vitro, preclinical, and clinical data. *J Pharmacol Exp Ther* 323:346-355.

Lankas GR, Cartwright ME and Umbenhauer D (1997) P-glycoprotein deficiency in a subpopulation of CF-1 mice enhances avermectin-induced neurotoxicity. *Toxicol Appl Pharmacol* 143:357-365.

Schinkel AH (1997) The physiological function of drug-transporting P-glycoproteins. *Semin Cancer Biol* 8:161-170.

Schinkel AH, Wagenaar E, Mol CA and van Deemter L (1996) P-glycoprotein in the blood-brain barrier of mice influences the brain penetration and pharmacological activity of many drugs. *J Clin Invest* 97:2517-2524.

Thompson SJ, Koszdin K and Bernards CM (2000) Opiate-induced analgesia is increased and prolonged in mice lacking P-glycoprotein. *Anesthesiology* 92:1392-1399.

Tuk B, Danhof M and Mandema JW (1997) The impact of arteriovenous concentration differences on pharmacodynamic parameter estimates. *J Pharmacokinet Biopharm* 25:39-62.

Umbenhauer DR, Lankas GR, Pippert TR, Wise LD, Cartwright ME, Hall SJ and Beare CM (1997) Identification of a P-glycoprotein-deficient subpopulation in the CF-1 mouse strain using a restriction fragment length polymorphism. *Toxicol Appl Pharmacol* 146:88-94.

Upton RN and Doolette DJ (2002) A quantitative alternative to the hysteresis plot for measurement of drug transit time. *J Pharmacol Toxicol Methods* 47:45-51.

Verotta D, Beal SL and Sheiner LB (1989) Semiparametric approach to pharmacokinetic-pharmacodynamic data. *Am J Physiol* 256:R1005-1010.

CHAPTER 10

YOU CAN'T HAVE ONE WITHOUT THE OTHER: IMPROVING THE MARRIAGE BETWEEN PHARMACOKINETICS AND PHARMACODYNAMICS

In contrast to the straightforward situation of time-independent pharmacokinetics and pharmacodynamics (PK-PD), the relationship between drug concentrations and pharmacologic response is often complex and time-dependent. Describing the time course of drug concentrations is a relatively uncomplicated process for most drugs, a feat largely attributed to improvements in analytical sensitivity and specificity coupled with advances in computational power. In contrast, pharmacologic response is often poorly understood, making PD model development difficult. Since therapeutic outcomes are based on whether a drug can produce the designated effect, to the desired extent, in the absence of toxicity and unwanted side effects, it is critical that pharmacologic effect is described adequately. Ultimately, the development of more precise and robust PD models requires an understanding of both the mechanisms that mediate pharmacologic response and a thorough understanding of pharmacokinetics and associated sources of variability.

Describing the marriage between pharmacokinetics and pharmacodynamics is often difficult because the latter relies on the former. Take the example of a central nervous system (CNS) active drug. Systemic concentrations are dictated by absorption, distribution, metabolism and elimination (ADME) processes. Entry into, and exit out of, the CNS is dependent not only on systemic drug distribution but also on passive and active uptake/efflux transport at the blood-brain (BBB) and -cerebrospinal fluid (BCSFB) barriers, protein

binding, CSF turnover, and biotransformation. Moreover, drug distribution to the receptor biophase within the CNS is dependent on cerebral blood flow rate, brain capillary density and residence time, expression of transport proteins and metabolic enzymes, receptor distribution, and expression levels. Finally, manifestation of pharmacologic effect is dictated by factors such as binding affinity and the specific downstream signaling events that mediate response. Considering the magnitude and diversity of events that influence pharmacologic effect and the corresponding population variability around each of these factors, it is no surprise that characterizing the link between effect and concentration is challenging.

The central aim of this dissertation project was to improve the analytical link between pharmacokinetics and pharmacodynamics. This objective was addressed in two parts. The first section of this dissertation characterized factors that mediate systemic and CNS drug disposition, and explored how these attributes might modulate pharmacologic response. Specifically, utilizing a series of opioids, the influence of protein binding on *in* vitro-to-preclinical and preclinical-to-clinical relationships was characterized and the role of P-gp at the BBB on attenuating brain concentrations and antinociception. The second part of this project employed novel parametric and non-parametric approaches to characterize the link between drug concentrations and responsivity, again utilizing opioids as a model pharmacologic class. A PK-PD model was used to relate opioid-receptor binding within structurally distinct locales to different behavioral responses to nociceptive input. A modification of the sigmoidal E_{max} model assessed the influence of artificially truncating the value of E_{max} on resultant PD parameter estimates. The non-parametric approach utilized in this section related the calculated area bounded by a hysteresis loop (ABH) present in the effect versus serum concentration relationship to PK-PD parameters. This effort required

development of a new analytical approach, validation of that approach, and exploration of the potential utility of this new metric.

The intent of this concluding chapter is to integrate the results of this dissertation project, to place these results in perspective within a larger body of scientific research, and to discuss the implications of these results and potential areas for future investigation.

OPIOID TOLERANCE DEVELOPMENT

The opioids are a classic example of compounds that exhibit reductions in pharmacologic effect following long-term, repeated drug exposure. The rapid development of tolerance to the analgesic effects, but not the side effects of respiratory depression, nausea, and decreased gastrointestinal motility, limits dose-escalations and ultimately results in loss of analgesic efficacy (Inturrisi, 2002). Despite significant research on the topic, a comprehensive characterization of the pharmacokinetic and pharmacodynamic alterations that accompany tolerance development was lacking. Chapter 2 addressed this issue in detail, and discussed the pharmacokinetic mechanisms that may underlie opioid tolerance development, such as changes in metabolic enzyme activity and expression, or transporter functionality. PK alterations are not the predominant mediators of opioid tolerance. Pharmacodynamic alterations, however, are responsible and can be attributed to changes in receptor expression and functionality, variations in the signal transduction pathways and existence of cross-tolerance. The integrated PK-PD models that have developed to characterize the link between pharmacokinetics and pharmacodynamics were discussed in some detail.

While a number of approaches have been implemented to delay the onset and severity of opioid tolerance, the underlying problem has not been addressed (World Health

Organization, 1996). The prospect of developing drugs targeted to peripheral opioid receptors is particularly promising in that they are capable of producing antinociception while minimizing side effects associated with centrally-acting drugs (DeHaven-Hudkins, 2003; DeHaven-Hudkins and Dolle, 2004). While this approach could be used alone or in conjunction with a low-dose, centrally-active opioid, it requires the development of antinociceptive assays capable of differentiating peripheral and central contributions to antinociception.

The feasibility of targeting peripheral opioid receptors is supported by a number of studies. Rodents and humans express the μ-opioid receptor on and near cutaneous nerve fibers in normal and inflammatory states (Stein, 1993; Wittert et al., 1996; Labuz et al., 2007). These receptors are functional, as evidenced by analgesia produced following intra-articular or intra-ligamentary injections of morphine sulfate in the treatment of pain associated with inflammation or post-surgical traume (Stein et al., 1991; Dionne et al., 2001). Topical application of morphine-6-glucuronide (M6G) or DAMGO (D-Ala^2-MePhe^4-Gly(ol)^5]enkephalin) to a mouse tail evidenced peripherally-mediated antinociception (Kolesnikov and Pasternak, 1999). If opioids targeted to peripheral receptors are to increase in prevalence, assays of antinociception must be modified and improved to address antinociception mediated in the periphery.

The predominant antinociception assays involve exposure of experimental animals or subjects to thermal stimuli (Le Bars et al., 2001). One advantage of thermal assays is that, depending on the methodology, peripheral, spinal, or supraspinally-mediated antinociception can be assessed. The hotplate latency assay is considered an approach to evaluate supraspinally-mediated antinociception, whereas the radiant heat tail-flick assay is

considered a measure of spinally-mediated antinociception (Woolfe and Macdonald, 1944; Irwin et al., 1951). The primary method of characterizing peripheral antinociception involves a modified tail-flick assay where a low-dose opioid is topically applied to a segment of the tail and exposure to the radiant heat source is used to assess antinociception (Kolesnikov and Pasternak, 1999).

A novel approach to differentiating central and peripheral antinociception was developed in this dissertation project (Chapter 6). This assay characterizes two sets of behavioral responses following exposure to the hotplate: a reflexive response (hind-paw lifting and shaking) or a processed response (jumping or licking of the hind-paw). Latency to processed responses, such as jumping and licking was driven by brain concentrations, whereas reflexive responses, such as lifting and shaking of the paw, were predominately driven by serum concentrations with slight additive central contribution. Prior to widespread implementation of this assay, further validation will be required. Such validation steps could involve co-administration of a peripherally-restricted opioid receptor antagonist such as naloxone methiodide or a peripherally-restricted NMDA receptor antagonist such as LY235959 with an opioid to decrease or increase peripheral antinociception, respectively (Labuz et al., 2007). This novel antinociceptive assay could be especially valuable in characterizing the results of co-administration of peripherally- and centrally-acting opioids. Chapter 6 improved the marriage between pharmacokinetics and pharmacodynamics by linking different behavioral responses to concentrations in brain and serum.

P-GP-MEDIATED ATTENUATION OF CNS EXPOSURE

The passage of endogenous and exogenous substances between blood and the CNS is restricted by the presence of the BBB and BCSFB. The highly-developed structure of the

BBB contributes to its role as an anatomical, biochemical, and functional impediment to CNS penetration. These structures include brain capillary endothelial cells linked with tight junctions, an absence of fenestrations, low pinocytotic activity and structural support provided by astrocytes and glial cells (Engelhardt, 2003; Ohtsuki and Terasaki, 2007). Passive penetration of the BBB is largely dependent on chemical structure and physicochemical properties such as molecular weight, polar surface area, lipophilicity, and hydrogen bonding (Feng, 2002). In order to maintain homeostasis, the CNS relies on the expression of active uptake and efflux transporters for essential nutrients, physiologic substrates and xenobiotics (Graff and Pollack, 2004; Hawkins et al., 2006).

The diversity in chemical structure, BBB penetration, physicochemical properties, potency, and duration of effect exhibited by opioids makes this an ideal class of compounds for examining CNS disposition. Some opioids readily penetrate the CNS, whereas others (e.g., loperamide) do not cross the BBB effectively and are devoid of centrally-mediated activity at therapeutic doses (Niemegeers et al., 1979). This situation is, in part, due to P-gp expression on expression on the luminal surface of brain endothelial cells (Cordon-Cardo et al., 1989). The use of P-gp-deficient knockout mice or naturally-occurring mutants has been instrumental in assessing the role of P-gp in attenuating brain uptake and antinociception of loperamide, methadone, and DPDPE ([D-penicillamine(2,5)] enkephalin) (Chen and Pollack 1998; Thompson, Koszdin et al., 2000; Dagenais, Graff et al., 2004). The readily measurable effect of antinociception makes this class of drugs ideal for characterizing the influence of P-gp on CNS exposure and pharmacologic effect.

Loperamide and methadone exhibit enhanced antinociception in P-gp deficient mice, suggesting the role of P-gp efflux in mediating CNS concentrations and effect of these

compounds (Thompson et al., 2000). Chapters 4 and 5 characterized the impact of BBB P-gp on the time course of brain concentrations and antinociception of loperamide, methadone, fentanyl and alfentanil; the latter was identified as a P-gp substrate for the first time in this series of experiments (Chapter 5). The higher opioid doses required to achieve equipotent antinociception in P-gp competent versus deficient mice compensated for the role of BBB P-gp. While the results of earlier studies led to speculation that an increase in brain tissue EC_{50} of opioids in the presence of P-gp was related to P-gp-related impairment of opioid approach to receptor targets, the results of the present studies did not support that hypothesis (Chen and Pollack, 1998). Ultimately, P-gp at the BBB impacts the relationship between systemic and central concentrations and subsequently, pharmacologic effect. Yet, by understanding its role on CNS penetration of opioids and compounds representing other drug classes, the relationship between PK and PD is strengthened.

IMPROVING ESTIMATES OF EC_{50}

Drug potency is commonly expressed as K_i or EC_{50}, depending on whether measurements are obtained *in vitro* or *in vivo*, respectively. EC_{50} tends to be more a more useful descriptor than K_i because it incorporates the influence of drug disposition and other dynamic factors (Leysen et al., 1983; Visser et al., 2003). In situations of time-independent PK-PD, estimates of EC_{50} can be recovered from the relationship between effect and serum concentration. As is more often the case, time-dependent PK-PD relationships, that is, the dissociation between the time course of effect and the time course of systemic concentrations, are observed, and are commonly addressed with the inclusion of k_{e0}, the rate constant of distribution between serum and a hypothetical effect compartment containing the receptor biophase (Chapters 7 and 9). While this approach is useful for recovering estimates

of relevant PD parameters (e.g., EC_{50} in the hypothetical effect compartment), it is no substitute for knowing actual biophase concentrations. Seven μ-opioid agonists (alfentanil, fentanyl, loperamide, methadone, meperidine, morphine, and sufentanil) were selected in Chapter 3 to determine which measures of potency correlate best between *in vitro*-preclinical-and-clinical situations. The strongest *in vitro*-to-*in vivo* correlation was observed between K_i and unbound brain EC_{50}. While a strong correlation was observed between mouse serum and human plasma EC_{50}, it was improved by correcting for protein binding. Improving estimates of EC_{50}, by accounting for biophase concentrations and/or the free drug fraction, strengthens the link between pharmacokinetics and pharmacodynamics for the opioids and provides a basis for future studies of the importance of free drug fractions on estimates of EC_{50}.

Estimates of EC_{50} also are influenced both by pharmacodynamic and pharmacokinetic processes. Chapter 7 examined the role of artificially truncating the value of E_{max} on estimates of PD parameters. Assessing antinociception with the hotplate latency assay requires the implementation of a 60 sec latency cut-off time to prevent tissue damage (Hammond, 1989). This requirement imposes an artificial ceiling of effect that results in skewed data when the cut-off time is reached. In this study, mice receiving fentanyl (0.09 mg/kg s.c.) or morphine (3.6 mg/kg s.c.) exhibited responses of 100% MPR at one or more time points. A linked PK-PD model, including a sigmoidal relationship between effect and hypothetical effect-compartment concentrations, was fit to the time course of drug disposition and antinociception after opioid administration. The data were best described when an estimate of the E_{max} was recovered from the model, rather than utilizing a truncated fixed value as a constant in the model. Increasing the dynamic range of effect (by 65 to

100%) of the theoretical E_{max} improved estimates of k_{e0}, EC_{50} and γ. Simulations revealed that artificial E_{max} truncation influences parameter estimates to a greater extent when sigmoidicity is low (γ=1 vs. γ=4). These results highlight the importance of assay methodology in measurements of pharmacologic response and the availability of modeling approaches to address limitations imposed by assay methodology. Ultimately, incorporating new data analysis techniques the approach presented in Chapter 7 will improve the relationship between pharmacokinetics and pharmacodynamics.

ABH: A NON-PARAMETRIC DESCRIPTOR OF PK-PD DISSOCIATIONS

The time-dependent dissociation between pharmacologic effect and blood concentrations can result from a number of physiologic processes: indirect responses following drug-receptor binding, production of a pharmacologically active metabolite, or drug distribution to a structurally distinct compartment containing the receptor biophase. Dissociations between concentration and effect, known as hysteresis loops, can progresses temporally in the clockwise direction, such as in situations such as tolerance development or progress in the counterclockwise direction, such as in situations of distributional delays between serum and the receptor biophase. It is assumed that the relationship between the receptor biophase and pharmacologic response is time-independent and sigmoidal. Since biophase concentrations are unknown, PD estimates must be made using the relationship between serum and effect.

The approach developed by Holford and Sheiner (1982), predicting the time course of drug concentrations in a hypothetical effect compartment based on the temporal relationships between effect and blood concentrations, was utilized in Chapters 8 and 9 to recover estimates of fundamental pharmacodynamic parameters (EC_{50} and γ). The novel, non-

parametric approach of calculating the area bounded by the effect-serum concentration hysteresis (ABH), described in Chapter 8, was utilized to determine if ABH may serve as a model-independent metric of the dissociation between serum concentrations and effect. The time course of serum concentrations and antinociception for 5 μ-opioid receptor agonists (alfentanil, fentanyl, loperamide, methadone and morphine), administered at equipotent doses to P-gp-competent and P-gp-deficient mice, was used in Chapter 9 to recovered estimates of relevant PK-PD parameters and to calculate ABH.

The ABH values calculated for this series of opioids correlated with the area under the concentration curve (AUC) and PK-PD model-derived descriptors, k_{e0} and EC_{50}. An alternative model-independent descriptor, the normalized time difference between maximum serum concentrations and peak effect, appeared to be a predictive metric of k_{e0}. While further validation of the relationships between ABH and model-derived parameters is necessary, Chapters 8 and 9 present a potentially high-impact, alternative approach to addressing concentration-effect hysteresis loops.

SUMMARY

This dissertation project addressed two methods of improving the link between pharmacokinetics and pharmacodynamics. The first component addressed methods of improving correlations between concentration and response. The influence of P-gp-mediated efflux on drug disposition was highlighted in Chapters 4 and 5, Chapter 3 identified the utility of correcting for protein binding, and Chapters 6 and 7 presented novel methods of relating concentration and response, by distinguishing central and peripheral contributions to antinociception based on behavioral responses and by using the theoretical value of E_{max} to improve PD parameter estimates. The second component of this project identified ABH as a

model-independent descriptor of the relationship between concentration and response (Chapters 8 and 9). The results of each of these global efforts indicated that the marriage between pharmacokinetics and pharmacodynamics can be improved by incorporating the components that influence concentration and response (e.g., protein binding, P-gp efflux, or distribution of the receptor biophase in different compartments) and by characterizing this relationship in novel manners (e.g. calculations of ABH).

REFERENCES

Chen C and Pollack GM (1998) Altered disposition and antinociception of [D-penicillamine(2,5)] enkephalin in mdr1a-gene-deficient mice. *J Pharmacol Exp Ther* **287**:545-552.

Cordon-Cardo C, O'Brien JP, Casals D, Rittman-Grauer L, Biedler JL, Melamed MR and Bertino JR (1989) Multidrug-resistance gene (P-glycoprotein) is expressed by endothelial cells at blood-brain barrier sites. *Proc Natl Acad Sci U S A* **86**:695-698.

DeHaven-Hudkins DL (2003) Peripherally restricted opioid drugs: advances and retreats. *Current Opinion in Anaesthesiology* **16**:541-545.

DeHaven-Hudkins DL and Dolle RE (2004) Peripherally restricted opioid agonists as novel analgesic agents. *Curr Pharm Des* **10**:743-757.

Dionne RA, Lepinski AM, Gordon SM, Jaber L, Brahim JS and Hargreaves KM (2001) Analgesic effects of peripherally administered opioids in clinical models of acute and chronic inflammation. *Clin Pharmacol Ther* **70**:66-73.

Engelhardt B (2003) Development of the blood-brain barrier. *Cell Tissue Res* **314**:119-129.

Feng MR (2002) Assessment of blood-brain barrier penetration: in silico, in vitro and in vivo. *Curr Drug Metab* **3**:647-657.

Graff CL and Pollack GM (2004) Drug transport at the blood-brain barrier and the choroid plexus. *Curr Drug Metab* **5**:95-108.

Hammond DL (1989) Inference of Pain and Its Modulation from Simple Behaviors, in *Issues in Pain Management* (Chapman CR and Loeser JD eds) pp 69-89, Raven Press, Ltd., New York.

Hawkins RA, O'Kane RL, Simpson IA and Vina JR (2006) Structure of the blood-brain barrier and its role in the transport of amino acids. *J Nutr* **136**:218S-226S.

Holford NH and Sheiner LB (1982) Kinetics of pharmacologic response. *Pharmacol Ther* **16**:143-166.

Inturrisi CE (2002) Clinical pharmacology of opioids for pain. *Clin J Pain* **18**:S3-13.

Irwin S, Houde RW, Bennett DR, Hendershot LC and Seevers MH (1951) The effects of morphine methadone and meperidine on some reflex responses of spinal animals to nociceptive stimulation. *J Pharmacol Exp Ther* **101**:132-143.

Kolesnikov Y and Pasternak GW (1999) Topical opioids in mice: analgesia and reversal of tolerance by a topical N-methyl-D-aspartate antagonist. *J Pharmacol Exp Ther* **290**:247-252.

Labuz D, Mousa SA, Schafer M, Stein C and Machelska H (2007) Relative contribution of peripheral versus central opioid receptors to antinociception. *Brain Res* **1160**:30-38.

Le Bars D, Gozariu M and Cadden SW (2001) Animal Models of Nociception. *Pharmacol Rev* **53**:597-652.

Leysen JE, Gommeren W and Niemegeers CJ (1983) [3H]Sufentanil, a superior ligand for mu-opiate receptors: binding properties and regional distribution in rat brain and spinal cord. *Eur J Pharmacol* **87**:209-225.

Niemegeers CJ, McGuire JL, Heykants JJ and Janssen PA (1979) Dissociation between opiate-like and antidiarrheal activities of antidiarrheal drugs. *J Pharmacol Exp Ther* **210**:327-333.

Ohtsuki S and Terasaki T (2007) Contribution of carrier-mediated transport systems to the blood-brain barrier as a supporting and protecting interface for the brain; importance for CNS drug discovery and development. *Pharm Res* **24**:1745-1758.

Stein C (1993) Peripheral mechanisms of opioid analgesia. *Anesth Analg* **76**:182-191.

Stein C, Comisel K, Haimerl E, Yassouridis A, Lehrberger K, Herz A and Peter K (1991) Analgesic effect of intraarticular morphine after arthroscopic knee surgery. *N Engl J Med* **325**:1123-1126.

Thompson SJ, Koszdin K and Bernards CM (2000) Opiate-induced analgesia is increased and prolonged in mice lacking P-glycoprotein. *Anesthesiology* **92**:1392-1399.

Visser SA, Wolters FL, Gubbens-Stibbe JM, Tukker E, Van Der Graaf PH, Peletier LA and Danhof M (2003) Mechanism-based pharmacokinetic/pharmacodynamic modeling of the electroencephalogram effects of GABAA receptor modulators: in vitro-in vivo correlations. *J Pharmacol Exp Ther* **304**:88-101.

Wittert G, Hope P and Pyle D (1996) Tissue distribution of opioid receptor gene expression in the rat. *Biochem Biophys Res Commun* **218**:877-881.

Woolfe G and Macdonald AD (1944) The evaluation of the analgesic action of pethidine hydrochloride (Demerol). *J Pharmacol Exp Ther* **80**:300-307.

World Health Organization (1996) Cancer Pain Relief, Second Edition, in pp 1-69, World Health Organization, Geneva, Switzerland.

APPENDIX: MATLAB CODE

```
%*******************************************************************************************
% Hysteresis.m - Calculates area of hysteresis loops
%*******************************************************************************************

clear all;
close all;
format compact;
tic;

%=========================================================================
% Read List of Files to Analyze
%=========================================================================
FileList='FileList.csv';
st=strcat(cd,'\',FileList);
fid=fopen(st,'r');

f=0;
while feof(fid)~=1            % while "end of file" has not been reached
    f=f+1;                    % increment counter
    line=fgetl(fid);          % get 1 line from file list. Format = 'foldername','filename'
    [a,b]=strtok(line,',');   % get folder and file names from 'line' variable.
    b=b(2:length(b));         % strip leading comma (from strtok command) from filename
    FolderName{f}=a;          % save folder name to variable 'FolderName'
    FileName{f}=b;            % save file name to variable 'filename'
    FilePath{f}=strcat(cd,'\',a,'\',FileName{f},'.csv');   % create and save full file path
end
fclose(fid);

%=========================================================================
% Count files in each folder to group for figures
%=========================================================================
for f=1:length(FileName)
    if f==1;                                        %If first file in list, then
        FigNum(f)=1;                                %   assign to subplot #1 on figure #1
        FigSubplotNum(f)=1;
    else                                            %If file is not first on list, then
        if strcmp(FolderName{f},FolderName{f-1})==1  %If foldername matches previous, then
            FigNum(f)=FigNum(f-1);                  %  assign to next subplot on same figure
            FigSubplotNum(f)=FigSubplotNum(f-1)+1;
        else                                       %If foldername doesn't match previous, then
            FigNum(f)=FigNum(f-1)+1;                %   assign to subplot #1 on new figure
            FigSubplotNum(f)=1;
        end
    end
    GrpSize(FigNum(f))=FigSubplotNum(f);            % Determine size of each figure group
end

%=========================================================================
% Get and Analyze Data From Files
%=========================================================================
for f=1:length(FileName);

    %=====================================================================
    % Get Header Info
    %=====================================================================
    fid=fopen(FilePath{f},'r');       % Open data file
    x=fgetl(fid);                     % Get first line (column headers)
    i=0;
    while isempty(x)~=1;              % While x is not empty, look for more column headers
        i=i+1;                        % Increment counter
        [a,x]=strtok(x,',');          % Search for delimiters (comma) to separate header name
        ColHdr{i}=a;                  % Save column header name
        if isempty(x)~=1              % If another column is detected,
            if strcmp(x(1:2),',,')==1   %    then check next column for text
                break;                % Break if no header text detected
            end
        end
    end
```

```
%=========================================================================
% Read numerical data from file
%=========================================================================
numrowsmax=10000;                       % Maximum number of data rows to search
for i=1:numrowsmax
    x=fgetl(fid);                       % Get data line from file
    if feof(fid)==1;                    % Test to see if end of file has been reached
        break;                          % Break loop if end of file
    elseif strcmp(x(1:2),',,')==1;      % Test to see if line has no data, but has comma
                                        %  delimiters
        break;                          % Break loop if line has no data
    else
        for j=1:length(ColHdr)
            [a,x]=strtok(x,',');
            if isempty(str2num(a))~=1
                data(i,j)=str2num(a);
            else
                data(i,j)=NaN;
            end
        end
    end
end
fclose(fid);                            % Close data file

%=========================================================================
% Select Data Columns and Calculate Area
%=========================================================================

% Select Data Columns for X and Y Axes;
xcolnum=3;
ycolnum=5;

x_hdr=ColHdr{xcolnum};
y_hdr=ColHdr{ycolnum};
x=data(:,xcolnum);
y=data(:,ycolnum);

% Find index of maximum x value
[val,maxind]=max(x);
x1=x(1:maxind);
x2=x(maxind:length(x));
y1=y(1:maxind);
y2=y(maxind:length(x));

% Calculate Area
for i=1:(length(x1)-1)
    Area1(i)=abs(mean(y1(i:i+1))*diff(x1(i:(i+1))));
end
Area1=sum(Area1);

for i=1:(length(x2)-1)
    Area2(i)=abs(mean(y2(i:i+1))*diff(x2(i:(i+1))));
end
Area2=sum(Area2);

CurveArea(f)=abs(Area1-Area2);
if Area1-Area2<0
    Direction{f}='CCW';
else
    Direction{f}='CW';
end

%=========================================================================
% Plot Curves
%=========================================================================

% Set Location for Plot(figure number, subplot number)
figure(FigNum(f));
if FigSubplotNum(f)==1                  % If first subplot in group,
    rows=round(sqrt(GrpSize(FigNum(f))));      %   set subplot layout for rest of group
```

```
        cols=rows;
    end

    % Plot Data
    subplot(rows,cols,FigSubplotNum(f));
    plot(x1,y1,'b',x2,y2,'r')

    % Set Titles and Axis Labels
    title(FileName{f},'fontsize',8,'verticalalignment','middle');
    xlabel(x_hdr,'fontsize',8,'verticalalignment','middle');
    if rem(FigSubplotNum,rows)==1
        ylabel(y_hdr,'fontsize',8,'verticalalignment','middle');
    end
    set(gca,'fontsize',8)

    % Normalize axes for all plots on figure if plot is last in group
    if FigSubplotNum(f)==GrpSize(FigNum(f));
        % Get X and Y axis limits for each plot
        for i=1:FigSubplotNum(f);
            figure(FigNum(f));
            subplot(4,4,i);
            a=get(gca,'xlim');
            xlim_min(i)=a(1);
            xlim_max(i)=a(2);
            a=get(gca,'ylim');
            ylim_min(i)=a(1);
            ylim_max(i)=a(2);
        end
        % Set Equal X and Y axis limits for each plot
        for i=1:FigSubplotNum(f);
            figure(FigNum(f));
            subplot(4,4,i);
            set(gca,'xlim',[min(xlim_min) max(xlim_max)]);
            set(gca,'ylim',[min(ylim_min) max(ylim_max)]);
        end
    end;

    %=========================================================================
    % Save Output Values
    %=========================================================================
    Output{f,1}=FigNum(f);
    Output{f,2}=FigSubplotNum(f);
    Output{f,3}=FolderName{f};
    Output{f,4}=FileName{f};
    Output{f,5}=x_hdr;
    Output{f,6}=y_hdr;
    Output{f,7}=CurveArea(f);
    Output{f,8}=Direction{f};

    %=========================================================================
    % Display Progress
    %=========================================================================
    clc;
    disp(strrep(strcat('Completed:_',num2str(round(100*f/length(FileName))),'%'),'_',' '))
end

% Plot loop area values for each figure group
figure;
for i=1:max(FigNum);
    y=CurveArea(find(FigNum==i));
    subplot(3,2,i);
    plot([1:length(y)],y,'-vb');
    xlim([0 length(y)+1]);

    title(FolderName{min(find(FigNum==i))},'fontsize',8,'verticalalignment','middle');
    ylabel('Area','fontsize',8,'verticalalignment','middle');
    set(gca,'fontsize',8);
end

% Clear screen and display elapsed time
clc;
```

```
t=toc;
disp(strrep(strcat('Time Elapsed:_',num2str(round(10*t/60)/10),'_min'),'_',' '))

%=========================================================================
% Select output filename and verify overwrite of existing file if needed
%=========================================================================
WriteOutputFile=0;
while WriteOutputFile==0;
    beep
    disp(' ');
    disp('Waiting for user input...');
    disp(' ');
    OutputFileName=input('Name for output file: ','s');

    x=dir(cd);
    for i=1:length(x)
        MatchingFile(i)=strcmp(lower(x(i).name),lower(strcat(OutputFileName,'.txt')));
    end
    MatchingFile=sum(MatchingFile);

    if MatchingFile==0;
        WriteOutputFile=1;
    else
        disp(' ');
        disp(strcat(OutputFileName,'.txt already exists.'))
        OverwriteFile=input('Do you want to replace it? (Y/N): ','s');
        if strcmp(lower(OverwriteFile(1)),'y')==1
            WriteOutputFile=1;
        else
            WriteOutputFile=0;
        end
    end
end

%=========================================================================
% Write to Output File
%=========================================================================
fid=fopen(strcat(cd,'\',OutputFileName,'.txt'),'w');
fprintf(fid,'Folder\tFile\tX_Data\tY_Data\tCurve Area\tDirection\r\n');
fprintf(fid,'------\t----\t------\t------\t----------\t---------\r\n');
for f=1:size(Output,1)
    if f~=1
        if Output{f,1}~=Output{f-1,1}
            fprintf(fid,'\r\n');
        end
    end
%     fprintf(fid,'%s\t%s\t%s\t%s\t%s\t%g\r\n',...
%         Output{f,3},Output{f,4},Output{f,5},Output{f,6},Output{f,7},Output{f,8});

    fprintf(fid,'%s\t',Output{f,3});
    fprintf(fid,'%s\t',Output{f,4});
    fprintf(fid,'%s\t',Output{f,5});
    fprintf(fid,'%s\t',Output{f,6});
    fprintf(fid,'%g\t',Output{f,7});
    fprintf(fid,'%s\r\n',Output{f,8});
end
fclose(fid);

%=========================================================================
% Save Plots to jpeg Format
%=========================================================================
for f=1:length(FileName)
    n=Output{f,1};
    PlotName{n}=strcat(OutputFileName,'_',Output{f,3});
end
PlotName{max(FigNum)+1}=strcat(OutputFileName,'_','Area Curves');

for i=1:length(PlotName)
    figure(i)
    set(figure(i),'PaperOrientation','portrait')
    set(figure(i),'PaperPosition',[0.25 0.25 8 10.5])
```

```
    disp(strrep(strcat('Generating
Image_',num2str(i),'_of_',num2str(Output{size(Output,1),1}), '...'),'_',' '))
    print(i,'-dtiff','-r300',PlotName{i})
end


%=========================================================================
% Display Status
%=========================================================================
clc;
fprintf('***DONE***\r\n\r\n')
fprintf('Output data saved to:\r\n\t%s\r\n\r\n',strcat(OutputFileName,'.txt'))
fprintf('Plots saved to: \r\n')
for i=1:length(PlotName)
    fprintf('\t%s\r\n',strcat(PlotName{i},'.tiff'))
end
fprintf('\r\n')
fprintf('File Location: %s\r\n\r\n',strcat(cd,'\'));
disp(strrep(strcat('Time Elapsed:_',num2str(round(10*t/60)/10),'_min'),'_',' '))
beep
```